Vol. 280, No. 2, August 16, 1993
Completing Volume 280

ISSN 0003-2670

Please Note
Cumulative Indexes for Volumes 271–280 will be published later

ANALYTICA CHIMICA ACTA

An international journal devoted to all branches of analytical chemistry

ELSEVIER

ANALYTICA CHIMICA ACTA

Scope. *Analytica Chimica Acta* publishes original papers, preliminary communications and reviews dealing with every aspect of modern analytical chemistry. Reviews are normally written by invitation of the editors, who welcome suggestions for subjects. Preliminary communications of important urgent work can be printed within four months of submission, if the authors are prepared to forego proofs.

Submission of Papers

Americas

Prof. Harry L. Pardue
Department of Chemistry
1393 BRWN Bldg, Purdue University
West Lafayette, IN 47907-1393
USA

Tel:(+1-317) 494 5320
Fax:(+1-317) 496 1200

Computer Techniques

Prof. J.T. Clerc
Universität Bern
Pharmazeutisches Institut
Baltzerstrasse 5, CH-3012 Bern
Switzerland

Tel:(+41-31) 654171
Fax:(+41-31) 654198

Prof. Sarah C. Rutan
Department of Chemistry
Virginia Commonwealth University
P.O. Box 2006
Richmond, VA 23284-2006
USA
Tel:(+1-804) 367 1298
Fax:(+1-804) 367 8599

Other Papers

Prof. Alan Townshend
Department of Chemistry
The University
Hull HU6 7RX
Great Britain

Tel:(+44-482) 465027
Fax:(+44-482) 466410

Prof. Willem E. van der Linden
Laboratory for Chemical Analysis
Department of Chemical Technology
Twente University of Technology
P.O. Box 217, 7500 AE Enschede
The Netherlands
Tel:(+31-53) 892629
Fax:(+31-53) 356024

Prof. Paul Worsfold
Dept. of Environmental Sciences
University of Plymouth
Plymouth PL4 8AA
Great Britain

Tel:(+44-752) 233006
Fax:(+44-752) 233009

Submission of an article is understood to imply that the article is original and unpublished and is not being considered for publication elsewhere. *Anal. Chim. Acta* accepts papers in English only. There are no page charges. Manuscripts should conform in layout and style to the papers published in this issue. See inside back cover for "Information for Authors".

Publication. *Analytica Chimica Acta* appears in 14 volumes in 1993. The subscription price for 1993 (Vols. 267–280) is Dfl. 4214.00 plus Dfl. 462.00 (p.p.h.) (total approx. US$ 2597.75). *Vibrational Spectroscopy* appears in 2 volumes in 1993. The subscription price for *Vibrational Spectroscopy* (Vols. 4 and 5) is Dfl. 700.00 plus Dfl. 66.00 (p.p.h.) (total approx. US$ 407.50). The price of a combined subscription (*Anal. Chim. Acta* and *Vib. Spectrosc.*) is Dfl. 4592.00 plus Dfl. 528.00 (p.p.h.) (total approx. US$ 2844.50). All earlier volumes (Vols. 1–266) except Vols. 23 and 28 are available at Dfl. 259.50 (US$ 144.00), plus Dfl. 18.00 (US$ 10.00) p.p.h., per volume. The Dutch guilder price is definitive. The U.S. dollar price is subject to exchange-rate fluctuations and is given only as a guide. Subscriptions are accepted on a prepaid basis only, unless different terms have been previously agreed upon.
Our p.p.h. (postage, packing and handling) charge includes surface delivery of all issues, except to subscribers in the U.S.A., Canada, Australia, New Zealand, China, India, Israel, South Africa, Malaysia, Thailand, Singapore, South Korea, Taiwan, Pakistan, Hong Kong, Brazil, Argentina and Mexico, who receive all issues by air delivery (S.A.L.–Surface Air Lifted) at no extra cost. For Japan, air delivery requires 25% additional charge of the normal postage and handling charge; for all other countries airmail and S.A.L. charges are available upon request.

Subscription orders. Subscription orders can be entered only by calendar year and should be sent to: Elsevier Science Publishers B.V., Journals Department, P.O. Box 211, 1000 AE Amsterdam, The Netherlands. Tel: (+31-20) 5803 642, Telex: 18582, Telefax: (+31-20) 5803598, to which requests for sample copies can also be sent. Claims for issues not received should be made within six months of publication of the issues. If not they cannot be honoured free of charge. Readers in the U.S.A. and Canada can contact the following address: Elsevier Science Publishing Co. Inc., Journal Information Center, 655 Avenue of the Americas, New York, NY 10010, U.S.A. Tel: (+1-212) 6333750, Telefax: (+1-212) 6333990, for further information, or a free sample copy of this or any other Elsevier Science Publishers journal.
Advertisements. Advertisement rates are available from the publisher on request.

US mailing notice – Analytica Chimica Acta (ISSN 0003-2670) is published biweekly by Elsevier Science Publishers (Molenwerf 1, Postbus 211, 1000 AE Amsterdam). Annual subscription price in the USA US$ 2597.75 (subject to change), including air speed delivery. Second class postage paid at Jamaica, NY 11431. *USA Postmasters*: Send address changes to Anal. Chim. Acta, Publications Expediting, Inc., 200 Meacham Av., Elmont, NY 11003. Airfreight and mailing in the USA by Publication Expediting.

ANALYTICA CHIMICA ACTA

An international journal devoted to all branches of analytical chemistry

(Full texts are incorporated in CJELSEVIER, a file in the Chemical Journals Online database available on STN International; Abstracted, indexed in: Aluminum Abstracts; Anal. Abstr.; Biol. Abstr.; BIOSIS; Chem. Abstr.; Curr. Contents Phys. Chem. Earth Sci.; Engineered Materials Abstracts; Excerpta Medica; Index Med.; Life Sci.; Mass Spectrom. Bull.; Material Business Alerts; Metals Abstracts; Sci. Citation Index)

VOL. 280 NO. 2 CONTENTS AUGUST 16, 1993

(Continued overleaf)

Contents (continued)

Analytica Chimica Acta, 280 (1993) 179–184
Elsevier Science Publishers B.V., Amsterdam

Selective flow-injection determination of methanol in the presence of ethanol based on a multi-enzyme system with chemiluminescence detection

Yoshiie Sekine

Food Research Laboratory, Quality Assurance Department, Snow Brand Milk Products Co., Ltd., 1-1-2, Minamidai, Kawagoe-shi, Saitama 350 (Japan)

Masayasu Suzuki [1], Toshifumi Takeuchi, Eiichi Tamiya and Isao Karube

Research Centre for Advanced Science and Technology, University of Tokyo, 4-6-1, Komaba, Meguro-ku, Tokyo 153 (Japan)

(Received 19th October 1992; revised manuscript received 16th February 1993)

Abstract

A highly selective flow-injection system was developed for the determination of methanol. The system consisted of three immobilized enzymes with luminol chemiluminescence detection. First, methanol was oxidized in the presence of alcohol oxidase to yield formaldehyde and hydrogen peroxide. The hydrogen peroxide produced was then destroyed by catalase. The formaldehyde formed in the first stage was further oxidized by NAD^+–formaldehyde dehydrogenase. The NADH formed was oxidized by 1-methoxy-5-methylphenazinium methylsulphate (1-MPMS), and finally the reduced 1-MPMS was spontaneously oxidized and hydrogen peroxide was produced. The concentration of the hydrogen peroxide produced, which was proportional to the initial concentration of methanol, was determined by luminol chemiluminescence. The determination range was from 0.1 to 100 mg l^{-1} and the response time was less than 2 min per sample with a relative standard deviation of less than 3%. The system showed good selectivity for methanol; the response was ca. 50 times higher than for ethanol.

Keywords: Chemiluminescence; Enzymatic methods; Flow injection; Methanol

It is well known that central nervous system disorders, particularly optic disorders, may occur from ingestion or inhalation of methanol, hence the development of simple and sensitive methods for the detection of methanol is important. Several detection methods are currently employed for the detection of methanol as a contaminant in alcoholic beverages, wines and spirits, e.g., chromatographic, spectrophotometric and biochemical methods.

Gas chromatography has been widely used for this purpose, but it requires a long time (at least 30 min) for each sample. Near-infrared spectrometry using fibre optics has been applied for the detection of methanol [1]. This method is highly selective but the sensitivity is insufficient for determination at low concentration levels.

Correspondence to: Y. Sekine, Food Research Laboratory, Quality Assurance Department, Snow Brand Milk Products Co., Ltd., 1-1-2, Minamidai, Kawagoe-shi, Saitama 350 (Japan).

[1] Present address: Department of Biochemical Engineering and Science, Faculty of Computer Science and Systems Engineering, Kyusyu Institute of Technology, 680-4 Kawazu, Iizuka-shi, Fukuoka 820 (Japan).

Biological methods using microorganisms or enzymes have also been reported [2–7]. A microbial sensor consisting of an oxygen electrode covered with a membrane with immobilized microorganisms has been proposed [2]. However, this sensor may be difficult to handle, because the metabolic conditions of the immobilized microorganisms could be easily changed. In enzyme sensors for alcohols, alcohol oxidase (EC 1.1.3.13) (AOD) or alcohol dehydrogenase (EC 1.1.1.1) (ADH) is generally used [3–7]. For the detection of methanol, AOD is employed because ADH does not react with methanol. The selectivity of the methanol sensors depend totally on the substrate specificity of AOD and it appears that the sensor's selectivity for methanol is insufficient because of the low methanol selectivity of AOD. Recently, an enzyme sensor using methanol dehydrogenase (EC 1.1.99.8) (MDH) was reported [8]. However, the selectivity of this sensor for methanol was not high as the response for methanol of MDH is only twice that for ethanol.

In this study, a multi-enzyme system was employed for the detection of methanol in order to enhance selectivity, consisting of AOD, formaldehyde dehydrogenase (EC 1.2.1.1) (FDH) and catalase (EC 1.11.1.6) (Cat), and a flow-injection (FI) system was constructed with luminol chemiluminescence detection, involving en enzyme reactor with AOD, Cat and FDH, which are sequentially immobilized. The efficiency of the system was demonstrated on the determination of methanol; especially the selectivity for methanol was examined in the presence of a large excess of ethanol.

EXPERIMENTAL

Apparatus

A schematic diagram of the FI system is shown in Fig. 1. Two piston pumps (880-PU; Japan Spectroscopic, Tokyo) were used for the reaction reagent [50 mM phosphate buffer (pH 7.0) containing 30 mg l^{-1} 1-methoxy-5-methylphenazinium methylsulphate (1-MPMS), 5 mM EDTA and 200 μM NAD^+] and the chemiluminescence reagent [200 mM borate buffer (pH 9.5) containing 1 mg l^{-1} luminol and 5 mM EDTA]. The immobilized enzymes were packed into a stainless-steel column (30 mm × 2 mm i.d. × 1/8 in o.d.). Samples were injected through a sample injector with a 20-μl sample loop (Model 7125M; Rheodyne, Cotati, CA). Luminescence intensities were monitored by a chemiluminescence detector (825-CL; Japan Spectroscopic) with a single-channel chart recorder (Unicorder U-228; Nippon Denshi Kagaku, Kyoto).

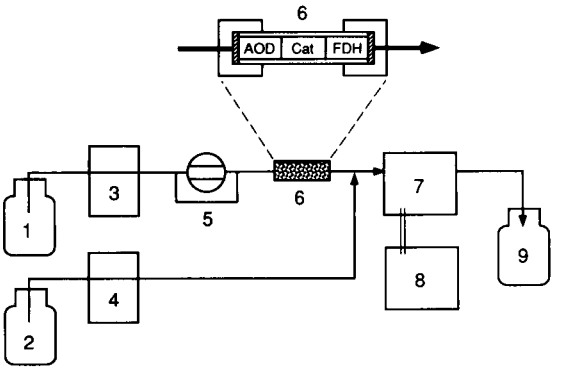

Fig. 1. Schematic diagram of the FI system: 1 = reaction reagent; 2 = chemiluminescence reagent; 3 = piston pump (flow-rate, 1.0 ml min^{-1}); 4 = piston pump (flow-rate, 1.5 ml min^{-1}); 5 = sample injector (sample size, 20 μl); 6 = immobilized enzyme column (30 mm × 2.0 mm i.d.); 7 = chemiluminescence detector; 8 = single-pen chart recorder; 9 = waste.

Reagent

Alcohol oxidase (AOD) (EC 1.1.3.13) from yeast and formaldehyde dehydrogenase (FDH) (EC 1.2.1.1) from *Pseudomonas* sp. were purchased from Toyobo (Tokyo). Catalase (Cat) (EC 1.11.1.6) from beef liver was purchased from Tokyo Kasei Kogyo (Tokyo). NAD^+ and 1-MPMS were purchased from Wako. All other reagents were of analytical-reagent grade and used as received.

Enzyme immobilization

AOD, Cat and FDH were covalently immobilized on commercially available controlled-pore glass beads (aminopropyl-CPG; particle size 200–400 mesh, mean pore diameter 500 Å; CPG Inc., Fairfield, NJ) by a conventional method [9].

Briefly, 0.2 g of aminopropyl-CPG was washed with 100 ml of distilled water on a glass-fibre filter and added to 10 ml of 2.5% glutaraldehyde solution. The mixture was gently stirred for 1 h at room temperature. The glutaraldehyde-treated CPG was washed with 100 ml of 50 mM phosphate buffer (pH 7.0) and then mixed with 3 ml of the same buffer containing 100 μl of AOD (ca. 5 mg of protein) and kept overnight at 4°C. After the immobilization, the CPG was washed sequentially with 250 ml of 50 mM phosphate buffer containing 0.5 M NaCl (pH 7.0) and 50 ml of 50 mM phosphate buffer (pH 7.0). This immobilized enzyme was stored at 4°C in 50 mM phosphate buffer (pH 7.0) containing 0.2% bovine serum albumin and 0.02% sodium azide. For the immobilization of Cat and FDH, 5 mg of each enzyme were dissolved in 3 ml of phosphate buffer and then mixed with the glutaraldehyde-treated CPG. The following procedure was the same as described for the immobilization of AOD.

Chemiluminescent assay for methanol

Each alcohol standard was prepared in 50 mM phosphate buffer (pH 7.0). The sample solutions were injected into the FI system and each determination was made by calculation from relative chemiluminescence intensity values which were measured as signal peak height on a chart recorder. A column packed with the immobilized AOD alone was prepared in order to examine the substrate specificity. In this experiment, 50 mM phosphate buffer (pH 7.0) containing 5 mM EDTA was used as the reaction reagent.

RESULTS AND DISCUSSION

Multi-enzyme reaction system in the FIA system

Figure 2 shows the principle of the enzymatic reaction system. In this system, methanol is oxidized to formaldehyde by AOD, followed by the further oxidation of formaldehyde by FDH with NAD^+ to yield formic acid and NADH. The NADH is oxidized by 1-MPMS and reduced 1-MPMS is produced. The reduced 1-MPMS is non-enzymatically oxidized and produces hydrogen peroxide [10], corresponding to the initial amount of methanol, which is finally determined by luminol chemiluminescence.

During the first oxidation process mediated by AOD, hydrogen peroxide was produced, which interfered with the determination of the hydrogen peroxide produced in the reduced 1-MPMS

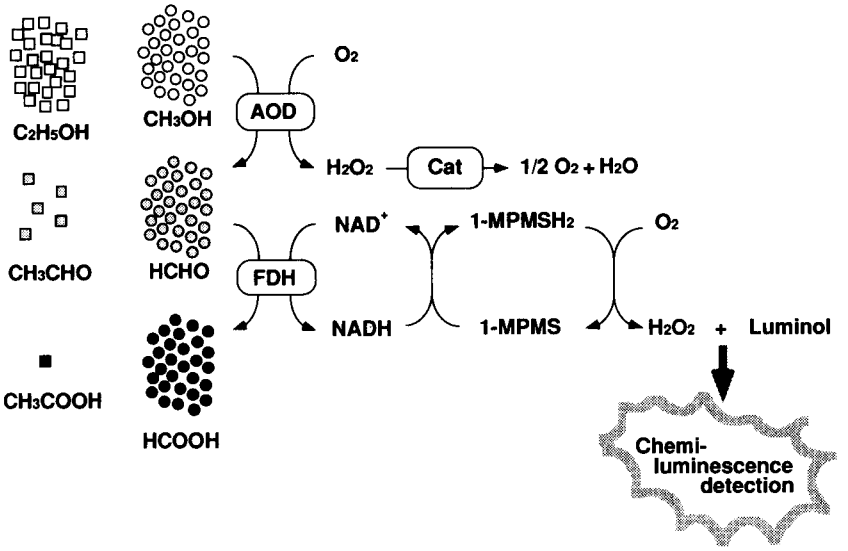

Fig. 2. Schematic diagram of the sequential reaction system for methanol. AOD, alcohol oxidase; FDH, formaldehyde dehydrogenase; Cat, catalase; 1-MPMS, 1-methoxy-5-methylphenazinium methylsulphate.

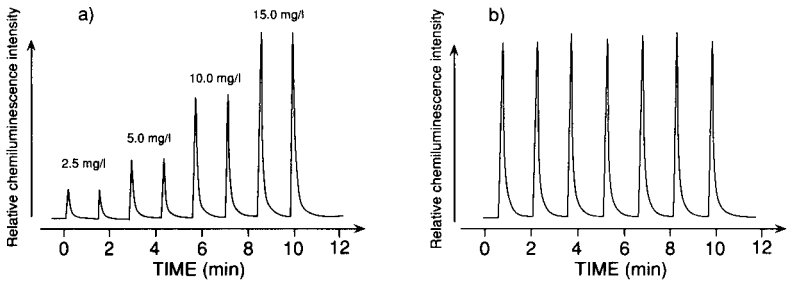

Fig. 3. Flow signals of the FI system for methanol. Responses for 2.5, 5.0, 10.0 and 15.0 mg l^{-1} methanol; repetitive determinations of 15.0 mg l^{-1} methanol.

oxidation step. In our system, Cat was employed to eliminate hydrogen peroxide produced by the AOD oxidation process. The immobilized AOD, Cat and FDH were packed into the column sequentially, and therefore hydrogen peroxide produced by the AOD oxidation was destroyed by the immobilized Cat and only the product, formaldehyde, could pass through this region.

This system is based on sequential enzyme reactions using AOD and FDH. AOD and FDH were used in order to enhance the selectivity for methanol. Because the amount of NADH produced by the FDH oxidation corresponds to the amount of formaldehyde formed by the AOD oxidation, the substrate specificity of both AOD and FDH governs the selectivity of the complete system, so the selectivity of the system for methanol is expected to be higher than that of mono-enzyme systems.

Response and calibration graphs for methanol

Figure 3 shows typical flow signals for methanol in the present system. In these experiments, each sample was analyzed within 2 min and a relative standard deviation (R.S.D.) of 1.9% was obtained at a concentration of 15.0 mg l^{-1} methanol ($n = 7$)

TABLE 1

Relative responses of the mono-enzyme and multi-enzyme systems to various alcohols

Substrate [a]	Relative sensitivity (%)	
	AOD	AOD/Cat/FDH
Methanol	100	100
Ethanol	9.1	1.8
Propanol	3.4	0.0
Butanol	3.4	0.0

[a] 10 mg l^{-1} alcohol.

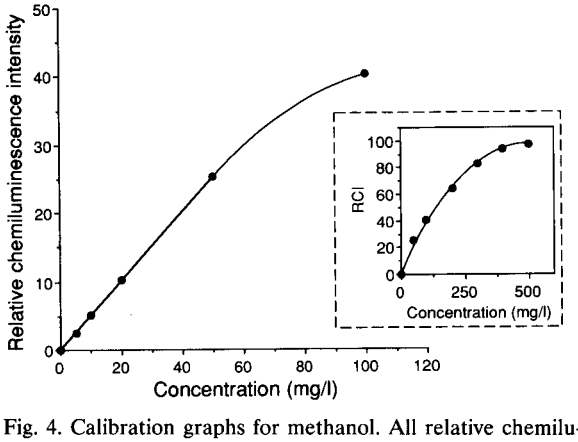

Fig. 4. Calibration graphs for methanol. All relative chemiluminescence intensities were calculated by measuring peak heights.

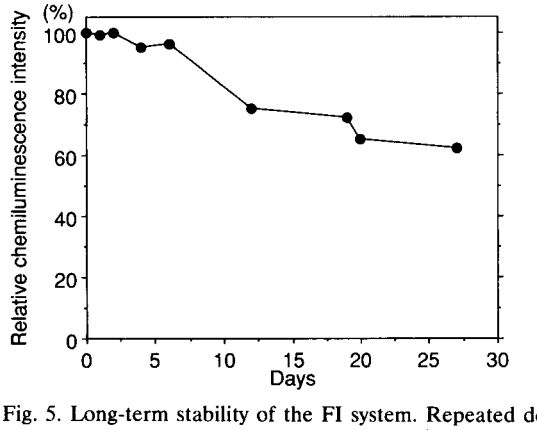

Fig. 5. Long-term stability of the FI system. Repeated determinations were carried out for 10 mg l^{-1} methanol. All relative chemiluminescence intensities were calculated based on the peak height of the initial determination as 100%.

and 2.2% ($n = 5$) at 100 mg l^{-1}. A linear calibration graph was obtained up to 50 mg l^{-1} with a saturation limit over 500 mg l^{-1} (Fig. 4). The detection limit was 0.1 mg l^{-1} for a signal-to-noise ratio of 5.

Table 1 indicates that the substrate selectivity of an AOD mono-enzyme system is less than that of the multi-enzyme system. It is clear that the selectivity in the multi-enzymate system is greater than that in the mono-enzymate system. The relative response for methanol over ethanol increased as a factor of 4 in the multi-enzyme system, and propanol and butanol did not respond in the present system. The specifications of enzymes given by each manufacturer indicated that the response of AOD for methanol is ca. ten times higher than that for ethanol and that of FDH for formaldehyde is ca. five times higher than that for acetaldehyde. These specifications were consistent with the present results as the selectivity of the present system for methanol can be estimated as a multiple of the selectivity of AOD and FDH, which is 50 times greater than that for ethanol.

Figure 5 shows the results for the repetitive determination of 10 mg l^{-1} methanol in order to examine the long-term stability of the system. They showed that the response to methanol was decreased by 60% of the initial value after 4 weeks. The reason for the decrease may be the inactivation of immobilized enzymes. Although the response decreased, the reproducibility had not significantly changed: 1.28% 1 day after immobilization, 1.62% after 6 days, 2.11% after 12 days, 1.30% after 20 days and 2.17% after 27 days ($n = 10$).

Determination of methanol in the presence of ethanol

Chemiluminescence intensities of 5 mg l^{-1} methanol (0.16 mM) were measured in the presence of 100–20 000 mg l^{-1} ethanol (Fig. 6a). The intensity rapidly decreased at ethanol concentrations above 1 g l^{-1}. Because the non-enzymatic oxidation of reduced 1-MPMS (Fig. 6b) and the FDH oxidation (Fig. 6c) were unaffected by the presence of ethanol, the decrease could be caused by the inhibition of the first step of the reaction scheme (Fig. 2), i.e., the AOD oxidation.

Although the chemiluminescence intensity derived from methanol decreased in the presence of large excess of ethanol, calibration graphs showed a linear relationship between methanol concentration and chemiluminescence intensity (Fig. 7). These results suggested that a linear calibration graph for methanol can be obtained at any given concentration of ethanol.

According to the Japanese Pharmacopoeia, the contamination of ethanolic medicines by methanol must be less than 0.2%. Because 1 mg l^{-1} methanol could be determined using the present system for samples containing 500, 1000 or 2500

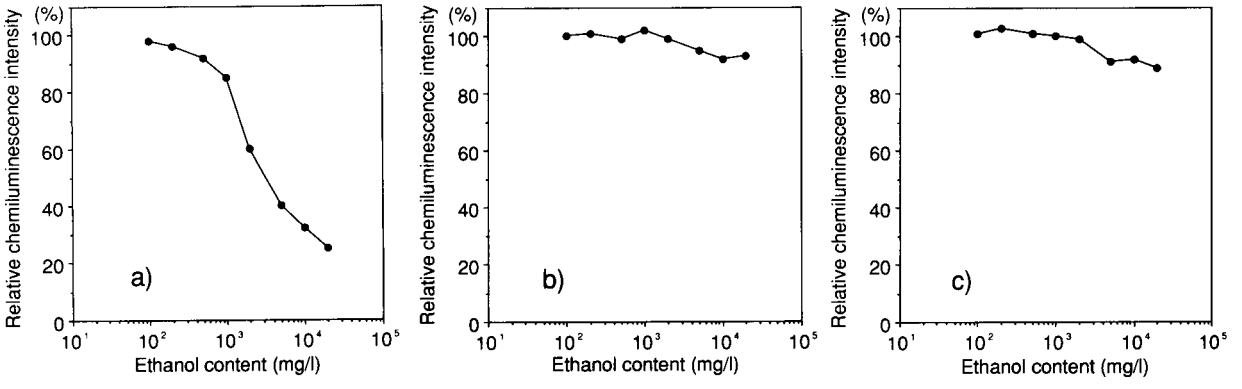

Fig. 6. Effect of ethanol on the methanol response for (a) the whole determination system, (b) the self-oxidation of 1-MPMS and (a) the FDH oxidation stage. The determinations were carried out using (a) 0.16 mM (5 mg l^{-1}) methanol, (b) 0.16 mM NADH and (c) 0.16 mM formaldehyde containing 100–20 000 mg l^{-1} ethanol. All relative chemiluminescence intensities were calculated as the percentage of the peak height measured for each ethanol-free substrate.

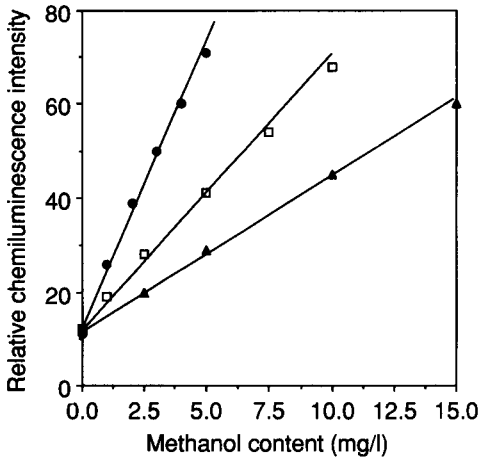

Fig. 7. Relationships between relative chemiluminescence intensity and methanol concentration in the presence of ethanol at concentrations of (●) 500, (□) 1000 and (▲) 2500 mg l^{-1}. Relative chemiluminescence intensities were calculated by measuring peak response heights. Regression equations and correlation coefficients were obtained as follows: 500 mg l^{-1} ethanol, $y = 13.33 + 11.80x$, $r = 0.994$; 1000 mg l^{-1} ethanol, $y = 13.17 + 5.499x$, $r = 0.999$; 2500 mg l^{-1} ethanol, $y = 12.31 + 3.214x$, $r = 0.999$ [y = relative chemiluminescence intensity; x = methanol concentration (mg l^{-1})].

mg l^{-1} ethanol (Fig. 7), the system could be used for quality control of not only alcoholic drinks and spirits but also pharmaceuticals.

Conclusion

In the proposed determination system, the selectivity for methanol was improved because of the combined use of three enzymes, AOD, Cat and FDH. The selectivity was 50 times greater than that for ethanol. The system was stable enough to operate for at least 4 weeks and, during this period, repeated assays showed high reproducibility with R.S.D.s less than 3%. The determination range was 0.1 and 100 mg l^{-1} and the response time was less than 2 min per sample. These features could be useful for monitoring methanol in routine quality control applications.

REFERENCES

1 B.R. Buchanan and D.E. Honigs, Appl. Spectrosc., 41 (1987) 1388.
2 M. Hikuma, T. Kubo and T. Yasuda, Biotechnol. Bioeng., 21 (1979) 1845.
3 G.G. Guilbault, B. Danielsson, C.F. Mandenius and K. Mosbach, Anal. Chem., 55 (1983) 1582.
4 J.A. Klavons and R.D. Bennett, J. Agric. Food Chem., 34 (1986) 597.
5 A. Maquieria, M.D. Luque de Castro and M. Valcarcel, Microchem. J., 26 (1987) 309.
6 V.J. Smith, R.A. Green and T.R. Hopkins, J. Assoc. Off. Anal. Chem., 72 (1989) 30.
7 Y. Kitagawa, K. Kitabatake, I. Kubo, E. Tamiya and I. Karube, Anal. Chim. Acta, 218 (1989) 61.
8 S. Zhao and R.B. Lennox, Anal. Chem., 63 (1991) 1174.
9 H.H. Weetall, Immobilized Enzymes, Antibodies and Peptides, Marcel Dekker, New York, 1975.
10 K. Tabe, T. Kawasaki, M. Maeda, A. Tuji and M. Yabuuchi, Bunseki Kagaku, 36 (1987) 82.

Analytica Chimica Acta, 280 (1993) 185–189
Elsevier Science Publishers B.V., Amsterdam

Chemiluminometric L-lysine determination with immobilized lysine oxidase by flow-injection analysis

F. Preuschoff and U. Spohn

Institute of Biotechnology, University of Halle (Saale), Weinbergweg 16a, D-O-4050 Halle (Germany)

E. Weber

Institute of Biochemistry, Medical Department of University of Halle (Saale), Hollystr. 1, D-O-4020 Halle (Germany)

K. Unverhau

Institute of Microbiology, University of Halle (Saale), Weinbergweg 16a, D-O-4050 Halle (Germany)

K.-H. Mohr

Institute of Biotechnology, University of Halle (Saale), Weinbergweg 16a, D-O-4050 Halle (Germany)

(Received 31st August 1992; revised manuscript received 11th February 1993)

Abstract

An enzymatic flow-injection procedure for the determination of L-lysine was developed. A lysine oxidase reactor is combined with a fibre-optic hydrogen peroxide detector. Hydrogen peroxide detection is based on the peroxidase-catalysed luminol reaction. The chemiluminescent light is detected by a photomultiplier. L-Lysine can be determined in the range 10–1000 μM. A sampling rate of up to 90 h^{-1} can be achieved. The whole sensing assay works for more than 1 month. The double logarithmic graph of the peak signal height vs. the lysine concentration is linear, the slope being larger than unity ($r^2 = 0.991$, $n = 4$).

Keywords: Chemiluminescence; Enzymatic methods; Flow injection; Lysine

L-Lysine is an essential amino acid for animal feed and human nutrition. It occurs as an important component in many animal proteins, but less in plant proteins. L-Lysine is added to human food, especially dietary products, and plays an important role as an additive to animal feed in cattle raising. It is also used in medicine for preparing infusion solutions. L-Lysine is also produced by fermentation. However, there is a lack of simple, specific methods for the rapid on-line monitoring of amino acids in technological processes.

Correspondence to: U. Spohn, Institute of Biotechnology, University of Halle (Saale), Weinbergweg 16a, D-O-4050 Halle (Germany).

Selective methods for L-lysine determination are based on enzymatic assays using lysine decarboxylase or, more recently, lysine oxidase (LOD). The employment of the Clark oxygen electrode and of gas-sensitive potentiometric carbon dioxide and ammonia sensors considerably improved the methods for the rapid determination of several amino acids [1–8]. Nakatani et al. [9] proposed the use of saccharopine dehydrogenase for the photometric detection of lysine. However, despite of the high substrate specificity of the assay, the dehydrogenase is strongly inhibited by leucine, isoleucine, valine and ornithine.

Romette et al. [10] described a lysine sensor based on a lysine oxidase membrane attached to a Clark electrode. Suzuki et al. [11] reported

investigations with a bacterial amperometric L-lysine miniature sensor with a detection limit of 25 μM. Weber and co-workers [12,13] isolated a highly stable lysine oxidase and investigated its use in an L-lysine sensor based on amperometric hydrogen peroxide detection. Pohlmann et al. [14] used immobilized lysine oxidase combined with photometric hydrogen peroxide detection in a flow-injection analysis (FIA) system. They observed good long-term stability of the enzyme reactor.

This paper describes a FIA procedure for the chemiluminometric determination of L-lysine. The L-lysine sample reacts according to the following equation:

$$\text{L-lysine} + O_2 + H_2O \xrightarrow{\text{LOD}} \alpha\text{-keto-}\epsilon\text{-aminocaproate} + NH_3 + H_2O_2$$

EXPERIMENTAL

Reagents

The enzyme L-lysine oxidase (L-lysine: O_2-oxidoreductase; EC 1.4.3.14) was isolated from culture extracts of *Trichoderma viride* i4 and purified as described elsewhere [13]. Microbial peroxidase from *Arthromyces ramosus* (EC 1.11.1.7; 60 U mg^{-1}) and luminol were purchased from Sigma (Deisenhofen, Germany). All chemicals were of analytical-reagent grade. Working standard solutions of L-lysine were prepared by successive dilution of a 10 mM stock standard solution with doubly distilled, deionized water immediately before the measurements. For the immobilization of the peroxidase a phosphate buffer solution was used containing 137 mM NaCl, 2.7 mM KCl, 8.0 mM Na_2HPO_4 and 1.5 mM KH_2PO_4.

Immobilization of lysine oxidase on glass particles

Immobilization was carried out according to Weetall and Filbert [16]. A 200-mg amount of aminosilylated Bioran (sieve fraction 190–200 μm) (Schott, Mainz, Germany) was activated with 2.5% (v/v) glutaraldehyde in 5 ml of 0.1 M potassium phosphate buffer (pH 6.5) for 1 h, the first 30 min being under a water-jet vacuum. After stirring the suspension for 30 min the activated carrier was filtered and washed with 200 ml of distilled water. A 5-mg amount of lysine oxidase and 15 mg of bovine serum albumin (BSA) (Boehringer, Mannheim, Germany) were dissolved in 1–2 ml of cold 0.1 M phosphate buffer (pH 6.5). Thereafter, the activated carrier was added. After 30 min under vacuum the reaction mixture was stored for 12 h at 4°C, then it was filtered and washed with 200 ml of cold phosphate buffer. Finally, the immobilized enzyme was packed into a Plexiglas tube (15 mm × 2 mm i.d.).

Membrane immobilization of peroxidase

A 7-mg amount of peroxidase was dissolved in 200 μl of phosphate buffer solution. An aliquot of this solution was dropped on to a rectangular sector of a commercially available membrane (Ultrabind; Gelman Sciences, Ann Arbor, MI), then the membrane was dried. The whole process was repeated three times.

Hydrogen peroxide sensor

The hydrogen peroxide sensor is described elsewhere [15]. Figure 1 shows a schematic diagram of the sensor, which is based on a flow-through cell with an integrated peroxidase membrane. A groove is formed by a PTFE spacer (0.5 or 1 mm thickness) with a rectangular slit (15 × 1 mm) providing a sensor with an effective measuring volume of only 7.5 or 15 μl. A transparent PVC foil separates the fibre bundle tip from the flow cell. The foil transmits ca. 80% of the chemiluminescent light.

Apparatus and procedure

Figure 2 shows a schematic diagram of the FIA set-up combined with the chemiluminometer. A FIAstar 5010 system (Perstorp Analytical, Höganäs, Sweden) was used with V-200 injection valve. Carrier and reagent solutions were propelled with two precision piston pumps (Dosimat 665; Metrohm, Herisau, Switzerland). The injection valve, both peristaltic pumps of the FIAstar 5010 and the piston pumps were controlled by

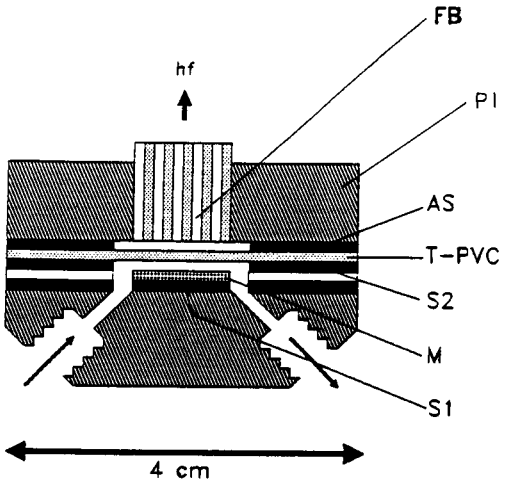

Fig. 1. Hydrogen peroxide sensor: hf = chemiluminescent light; FB = fibre bundle; PJ = light-tight PVC jacket; AS = aluminium spacer with a rectangular slit; T-PVC = transparent PVC foil; S1 and S2 = PTFE spacers; M = membrane with immobilized peroxidase.

means of a PC with a timer card. The sample solution was propelled by one of the peristaltic pumps.

The base of the flow cell is adapted geometrically to the rectangular end of a specially designed fibre-optic bundle (Model 77539, LOT, Darmstadt, Germany). The circular end of the fibre bundle was faced to a photomultiplier tube (PMT), (Model 77348, LOT) built into a light-tight housing (Model, 70680, LOT). The chemiluminescent light produced in the channel was conducted via the fibre bundle to the PMT, where the light was transformed into an analogue current signal.

The PMT was powered by a high-voltage power supply integrated in an Oriel 7070 detection system. The PMT voltage was maintained constant at 800 V (d.c.). The PMT signal was amplified and displayed by the Oriel 7070 detector. The output voltage was recorded by a TZ 4100 pen recorder (Laboratórnije Přístoje, Prague).

A 0.1 M potassium phosphate buffer solution (pH 7.4) and 0.677 mM luminol dissolved in 33 mM sodium carbonate (pH 10.4) were used as the carrier and reagent stream, respectively. The pH within the chemiluminometric flow cell was set to 8.5 by adjusting the flow-rates of the carrier and reagent stream. The total flow-rate through the sensor was set to 0.5 ml min^{-1}. L-Lysine standard solutions were prepared in the range 10 μM–1.5 mM. The sample injection volume was set at 40 μl.

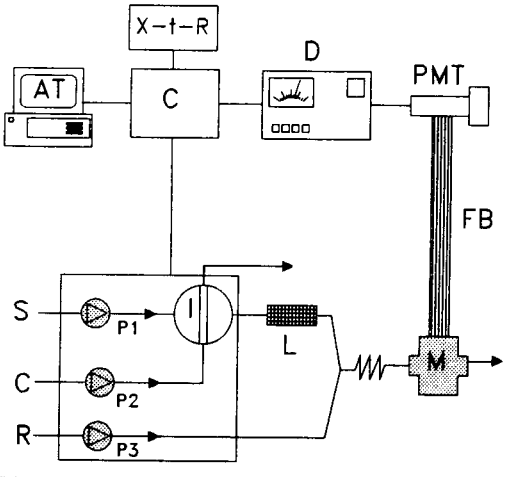

Fig. 2. FIA set-up for the chemiluminometric determination of L-lysine: C = 0.1 M phosphate buffer (pH 7.4); S = sample R = luminol reagent; P1–3 = pumps; I = injection valve; L = L-lysine α-oxidase reactor; M = hydrogen peroxide sensor; AT = personal computer; C = PC timer card; *X–t-R* = pen recorder; D = Oriel 7070 detector; PMT = photomultiplier; FB = fibre bundle.

RESULTS AND DISCUSSION

L-Lysine can be determined in the concentration range 10 μM–1 mM. A double logarithmic relationship between the peak height S in mV and the concentration c in μM was found:

$$\log S = (1.28 \pm 0.02) \log c + (2.49 \pm 0.02)$$

with $r^2 = 0.991$ ($n = 4$) for the 95% confidence interval.

The mean measuring time for one sample is given by the peak bases width, which was 30–50 s depending on the L-lysine concentration. Therefore, a sampling rate of up to 90 h^{-1} can be achieved. The detection limit was 5 μM L-lysine.

Figure 3 shows part of a measurement series. The relative signal stability is mainly influenced by the operational stability of the hydrogen peroxide sensor as shown in Fig. 4. To determine the stability of the enzyme reactor, the H_2O_2 sensor

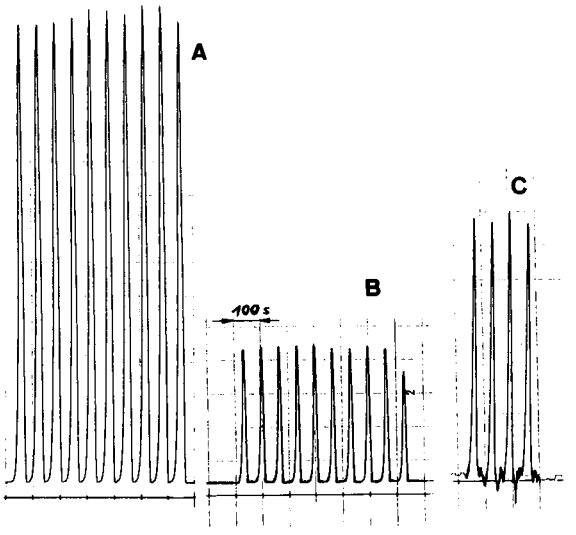

Fig. 3. Measured series of peak of L-lysine samples. Lysine concentrations and amplification factor, f: (A) 1 mM, $f = 10^7$; (B) 0.333 mM, $f = 10^7$; (C) 0.0333 mM, $f = 10^9$.

was calibrated with H_2O_2 standard solutions before each measurement. A 0.5 mM lysine solution was injected throughout the stability test. The measured H_2O_2 concentrations were standardized with respect to those measured at the beginning of the stability test, indicating a decrease in sensitivity of 12% after 2 months. In spite of the greater sensitivity decrease caused by the H_2O_2 sensor, the enzymatic FIA set-up worked for more than 1 month, exhibiting a good linear double

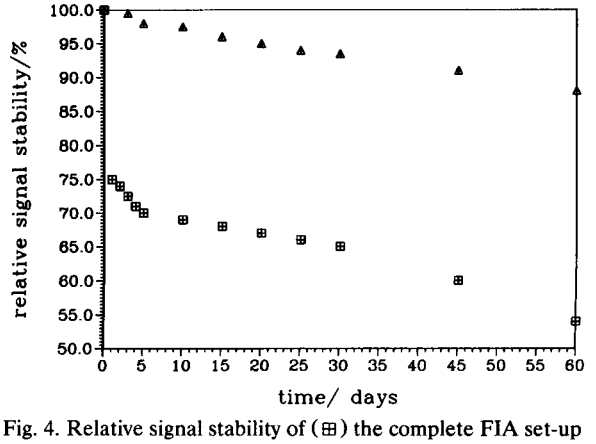

Fig. 4. Relative signal stability of (⊞) the complete FIA set-up in comparison with (△) the stability of the lysine oxidase reactor. Lysine concentration, 0.05 mM; amplification factor, $f = 10^7$.

TABLE 1

Influence of some amino acids and ascorbic acid on determination of lysine

Interferent	Limit of the concentration ratio (mM interferent/ 0.5 mM lysine)	Ratio $S_{\text{with interferent}} / S_{\text{without interferent}}$ (0.5 mM interferent/ 0.5 mM lysine)
Ascorbic acid	0.001	< 0.2
L-Ornithine	0.05	1.12
L-Histidine	1.5	1.01
L-Arginine	1.5	1.01
L-Glutamine	5.0	1.00
L-Glutamate	5.0	0.99

logarithmic correlation between peak height and lysine concentration.

Table 1 shows the influence of some amino acids and ascorbic acid on the determination of lysine. The interference by ornithine is significant. Ascorbic acid reacts rapidly with the enzymatically generated hydrogen peroxide causing decreased peak heights. Co(II), Fe(II) and Ni(II) ions in the μM and lower mM range cause an increase in the lysine peak signal because of their catalytic effect on the reaction of luminol with hydrogen peroxide. This effect can be suppressed by adding a 3–5-fold excess of ethylenediaminetetraacetate and depends on the lysine concentration.

The authors acknowledge financial support for this research from the Federal Ministry of Research and Technology, support index 0319658A.

REFERENCES

1 N.J. Vogel and Y. Shimura, Methods Enzymol., 17B (1971) 228.
2 J. Hutzler, M. Odievre and J. Dancis, Anal. Biochem., 19 (1967) 529.
3 Y. Nakatani, M. Fujioka and K. Higashino, Anal. Biochem., 49 (1972) 225.
4 E.F. Gale, in H.U. Bergmeyer (Ed.), Methods of Enzymatic Analysis, Vol. 4, VCH, Weinheim, and Academic Press, New York, 1974, p. 1662.
5 J. Hutzler, in H.U. Bergmeyer (Ed.), Methods of Enzymatic Analysis, Vol. 4, VCH, Weinheim, and Academic Press, New York, 1974, p. 1669.

6 S.L. Tong and G.A. Rechnitz, Anal. Lett., 9 (1976) 1.
7 K. Soda, T. Hirasawa and T. Fukumura, Anal. Biochem., 87 (1978) 283.
8 N.D. Tran, J.L. Romette and D. Thomas, Biotechnol. Bioeng., 25 (1983) 329.
9 Y. Nakatani, M. Fujioka and K. Higashino, Anal. Biochem., 49 (1972) 225.
10 J.L. Romette, J.S. Yang, H. Kusakabe and D. Thomas, Biotechnol. Bioeng., 25 (1983) 2557.
11 H. Suzuki, E. Tamiya and I. Karube, Anal. Chim. Acta, 229 (1990) 197.
12 E. Weber, K. Siegler, B. Weber, K. Tonder, K. Unverhau, H. Weide and H. Aurich, in F. Scheller and R.D. Schmid (Eds.), Biosensors: Fundamentals, Technologies and Applications (GBF Monographs, Vol. 17), VCH, Weinheim, 1992, p. 303.
13 E. Weber, K. Tonder, H. Aurich, K. Unverhau, H. Weide, K. Siegler and B. Weber, Bioengineering, (1993) in press.
14 A. Pohlmann, W.W. Stamm, H. Kusakabe and M.-R. Kula, Anal. Chim. Acta, 235 (1990) 329.
15 F. Preuschoff, U. Spohn, G. Blankenstein, K.-H. Mohr and M.-R. Kula, Fresenius' J. Anal. Chem., (1993) in press.
16 H.H. Weetall and A.M. Filbert, Methods Enzymol., 34 (1974) 59.

Analytica Chimica Acta, 280 (1993) 191–196
Elsevier Science Publishers B.V., Amsterdam

Immunoaffinity chromatographic method for the detection of pesticides

Boris B. Kim and Eugenii V. Vlasov

Chemistry Department, Lomonosov Moscow University, 199899 Moscow (Russian Federation)

Peter Miethe

Biotechnikum der Martin-Luther-Universität, D-O-4020 Halle (Germany)

Alexey M. Egorov

Chemistry Department, Lomonosov Moscow University, 199899 Moscow (Russian Federation)

(Received 26th October 1992)

Abstract

An immunoaffinity chromatographic (IC) method for the determination of 2,4-dichlorophenoxyacetic acid (2,4-D) and atrazine was developed. The sensitivity was 1 and 0.1 $\mu g\ l^{-1}$ for 2,4-D and atrazine, respectively, the relative standard deviation was in the range 3–8% and the total assay time per sample was 10 min. IC was combined with three detection systems: spectrophotometric, chemiluminescence and fluorescence. The whole procedure can be fully automated and applied to the quasi-continuous control of pesticide contamination and a rapid assay under out-of-laboratory conditions.

Keywords: Immunoassay; Liquid chromatography; Atrazine; Dichlorophenoxyacetic acid; Pesticides; Waters

During the last decade, enzyme immunoassay techniques have attracted growing interest as a method for pesticide analysis [1]. Immunoassays have the advantage of being less expensive, more sensitive and faster than conventional methods [2]. Their main drawback appears to be the relatively low specificity, which makes it impossible to distinguish between structurally related pesticides. For this reason, the immunoassay is mainly considered as a screening and quality assurance tool to be used before gas chromatography–mass spectrometry [3]. Several different formats for pesticide immunoassays have been developed: in microplates [4], in tubes [5], on magnetic particles [6] and flow-injection immunoassay (FIIA) using hydrophobic membranes as supports [7]. The first three variants require substantial manual work and FIIA suffers from relatively low reproducibility [7].

Immunoaffinity chromatography (IC) has been demonstrated to be a useful alternative to conventional immunoassay methods, combining the advantages of liquid chromatography and immunoanalysis [8,9]. The purpose of this work was to adopt this technique to the determination of pesticides in water samples.

Correspondence to: B.B. Kim, Chemistry Department, Lomonosov Moscow University, 199899 Moscow (Russian Federation).

EXPERIMENTAL

Chemicals, substrates for horseradish peroxidase (HRP), keyhole lymphet haemocyanin (KLH)

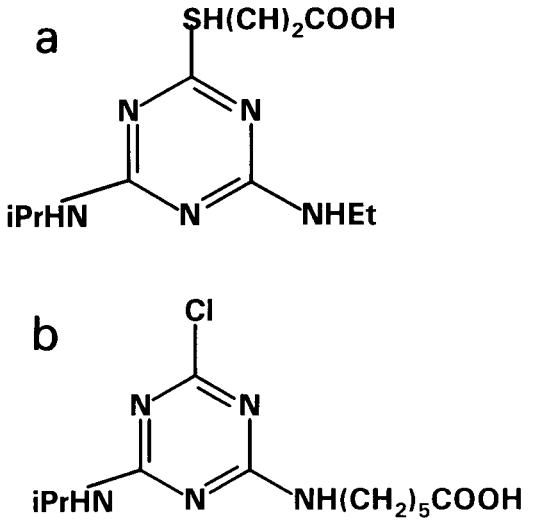

Fig. 1. Structures of (a) 3-({4-(ethylamino)-6-[(1-methylethyl)amino]-1,3,5-triazin-2-yl}thio)propanoic acid and (b) 6-({4-chloro-6-[(1-methylethyl)amino]-1,3,5-triazin-2-yl}amino) hexanoic acid.

and protein A were supplied by Sigma (St. Louis, MO). Atrazine and 2,4-dichlorophenoxyacetic acid (2,4-D) were purchased from Riedel-de Haën (Hannover, Germany) HRP (RZ 3.1) was obtained from Agrotecnika (Kiev, Ukraine). Acids and salts of analytical-reagent grade were supplied by Reakhim (Moscow). Luminol and *p*-iodophenol were recrystallized; the other reagents were used without further purification. All solutions were prepared with water purified with a Milli-Q system (Millipore, Bedford, MA).

Rabbit polyclonal antibodies against 2,4-D were obtained from Dr. Dzantiev (Bakh Institute for Biochemistry, Moscow). A conjugate of 2,4-D with HRP was prepared via the *N*-hydroxysuccinimide (NHS) ester [10]. Polyclonal antibodies against atrazine were raised in female New Zealand white rabbits. The conjugate for immunization was obtained by coupling of KLH with 3-({4-(ethylamino)-6-[(1-methylethyl)amino]-1,3,5-triazin-2-yl}thio)propanoic acid (Fig. 1a) via the NHS ester as described [11]. The hapten was synthesized [11] from atrazine and 3-mercaptopropanoic acid. To prepare the enzyme conjugate 6-({4-chloro-6-[(1-methylethyl)amino]-1,3,5-triazin-2-yl}amino)hexanoic acid (Fig. 1b) was used. It was obtained from 6-aminohexanoic acid and 4,6-dichloro-*N*-(1-methylethyl)-1,3,5-triazin-2-amine [11]. The procedure of conjugation was essentially the same as for the preparation of immunogen. The haptens were characterized by melting point and ^{1}H NMR measurements. NMR spectra were recorded with a Varian VRX-400 instrument at 400 MHz in DMSO-d_6. The hapten density of HRP conjugate was estimated by measuring ratios of absorbance at 263 and 403 nm, using the following molar absorptivities: $\epsilon_{263,1b} = 4160$ [11], $\epsilon_{403,HRP} = 1.02 \times 10^5$ [12], $\epsilon_{263,HRP} = 3.4 \times 10^4$ l mol^{-1} cm^{-1} (this work).

An ABICAP (antibody immuno column for analytical processes; Abion, Germany) was used as the main unit for IC. The column contains immobilized antibodies to IgG of different animals. The scheme of the assay used is based on a sequential competitive enzyme immunoassay procedure [13]. In the first step free hapten binds to a limited number of antibodies. The unbound antibodies are determined with a hapten–HRP conjugate in the second step. The routine protocol of the assay was as follows: apply 50 μl of rabbit antiserum; wait for 1.5 min; wash with 500 μl of phosphate-buffered saline supplemented with 0.05% Triton X-100 (PBST) twice; add 200 μl of standard solution; wait for 1.5 min; add 50 μl of conjugate solution; wait for 1.5 min; wash with 500 μl of PBST twice. All these steps may be done either manually or automatically using the ABION dispensing device.

The activity of enzyme label was measured by three methods: spectrophotometric, fluorescence and chemiluminescence. The substrate mixture for spectrophotometric detection contained 70 μM 3,3′,5,5′-tetramethylbenzidine (TMB) and 2 mM sodium perborate in phosphate–citrate buffer (pH 4.5). Two aliquots of 500 μl of the mixture were passed through the column. The outflow was collected and neutralized with 1 ml of 1 M H_2SO_4 and the absorbance of the solution was measured at 450 nm using an Abbot (North Chicago, USA) Quantum II spectrophotometer.

The substrate mixture for fluorescence detection contained 0.5 mM 3-*p*-hydroxyphenylpropionic acid (HPPA) and 2 mM sodium perborate in phosphate–citrate buffer (pH 4.0). Two aliquots

of 500 μl of the mixture were passed through the column. The outflow was collected and 500 μl of 1.5 M glycine buffer were added to increase the fluorescence efficiency of the product [14]. The fluorescence intensity was measured downstream using a Kontron spectrofluorimeter equipped with a flow-through cell, with a flow-rate of 1 ml min^{-1}, λ(ex) = 320 nm, λ(em) = 404 nm. Peak heights and areas were registered with a Merck–Hitachi D 2500 integrator.

An enhanced chemiluminescence reaction was used for chemiluminescence detection [15]. The IC procedure was performed in transparent columns in order to measure the activity of the HRP label directly. The substrate mixture contained 5×10^{-5} M luminol and *p*-iodophenol and 1 mM H_2O_2 in Tris–HCl buffer (pH 8.6). A 0.5-ml volume of substrate mixture was applied to the column. The column was then placed in the measuring chamber of a luminometer (LKB 1250) and maximum light intensity was recorded after 1 minute.

Enzyme-linked immunosorbent assay (ELISA) experiments were done as follows. Microplates (Nunc Immunoplates, MaxiSorp.) were coated at 4°C overnight with 300 μl of 10 μg ml^{-1} protein A solution. After washing three times with PBST 300 μl of antiserum to pesticide were added to each well of a microplate. After incubation for 2 h at room temperature and washing with PBST, standard (200 μl) and conjugate (50 μl) were added and incubated for 1 h. The wells were washed out and 200 μl of TMB substrate solution (see above) were added. After 15 min of incubation the reaction was stopped with 50 μl of 2 M H_2SO_4. The absorbance was measured at 450 nm (reference 650 nm) using a V_{max} reader (Molecular Devices, Palo Alto, CA). All standards were measured in quadruplicate.

The software package Softmax (Molecular Devices) was used for fitting the calibration graphs to a four-parameter equation:

$$B/B_0(\%) = [100 - B_{ex}/B_0(\%)]/[1 + (C/C_{50})^x] + B_{ex}/B_0(\%)$$

where C = concentration of analyte; B = concentration of bound tracer; B_0 = concentration of bound tracer at $C \to 0$; B_{ex} = concentration of bound tracer at $C \to \infty$; C_{50} = concentration of analyte at which 50% of tracer is bound to antibodies; and x = an empirical coefficient reflecting the slope of the plot at $C = C_{50}$.

Atrazine and 2,4-D working standard solutions were prepared from 1 mg ml^{-1} stock standard solutions in dimethyl sulphoxide.

RESULTS AND DISCUSSION

The properties of immunogen greatly affect the quality of antibodies obtained. The most crucial factors in immunogen design are the proper choice of the carrying protein, the hapten density and the mode of conjugation of hapten to a protein [1]. In this work KLH, which had been successfully applied to immunogen preparation [16], was used. This protein is highly immunogenic and is assumed to enhance an anti-hapten response via general stimulation of the immune system. Different types of spacer groups were used to synthesize the immunogen and tracer. This may help to avoid problems associated with antibodies directed to the spacer group rather than to the hapten itself. In some instances the use of heterological spacers improves the sensitivity of the assay [11].

Using a checkboard titration the best combination of antiserum and conjugate dilutions giving the highest sensitivity towards the analyte was found. The calibration graphs constructed using the optimum conditions are shown in Fig. 2. To facilitate a comparison the graphs are presented as $\%B/B_0$ plots. The sensitivity (as concentration of hapten at $B/B_0 = 90\%$) of the assay was 0.1 and 1 μg l^{-1} for atrazine and 2,4-D, respectively. EEC regulations stipulate a maximum allowable concentration of 0.1 μg l^{-1} for a single pesticide and 0.5 μg l^{-1} for the total pesticide contents [17]. For 2,4-D the maximum contaminant level is 70 μg l^{-1} as proposed by the US EPA [18]. The sensitivity of the assay depends mainly on the quality of antibodies and on fine matching within the antibody–tracer pair. Atrazine, for example, can be detected at concentrations as low as 1 ng l^{-1} [4]. The reproducibility of the assay expressed

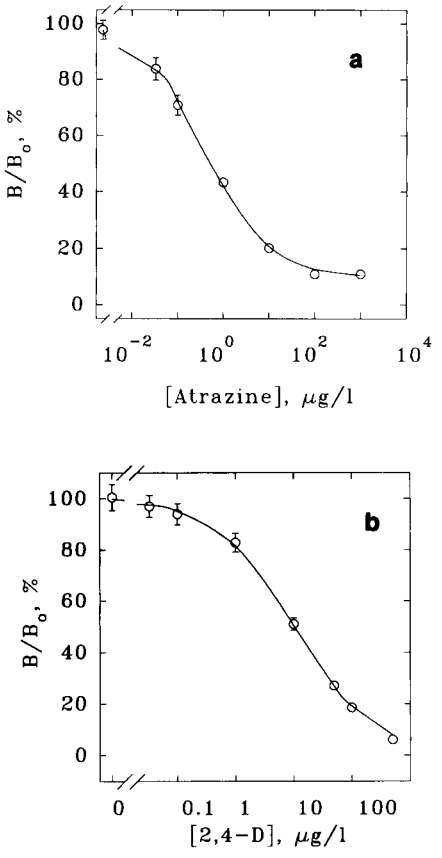

Fig. 2. Calibration graphs for (a) atrazine determination and (b) 2,4-D determination in ELISA.

as relative standard deviation (R.S.D.) was in the range 3–5% ($n = 7$). The performance characteristics of standard ELISA were then compared with those of affinity chromatography for the same antibody–tracer pair.

For IC the calibration graph consisted of four points: 0, 0.1, 1 and 10 $\mu g\ l^{-1}$ for atrazine and 0, 1, 10 and 100 $\mu g\ l^{-1}$ for 2,4-D. The results of the assays (as $\%B/B_0$) are shown in Figs. 3 and 4. All steps of the antigen–antibody interactions in this instance proceed in the kinetic, non-equilibrium mode. This allowed the incubation steps to be decreased to a few minutes. The main reason for such rapid kinetics is that beads provide many accessible surface sites on which antigen–antibody interaction takes place. Antigen and tracer rapidly diffuse into the particles where the diffusion path is much shorter than in a well of a

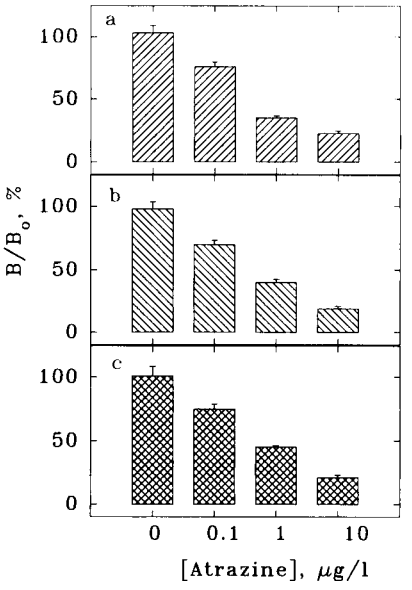

Fig. 3. Assay of atrazine by immunoaffinity chromatography using different detection systems: (a) spectrophotometric; (b) fluorescence; (c) chemiluminescence.

microplate. The overall time of assay was about 10 min per sample. All steps of the procedure, including detection, can be easily automated us-

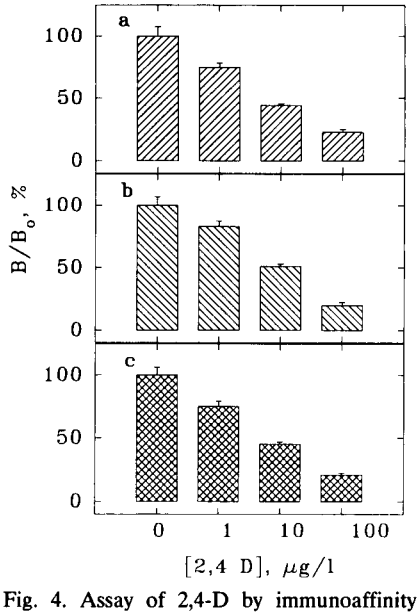

Fig. 4. Assay of 2,4-D by immunoaffinity chromatography using different detection systems: (a) spectrophotometric; (b) fluorescence; (c) chemiluminescence.

ing commercially available units for sample preparation for liquid chromatography and flow-through spectrophometric or fluorescence detection. In the automatic mode, several samples can be processed in parallel, which reduces the effective assay time per sample.

The sensitivity of IC was 0.1 and 1 $\mu g\ l^{-1}$ for atrazine and 2,4-D, respectively. The concentration ranges for both analytes are narrower than for ELISA. This usually occurs in sequential types of assays when the analyte and tracer are not competing for binding sites simultaneously [13].

The R.S.D. for all detection systems with affinity chromatography was in the range 3–8% (n = 7). This is higher than that with ELISA but less than that for FIIA of atrazine (20–40% at mid-concentration) [7]. Any non-equilibrium immunoassay scheme suffers from relatively low precision (compared with the equilibrium method). As the antigen–antibody reaction does not reach equilibrium, such procedures need careful time control. This requirement also limits the maximum number of samples that can be analysed simultaneously. The problem may be overcome by using a microprocessor-controlled dispensing unit. Up to 9 and 50 samples can be analysed in parallel using manual and automatic dispensing, respectively. The other possible sources of error are connected with column-to-column variations of flow-rate and sorption capacity of the gel. Experiments showed that these factors do not contribute significantly to the total error of assay with the ABICAP system.

The IC system can be easily combined with detection method widely used in enzyme immunoassay (spectrophotometric, fluorescence and chemiluminescence). Although they all give comparable results in terms of sensitivity and precision, each of them may be particularly suited for specific applications. Reaction with chromogenic dye, for example, may be used for visual control which can be performed without any device. This is especially important when the assay is carried out under out-of-laboratory conditions. Fluorescence detection allows the downstream determination of the product of enzymatic reactions. It may therefore be built into a fully automatic quasi-continuous system for the determination of

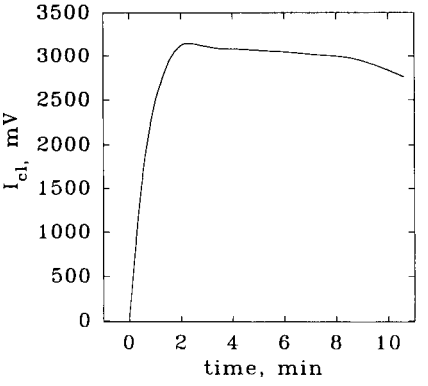

Fig. 5. Time course of the enhanced chemiluminescence reaction.

pesticides. Chemiluminescence detection seems to be the most sensitive. Another advantage of chemiluminescence reactions is the short detection time. The kinetic behaviour of the signal is shown in Fig. 5. The peak of the signal is observed 1–2 min after addition of substrate mixture. In fluorescence and spectrophotometric detection it is necessary to wait until sufficient dye has accumulated. To increase the incubation time a double portion of substrate mixture was added (see Experimental), but even then the maximum signal was not reached. Short detection times are of special importance for non-equilibrium types of immunoassays. Given a total time for all steps of antigen–antibody interaction of 5 min, a detection time of 5–15 min as required in conventional methods becomes inappropriate. Such direct techniques may benefit from switching to "faster" detection systems such as enhanced chemiluminescence reaction.

In IC the same volume and dilution of antibodies and conjugate as in ELISA were used. In FIIA reagent consumption is 10–100 times higher [7]. The flow-through construction of the main unit for IC allows variations of the sample volume over a wide range. This option can be used to adopt the sensitivity of the assay to the concentration of the analyte. When the concentration is low, a large volume of sample can be passed through the column to concentrate the analyte. Conversely, concentrated samples may be applied to the column in a very small volume, down to 1

μl. This option enables dilution steps, which are significant sources of error in ELISA to be avoided.

Previously, IC was mainly used with a sandwich scheme of immunoassays [9,19,20]. In that case a large excess of antibodies over the analyte helps its rapid capture. The possibility of applying the IC technique to competitive types of assays where the number of binding sites is limited was demonstrated.

In this work, an IC method for the determination of 2,4-D and atrazine was developed. The sensitivity of the assays was the same and the precision was slightly than with ELISA. The total assay time per sample was 10 min and may be further decreased in the automatic mode. IC is combined with different detection systems (spectrophotometric, chemiluminescence and fluorescence). The procedure can be easily adopted for quasi-continuous control of pesticide contamination. IC may well be used as a rapid assay under out-of-laboratory conditions.

B. Kim thanks the German Academic Exchange (DAAD) for a fellowship.

REFERENCES

1 J.M. Van Emon, J.N. Seiber and B.D. Hammock, in J. Sherma (Ed.), Analytical Methods for Pesticides and Plant Growth Regulators, Academic, San Diego, 1989, p. 217.
2 E.M. Thurman, M. Meyer, M. Pomes, C.A. Perry and A.P. Schwab, Anal. Chem., 62 (1990) 2043.
3 D.A. Goolsby, E.M. Thurman, M.L. Clark and M.L. Pomes, in M. Vanderlaan, L.H. Stanker, B.E. Watkins and D.W. Roberts (Eds.) Immunoassay for Trace Chemical Analysis. Monitoring Toxic Chemicals in Humans, Food, and the Environment, American Chemical Society, Washington, DC, 1991, p. 86.
4 C. Wittmann and B. Hock, Food Agric. Immunol., 1 (1989) 211.
5 R.J. Bushway, B. Perkins, S.A. Savage, S.J. Lekousi and B.S. Ferguson, Bull. Environ. Contam. Toxicol., 40 (1988) 647.
6 T.S. Lawruk, C.S. Hottenstein, C.E. Lachman, J.X. Dautlick, D.P. Herzog, M.R. Fernando and J.R. Fleeker, presented at the 105th AOAC Annual International Meeting and Exposition, Phoenix, Az, 1991.
7 P.M. Kramer and R.D. Schmid, Biosensor Bioelectron., 6 (1991) 239.
8 W.U. De Alwis and G.S. Wilson, Anal. Chem., 57 (1985) 2754.
9 D.S. Hage and P.C. Kao, Anal. Chem., 63 (1991) 586.
10 J.C. Hall, R.J.A. Deschamps and K.K. Krieg, J. Agric. Food Chem., 37 (1989) 981.
11 M.H. Goodrow, R.O. Harrison and B.D. Hammock, J. Agric. Food Chem., 38 (1990) 990.
12 J.E. Frew and P. Jones, Adv. Inorg. Bioinorg. Mech., 3 (1984) 175.
13 P. Tijssen, Practice and Theory and Enzyme Immunoassays, Elsevier, Amsterdam, 1985.
14 T. Tuuminen, P. Palomaki, A. Rakkolainen, M.-G. Welin, T. Weber and K. Kapyaho, J. Immunoassay, 12 (1991) 29.
15 T.P. Whitehead, G.H.G. Thorpe, T.J.N. Carter, C. Groucutt and L.J. Kricka, Nature, 305 (1983) 158.
16 A.E. Karu, O.R. Harrison, D.J. Schmidt, C.E. Clarkson, J. Grassman, M.H. Goodrow, A. Lucas, B.D. Hammock, J.M. Van Emon and R.J. White, in M. Vanderlaan, L.H. Stanker, B.E. Watkins and D.W. Roberts (Eds.), Immunoassay for Trace Chemical Analysis. Monitoring Toxic Chemicals in Humans, Food, and the Environment, American Chemical Society, Washington, DC, 1991, p. 59.
17 EEC Drinking Water Directive. Europäische Gemeinschaften. Richtlinie des Rates vom 15 Juli 1980 uber die Qualitat von Wasser für den menschlichen Gerbrauch (80/778/EWG). Armtsblatt der EG Nr. L 229 (30 August 1980), 1980, pp. 11–29.
18 US Environmental Protection Agency, Drinking Water Health Advisory: Pesticides, Lewis, Chelsea, MI, 1989.
19 N.B. Afeyan, N.F. Gordon and F.E. Regnier, Nature, 358 (1992) 603.
20 W. Stocklein, V. Jager and R.D. Schmid, Anal. Chim. Acta, 245 (191) 1.

Analytica Chimica Acta, 280 (1993) 197–208
Elsevier Science Publishers B.V., Amsterdam

Lipophilic and immobilized anionic additives in solvent polymeric membranes of cation-selective chemical sensors

Thomas Rosatzin, Eric Bakker, Koji Suzuki [1] and Wilhelm Simon [2]

Swiss Federal Institute of Technology (ETH), Department of Organic Chemistry, Universitätstrasse 16, CH-8092 Zürich (Switzerland)

(Received 5th January 1993; revised manuscript received 16th February 1993)

Abstract

Lipophilic borate salts are frequently used as anionic additives in potentiometric and optical cation-selective sensors based on solvent polymeric membranes. The lifetime of such membranes may be limited owing to chemical decomposition and leaching of the components. Borate salts, in particular, are decomposed in the presence of acids in the membrane. Adequately substituted borate salts and sulphonic acids, such as sodium tetrakis[3,5-bis(trifluoromethyl)phenyl]borate, sodium tetrakis[3,5-bis(2-methoxyhexafluoro-2-propyl)phenyl]borate and dinonylnaphthalenesulphonic acid (DNNS), are shown to be sufficiently stable as membrane additives. Furthermore, lipophilic mobile or immobilized sulphonic acids [DNNS or poly(2-acrylamido-2-methyl-1-propanesulphonic acid–co-styrene), respectively] were also tested as anionic additives. Their influence on the selectivity behaviour of the sensor is attributed to their strong association with positively charged species in the membrane phase. It may be kept small by choosing ionophores that form stable complexes with the analyte.

Keywords: Ion selective electrodes; Sensors; Membrane electrodes; Optodes; Solvent polymeric membranes

A large number of chemical sensors with potentiometric and optical transduction [ion-selective electrodes (ISEs) and optodes] based on solvent polymeric membranes have been described that require the addition of lipophilic salts for a good working performance (for reviews see [1–5]). As was seen, e.g., with cation-selective membranes containing an anionic polymer [6], such additives induce permselectivity.

Moreover, the presence of lipophilic anionic sites in cation-selective membrane electrodes proved to have a beneficial effect on various sensor parameters. In general, the ohmic resistance and detection limit are lower, with less interference from anions at high sample activities [7,8], the selectivity and response behaviour are improved [9,10] and, in cases where the ionophore has poor extraction capabilities, the sensitivity of the sensor is enhanced [2]. In addition, anionic sites may catalyse phase-transfer processes in cases when the kinetics at the sample/membrane interface are limited [11]. In analogy, salts of lipophilic cations are used as additives in anion-selective electrodes [12], mainly for neutralizing anionic impurities present in the membrane phase [13] and thereby inducing permselectivity for anions. Even though the influence of additives on the behaviour of anion-selective electrodes has not been investigated as thoroughly as in the case of cation-selective electrodes, analogous effects can be expected.

Correspondence to: E. Bakker, Swiss Federal Institute of Technology (ETH), Department of Organic Chemistry, Universitätstrasse 16, CH-8092 Zürich (Switzerland).

[1] On leave from Department of Applied Chemistry, Faculty of Science and Technology, Keio University, 3-14-1, Hiyoshi, Kohoku-ku, Yokohama 233 (Japan).

[2] Deceased, 17th November 1992.

For bulk optodes, the membrane must be in thermodynamic equilibrium with the sample, hence a mass transfer of analyte into the membrane is required [14]. In this case, an anionic additive is used in cation-selective optodes containing a neutral chromoionophore (ion-exchange system), while a cationic additive is incorporated in anion-selective optodes based on an charged chromoionophore (coextraction system).

In order to improve the lifetime of sensors based on solvent polymeric membranes, efforts have been focused on the lipophilicity of the neutral membrane components, such as ionophores [2], chromoionophores [15] and plasticizers [16], and little or no attention has been paid to the properties of the ionic additives. Just like all other components of the membrane phase, additives have a finite lifetime owing to their chemical decomposition and the leaching process. Therefore, various additives, such as borate salts [8,17], sulphonic acids [18,19] or dipicrylamine [20], and also anions or cations, covalently immobilized on a polymer matrix [6,21,22], have been investigated.

This paper reports on the use and stability of these anionic additives in the membrane phase and on their influence on the selectivity of cation-selective electrodes. Sulphonic acids were found to be chemically as stable as highly substituted borates in sensing membranes and can serve as anionic sites, even though they may influence the selectivity, presumably owing to strong ion-pair formation. Further, the selectivity coefficients are treated theoretically, taking into account the association of charged species in the membrane phase.

EXPERIMENTAL

Reagents

Aqueous solutions were prepared with doubly quartz-distilled water. Salts and solvents of the highest purity available were used.

Membrane components

Bis(2-ethylhexyl) sebacate (DOS), 2-nitrophenyl octyl ether (o-NPOE), poly(vinyl chloride) (PVC) (high molecular weight) and tetrahydrofuran (THF) (distilled prior to use) were Selectophore material from Fluka (Buchs, Switzerland).

Anionic additives. Sodium tetraphenylborate (NaTPB, **1**), potassium tetrakis(4-chlorophenyl)-borate (KTpClPB, **2**), sodium tetrakis[3,5-bis(trifluoromethyl)phenyl]borate (NaTFPB, **3**) and tetradodecylammonium tetrakis(4-chlorophenyl) borate (ETH 500) were Selectophore materials from Fluka; sodium tetrakis[3,5-bis(2-methoxyhexafluoro-2-propyl)phenyl]borate (NaHFPB, **4**) was kindly provided by Professor H. Kobayashi (Kyushu University, Fukuoka, Japan). Dinonylnaphthalenesulphonic acid (DNNS, **5**) was obtained from Pfaltz & Bauer (Waterbury, CT) as a 50% solution in kerosene, which was removed by distillation. Sodium dipicrylamine (**6**) was purchased from Dojindo Labs. (Kumamoto, Japan) and poly(2-acrylamido-2-methyl-1-propanesulphonic acid–co-styrene) (Polymer-SO_3H, **7**) from Janssen (Beerse, Belgium).

Ionophores. Dicyclohexyl-18-crown-6 and *N,N,N′,N′*-tetracyclohexyl-3-oxapentanediamide (ETH 129) (Selectophore) were obtained from Dojindo Labs. and Fluka, respectively. The syntheses of the remaining ligands have been described: 4-octadecylaminoazobenzene (ETH 5315) [23]; *N*-heptyl-*N,N′*-bis-(8-{[3-(heptylmethylamino)-1,3-dioxopropyl]amino}octyl)-*N*-methyl propanediamide (ETH 7025) [24]; *N,N′*-diheptyl-*N,N′*-dimethyl-3,6-dioxaoctanediamide (ETH 64); *N,N,N′,N′*-tetraoctyl-3,6-dioxaoctanediamide (ETH 1095) [25] and *N,N,N′,N′*-tetradodecyl-3,6-dioxaoctanediamide (ETH 5428) [23]. For determining the kinetic limitation (see Table 1), ETH 1095 was further purified by flash chromatography on silica gel [hexane–ethyl acetate (4:6)], obtaining a yellowish oil which, according to gel permeation and thin-layer chromatography, consisted of one compound only whose ^1H NMR spectrum was identical with that described [23]. Calculated for $C_{38}H_{76}N_2O_4$ (625.03), C 73.02, H 12.26, N 4.48; found, C 72.96, H 12.47, N 4.75%.

Optical measurements

Optode membranes contained 3.0 mg (1.2 wt.%) ETH 5315, 80 mg (32 wt.%) DOS and 160 mg (64 wt.%) PVC, and also either 4.6 mg (1.8

wt.%) NaTPB, 4.6 mg (1.8 wt.%) KTpClPB, 11.1 mg (4.2 wt.%) KTFPB, 11.0 mg (4.3 wt.%) NaHFPB, 6.1 mg (2.3 wt.%) DNNS or 4.7 mg (1.9 wt.%) sodium dipicrylamine. The components were dissolved in THF (8 ml g^{-1}). Two membranes of the same composition and ca. 2.0 μm thickness were prepared on two quartz plates (35 mm diameter) by means of a spin-on device (630 rpm) [26]. They were then mounted in a specially designed measuring cell [26] which was filled with 0.2 M HOAc. This solution was not replaced in order to minimize leaching effects. Absorption spectra were recorded between 650 and 350 nm at intervals of 1 h for optode membranes containing NaHFPB, KTFPB, DNNS or sodium dipicrylamine, and of 15 min for those with KTpClPB. With NaTPB, owing to its rapid decomposition, continuous recording at 515 nm was necessary. Finally, the spectrum of all membranes was taken after equilibration with 0.01 M NaOH in order to determine the baseline at complete deprotonation of the chromoionophore.

Potentiometric measurements

All electrochemical measurements were performed at 21 ± 1°C with cells of the type $Hg|Hg_2Cl_2|KCl$ (sat.)¦3 M KCl ¦¦sample ‖membrane ‖0.01 M $MCl_2|AgCl|Ag$ with a free-flowing free-diffusion liquid-junction calomel reference electrode [27]. For measurements with K^+-selective membranes, 1 M LiOAc was used as bridge electrolyte. Plasticized PVC membranes (for compositions, see Tables 1–4) of ca. 200 μm thickness were mounted in electrode bodies (IS-561; Philips, Eindhoven, Netherlands). All e.m.f. values were corrected for changes in the liquid-junction potential using the Henderson formalism, and single-ion activities were calculated according to Debye–Hückel [28]. Selectivity coefficients, log K^{pot}_{MJ}, were determined in unbuffered 0.1 M metal chloride solutions by the separate solution method (SSM) [29]. Resistance measurements were carried out as described [30].

Equipment

The measuring cell for optodes, whose temperature was kept at 22 ± 1°C [19], was placed in a UV–visible spectrophotometer (Uvikon 810; Kontron, Zürich, Switzerland) to record the absorption spectra of the membranes in the transmission mode. The equipment used for potentiometric measurements is specified elsewhere [10].

THEORY

Decomposition of tetraphenylborates

In recent years, different derivatives of tetraphenylborate salts (**1–4**, see Fig. 1) have been successfully used as anionic additives in solvent polymeric membranes of cation-selective electrodes and optodes (Fig. 1). Taking advantage of their ability to form lipophilic salts with different cations, these compounds originally served as agents in precipitation and liquid–liquid extraction processes of inorganic and organic cations in aqueous solutions [31,32].

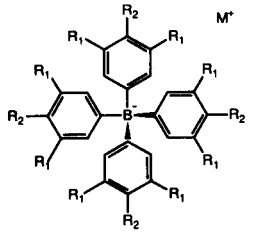

Additive (R^-)		R_1	R_2
TPB^-	1	H	H
$TpClPB^-$	2	H	Cl
$TFPB^-$	3	CF_3	H
$HFPB^-$	4	$C(CF_3)_2OCH_3$	H

1-4
Tetraphenylborate

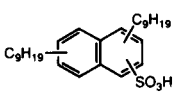

5
Dinonylnaphthalene-sulfonic acid (DNNS)

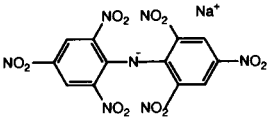

6
Sodium Dipicrylamine

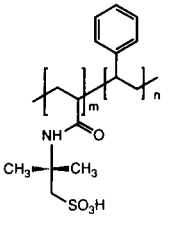

7
Poly(2-acrylamido-2-methyl-1-propane-sulfonic acid co-styrene) (Polymer - SO_3H)

Fig. 1. Constitutions of anionic additives.

However, the chemical stability of tetraphenylborate (TPB^-) is limited, especially in the presence of acids, oxidants and light, as the hydrogen ion probably attacks a phenyl substituent (Ph) [31]:

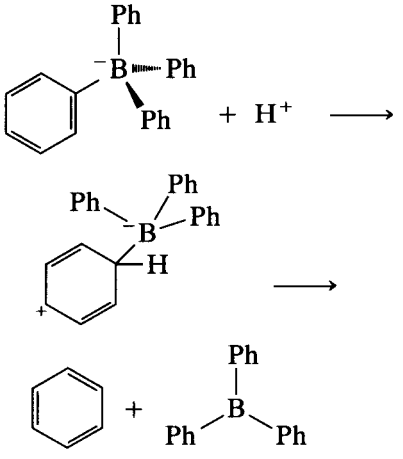

The decomposition of tetraphenylborate derivatives under acidic conditions is slowed by substituting the phenyl rings with electron-withdrawing groups in *para* or *meta* positions (**1–4**, see Fig. 1). Hence their chemical stability in protic media is increased [31,32]. Assuming that the mechanism of the decomposition of tetraphenylborate derivatives in organic membrane phases is similar to that in aqueous solvents, the rate of the decomposition reaction can be described as follows:

$$-d[R^-]/dt = k[R^-][H^+] \quad (1)$$

the rate of decomposition being determined by the concentrations of the borate, $[R^-]$, and of the so-called free hydrogen ion, $[H^+]$, in the organic phase (square brackets referring to concentrations).

With the help of optode membranes containing an anionic additive and a neutral chromoionophore (chromogenic pH indicator) with the acidity constant K_a, the chemical decomposition of the additive in the membrane environment was studied. According to the principle of electroneutrality, the content of anionic sites, $[R^-]$, can be directly correlated with the concentration of the protonated chromoionophore, $[CH^+]$, which, on decomposition of the anions, is subsequently deprotonated (Fig. 2).

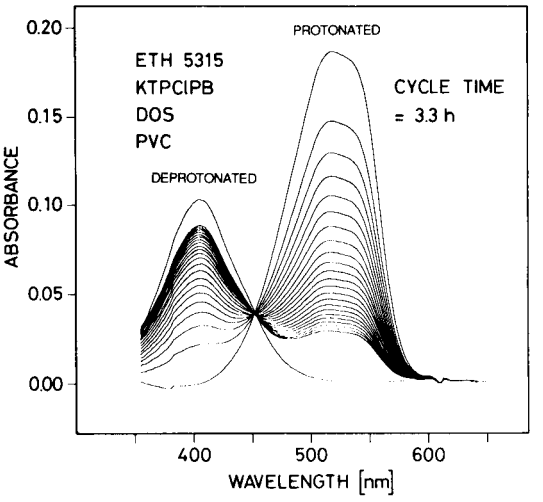

Fig. 2. Absorption spectra of solvent polymeric optode membranes [DOS–PVC (2+1)] with KTpClPB (**2**) and ETH 5315 [λ_{max} (prot.) = 520 nm, λ_{max} (deprot.) = 400 nm] in contact with 0.2 M HOAc for 72 h, evidencing the decomposition of the borate (see Theory). Recording cycle time = 3.3 h.

As $[H^+]$ is given by the basicity of the indicator, the rate of the decomposition reaction can be expressed as

$$-d[R^-]/dt = k[R^-]K_a([CH^+]/[C]) \quad (2)$$

Selectivity

When theoretically treating the selectivity of sensor membranes containing ionic additives, association between oppositely charged species is usually neglected [10,14]. The following theoretical description gives a general relationship for the selectivity coefficients of potentiometric sensors considering ion-pair formation within the organic membrane phase. Under specific assumptions, several equations for the selectivity coefficient, given in the literature [33], can be derived from this general formalism.

The following theoretical expressions are based on the model for cation-selective membranes [33] containing an electrically neutral ionophore (S) and an anionic additive (R^-). Selectivity coefficients are assumed to be determined by the separate solution method (SSM) [29], with only the primary ion, I, or the interfering ion, J, being present in the aqueous sample solution. For sim-

plicity, activities within the organic phase are assumed to be equal to concentrations, which is justified as long as the ionic strength in the membrane phase is small.

On the assumption that the diffusion potential within the membrane is constant, and primary ions I are present in the internal filling solution, the membrane potentials for I and J, E_i and E_j, are given by the boundary potentials:

$$E_i = E^0 + \frac{RT}{z_i F} \ln\left(\frac{a_i [\mathrm{I}]'}{[\mathrm{I}] a_i'}\right) \tag{3}$$

$$E_j = E^0 + \frac{RT}{z_i F} \ln\left\{K_{ij}\left(\frac{a_j}{[\mathrm{J}]}\right)^{z_i/z_j} \frac{[\mathrm{I}]'}{a_i'}\right\} \tag{4}$$

where K_{ij} is the ion-exchange constant for the uncomplexed ions between the aqueous and organic phases:

$$K_{ij} = \left(\frac{[\mathrm{J}]}{a_j}\right)^{z_i/z_j} \frac{a_i}{[\mathrm{I}]} \tag{5}$$

where a_i, a_j and a_i' refer to the activities of primary and interfering ions, I and J, in the aqueous sample solution and internal buffer solution, respectively, [I], [J] and [I]', [J]' are the concentrations of the uncomplexed ions in the organic phase boundary contacting the sample solution and the internal filling solution, respectively, z_i and z_j are the charges of the ions I and J and R, T and F have their usual meanings. All other potentials are assumed to be constant and are included in E^0. The selectivity coefficient, $\log K_{ij}^{\mathrm{pot}}$, for SSM measurements is defined as follows [34,35]:

$$\log K_{ij}^{\mathrm{pot}} = \frac{(E_j - E_i) z_i F}{2.303 RT} + \log a_i - \frac{z_i}{z_j} \cdot \log a_j \tag{6}$$

By inserting Eqns. 3 and 4 in Eqn. 6, the following fundamental equation is obtained:

$$\log K_{ij}^{\mathrm{pot}} = \log K_{ij} \cdot \frac{[\mathrm{I}]}{[\mathrm{J}]^{z_i/z_j}} \tag{7}$$

For simplicity reasons, all the following considerations are given for monovalent ions ($z_i = z_j = 1$), but analogous results are obtained for ions with higher valencies.

The concentration of the uncomplexed ions, I and J, in the organic boundary phase depends on the membrane composition. With the ionophore forming charged complexes, $[\mathrm{IS}_n^+]$ and $[\mathrm{JS}_m^+]$, with I and J, the corresponding stability constants are given by

$$\beta_{\mathrm{IS}} = \frac{[\mathrm{IS}_n^+]}{[\mathrm{I}^+][\mathrm{S}]^n} \tag{8}$$

and

$$\beta_{\mathrm{JS}} = \frac{[\mathrm{JS}_m^+]}{[\mathrm{J}^+][\mathrm{S}]^m} \tag{9}$$

The ion-pair formation in the membrane phase can be described by the respective association constants, K:

$$K_{\mathrm{RI}} = \frac{[\mathrm{RI}]}{[\mathrm{R}^-][\mathrm{I}^+]} \tag{10}$$

$$K_{\mathrm{RIS}} = \frac{[\mathrm{RIS}_n]}{[\mathrm{R}^-][\mathrm{IS}_n^+]} = \frac{[\mathrm{RIS}_n]}{[\mathrm{R}^-]\beta_{\mathrm{IS}}[\mathrm{I}^+][\mathrm{S}]^n} \tag{11}$$

$$K_{\mathrm{RJ}} = \frac{[\mathrm{RJ}]}{[\mathrm{R}^-][\mathrm{J}^+]} \tag{12}$$

$$K_{\mathrm{RJS}} = \frac{[\mathrm{RJS}_m]}{[\mathrm{R}^-][\mathrm{JS}_m^+]} = \frac{[\mathrm{RJS}_m]}{[\mathrm{R}^-]\beta_{\mathrm{JS}_m}[\mathrm{J}^+][\mathrm{S}]^m} \tag{13}$$

With the principle of electroneutrality, the mass balance for the total concentration of anionic sites, $[\mathrm{R}_{\mathrm{T}}^-]$, can be expressed as

$$[\mathrm{R}_{\mathrm{T}}^-] = [\mathrm{I}^+] + [\mathrm{IS}_n^+] + [\mathrm{RI}] + [\mathrm{RIS}_n] \tag{14}$$

or

$$[\mathrm{R}_{\mathrm{T}}^-] = [\mathrm{J}^+] + [\mathrm{JS}_m^+] + [\mathrm{RJ}] + [\mathrm{RJS}_m] \tag{15}$$

Combination of Eqn. 14 with Eqns. 8, 10 and 11 leads to

$$[\mathrm{I}^+] = \frac{[\mathrm{R}_{\mathrm{T}}^-]}{1 + \beta_{\mathrm{IS}}[\mathrm{S}]^n + K_{\mathrm{RI}}[\mathrm{R}^-] + K_{\mathrm{RIS}}\beta_{\mathrm{IS}}[\mathrm{S}]^n[\mathrm{R}^-]} \tag{16}$$

and of Eqn. 15 with Eqns. 9, 12 and 13 to

$$[\mathrm{J}^+] = \frac{[\mathrm{R}_{\mathrm{T}}^-]}{1 + \beta_{\mathrm{JS}}[\mathrm{S}]^m + K_{\mathrm{RJ}}[\mathrm{R}^-] + K_{\mathrm{RJS}}\beta_{\mathrm{JS}}[\mathrm{S}]^m[\mathrm{R}^-]} \tag{17}$$

With Eqns. 16 and 17, Eqn. 7 can be solved, giving the following general description for the selectivity coefficient:

$$K_{ij}^{pot} = K_{ij}\left(1 + \beta_{JS}[S]_j^m + K_{JR}[R^-]_j + K_{JSR}\beta_{JS}[S]_j^m[R^-]_j\right) / \left(1 + \beta_{IS}[S]_i^n + K_{IR}[R^-]_i + K_{ISR}\beta_{IS}[S]_i^n[R^-]_i\right) \quad (18)$$

the subscripts i and j designating aqueous solutions containing only I or J alone. For ligand-free membranes and complete dissociation of all ionic species, Eqn. 18 is reduced to

$$\log K_{ij}^{pot} = \log K_{ij} \quad (19)$$

If the complexes of the ionophore with the cations of the sample solution are highly stable ($\beta[S] \gg 1$) and of identical stoichiometry (i.e., $n = m$), and assuming that the concentrations of the uncomplexed ionophore, $[S]_i$ and $[S]_j$, are equal and complete dissociation of all ionic species ($[R^-]_i = [R^-]_j$), Eqn. 18 yields

$$\log K_{ij}^{pot} = \log K_{ij} \cdot \frac{\beta_{JS}}{\beta_{IS}} \quad (20)$$

In the case of very strong ion-pair formation, the selectivity coefficient can be approximated as

$$\log K_{ij}^{pot} = \log K_{ij} \cdot \frac{K_{RJ} + K_{RJS}\beta_{JS}[S]_j^m}{K_{RI} + K_{RIS}\beta_{IS}[S]_i^n} \quad (21)$$

Equation 21 reduces to Eqn. 20 if all association constants are equal and highly stable complexes ($\beta[S] \gg 1$) of equal stoichiometry are assumed. With tetraphenylborate salts in an apolar membrane phase [DOS–PVC (2 + 1)], it was shown experimentally that, in this instance, such a simplification is justified ($K_{RI} \approx K_{RIS}$ and $K_{RJ} \approx K_{RJS}$) [36]. However, if the association constants are not negligibly small, it must be assumed that $K_{RI} > K_{RIS}$ and $K_{RJ} > K_{RJS}$ because of higher charge densities for uncomplexed ions.

Figure 3 shows the selectivity coefficient as a function of the stability constant β. It is assumed that the primary ion forms more stable complexes than the interfering ion [$\log \beta_{JS} = (\log \beta_{IS}) - 4$], but all other characteristics are equal ($K_{ij} = 1, K_{RI} = K_{RIS}$ and $K_{RJ} = K_{RJS}$). In membranes containing ionophores with high complex stability, the ion pairs between uncomplexed sample ions and ionic sites have a smaller influence than

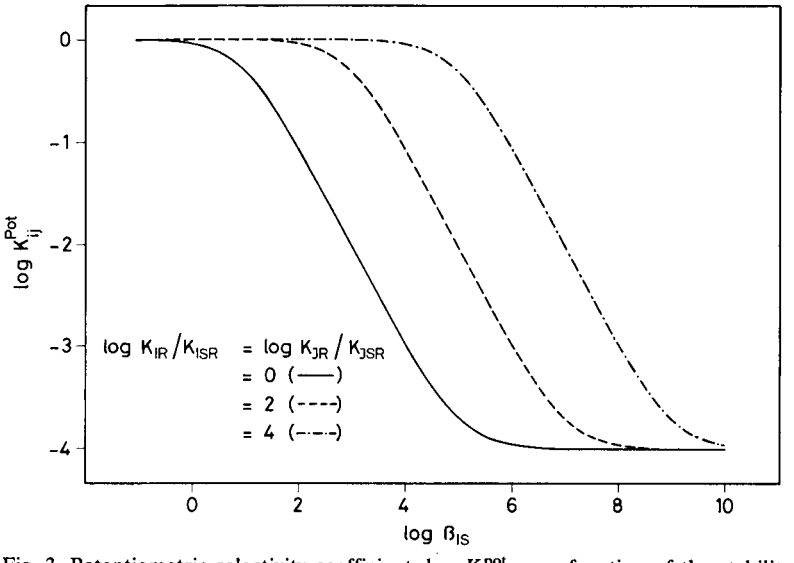

Fig. 3. Potentiometric selectivity coefficient, $\log K_{ij}^{pot}$, as a function of the stability constant, β_{IS}, of the primary ion–ionophore complex for different ratios of ion pair association constants, $\log(K_{RI}/K_{RIS}) = \log(K_{RJ}/K_{RJS})$, in the membrane phase, according to Eqn. 21, with $K_{ij} = 1$, [S] = 0.1 M and the complex stability constant for JS 10^4 times smaller than for IS [$\log \beta_{JS} = (\log \beta_{IS}) - 4$].

in membranes with weaker complexes. The selectivity coefficient consequently increases if the ratio of the association constants, K_{RI}/K_{RIS} and K_{RJ}/K_{RJs}, also increases. In consequence, a dependence of the selectivity of an electrode membrane on the complex stability of the ionophore can be expected as long as the association of charged species cannot be neglected.

RESULTS AND DISCUSSION

Stability of anionic additives

The chemical stability of tetraphenylborate (TPB) was found to be correlated with the basicity of the chromoionophore incorporated in the membrane phase (see Eqn. 2). TPB (**1**) decomposed $10^{3.6}$ times faster with 4-octadecylaminoazobenzene {ETH 5315; $pK_a = 3.6$ in MeOH and ≈ 5.2 in a PVC–DOS (2 + 1) membrane [15]} than with ETH 5292, which is $10^{3.3}$ times more basic [37]. The results on the chemical decomposition of different tetraphenylborate salts in optode membranes containing the acidic chromoionophore ETH 5315 are in agreement with previous findings in acidic aqueous media [31]. The decomposition rate was found to be unaffected by the pH of the sample solution as long as the chromoionophore in the membrane could be fully protonated. As can be seen from Fig. 4, the highly substituted borates sodium tetrakis[3,5-bis(trifluoromethyl)phenyl]borate (NaTFPB, **3**) and sodium tetrakis[3,5-bis(2-methoxyhexafluoro-2-propyl)phenyl]borate (NaHFPB, **4**) are much more stable in the membrane phase than the unsubstituted sodium tetraphenylborate (NaTPB, **1**) or the *p*-chloro-substituted analogue (KTpClPB, **2**). Surprisingly, dinonylnaphthalenesulphonic acid (DNNS, **5**) did not show an unlimited lifetime under the conditions chosen, which could be attributed to insufficient lipophilicity. Notwithstanding, the absorbance of membranes with DNNS proved to be nearly as stable as the borates **3** and **4**. Under the same conditions, the decomposition and/or leaching process of dipicrylamine (**6**) as additive could not be monitored because the degree of protonation of ETH 5315 was too low. Only a rapid decrease in absorbance was observed (not shown in Fig. 4), which was comparable to that for analogous membranes with KTpClPB (**2**).

If the lipophilicity of sulphonic acids is the limiting factor, a very long lifetime of such additives in membranes can probably only be achieved

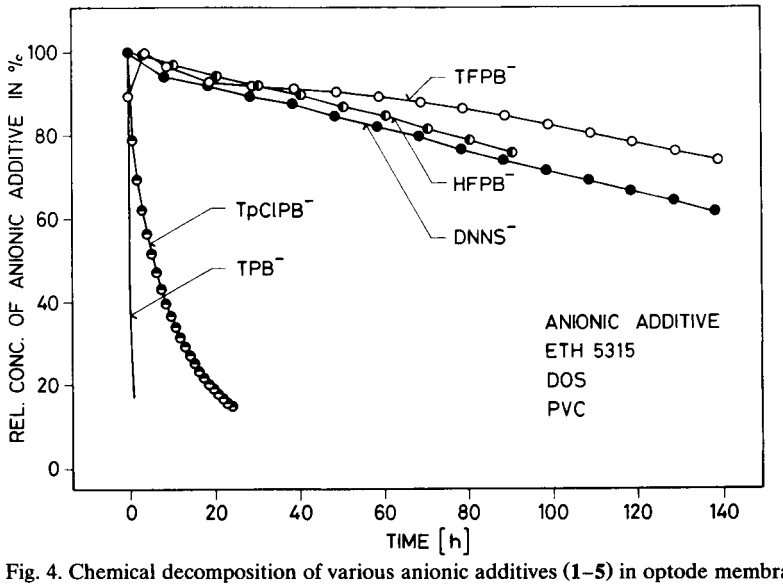

Fig. 4. Chemical decomposition of various anionic additives (**1–5**) in optode membranes [DOS–PVC (2 + 1), ETH 5315] exposed to 0.2 M HOAc, visualized by a loss of absorbance at 520 nm (see also Fig. 2).

TABLE 1

Potentiometric properties [a] of Ca^{2+}-selective membrane electrodes with different anionic additives [b]

Ligand	Additive	Slope (mV) [c]	Detection limit log a_i [d]	Resistance (MΩ)
None	None	ca. 0	–	23.5 ± 5.0
ETH 1095	None	ca. 0	–	2.2 ± 1.3
ETH 1095	KTpClPB	29.2 ± 0.5	−5.4	0.3 ± 0.1
ETH 1095	DNNS	29.1 ± 0.1	−5.0	$0.4 \pm 0.0_3$
ETH 1095	Polymer-SO_3H	30.1 ± 0.2	−5.4	1.2 ± 0.4
ETH 1095 [e]	None	28.0 ± 0.2	−5.5	4.4 ± 0.1
ETH 64	None	25.0 ± 1.4	−5.6	4.3 ± 0.9
ETH 64	KTpClPB	29.4 ± 0.1	−5.9	0.2 ± 0.1
ETH 64	DNNS	28.6 ± 0.1	−5.2	$0.3 \pm 0.0_2$
ETH 64	Polymer-SO_3H	29.4 ± 0.1	−5.7	$1.2 \pm 0.0_4$
ETH 5428	None	24.1 ± 0.6	−4.7 [c]	n.d. [f]

[a] Average of 3–6 values. [b] Membrane composition: 1 wt.% ligand, 73 mol% anionic additive (relative to ligand) in o-NPOE–PVC (2 + 1). [c] Calculated from linear regression between 10^{-1} and $10^{-5.2}$ M $CaCl_2$ ($s_{theor.}$ = 29.2 mV). [d] For linear regression between 10^{-1} and $10^{-6.2}$ M $CaCl_2$. [e] After extensive purification of the ligand (see Experimental). [f] Not determined.

by covalently immobilizing them on the polymer matrix. As an example, poly(2-acrylamido-2-methyl-1-propanesulphonic acid–co-styrene) (Polymer-SO_3H, **7**) was chosen, but its chemical stability in DOS–PVC (2 + 1) membranes could not be quantified because the spectra showed unstable baselines, probably owing to substantial water uptake and subsequent turbidity of the membrane.

Influence on cation-selective electrodes

General properties. The suitability of mobile and immobilized anionic additives was investigated for cation-selective electrodes containing four different Ca^{2+} or Mg^{2+} selective neutral ligands. As shown for the two Ca^{2+}-selective electrodes based on *N,N'*-diheptyl-*N,N'*-dimethyl-3,6-dioxaoctanediamide (ETH 64) and *N,N,N',N'*-tetraoctyl-3,6-dioxaoctanediamide (ETH 1095), the substitution of the borate salt KTpClPB (**2**) by the sulphonate DNNS (**5**) does not affect the general properties of the electrode such as slope, anion interference, detection limit and electrical resistance (Table 1). Further, the use of immobilized anionic additives such as Polymer-SO_3H (**7**) did not cause drastic changes in

TABLE 2

Calibration functions and selectivity coefficients of Ca^{2+}-selective electrodes with mobile (KTpClPB) and immobilized anionic additive (Polymer-SO_3H) after 55 days in running tap water (200 ml min^{-1}) [a]

Anionic additive	1 day [b]		55 days [c]										Decrease in slope [f]
	Slope [d] (mV)	Detection limit log(a_{Ca}/M)	Slope [d] (mV)	Detection limit log(a_{Ca}/M)	Log K^{pot}_{CaJ} [e]								
					Li^+	Na^+	K^+	NH_4^+	Rb^+	Cs^+	Mg^{2+}	Sr^{2+}	Ba^{2+}	
KTpClPB	29.8 ± 0.4	−5.5	28.4 ± 0.3	−5.0	−3.2	−3.1	−3.1	−3.2	−3.0	−3.2	−3.9	−1.0	−2.8	4.6%
Polymer-SO_3H	29.3 ± 0.6	−5.5	28.7 ± 0.1	−5.1	−3.5	−3.5	−3.6	−3.5	−3.1	−3.6	−3.9	−1.1	−2.8	2.1%

[a] All membranes contained ETH 129 (1 wt.%) and anionic additive (46 mol% relative to ligand) in o-NPOE–PVC (2 + 1). [b] After conditioning during 24 h in 0.01 M $CaCl_2$. [c] In running tap water (200 ml min^{-1}). [d] Calculated from the calibration function between $10^{-4.2}$ and 10^{-2} M $CaCl_2$ ($s_{theor.}$ = 29.2 mV). [e] All selectivity coefficients were determined in 0.1 M unbuffered solutions of the metal chloride salt (separate solution method). [f] Calculated from the change of slope between the 1st and 55th days.

these properties. However, a slightly higher electrical resistance was observed in comparison with the membranes with mobile additives, obviously influenced by the lack of mobility of the additive or its ion pairs in the membrane phase.

Similar effects were observed for the Ca^{2+}-selective ligand *N,N,N',N'*-tetracyclohexyl-3-oxapentanediamide (ETH 129), where the use of immobilized anionic additives even tends to improve the long-term behaviour with respect to electrode slope, detection limit and selectivities (see Table 2).

Again, Polymer-SO_3H (**7**) proved to be a suitable anionic additive in electrodes with the Mg^{2+}-selective ligand *N*-heptyl-*N,N'*-bis-(8-{[3-(heptylmethylamino)-1,3-dioxopropyl]amino}octyl)-*N*-methylpropanediamide (ETH 7025), which showed no response to $MgCl_2$ samples in the absence of sites (see Fig. 5). As pointed out by Perry et al. [6], the permselectivity of a cation-selective membrane can be induced by incorporating immobilized anionic sites.

Kinetic limitation. As reported previously [11], Ca^{2+}-selective electrodes based on the symmetrically substituted ligand ETH 1095 without additive exhibited no response. This lack of response was eliminated by incorporating anionic additives in the membrane. This effect was explained by a kinetic limitation of the ion transfer process between the aqueous sample and the organic phase. A more thorough study on this ionophore now revealed that the phenomenon had been due to an impurity and was not caused by the symmetrical constitution of this ligand (Table 1). Nevertheless, the possibility of kinetic limitations at the interface between the sample and membrane caused by the constitution of the ligand should, in principle, not be excluded. Membrane electrodes with an ionophore carrying even longer alkyl chains, such as *N,N,N',N'*-tetradodecyl-3,6-dioxaoctanediamide (ETH 5428), clearly give a reduced slope of the calibration function (Table 1).

Selectivity. In the theoretical considerations above, the contribution of diffusion processes was omitted. Therefore, the selectivity should be given by the phase-transfer equilibrium and be independent of the mobility of the ionic species in the membrane phase. By comparing membranes with sites of different mobility, the suitability of this assumption was investigated.

As shown in Fig. 6, different anionic additives influence the selectivity behaviour of membranes based on the neutral Ca^{2+} ionophore ETH 1095. While the addition of KTpClPB (**2**) induces a Nernstian slope and a distinct selectivity for Ca^{2+} (see also Table 1), the latter is significantly reduced in the presence of sulphonic acids. This effect seemed to be the same with both the mobile form (**6**) and the immobilized form (**7**). The loss of selectivity can be understood from the

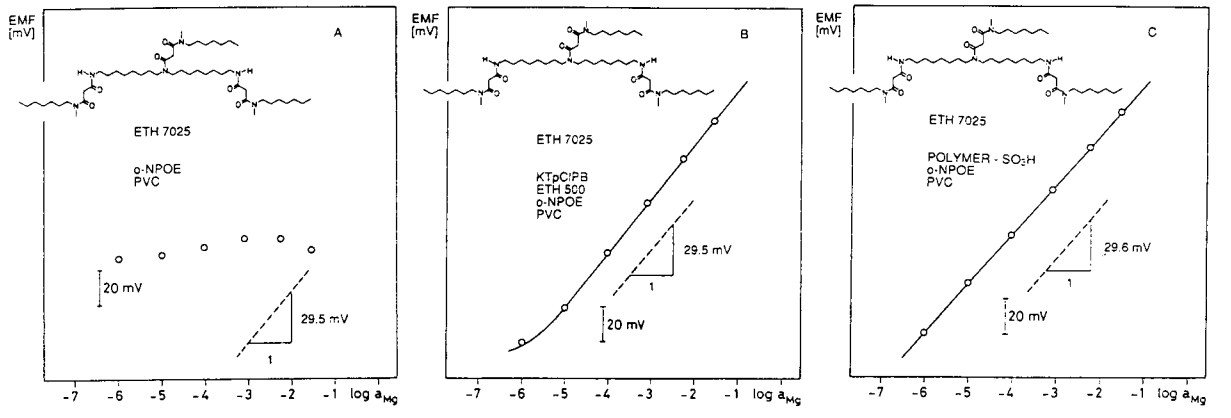

Fig. 5. E.m.f. response of Mg^{2+}-selective membrane electrodes based on o-NPOE–PVC (2 + 1). (A) Without additives, 1.0 wt.% ETH 7025; (B) KTpClPB (**2**) (155 mol% relative to ETH 7025), 3.5 wt.% ETH 500 and 3.0 wt.% ETH 7025 (composition optimized for physiological applications [24]); (C) with immobilized sulphonic acid [Polymer-SO_3H (**7**)] (155 mol% relative to ETH 7025) and 1 wt.% ETH 7025.

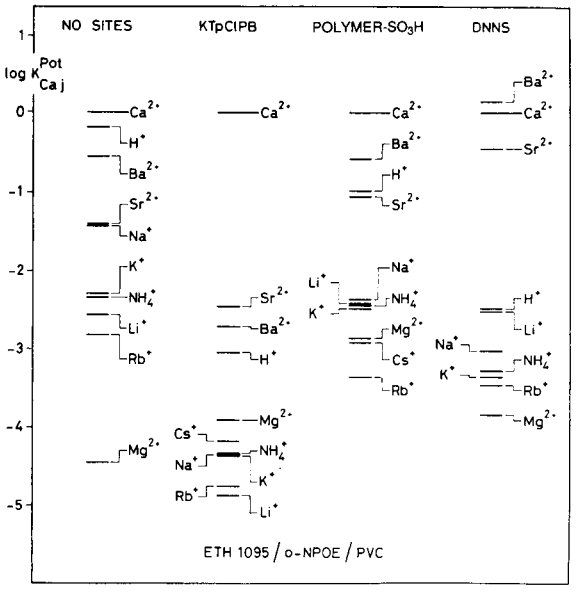

Fig. 6. Selectivity coefficients, log K^{pot}_{CaJ}, for solvent polymeric membranes containing ETH 1095 (1 wt.%) and different anionic additives (73 mol% relative to the ionophore) in o-NPOE–PVC (2 + 1).

differences in the association constants between borate or sulphonate and the positively charged species in the membrane phase. This interpretation is supported by the fact that immobilization of the sulphonic acid additive influences the selectivity behaviour only slightly (Fig. 6).

The complex stability constant, β, of the neutral ionophore may, however, contribute to the selectivity of such membranes (see Theory). Recent studies revealed that the Mg^{2+}-selective carrier ETH 7025 forms much weaker complexes than the Ca^{2+}-selective ionophore ETH 129 [38]. Accordingly, the addition of sulphonic acid completely eliminates the Mg^{2+} selectivity observed with membranes containing ETH 7025 and KTpClPB (2) (Fig. 7). On the other hand, membrane electrodes based on ETH 129 exhibited virtually the same selectivities with different sites (Fig. 8). A careful evaluation of the ligand is therefore important for the practical application of these additives.

By choosing the ratio of anionic additive to neutral ligand, the selectivity for a divalent primary ion, I^{2+}, against a monovalent interfering

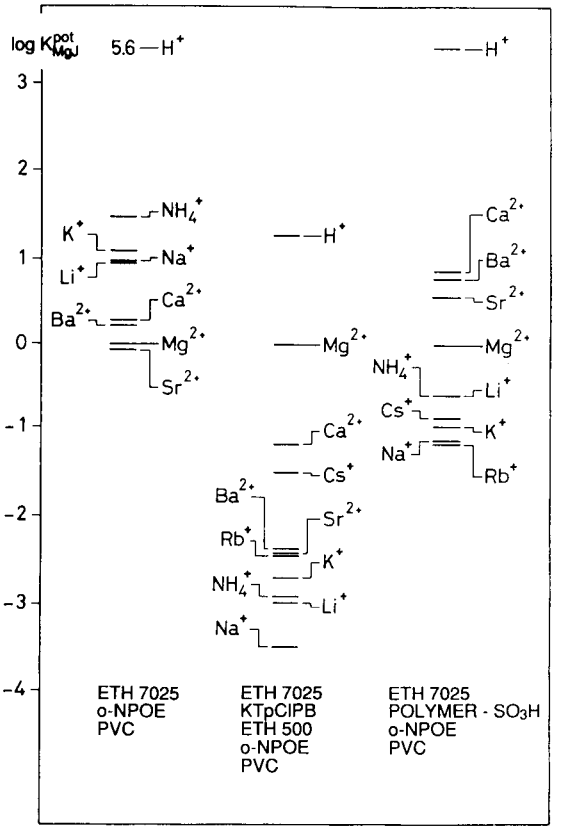

Fig. 7. Selectivity coefficients, log K^{pot}_{MgJ}, for solvent polymeric membranes containing ETH 7025 and different anionic additives (for membrane composition, see Fig. 5).

TABLE 3

Selectivity coefficients, log K^{pot}_{KM}, of K^+-selective membrane electrodes in relation to their ligand-to-additive ratio [a]

M [b]	Log K^{pot}_{Km}				
	KTpClPB (mol%) [c]				Without ligand [d]
	20	40	60	100	
Li^+	−2.7	−2.7	−2.2	−1.7	−0.6
Na^+	−1.3	−1.2	−1.2	−0.8	−0.5
NH_4^+	−0.7	−0.7	−0.7	−0.3	−0.1
Rb^+	−0.5	−0.5	−0.5	0	0
Cs^+	−1.2	−1.2	−1.0	−0.2	0.1
Mg^{2+}	−4.6	−4.3	−4.3	−2.4	−2.4
Ca^{2+}	−3.8	−3.5	−2.9	−1.7	−3.1
Sr^{2+}	−3.6	−3.3	−2.5	−1.5	−3.4
Ba^{2+}	−3.5	−3.3	−2.4	−1.6	−3.5

[a] All membranes contained 2 wt.% dicyclohexyl-18-crown-6, KTpClPB as anionic additive in DOS–PVC (2+1). [b] All selectivity coefficients were determined in 0.1 M unbuffered solutions of the respective metal chloride (SSM). [c] Relative to the ligand. [d] Ligand-free cation-exchange membrane.

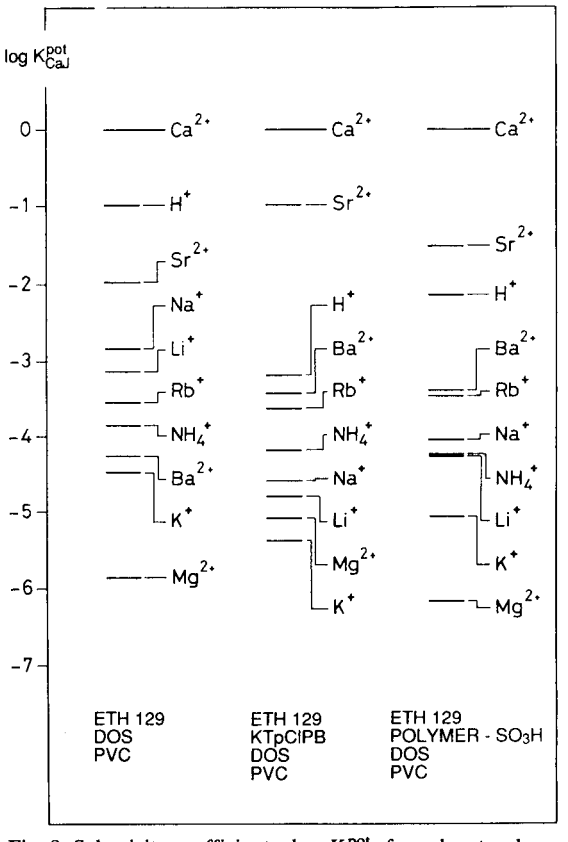

Fig. 8. Selectivity coefficients, log K^{pot}_{CaJ}, for solvent polymeric membranes containing ETH 129 (1 wt.%) and different anionic additives (56 mol% relative to the ionophore) in DOS–PVC (2+1).

TABLE 4

Selectivity coefficients, log K^{pot}_{KM}, of K^+-selective membrane electrodes in relation to their ligand-to-additive ratio [a]

M [b]	Log K^{pot}_{KM}				
	Polymer-SO_3H (mol%) [c]				Without ligand [d]
	20	40	60	100	
Li^+	−2.0	−2.2	−2.3	−2.1	−0.7
Na^+	−1.1	−1.2	−1.3	−1.3	−0.5
NH_4^+	−0.5	−0.5	−0.6	−0.5	0.1
Rb^+	−0.4	−0.4	−0.4	−0.4	0
Cs^+	−0.9	−0.9	−1.1	−1.0	0.2
Mg^{2+}	−2.3	−2.5	−2.6	−1.9	−1.7
Ca^{2+}	−2.4	−2.4	−2.4	−2.1	−2.0
Sr^{2+}	−2.4	−2.3	−2.6	−2.0	−1.6
Ba^{2+}	−2.1	−2.1	−2.3	−2.0	−1.4

[a] All membranes contained 2 wt.% dicyclohexyl-18-crown-6, Polymer-SO_3H as anionic additive in DOS–PVC (2+1). [b–d] See Table 3.

ion, J^+, can be optimized. The exact ratio can be calculated theoretically and depends on the ion charges and stoichiometries of the ion–ligand complexes [10]. As expected, for membrane electrodes with 18-crown-6 and KTpClPB (**2**), the selectivities of K^+ against divalent cations depend on the ratio of additive to ligand (Table 3). This was not observed with the corresponding membranes containing an immobilized sulphonic acid (**7**) (Table 4). The K^+ selectivity of these membranes against divalent ions is reduced in comparison, with membranes with KTpClPB (**2**) and is hardly influenced by the ligand-to-additive ratio (Table 4). Obviously, divalent ions are even better stabilized by the ionic additive than by the carrier. Similar effects were observed with Mg^{2+}-selective electrodes based on the ionophore ETH 7025 (data not shown).

Conclusions

Under acidic conditions, the stability of different borate salts in solvent polymeric membranes is shown to be seriously limited in the presence of weakly basic or acidic substances. However, highly substituted borates, e.g., NaTFPB (**3**) or NaHFPB (**4**), and the sulphonic acid DNNS (**5**) show a sufficiently long lifetime. In cases where the concentration of anionic additive in the membrane phase is crucial for the sensor performance, chemically stable additives such as NaTFPB (**3**), NaHFPB (**4**) or DNNS (**5**) should be used.

In cation-selective solvent polymeric membranes, mobile [DNNS (**5**)] or immobilized sulphonic acids [Polymer-SO_3H (**7**)] can be used as anionic additives. Owing to strong association with positively charged species in the membrane phase, they both influence the selectivity behaviour. The synthesis of sulphonic acids with their negative charge being delocalized and the association hindered by appropriate substitution could provide a new class of stable anionic additives for cation-selective sensor.

Part of this work was supported by the Swiss National Science Foundation and Ciba Corning Diagnostics. Thanks are due to D. Rüegg and B. Rusterholz for the synthesis and purification of some of the compounds and to Professor Dr. E.

Pretsch and especially to Dr. D. Wegmann for careful reading of the manuscript. We gratefully keep in mind the many fruitful discussions with the late Professor Dr. W. Simon and his generous support of our work.

REFERENCES

1 J. Koryta, Anal. Chim. Acta, 233 (1990) 1.
2 D. Ammann, W.E. Morf, P. Anker, P.C. Meier, E. Pretsch and W. Simon, Ion-Sel. Electrode Rev., 5 (1983) 3.
3 R.L. Solsky, Anal. Chem., 62 (1990) 21R.
4 W.R. Seitz, Anal. Chem., 56 (1984) 16A.
5 O.S. Wolfbeis, Anal. Chim. Acta, 250 (1991) 181.
6 M. Perry, E. Löbel and R. Bloch, J. Membr. Sci., 1 (1976) 223.
7 D. Ammann, E. Pretsch, W. Simon, E. Lindner, A. Bezegh and E. Pungor, Anal. Chim. Acta, 171 (1985) 119.
8 W.E. Morf, G. Kahr and W. Simon, Anal. Lett., 7 (1974) 9.
9 M. Huser, P.M. Gehrig, W.E. Morf, W. Simon, E. Lindner, J. Jeney, K. Tóth and E. Pungor, Anal. Chem., 63 (1991) 1380.
10 R. Eugster, P.M. Gehrig, W.E. Morf, U. Spichiger and W. Simon, Anal. Chem., 63 (1991) 2285.
11 P.M. Gehrig, W.E. Morf, M. Welti, E. Pretsch and W. Simon, Helv. Chim. Acta, 73 (1990) 203.
12 M. Rothmaier and W. Simon, Anal. Chim. Acta, 271 (1993) 135.
13 A. van den Berg, P.D. van der Wal, M. Skowrońska-Ptasińska, E.J.R. Sudhölter, D.N. Reinhoudt and P. Bergveld, Anal. Chem., 59 (1987) 2827.
14 W.E. Morf, K. Seiler, P. Sørensen and W. Simon, in E. Pungor (Ed.), Ion-Selective Electrodes, Vol. 5, Akadémiai Kiadó, Budapest, 1989, p. 141.
15 E. Bakker, M. Lerchi, Th. Rosatzin, B. Rusterholz, and W. Simon, Anal. Chim. Acta, 278 (1993) 211.
16 R. Eugster, Th. Rosatzin, A. Schmid, B. Rusterholz, D. Rüegg, B. Aebersold, U. Pedrazza, U.E. Spichiger and W. Simon, in preparation.
17 G.H. Zhang, T. Imato, Y. Asano, T. Sonoda, H. Kobayashi and N. Ishibashi, Anal. Chem., 62 (1990) 1644.
18 J.B. Harrell, A.D. Jones and G.R. Choppin, Anal. Chem., 41 (1969) 1459.
19 Ch.R. Martin and H. Freiser, Anal. Chem., 52 (1980) 562.
20 K. Kimura, T. Miura, M. Matsuo and T. Shono, Anal. Chem., 62 (1990) 1510.
21 Th. Rosatzin, P. Holý, K. Seiler, B. Rusterholz and W. Simon, Anal. Chem., 64 (1992) 2029.
22 M.-J. Rocheleau and W.C. Purdy, Analyst, 117 (1992) 177.
23 M. Lerchi, E. Bakker, B. Rusterholz and W. Simon, Anal. Chem., 64 (1992) 1534.
24 R. Eugster, B. Rusterholz, A. Schmid, U.E. Spichiger and W. Simon, Clin. Chem., in press.
25 R. Bissig, U. Oesch, E. Pretsch, W.E. Morf and W. Simon, Helv. Chim. Acta, 61 (1978) 1531.
26 K. Seiler, Ionenselektive Optodenmembranen, Fluka, Buchs, 1991.
27 R.E. Dohner, D. Wegmann, W.E. Morf and W. Simon, Anal. Chem., 58 (1986) 2585.
28 P.C. Meier, Anal. Chim. Acta, 136 (1982) 363.
29 G.G. Guilbault, R.A. Durst, M.S. Frant, H. Freiser, E.H. Hansen, T.S. Light, E. Pungor, G. Rechnitz, N.M. Rice, T.J. Rohm, W. Simon and J.D.R. Thomas, Pure Appl. Chem., 48 (1976) 127.
30 U. Oesch and W. Simon, Anal. Chem., 52 (1980) 692.
31 M. Meisters, J.T. Vandeberg, F.P. Cassaretto, H. Posvic and C.E. Moore, Anal. Chim. Acta, 49 (1970) 481.
32 H. Nishida, N. Takada, M. Yoshimura, T. Sonoda and H. Kobayashi, Bull. Chem. Soc. Jpn., 75 (1984) 2600.
33 W.E. Morf, The Principles of Ion-Selective Electrodes and of Membrane Transport, Akadémiai Kiadó, Budapest, 1981.
34 B.P. Nicolskij, Zh. Fiz. Khim., 10 (1937) 495.
35 G. Eisenman (Ed.), Glass Electrodes for Hydrogen and Other Cations, Dekker, New York, 1967.
36 R.P. Armstrong and G. Horvai, Electrochim. Acta, 35 (1990) 1.
37 E. Bakker, PhD Thesis, ETH, Zürich, in preparation.
38 E. Bakker, M. Willer, M. Lerchi and E. Pretsch, in preparation.

Analytica Chimica Acta, 280 (1993) 209–216
Elsevier Science Publishers B.V., Amsterdam

Behaviour of series piezoelectric sensor in electrolyte solution

Part II. Applications in titrimetry

Da-Zhong Shen, Zhi-Yong Li, Li-Hua Nie and Shou-Zhuo Yao
New Materials Research Institute, Hunan University, Changsha 410082 (China)

(Received 23rd June 1992; revised manuscript received 20th January 1993)

Abstract

The applications of a series piezoelectric sensor for end-point determination in frequencimetric titrations, including neutralization, precipitation, complexation and redox titrations, are reported. The method is based on the fact that a series piezoelectric sensor shows a sensitive and selective frequency response to changes in conductivity of solution and can be applied to sample solutions containing large amounts of unreacted foreign electrolytes.

Keywords: Piezoelectric sensors; Titrimetry; Frequencimetric titration

Piezoelectric quartz crystals (PQCs) have been mostly used in analytical chemistry as gas-phase microgravimetric sensors. More recently, increasing attention has been paid to operations and applications of PQCs exposed to the liquid phase [1,2]. Deakin and Buttry [3,4] reviewed the applications of the quartz crystal "microbalance" in electrochemistry and Thompson et al. [5] reviewed thickness shear mode acoustic wave sensors in the liquid phase. Usually, piezoelectric devices are used as a "microbalance" in chemistry owing to the extremely sensitive nature of PQCs towards mass changes at the surface of the electrode. In addition to the mass effect, the frequency of PQCs is affected by liquid properties such as conductivity, density, viscosity and permittivity [6–8]. Frequencimetric tritrations based on the frequency response of a PQC to the conductivity of solution have been reported previously [9–13]. Frequencimetric method offers the advantage over classical conductimetric titration that it can be applied to sample solutions containing unreacted foreign electrolytes at concentrations is much higher than that of the analyte. The use of PQC has shortcomings as any variation in the conditions of the crystal, such as interfacial structure and surface free energy [14], roughness and porosity [15], electrodeposition [16], adsorption [17] and corrosion, and the viscoelastic properties of liquid phase would change the frequency.

In Part I [18], the frequency characteristics of a series piezoelectric quartz crystal (SPQC) in electrolyte solutions were investigated. Because the crystal is out of contact with solution, the conditions of the crystal are independent of the properties of solution, and the frequency of the SPQC depends only on the permittivity and conductivity of the solution. Additionally, the frequency stability of the SPQC is much better than that of normal PQCs operating in the liquid phase because the power dissipation arising from the radi-

Correspondence to: Shou-Zhuo Yao, New Materials Research Institute, Hunan University, Changsha 410082 (China).

ation of a shear wave into the media by the oscillating PQC surface in the SPQC is much less than that in normal PQCs in the liquid phase. The lifetime of the crystal is greatly prolonged. In this paper, an improved frequencimetric titration method with a sensitive and selective frequency response of the SPQC to conductivity is reported.

EXPERIMENTAL

Apparatus and reagents

The SPQC used in this work was constructed by connecting an AT-cut piezoelectric quartz crystal and a conductivity electrode with a cell constant of 0.0104 m in series. A universal frequency counter (Iwatsu Model SC-7201) was used to record the oscillating frequency of a TTL-IC oscillator made in this laboratory [19]. An impedance analyser (Hewlett-Packard Model 4192A) was employed to measure the parameters of the crystal and the conductivity and capacitance of the solution. A computer (Hewlett-Packard, Model 9153C) was used for data analysis. The solution temperature was controlled at 20.0 ± 0.1°C by a thermostated water jacket.

Analytical-reagent grade chemicals and doubly distilled water were used throughout.

Procedure for frequencimetric titration

A 20-ml volume of sample solution was placed in a 25-ml breaker and the conductivity electrode in SPQC was immersed in the solution. Whilst stirring with a magnetic stirrer, the stable frequency (F_0) was recorded and served as the reference, an exact amount of titrant was added with a microsyringe and the stable frequency (F_1) was recorded again. The titration curves were obtained by plotting the frequency shift ($\Delta F = F_1 - F_0$) versus the volume of the titrant.

RESULTS AND DISCUSSION

Dependence of frequency response to conductivity on the crystal parameters

As discussed in Part I [18], the frequency shift (ΔF) of the SPQC in an electrolyte solution with the pure solvent used as the reference is given by

$$\Delta F = -\{F_s C_q (G^2 + AG\omega_0 C_s)\} / \{2(C_0 + C_s) \times [G^2 - AG\omega_0 C_0 + \omega_0^2 C_s (C_0 + C_s)]\} \quad (1)$$

where $F_s = 1/2\pi\sqrt{L_q C_q}$ and $\omega_0 = 2\pi F_s$. F_s, L_q, C_q and C_0 are the resonant frequency, motional inductance, motional capacitance and static capacitance of the crystal, respectively. $G = k\chi$ and $C_s = k\epsilon + C_p$, are the conductivity and capacitance of solution. k is the cell constant of the conductivity electrode, χ and ϵ are the specific conductivity and permittivity of the solution. C_p is the parasitic capacitance between the leading wires of the conductivity electrode, and A is a parameter related to the oscillator. It can be seen that the frequency shift of the SPQC decreases with increase in conductivity.

If a solution with conductivity G_0 is chosen as the reference, and the change in conductivity in solution (ΔG) is much less than G_0, the frequency shift can be expressed as

$$\Delta F = -\frac{\pi F_s^2 C_q (2G_0\omega_0 C_s + A\omega_0^2 C_s^2 - AG_0^2)}{[G_0^2 - AG_0\omega_0 C_0 + \omega_0^2 C_s (C_s + C_0)]^2} \cdot \Delta G \quad (2)$$

Equations 1 and 2 show that the frequency shift of the SPQC resulting from the change in conductivity of the solution is related to the parameters of the crystal and circuit in addition to the properties of the solution.

Using the frequency in water as the reference, the frequency shifts of the SPQC in KCl solutions were measured using crystals of different fundamental frequencies and are illustrated in Fig. 1. The sensitivity to the conductivity is shown in Fig. 2. The parameters of the crystal and circuit are given in Table 1. It seems that the higher the fundamental frequency, the greater is the value of A and the higher the sensitivity. A 9-MHz crystal was used in frequencimetric titrations.

Application of the SPQC in frequencimetric titrations

The success of a titration depends mainly on the end-point determination. Usually, the indicator method is employed for this purpose, as it

TABLE 1

Parameter of the crystals and circuit

F_s (kHz)	C_0 (pF)	C_q (pF)	L_q (mH)	A [a]
4433	3.29	0.0148	87.1	0.347
9000	6.48	0.0310	10.1	0.625
14318 [b]	4.67	0.0216	5.71	0.911

[a] $A = \tan\theta$, θ is the phase shift in the oscillator. [b] The data in this line were measured in a network analyzer (Hewlett-Packard Model 4195A).

offers the advantages of simplicity and convenience. However, the change in the colour of the indicator becomes less sharp near the end-point as the concentration of the analyte decreases. Instrumental methods are preferable in the titration of low concentrations owing to their high sensitivity and accuracy and the capability of following the whole titration course. Conductimetry is one of the instrumental methods often used in titration as the conductivity of the solution varies significantly in the procedures in most titrations [20,21]. Unfortunately, it is not suitable for sample in which the concentration of unreacted foreign electrolytes is much higher than that of the analyte, because the sensitivity and accuracy of conductimetric measurement are poor. Frequencimetric titrimetry by using a PQC proved to be useful in the titration of analytes at low concentrations under the conditions of a high conductivity background. The problem with this method is that the frequency response is sensitive to changes in the conditions of the crystal. As a quasi-liquid-phase piezoelectric sensor, an SPQC can give information about liquid media with the crystal oscillating in air. As shown in Eqns. 1 and 2. The frequency response of the SPQC is sensitive only to changes in the permittivity and conductivity of the solution. As the permittivity hardly changes with conductivity, a selective frequency response of the SPQC to conductivity in electrolyte solutions can be expected.

As shown in Fig. 2, the sensitivities are nearly constant in solutions of low conductivity, hence the frequency shift of the SPQC is proportional

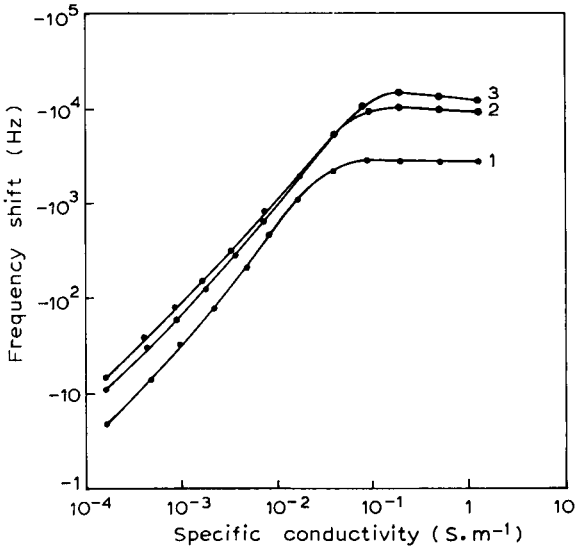

Fig. 1. Response curves of the SPQC with crystals of different fundamental frequency: (1) 4433; (2) 9000; (3) 14318 kHz.

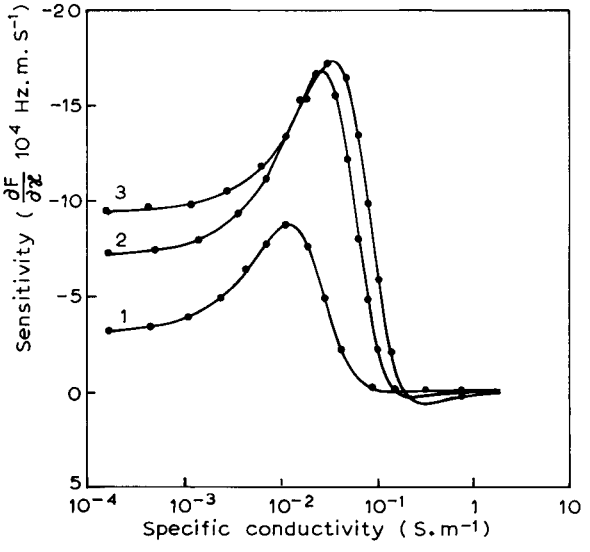

Fig. 2. Sensitivity to conductivity with crystals of different fundamental frequency: (1) 4433; (2) 9000; (3) 14318 kHz.

to the conductivity or the concentration of electrolyte in solutions of low concentration (1×10^{-5}–5×10^{-4} mol l^{-1} for KCl). According to Eqn. 2, slight changes in conductivity can be still detected by the SPQC even with a highly conducting background. It is more important to note that the sensitivity and linearity of the curve of frequency shift vs. conductivity change are improved under such conditions. For example, the frequency shift is linearly related to the concentration of KCl in the range 1×10^{-5} to 1×10^{-3} mol l^{-1} in the presence of 0.002 mol l^{-1} $NaNO_3$, and the slope of the response curves is about 2.5 times that in a pure water background. As an example of its applications, the SPQC was used for end-point determination in different titrations.

Acid–base titration. Both conductimetric and SPQC frequencimetric methods are suitable for acid–base titrations because H^+ and OH^- are the two ions with the highest equivalent conductivities. The frequencimetric titration curves for sodium hydroxide with hydrochloric acid are shown in Fig. 3. The lowest titratable concentration is 1×10^{-5} mol l^{-1}, which is much lower than that in conductometric titration. Moreover,

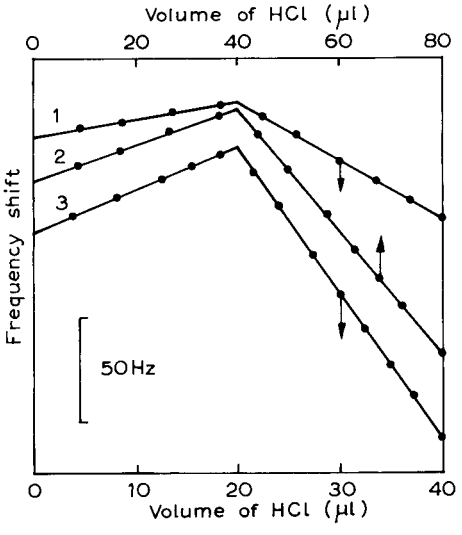

Fig. 3. Titration curves for sodium hydroxide with 0.01 mol l^{-1} hydrochloric acid. Concentration of analyte ($\times 10^{-5}$ mol l^{-1}): (1) 1.0; (2) 2.0; (3) 1.0 (with background of 0.001 mol l^{-1} KCl solution).

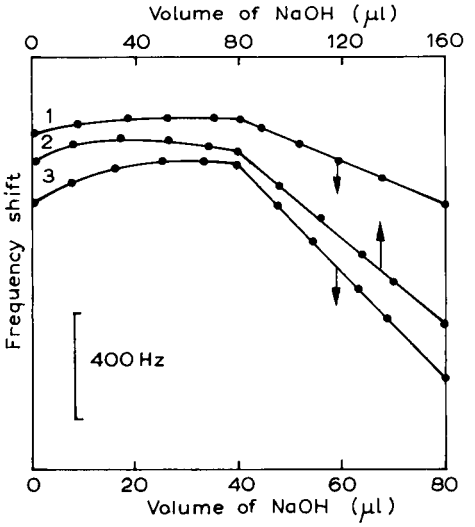

Fig. 4. Titration curves for acetic acid with 0.05 mol l^{-1} sodium hydroxide. Concentration of analyte ($\times 10^{-4}$ mol l^{-1}): (1) 1.0; (2) 2.0; (3) 1.0 (with background of 0.001 mol l^{-1} KCl solution).

intersection the angle of the titration curve in the presence of 0.001 mol l^{-1} KCl is sharper than that in its absence. Therefore, the detection limit of frequencimetric titration is improved in the presence of large amounts of unreacted foreign electrolyte.

Figure 4 shows the titration curves for acetic acid with sodium hydroxide. Because the analyte and the titration product form a buffer system, part of the titration curve is not strictly linear before the end-point. In addition, the shape of the titration curve is related to the concentration of acetic acid as the buffer capacity depends on the concentration. Again, the presence of foreign electrolytes is helpful for lowering the detection limit.

The titration curves for boric acid with sodium hydroxide are illustrated in Fig. 5. There is a distinct end-point for each concentration. However, it is not possible to use the classical conductimetric titration technique to determine boric acid at such low concentrations because the latter is a very weak acid.

EDTA complexation titration. EDTA is one of the most important titrants in complexation titration and it can react with many metal ions to

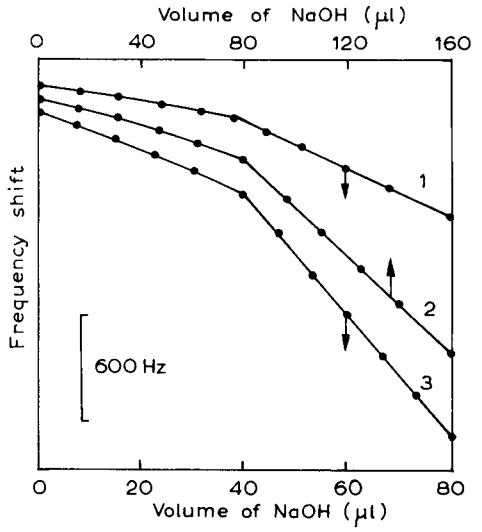

Fig. 5. Titration curves for boric acid with 0.05 mol l^{-1} sodium hydroxide. Concentration of boric acid ($\times 10^{-4}$ mol l^{-1}): (1) 1.0; (2) 2.0; (3) 1.0 (with background of 0.001 mol l^{-1} KCl solution).

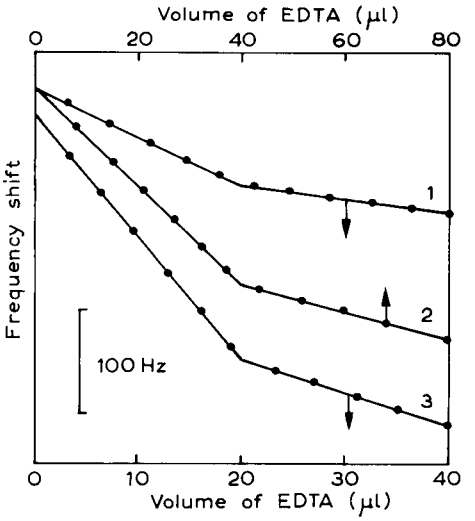

Fig. 6. Titration curves for zinc(II) with 0.01 mol l^{-1} EDTA without using of buffer solution. Concentration of zinc(II) ($\times 10^{-5}$ mol l^{-1}): (1) 1.0; (2) 2.0.

form stable 1:1 complexes. Because the form of EDTA present in solution depends on the pH of the solution, the shape of the titration curves should be related to the constitution of the solution.

Without a pH buffer and other acids or bases, the titration curves for zinc(II) are depicted in Fig. 6. Before the end-point, the frequency decreases sharply with the addition of EDTA, because H^+ is produced in the reaction. After the end-point, the decrease in frequency resulting from the excess of EDTA is very smooth. The end-point can be found accurately because the titration curve consists of two intersecting straight lines.

Usually, a buffer is required in complexiметric titration to improve the selectivity of analysis. The use of a buffer makes it difficult for the classical conductimetric method to monitor the course of titration because of the high background conductivity. As noted above, the SPQC method is still valid in such a case. The titration curves for iron(III) in 0.001 mol l^{-1} HCl are illustrated in Fig. 7. Before the end-point, the H^+ produced causes a decrease in frequency, but an increase in frequency is obtained after the end-point because part of the EDTA (H_2Y^{2-}) combines with H^+ to form H_3Y^-. Obviously, the intersection angles of the titration curves are sharper than those in Fig. 6, which is useful in improving the accuracy of determination.

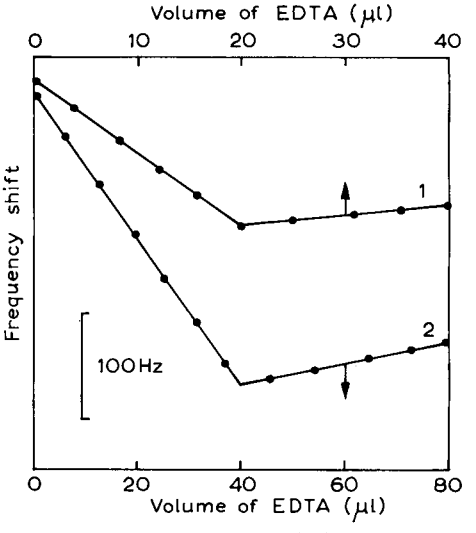

Fig. 7. Titration curves for iron(III) with 0.01 mol l^{-1} EDTA in 0.001 mol l^{-1} hydrochloric acid. Concentration of iron(III) ($\times 10^{-5}$ mol l^{-1}): (1) 1.0; (2) 2.0.

Figure 8 shows the titration curves for zinc(II) in acetate–acetic acid buffer solution. The decrease in frequency is slight before the end-point, because the increase in conductivity arising from the complexation reaction in this buffer is small. After the end-point, the decrease in frequency resulting from the excess of EDTA is more pronounced.

The titration curves for zinc(II) in ammonia–ammonium chloride buffer are illustrated in Fig. 9. Because the increase in conductivity in this buffer is similar before and after the end-point, the intersection angles of the frequencimetric titration curves are larger than those in Fig. 6.

Precipitation titration. The use of a PQC to monitor precipitation titration procedures could be questionable. For example, the adherence of the precipitate to the surface of the crystal would cause significant decrease in frequency, as the PQC is an extreme sensitive mass sensor, which makes it difficult to find the correct end-point. Addition of ethanol or a foreign electrolyte has been proposed [10]. It is worth pointing out that this shortcoming can be overcome by using an SPQC as the crystal is operated in air. On the other hand, the interface impedance between the

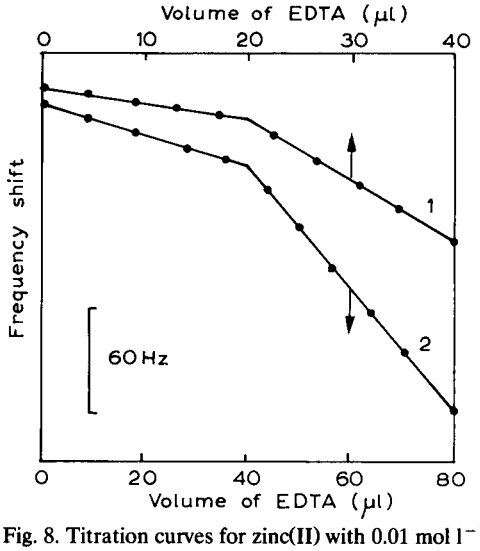

Fig. 8. Titration curves for zinc(II) with 0.01 mol l^{-1} EDTA in 0.001 mol l^{-1} acetate–0.001 mol l^{-1} acetic acid buffer solution. Concentration of zinc(II) ($\times 10^{-5}$ mol l^{-1}): (1) 1.0; (2) 2.0.

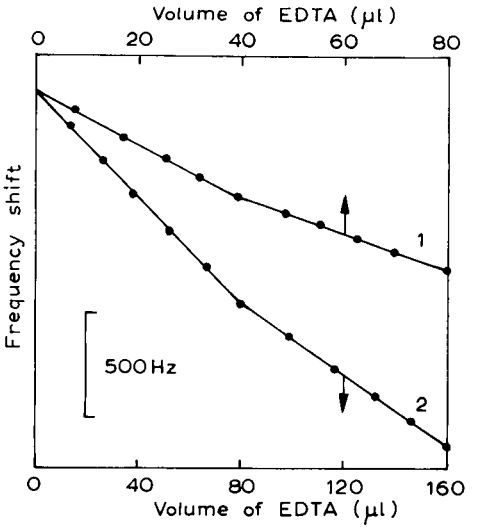

Fig. 9. Titration curves for zinc(II) with 0.05 mol l^{-1} EDTA in 0.001 mol l^{-1} ammonia–0.001 mol l^{-1} ammonium chloride buffer solution. Concentration of zinc(II) ($\times 10^{-4}$ mol l^{-1}): (1) 1.0; (2) 2.0.

electrodes and the solution is so small at high frequency that it can be neglected. Therefore, the adherence of the precipitate to the surface of conductivity electrodes has little influence on the interface impedance and the frequency of the SPQC. However, the adherence of the precipitate to the surface of the conductivity electrode would cause errors in conductimetry as it is operated at low frequency.

The titration curves for barium chloride with lithium sulphate and potassium bromide with silver nitrate are depicted in Figs. 10 and Fig. 11, respectively. It can be seen that the shape of the curve is related to the value of the solubility product (K_{sp}) of the precipitate. The end-point of the titration for Br^- is slightly more obvious than that for Ba^{2+} because the value of K_{sp} is 8.7×10^{-11} mol^2 l^{-2} for $BaSO_4$ and 3.2×10^{-13} mol^2 l^{-2} for AgBr [22].

Redox titration. The titration of iron(II) with permanganate is a typical example in redox titration. Although there is a change in conductivity during the course of titration, it is difficult for classical conductimetry to follow the titration of iron(II) at low concentrations, as large excesses of sulphuric and phosphoric acid are required in

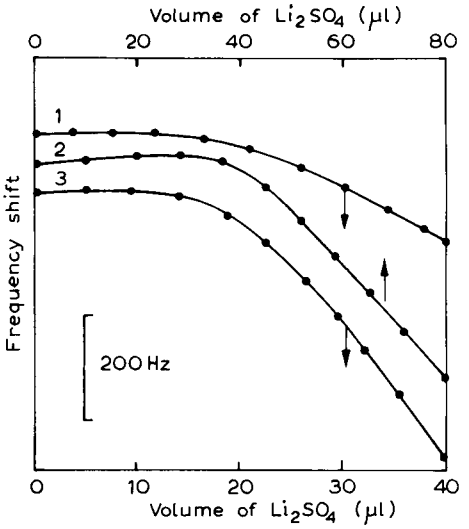

Fig. 10. Titration curves for barium chloride with 0.05 mol l^{-1} lithium sulphate. Concentration of barium ($\times 10^{-5}$ mol l^{-1}): (1) 5.0; (2) 10.0; (3) 5.0 (with background of 0.001 mol l^{-1} KCl solution).

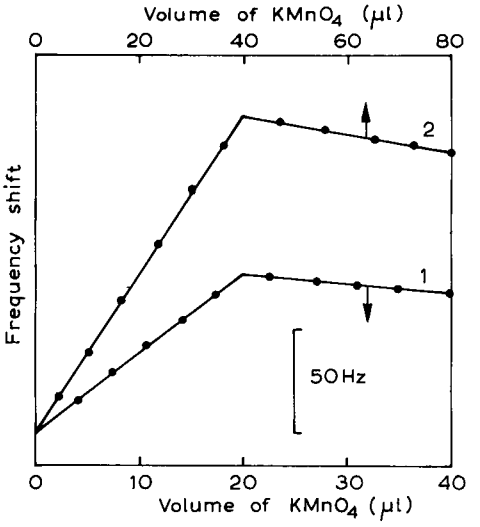

Fig. 12. Titration curves for iron(II) with 0.002 mol l^{-1} permanganate in 0.001 mol l^{-1} sulphuric and phosphoric acids solution. Concentration of iron(II) ($\times 10^{-5}$ mol l^{-1}): (1) 1.0; (2) 2.0.

this reaction. Although the background conductivity of the solution is high and the relative change in conductivity is small, this titration can still be detected by the PQC method owing to its high frequency resolution. However, the adsorption of iron(III) as its phosphate [23] and possible corrosion of crystal might cause errors in determination. As mentioned previously, the SPQC is a quasi-liquid-phase piezoelectric sensor, hence these factors have little influence on its frequency and the accuracy of the determination can be improved. In addition, the lifetime of the crystal is markedly prolonged for the same reason. The titration curves for iron(II) with $KMnO_4$ in 0.001 mol l^{-1} sulphuric and phosphoric acid medium are illustrated in Fig. 12. Distinct end-points were obtained in the titration of 1×10^{-5} mol l^{-1} iron(II) solutions.

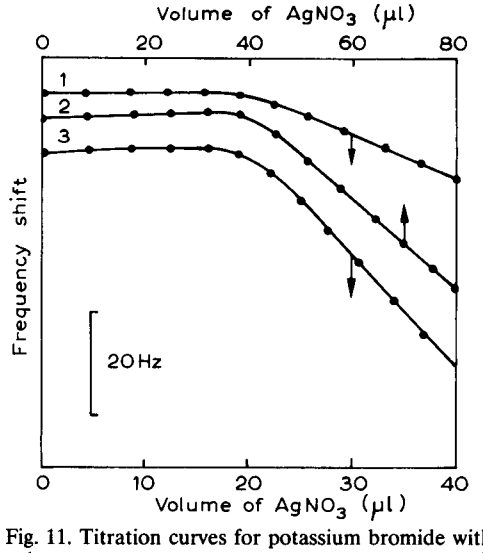

Fig. 11. Titration curves for potassium bromide with 0.01 mol l^{-1} silver nitrate. Concentration of bromide ($\times 10^{-5}$ mol l^{-1}): (1) 1.0; (2) 2.0; (3) 1.0 (with background of 0.001 mol l^{-1} KNO_3 solution).

It should be pointed out that the frequency stability and reproducibility of the SPQC are excellent. A frequency drift of 1 Hz per 10 min can be obtained in water at constant temperature. The reproducibility of the frequency shift is excellent. Each of the frequencimetric titrations was performed three times with good reproducibility. When 50 μl of 0.01 mol l^{-1} HCl were added to 20 ml of water, the frequency decreased by 143 Hz. The standard deviation for ten measurements of the frequency shift related to water was 0.63 Hz, hence the limit of detection for HCl is 3.3×10^{-7} mol l^{-1}. The limit of detection of this

method depends on the difference in the variation of conductivity before and after the endpoint. The greater the difference, the sharper is the intersection angle of titration curve and the lower is the detection limit. The concentrations at which determinations can be effected with sufficient accuracy are 1×10^{-5} mol l^{-1} for analytes under the conditions in Figs. 3, 7, 11 and Fig. 12, 2×10^{-5} mol l^{-1} for analytes under the conditions in Figs. 6 and 8 and 1×10^{-4} mol l^{-1} for analytes under the conditions in Figs. 4, 5, 9 and 10.

A 1.08×10^{-5} mol l^{-1} sodium hydroxide solution in the presence of 0.001 mol l^{-1} sodium chloride was titrated by this method and the recovery ranged from 98.6 to 101.7%. Additionally, as frequencimetric titrimetry is based on the frequency response to conductivity, the selectivity of this method is similar to that of classical conductimetry. Chemical treatment is required if chemical interferents are present.

Conclusions

An improved frequencimetric titrimetric method using an SPQC is proposed, which maintains the advantage of the PQC method of a high frequency response resolving power to the conductivity of solution. In the presence of large amounts of foreign electrolyte the sensitivity to conductivity of this method is even slightly improved. Compared with the previous method using PQC, the selectivity, reproducibility and stability of the frequency are markedly improved. The usable lifetime of the crystal in the SPQC method is significantly prolonged.

This work was supported by the Natural Science Foundation and the Education Commission Foundation of China.

REFERENCES

1 J.J. McCallum, Analyst, 114 (1989) 1173.
2 B.A. Čavić-Vlasak and L.J.V. Rajaković, Fresenius' J. Anal. Chem., 343 (1992) 339.
3 M.R. Deakin and D.A. Buttry, Anal. Chem., 61 (1989) 1147A.
4 D.A. Buttry, in A.J. Bard (Ed.), Electroanalytical Chemistry, Vol. 17, Dekker, New York, 1991, pp. 1–85.
5 M. Thompson, A.L. Kipling, W.C. Duncan-Hewitt, L.V. Rajaković, and B.A. Čavić-Vlasak, Analyst, 116 (1991) 881.
6 S.Z. Yao and L.H. Nie, Anal. Proc., 24 (1987) 336.
7 S.Z. Yao and T.A. Zhou, Anal. Chim. Acta, 212 (1988) 61.
8 T.A. Zhou, L.H. Nie and S.Z. Yao, J. Electroanal. Chem., 293, (1990) 1.
9 S.Z. Yao, Z.H. Mo and L.H. Nie, Anal. Chim. Acta, 229 (1990) 205.
10 Z.H. Mo, L.H. Nie and S.Z. Yao, Anal. Chim. Acta, 246 (1991) 421.
11 Z.H. Mo, L. H. Nie and S.Z. Yao, Anal. Chim. Acta, 246 (1991) 425.
12 S.Z. Yao, Z.H. Mo and L.H. Nie, Anal. Chim. Acta, 230 (1990) 51.
13 W.Z. Wei, L.H. Nie and S.Z. Yao, Anal. Chim. Acta, 269 (1992) 149.
14 M. Thompson, G.K. Dhaliwal and C.L. Arthur, Anal. Chem., 58 (1986) 1206.
15 R. Schmacher, J. Borges and K.K. Kanazawa, Surface Sci. 163 (1985) L621.
16 T. Nomura and M. Iijima, Anal. Chim. Acta, 131 (1981) 97.
17 S.Z. Yao, S.L. Dan and L.H. Nie, Anal. Chim. Acta, 209 (1988) 213.
18 D.-Z. Shen, W.-H. Zhu, L.-H. Nie and S.-Z. Yao, Anal. Chim. Acta, 276 (1993) 87.
19 S.Z. Yao and Z.H. Mo, Anal. Chim. Acta, 193 (1987) 97.
20 I.M. Kolthoff and P.J. Elvin, Treatise on Analytical Chemistry, Part I, Vol. 4, Interscience, New York, 1963, Chap. 51.
21 E. Pungor, Oscillometry and Conductometry, Pergamon, Oxford, 1965.
22 R.C. Weast, M.J. Astle and W.H. Beyer (Eds.), CRC Handbook of Chemistry and Physics, CRC Press, Boca Raston, FL, 65th edn., 1984.
23 T. Nomura and M. Maruyama, Anal. Chim. Acta, 147 (1983) 365.

Analytica Chimica Acta, 280 (1993) 217–222
Elsevier Science Publishers B.V., Amsterdam

Solubility of oxygen in glucose solutions

S.A.M. van Stroe-Biezen, A.P.M. Janssen and L.J.J. Janssen

Laboratory of Instrumental Analysis, Faculty of Chemical Technology, Eindhoven University of Technology, P.O. Box 513, 5600 MB Eindhoven (Netherlands)

(Received 2nd December 1992; revised manuscript received 9th February 1993)

Abstract

A knowledge of the solubility of oxygen in glucose-containing solutions is essential for the determination of the kinetics of the glucose oxidase-catalysed glucose oxidation. The enzyme glucose oxidase was used in a new glucose sensor. Combination of data for the dynamic viscosity and density from the literature and data from measurements with a rotating disc electrode (RDE) for hydrogen peroxide and hydroquinone showed that the factor ηD (η = dynamic viscosity; D = diffusion coefficient) remains constant in solutions with a glucose concentration ranging from 0 to 1 M. Assuming that this is also valid for oxygen, the diffusion coefficient of oxygen in glucose solutions was calculated and the solubility of oxygen was determined with RDE measurements. At both 25 and 37°C the relationship between the solubility of oxygen and the glucose concentration is a second-degree polynomial.

Keywords: Enzymatic methods; Glucose; Oxygen; Solubility

The enzyme glucose oxidase was used in a new design for a glucose sensor. In this approach, it is necessary to know the concentration profiles of all participating compounds and to determine the exact position of hydrogen peroxide production in the sensor. If the detection electrode is situated at this location, a maximum amount of hydrogen peroxide is detected. In the sensor the enzyme is immobilized in a hydrogel. When the kinetic parameters of the immobilized enzyme are determined, the enzyme-containing gel is brought into contact with solutions with a different glucose concentration. These solutions, and also the enzyme-containing gel, are saturated with oxygen. A knowledge of the solubility of oxygen in the glucose solutions is essential, as the kinetics of the enzyme also depend on the oxygen concentration.

Correspondence to: S.A.M. van Stroe-Biezen, Laboratory of Instrumental Analysis, Faculty of Chemical Technology, Eindhoven University of Technology, P.O. Box 513, 5600 MB Eindhoven (Netherlands).

The glucose solutions used in these studies were prepared with phosphate-buffered saline (0.050 M NaH_2PO_4, 0.050 M Na_2HPO_4 and 0.16 M NaCl, pH 7). The enzyme glucose oxidase (GOD) catalyses the oxidation of glucose:

$$\text{glucose} + \text{GOD}_{ox} \longrightarrow \text{gluconolactone} + \text{GOD}_{red}$$
$$O_2 + \text{GOD}_{red} \longrightarrow H_2O_2 + \text{GOD}_{ox} \qquad (1)$$

The rate of production of hydrogen peroxide (v) is given by [1]

$$\frac{1}{v} = \frac{1}{v_{max}}\left(1 + \frac{k_o}{C_o} + \frac{k_g}{C_g}\right) \qquad (2)$$

where v_{max} is the maximum reaction rate (mol m^{-3} s^{-1}), k_o and k_g are the Michaelis–Menten constants (mol m^{-3}) for oxygen and glucose, respectively, and C_o and C_g are the concentrations of oxygen and glucose (mol m^{-3}), respectively. To determine the kinetic parameters v_{max}, k_0 and k_g from the production rate of hydogen peroxide

(υ), the concentrations of oxygen and glucose must be known.

THEORY

The determination of the solubility of oxygen can be carried out by using a rotating disc electrode (RDE). The well known Levich relationship is used for RDE experiments [2]:

$$I_{lim} = 0.62nFA_eCD^{2/3}\nu^{-1/6}\omega^{1/2} \quad (3)$$

where I_{lim} is the limiting current (A), n the number of electrons involved in the electrode reaction, F the Faraday constant, i.e., the charge on 1 mol of electrons (A), A_e the electrode area (m^2), C the bulk concentration of the electroactive species (mol m^{-3}), D the diffusion coefficient of the electroactive species (m^2 s^{-1}), ν the kinematic viscosity of the solution (m^2 s^{-1}) and ω the angular rotation speed (rad s^{-1}). D and ν will alter as a result of changes in glucose concentration.

To solve this problem, a Stokes–Einstein-type relationship is used [3]:

$$\eta D = \text{constant} = B \quad (4)$$

where η is the dynamic viscosity of the solution (kg m^{-1} s^{-1}). From data for the dynamic viscosity and the density (ρ), the kinematic viscosity ν ($= \eta/\rho$) as a function of the glucose concentration was obtained. As the diffusion coefficient of oxygen in the absence of glucose is well known, it is possible to determine the diffusion coefficient of oxygen for several glucose concentrations from Eqn. 4. Equation 3 can be applied to calculate the solubility of oxygen.

The validity of Eqn. 4 was checked for two electroactive species, viz., hydrogen peroxide and hydroquinone, because for these species the concentrations in the glucose solution are chosen. However, this is not the case for oxygen.

EXPERIMENTAL

Reagents

Phosphate-buffered saline (PBS) was prepared with $NaH_2PO_4 \cdot 2H_2O$, $Na_2HPO_4 \cdot 2H_2O$ and NaCl purchased from Merck. Hydrogen peroxide [30% (w/w), aqueous solution] was obtained from Chempro Pack, hydroquinone from Merck and D-glucose from Janssen Chimica. Platinum black electrodes were prepared with a solution of $H_2PtCl_6 \cdot 6H_2O$ from H. Drijfhout and $PbCl_2$ from Merck. All solutions were prepared with demineralized, distilled water.

Instrumentation

For the RDE experiments, a Wenking POS 73 potentiostat was used, equipped with a digital multimeter (Fluke 8600 A) and a Motomatic E-550-M stirring motor. Recording was carried out with either an x–y recorder (Philips 8120) for polished platinum RDE cyclic voltammograms or an x–t recorder (Kipp BD40) for platinum black RDE experiments. A circulating water-bath (Colora NB-32981) was used for temperature control of the one-compartment cell.

For preparation of the platinum black electrodes, a Delta Elektronika E030-1 power supply was used, connected with a sliding resistance (Albert van der Perk) and an amperometer (Gossen).

Preparation of a platinum black RDE

A polished platinum RDE was scanned from -1500 to $+1500$ mV (vs. SCE) with a scan rate of 1 V s^{-1} in a 2 M H_2SO_4 solution to remove all impurities. The electrode was immersed in 3% (w/w) H_2PtCl_6 solution [containing 0.02% (w/w) $PbCl_2$] and connected as the cathode with a platinum sheet as the anode. A current of about 5 mA was used to prepare a platinum black layer on the platinum RDE within 10 min. Subsequently the platinum black electrode (platinized electrode) was washed in running tap water for at least 30 min and then washed with distilled, demineralized water for 5 min.

Procedures

For all experiments a platinum RDE (polished or platinized) was used as the working electrode ($A_e = 0.50 \times 10^{-4}$ m^2). Further, a platinum counter electrode with a surface area of 5×10^{-4} m^2 and a saturated calomel reference electrode (SCE) with a Luggin capillary were placed in the

one-compartment cell. A circulating water-bath was used to keep the temperature constant. As supporting electrolyte PBS (0.050 M NaH_2PO_4, 0.050 M Na_2HPO_4 and 0.16 M NaCl, pH 7) was used. The glucose concentrations in this electrolyte varied from 0 to 1.0 M.

Hydroquinone experiments (2–3 mol m^{-3}) were performed with an argon-saturated (1 atm) glucose solution. Hydroquinone was added before passing argon through. A cyclic voltammogram was recorded from −550 to +1200 mV (vs. SCE) at various rotation rates (1–9 rps). Rotation rates were varied in random order. A scan rate of 50 mV s^{-1} was used. After every set of measurements belonging to one glucose concentration the RDE was cleaned by scanning from −1500 to +1500 mV (vs. SCE) in 2 M H_2SO_4 with a scan rate of 1 V s^{-1}.

For hydrogen peroxide measurements (3–4 mol m^{-3}) the glucose solution was saturated with argon (1 atm) before adding hydrogen peroxide and cyclic voltammograms were scanned cathodically from +300 to −750 mV (vs. SCE) at 50 mV s^{-1}. Again the rotation speeds were varied in random order and the RDE was cleaned in 2 M H_2SO_4 after each set of measurements. Hydrogen peroxide diffusion coefficients were also determined by using a platinized RDE. An oxidation potential of +700 mV vs. SCE was applied and the electrode was allowed to reach a steady background current for a glucose solution without hydrogen peroxide at a certain rotation speed. Thereafter an aliquot of a hydrogen peroxide stock solution was added while leaving the potential at +700 mV. The solution was stirred magnetically for a few seconds to make it homogeneous and a steady current was obtained.

Oxygen measurements were carried out with a platinum black electrode. Glucose solutions were saturated with argon to determine the background current at −580 mV vs. SCE at a certain rotation speed. Subsequently the solution was saturated with oxygen (1 atm) while leaving all other conditions unchanged. After about 10 min a steady reduction current could be measured. Measurements for all three compounds were made at 25 and 37°C. The temperature was controlled with a circulating water-bath.

RESULTS

From the dynamic viscosity η [4] and the density ρ [5] as a function of the weight percentage of glucose, the dynamic viscosity was calculated as a function of the molar glucose concentration (Fig. 1), taking into account the influence of NaCl, NaH_2PO_4 and Na_2HPO_4. If mutual interactions between the salt ions and glucose are neglected, the Grunberg–Nissan relationship can be used [6]:

$$\log \eta_s = x_w \log \eta_w + x_1 \log \eta_1 + x_2 \log \eta_2 + x_3 \log \eta_3 \quad (5)$$

where x_w is the mole fraction of water, x_i is the mole fraction of compound i, η_s and η_w are the dynamic viscosity of the solution and pure water, respectively, and η_i is the apparent dynamic viscosity of compound i. Further,

$$\log \eta_a = x_{w,a} \log \eta_w + x_{1,a} \log \eta_1 \quad (6)$$

$$\log \eta_b = x_{w,b} \log \eta_w + x_{2,b} \log \eta_2 \quad (7)$$

$$\log \eta_c = x_{w,c} \log \eta_w + x_{3,c} \log \eta_3 \quad (8)$$

where the subscripts a, b and c refer to aqueous solutions of NaCl, sodium phosphate and glucose, respectively. When x_i is assumed to be equal in

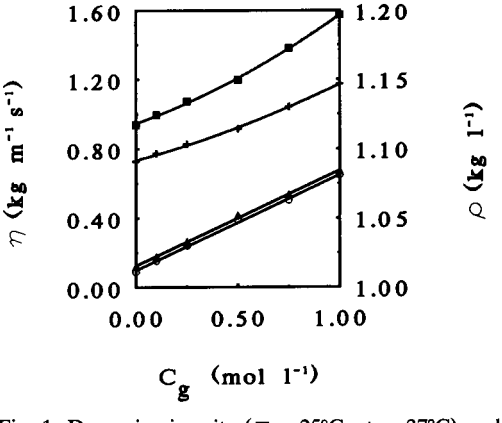

Fig. 1. Dynamic viscosity (■ = 25°C; + = 37°C) and density (▲ = 25°C; ○ = 37°C) as a function of the glucose concentration in PBS.

Eqn. 5 and in Eqns. 6–8 (viz., $x_{1,a} = x_1$; $x_{2,b} = x_2$; $x_{3,c} = x_3$) it follows that

$$\begin{aligned} x_w + x_1 + x_2 + x_3 &= 1 \quad \text{(from Eqn. 5)} \\ x_{w,a} + x_1 &= 1 \quad \text{(from Eqn. 6)} \\ x_{w,b} + x_2 &= 1 \quad \text{(from Eqn. 7)} \\ x_{w,c} + x_3 &= 1 \quad \text{(from Eqn. 8)} \end{aligned} \tag{9}$$

From this set of equations, the following can easily be derived:

$$x_w - x_{w,a} - x_{w,b} - x_{w,c} = -2 \tag{10}$$

Combining Eqns. 5–8 and 10 gives

$$\eta_s = \eta_a \eta_b \eta_c / \eta_w^2 \tag{11}$$

Values for η_w, η_a, η_b and η_c can be found in the literature [4,7]. The same procedure can be followed for calculating the density for the glucose–PBS solutions [5,8].

Cyclic voltammograms of hydrogen peroxide and hydroquinone in the glucose solutions have similar shapes to those in pure PBS. Plots of I_{lim} versus $\omega^{1/2}$ give straight lines although at higher rotation rates a small deviation is observed owing to kinetic limitations. Therefore, a reciprocal plot is made, which is linear even for high rotation rates. If, however, the original I_{lim} versus $\omega^{1/2}$ plot has an intercept (I^*), a correction should be performed by subtracting I^* from all measured limiting currents. Only from these corrected values can a proper reciprocal plot be obtained (see Figs. 2 and 3).

Contamination of the polished platinum electrodes easily occurs, especially in solutions with a high glucose concentration (≥ 0.5 M). Cleaning of the electrodes in sulphuric acid was necessary after every set of measurements (1–9 rps) for one glucose concentration. If measurements were performed going from a low to a high rotation speed, the Levich slope was different from measurements made going from a high to a low rotation speed (Fig. 4). This effect was not observed in a glucose-free solution (Fig. 4). The average of the two slopes, however, gave good results. A random order of measuring while alternating low and high rotation speeds yielded the same results. This is shown in Fig. 5 for hydroquinone and hydrogen peroxide.

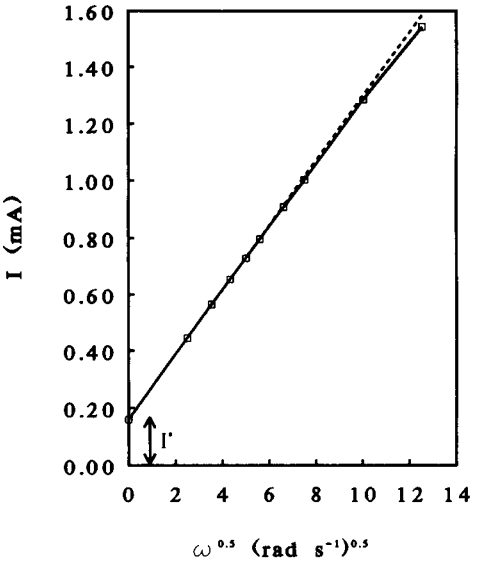

Fig. 2. Current as a function of square root of the angular rotation rate for 2 mM hydroquinone in PBS at 25°C. The continuous line follows the measured curve and the dashed line is the linear curve for rotation speeds from 1 to 5 rps. I^* denotes the intercept.

To check the validity of this adjusted method, experiments with a platinized electrode were carried out. With a platinized electrode, however, it

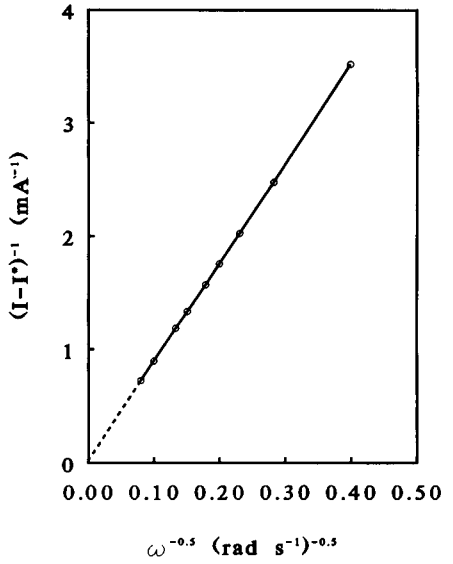

Fig. 3. Reciprocal of the corrected current $[(I - I^*)^{-1}]$ as a function of the reciprocal of the square root of the angular rotation rate for 2 mM hydroquinone in PBS at 25°C.

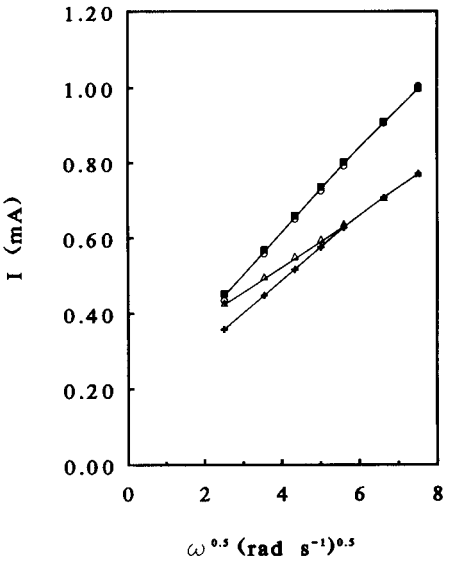

Fig. 4. Current plotted against square root of the angular rotation rate for 2 mM hydroquinone at 25°C. Measurements in PBS with (○) rising and (■) falling rotation speeds give the same results. For PBS containing 1 M glucose measurements with (+) rising or (△) falling rotation speeds do not match.

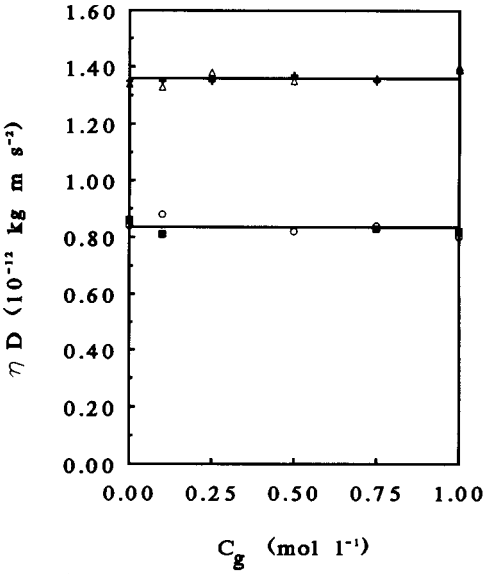

Fig. 6. ηD for hydrogen peroxide at (+) 25°C and (△) 37°C as a function of the glucose concentration in PBS, and for hydroquinone at (○) 25°C and (■) 37°C.

is not possible to obtain a voltammogram showing a limiting current, even if a low scan rate of 1 mV s^{-1} is used. Therefore, a potential at which a limiting current appears was directly applied. For a hydrogen peroxide-free medium it took 1–3 h (depending on the glucose concentration) to reach a background current at +700 mV. The results for the platinum black electrode were consistent with those for the polished platinum electrode. The advantage of the platinum black electrode is that the limiting current remains constant for at least 15 min.

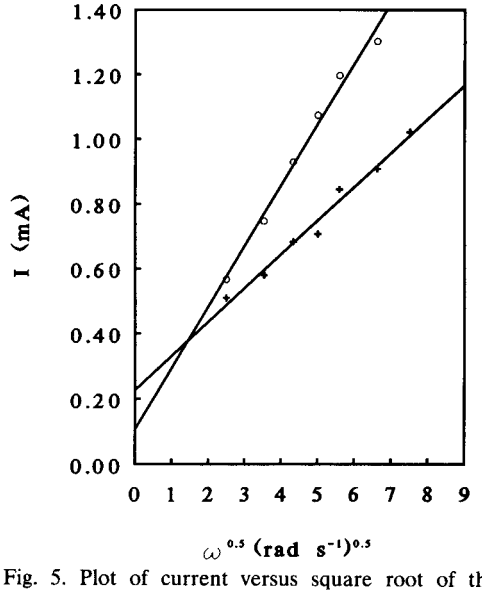

Fig. 5. Plot of current versus square root of the angular rotation rate, measured with rotation rates varied in random order for (○) 3.77 mM hydrogen peroxide and (+) 2.89 mM hydroquinone in PBS containing 1 M glucose at 25°C.

Figure 6 shows the factor ηD for both hydrogen peroxide and hydroquinone as a function of glucose concentration. It can be clearly seen that within the examined range of glucose concentrations ηD does not change significantly. Therefore, it is assumed that ηD for oxygen does not depend on the glucose concentration either. It is known that oxygen, hydrogen peroxide and hydroquinone behave similarly when diffusing through a hydrogel layer [9]. Further, it is known that the Stokes–Einstein relationship is valid for oxygen in NaCl solutions [10].

As the diffusion coefficient of oxygen in PBS is measured as 1.94×10^{-9} m^2 s^{-1} [9] and η for this solution is known to be 0.938×10^{-3} kg m^{-1} s^{-1} (Fig. 1), ηD can be calculated as 1.82×10^{-12}

kg m s^{-2}. At 37°C, ηD becomes $(2.47 \times 10^{-9}) \times (0.728 \times 10^{-3}) = 1.80 \times 10^{-12}$ kg m s^{-2}. From these values for ηD and the values for η (Fig. 1), the diffusion coefficient of oxygen was calculated as a function of the glucose concentration (Fig. 7). With a platinum black electrode the solubility of oxygen in glucose solutions was determined, using the diffusion coefficients from Fig. 7. The results are presented in Fig. 8 for 25 and 37°C.

The solubility of oxygen is likely to be slightly changed by the presence of salt ions (salting out effect [11]). The solubility of oxygen as a function of the glucose concentration at 25 and 37°C is given by

$$C_o = 1.045 - 0.2687C_g + 0.09714C_g^2 \quad (12)$$

$$C_o = 0.8607 - 0.1689C_g + 0.04571C_g^2 \quad (13)$$

respectively. These fitted relationships are applicable to a glucose concentration range of 0–1 M. The deviation between the measured values and values calculated with Eqn. 12 or 13 is $\leq 0.3\%$.

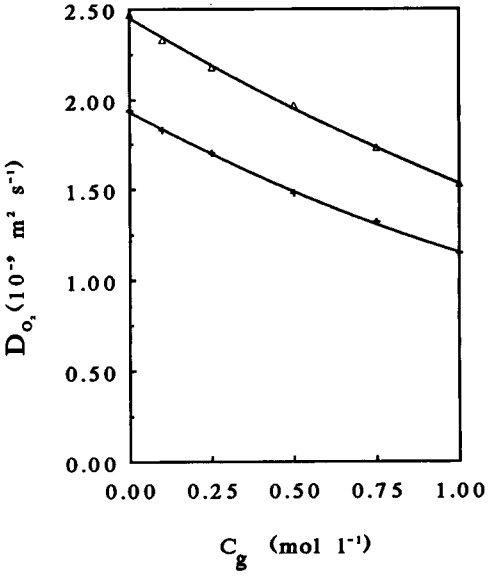

Fig. 7. Diffusion coefficient of oxygen as a function of glucose concentration in PBS at (+) 25°C and (△) 37°C.

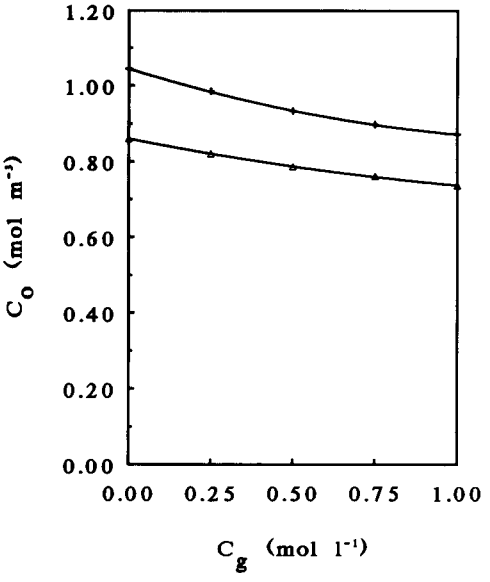

Fig. 8. Solubility of oxygen as a function of glucose concentration in PBS at (+) 25°C and (△) 37°C.

REFERENCES

1 P.H.S. Tse, J.K. Leypoldt and D.A. Gough, Biotechnol. Bioeng., 29 (1987) 696.
2 V.G. Levich, Physicochemical Hydrodynamics, Prentice Hall, Englewood Cliffs, NJ, 1962.
3 J. Joseph, E. Ackerman and R.L. Berger, J. Am. Chem. Soc., 78 (1956) 2979.
4 E.W. Washburn (Ed.), International Critical Tables of Numerical Data, Physics, Chemistry and Technology, Vol. V, McGraw-Hill, New York, 1st edn., 1929.
5 E.W. Washburn (Ed.), International Critical Tables of Numerical Data, Physics, Chemistry and Technology, Vol. II, McGraw-Hill, New York, 1st edn., 1927.
6 R.H. Perry, Perry's Chemical Engineers' Handbook, McGraw-Hill, New York, 6th edn., 1984.
7 Landolt-Börnstein, Zahlenwerte und Funktionen aus Physik, Chemie, Astronomie, Geophysik und Technik, 5. Teil, Bandteil 5, Springer, Berlin, 1969.
8 V.M.M. Lobo and J.L. Quaresma, Handbook of Electrolyte Solutions (Physical Sciences Data 41, Part B), Elsevier, Amsterdam, 1989.
9 S.A.M. van Stroe-Biezen, F.M. Everaerts, L.J.J. Janssen and R.A. Tacken, Anal. Chim. Acta, 273 (1993) 553.
10 J.C.P.A. Brock, Report, Eindhoven University of Technology, Eindhoven, 1981.
11 R. Battino and H.L. Clever, Chem. Rev., 66 (1966) 395.

Analytica Chimica Acta, 280 (1993) 223–229
Elsevier Science Publishers B.V., Amsterdam

Amperometric detection of amino acids in a flow-injection system with a nickel(II)-modified electrode with an Eastman-AQ polymer film

Anhua Liu and Erkang Wang

Laboratory of Electroanalytical Chemistry, Changchun Institute of Applied Chemistry, Chinese Academy of Sciences, Changchun, Jilin 130022 (China)

(Received 6th November 1992; revised manuscript received 15th February 1993)

Abstract

Amperometic flow measurements were made at +0.55 V (vs. Ag/AgCl) in 0.1 mol l^{-1} KOH electrolyte with an Ni(II) chemically modified electrode (CME) with an Eastman-AQ polymer film. The use and characteristics of a Ni(II)-containing crystalline and polymer-modified electrode obtained by a double coating step as a detector for amino acids in a flow-injection system using reversed-phase liquid chromatography are described. The detection of these analytes is based on the higher oxidation state of nickel (NiOOH) controlled by the applied potential. The electroanalytical parameters and the detection current for a series of amines and amino acids were investigated. The use of such a CME in the flow-injection technique was found to be suitable in a solution at low pH. The linear range for glycine is 5×10^{-6}–0.1 mol l^{-1} with a detection limit of 1.0×10^{-6} mol l^{-1}. A 1×10^{-4} mol l^{-1} mixture of serine and tyrosine was also detected after separation on an Nucleosil C_{18} column.

Keywords: Amperometry; Flow injection; Liquid chromatography; Amino acids; Chemically modified electrodes

The detection method for amino acids was initially based on the postcolumn reaction of amino acids with copper(II) ions added at a constant flow-rate and then the decrease in copper(II) ion concentration was monitored potentiometrically with a copper ion-selective electrode. The detection limits for glycine, valine and isoleucine are 75, 200 and 300 ng μl^{-1}, respectively [1–3]. There have been many studies of the detection of amino acids in liquid chromatography in recent years, and methods including direct detection, derivatization for reductive detection and derivatization for oxidative detection have been reported.

Direct amperometric detection [4,5] has been shown to be sensitive and versatile. Amino acids and peptides containing tyrosine have been detected directly using a glassy carbon electrode applied at +0.90 V [6]. Amino acids have also been detected at platinum electrode using pulsed electrocatalytic detection. Using pulsed amperometric detection for amino acids, Polta reported detection limits of 23 ng for hydroxyproline and 13 ng for glycine [5]. Several papers have been published on the use of derivatizing agents for the detection of amino acids using glassy carbon electrode [7–11].

Metallic electrodes have been utilized for the direct amperometric detection of amino acids. Mercury, cobalt, copper and nickel electrodes

Correspondence to: Erkang Wang, Laboratory of Electroanalytical Chemistry, Changchun Institute of Applied Chemistry, Chinese Academy of Sciences, Changchun, Jilin 130022 (China).

[12,13] have been reported. Fleischmann et al. [14] found that alcohols and amines can be oxidized at a nickel anode in aqueous alkaline solution. They showed that the rate-determining step was the oxidation of the substrate by a higher oxidation state species, NiOOH, on the hydrated nickel oxide surface. As the sample passes over the electrode, the amino acid is oxidized to a radical species and the nickel is reduced. The resulting current is proportional to the sample concentration. The electrode reaction has been applied to the determination of ethanol [15], amines and amino acids [12]. Yuan and Huber [16] reported a rapid and convenient detection method without derivatization for bovine serum albumin in the range 10–200 mg l^{-1} using a nickel oxide electrode. In addition, a chemically modified electrode (CME) has been used for the catalytic oxidation of amino acids and other carbohydrates [17–19]. For example, copper deposited on glassy carbon [20–22] and RuO_2-containing carbon paste [23] greatly enhanced the amperometric detection of carbohydrates and related compounds.

In a previous paper [17], a novel Eastman-AQ–Ni(II) CME prepared by a double coating step deposition of a poly(ester sulphonic acid) polymer film and Ni(II)-containing crystalline species on glassy carbon was reported; it exhibited stable electrocatalytic oxidation of α-hydrogen compounds. In this work, this kind of CME was applied to pH-matched samples and lower pH samples than the base electrolyte while the electrode surface activity was reproducibly restored from the stripping resulting at effect lower pH [12]. The CME was applied to the determination of amino acids in a flow-injection system. Glycine, serine and tyrosine could be detected over a linear concentration range from 5×10^{-6} to 0.1 mol l^{-1}, with a detection limit of 1×10^{-6} mol l^{-1} for glycine.

EXPERIMENTAL

Reagents

Analytical-reagent grade chemicals and doubly distilled water were used throughout, unless stated otherwise. Eastman-AQ was obtained from Eastman Kodak (Rochester, NY). Ni(II) solution was prepared by dissolving nickel sulphate (Beijing Chemical) in water. Amine and amino acid standard solutions were prepared in water from chemicals supplied by Shanghai Biochemical without further purification.

Apparatus

Cyclic voltammetry (CV) was performed with a Model 79-1 potentiostat (Jinan) with a three-electrode cell containing silver–silver chloride (with saturated potassium chloride) and a platinum wire as reference and counter-electrodes, respectively.

Flow-injection analysis (FIA) was performed with a Model 510 pump, a U6K injection valve (Waters, Milford, MA) and a Model TL-5A thin-layer electrochemical detector (Bioanalytical Systems, W. Lafayette, IN). The length of the connecting PTFE tubing (i.d. 0.013 cm) from the injection valve to the detector was 30 cm.

Liquid chromatographic (LC) experiments were carried out using a Model 510 pump, a U6K injection valve (Waters) and a 7-μm particle size Nucleosil C_{18} column (200 mm × 4.0 mm i.d.) as an analytical column.

The FIA–LC system was controlled by a laboratory-made potentiostat [24] used for amperometric detection. The mobile phase was 0.1 mol l^{-1} KOH to which 1.0×10^{-5} mol l^{-1} $NiSO_4$ had been added and was delivered at a flow-rate of 1.0 ml min^{-1}. All potentials were measured and recorded with respect to a saturated calomel electrode (SCE), unless stated otherwise.

Working electrode

Prior to its coating, a thin-layer glassy carbon (GC) disc electrode with an area of 0.071 cm^2 was hand-polished with alumina slurries of 1 and 0.05 μm. Residual polishing material was removed from the surface by sonication in a water-bath for 5 min after each polishing process. The surface was modified by a double coating step: the disc and its surrounding were first coated with a measured volume (5 μl) of dilute 2% Eastman-AQ–water polymer solution. The film dried in air to give a colourless, transparent, thin

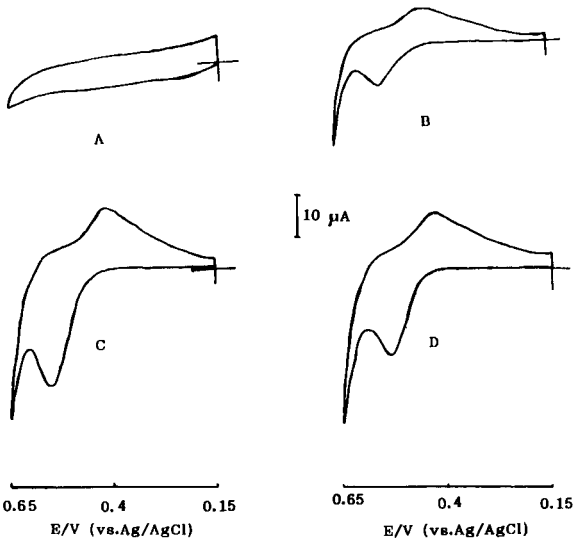

Fig. 1. Cyclic voltammograms of the CMEs. Scan potential range, +0.15–0.65 V (vs. Ag/AgCl); scan rate, 100 mV s^{-1}; base electrolyte, 0.1 mol l^{-1} KOH. (A) Eastman-AQ film electrode; (B) Eastman-AQ–Ni(II) electrode; (C) 1.0 mM glycine and (D) 1.0 mM tyrosine at Eastman-AQ–Ni(II) CME.

film on the GC substrate. In the second step, the film surface was coated with 10 μl of 1.0×10^{-4} mol l^{-1} $NiSO_4$ solution. Finally, the CME was allowed to dry under an infrared lamp. At this point, a white deposit appeared on the glassy carbon surface and the CME was ready for use.

RESULTS AND DISCUSSION

Electrochemistry

The cyclic voltammograms of the CME, measured in a conventional three-electrode voltammetric cell, were recorded in 0.1 mol l^{-1} KOH between +0.15 and +0.65 V (vs. Ag/AgCl) (Fig. 1). When an Eastman-AQ film electrode was employed, no oxidation or reduction response was observed within the potential range (Fig. 1A). However, when an Eastman-AQ–Ni(II) electrode was employed, a fairly large anodic peak with peak potential at ca. +0.55 V and a cathodic peak at ca. +0.45 V (vs. Ag/AgCl) were observed for the first cycle (Fig. 1B), which could be assigned to the formation of NiOOH according to Fleischmann et al. [14]. The anodic peak current varied linearly with scan rate up to 100 mV s^{-1}; the peak potential shifted positively with increasing scan rate. This indicates a slow Faradaic surface process. After a stable CV of the CME had been obtained in 0.1 mol l^{-1} KOH, the CME was used to obtain CVs of 1 mM glycine and tyrosine (Fig. 1C and D). Anodic current enhancements were observed at potentials between +0.55 and +0.60 V whereas no cathodic current enhancement was observed in potential range. In strongly alkaline medium, an active nickel(III) oxide (NiOOH) was formed in situ on the CME surface at ca. +0.55 V. The nickel(III) surface acts as a strong oxidant and reacts with amino acids, the resulting catalytic oxidation current being directly proportional to the concentration of the related species. In addition, the peak currents also increased significantly with increasing KOH concentration from 0.05 to 0.5 mol l^{-1} and the peak potential shifted negatively, indicating that hydroxide ion was involved in the reaction mechanism.

In a previous study [17] it was found that the catalytic function of the Eastman-AQ–Ni(II) CME obtained by the double coating step method was superior to that of obtained with one coating step. In this work, the double coating step method was also used with a Ni(II) concentration of 1.0×10^{-3} mol l^{-1} to prepare the CME (electrode area = 0.012 cm^2) with an increased background current. In FIA, 5 μl of the dilute Eastman-AQ polymer and 10 μl of 1.0×10^{-4} mol l^{-1} $NiSO_4$ solution were used to prepare the CME and then a long-lived and steady electrocatalytic current was obtained.

FIA and LC analysis

In the application of the FIA technique, the effects of the applied potential, the hydroxide concentration, the rate and other factors affecting the oxidation rate were investigated.

The hydrodynamic voltammetric (HDV) curve for glycine was obtained with 20-mV increments between +0.15 and +1.0 V (vs. SCE) (Fig. 2) for the CME, whereas no any significant current was observed within the potential range for a bare GC electrode. The optimum potential to obtain the largest analyte signal is about +0.55 V for

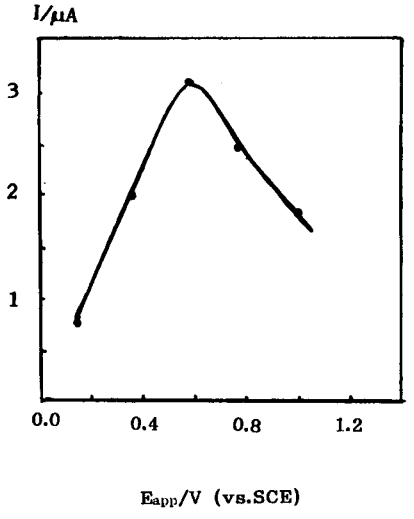

Fig. 2. Hydrodynamic voltammogram of glycine at the CME for a 20-μl injection of 1.0×10^{-3} mol l^{-1} glycine. Mobile phase, 0.1 mol l^{-1} KOH–1.0×10^{-5} mol l^{-1} $NiSO_4$; flow-rate, 1.0 ml min^{-1}.

amino acids. At applied potentials greater than the optimum, competition by excess of hydroxide ion and analyte for sites on the electrode surface apparently limited the current. Adsorption of hydroxide anions would be more sensitive than neutral analyte species to applied potential. At potentials less positive than the optimum value, the population of active sites on the electrode surface is apparently controlled by the applied potential. The HDV peak potentials at different concentrations of analytes are listed in Table 1. At lower

TABLE 1

HDV peak potentials of amino acids at different concentrations

Compound	Concentration (mmol l^{-1})	HDV peak potential (mV vs. Ag/AgCl)
Glycine	0.01	500
	0.1	550
	1.0	600
	5.0	Plateau
Serine	0.2	550
	1.0	590
	5.0	Plateau
Tyrosine	0.1	555
	1.0	600
	5.0	Plateau

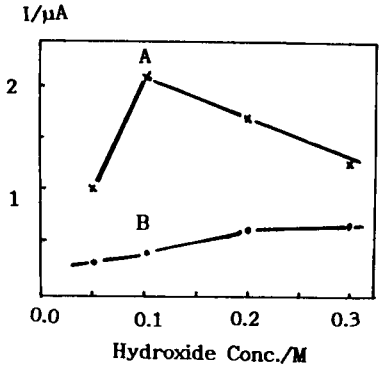

Fig. 3. Dependence of the peak current on the hydroxide concentration at the CME. Applied potential, +0.55 V (vs. SCE); 20-μl injection of 1.0×10^{-3} mol l^{-1} serine; flow-rate, 1.0 ml min^{-1}. (A) Peak current; (B) background current.

concentrations, fewer active sites are needed, hence lower optimum applied potentials observed. At concentrations higher than 5.0 mmol l^{-1}, a saturation effect occurred in the concentration data, i.e., the current was limited by available adsorption sites, rather than by reaction kinetics.

The effect of hydroxide concentration at an applied potential of +0.55 V is shown in Fig. 3. At lower concentrations, the formation of the higher oxide on the surface is limited, whereas at concentrations greater than 0.1 mol l^{-1}, solvent oxidation probably becomes competitive with that of the analyte. The peak current for 1.0×10^{-3} mol l^{-1} glycine increased with flow-rate up to 1.0 ml min^{-1} but there was no further increase up to 3.0 ml min^{-1}. At flow-rates up to 1.0 ml min^{-1}, the peak current dependence on flow-rate can be attributed to increasing convective mass transport at the electrode. Limitation of the analyte signal with increasing flow-rate can be attributed to the rate-limiting step for electron transfer at the electrode.

Analyte currents for a series of simple amines and common amino acids were determined in base electrolyte of 0.1 mol l^{-1} KOH under the conditions indicated above. Typical results for 20 μl of 1.0×10^{-3} mol l^{-1} samples are given in Table 2.

A major factor affecting the oxidation rate is steric effects on the adsorption and stoichiometry, i.e., the number of oxidizable sites such as

TABLE 2

FIA responses of Eastman-AQ–Ni(II) CME to various amines and amino acids at a concentration of 1.0×10^{-3} mol l^{-1} for a 20-μl injection [a]

Compound	Peak current (μA)	Detection limit (ng)
Propylamine	0.6	N.D. [b]
Butylamine	0.3	N.D.
Glycine	3.0	1.5
Serine	2.0	2.1
Tyrosine	1.4	3.6
Asparagine	1.0	13.2
Cysteine	0.8	20.4
Alanine	0.5	17.8
Arginine	0.3	34.8
Glutamic acid	0.32	29.4
Leucine	0.18	26.2
Tryptophan	0.15	40.8
Valine	0.10	117
Lysine	0.072	146
Proline	0.023	91.2

[a] Applied potential at +0.55 V (vs. Ag/AgCl); signal-to-noise ratio = 2. [b] N.D. = not determined.

amino groups. Stereochemical control of the oxidation rate can be observed; ethanol yields a larger signal than glycerol and primary amines yield much larger currents than secondary and tertiary amines [12]. For the amino acids, an increase in molecular weight corresponds to a decrease in peak current. As examples, glycine vs. serine, serine vs. lysine and alanine vs. phenylalanine can be noted. The stoichiometry effect is shown by comparing serine with alanine and tyrosine with phenylalanine. Both serine and lysine contain three hydrogens with two active groups, yet the more bulky lysine yields a current only 5% of that for serine. This indicates that the effect of steric hinderance exceeds that of stoichiometry.

In chromatography, and in other techniques, samples are often in a buffered medium at pH values considerably lower than that of the carrier electrolyte used here. Therefore, it was necessary to study the effect of pH on the detection signal from the CME. When a low-pH sample injected into the stream reaches the electrode, first a negative (cathodic) peak is observed as the oxide layer is reduced and then a positive (anodic) peak occurs owing to re-formation of an oxide layer at the tail of the sample plug where the pH is again increasing toward the base electrolyte pH. As the hydroxide concentration begins to increase during the tail of the passing sample zone, the active higher oxide surface is renewed. The amino acid sample is oxidized by the newly formed disordered nickel oxide surface, containing relatively many active sites. Analyte in the injected sample enhanced the positive peak height. In support of this mechanism, CV curves for Eastman-AQ–Ni(II) electrodes were obtained experimentally to show anodic NiOOH formation beginning at +0.4 V, in agreement with earlier reports [14]. The high rate of this process conforms to Fleischmann et al.'s report [14] showing that the layer of NiOOH initially formed is only a few monolayers thick following Langmuir adsorption behaviour.

Analyte signals were observed for the samples at various pH values: pH 10.5 (10 mM hydrogencarbonate buffer), pH 8.7 (10 mM phosphate buffer), pH 5.0 (10 mM acetate buffer) and pH 3.0 (10 mM phthalate buffer). Figure 4 shows the signals for 1.0×10^{-3} mol l^{-1} tyrosine in the four different buffers. The precision was examined for four replicate determinations of each sample at each pH value. The calculated relative standard

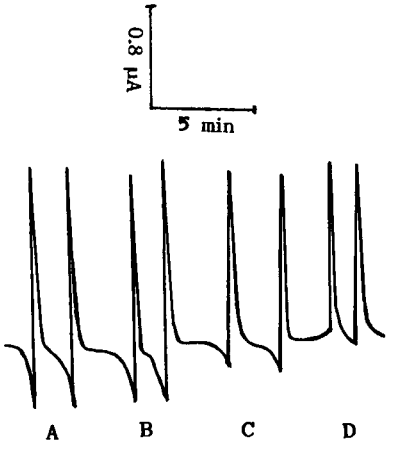

Fig. 4. Analytical signals for samples of different pH. Applied potential, +0.55 V (vs. SCE); 20-μl injection of samples of various pH; flow-rate, 1.0 ml/min; mobile phase, 0.1 mol l^{-1} KOH–1.0×10^{-5} mol l^{-1} $NiSO_4$. 1.0×10^{-3} mol l^{-1} tyrosine in (A) 0.1 mol l^{-1} phthalate buffer (pH 3.0), (B) 0.1 mol l^{-1} acetate buffer (pH 5.0), (C) 0.1 mol l^{-1} phosphate buffer (pH 8.7) and (D) 0.1 mol l^{-1} hydrogencarbonate buffer (pH 10.5).

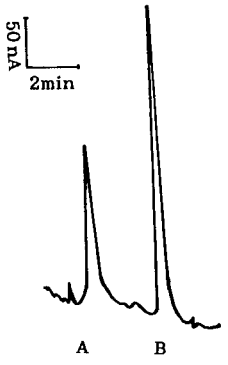

Fig. 5. Chromatographic detection at an Eastman-AQ–Ni(II) CME. Mobile phase, 0.05 mol l^{-1} KH_2PO_4/K_2HPO_4–1.0×10^{-5} mol l^{-1} $NiSO_4$, pH 8.7; flow-rate, 1.0 ml/min; E_{app} = +0.55 V (vs. SCE). (A) 1.0×10^{-4} mol l^{-1} serine; (B) 1.0×10^{-4} mol l^{-1} tyrosine.

deviation was 5.0% for all samples. This demonstrates that a reproducible higher oxide layer is formed after its temporary removal by the lower pH of the mid-portion of the sample zone. It should be noted that these results highlight the special advantage of the flow-injection technique in regenerating the surface when active electrode material is used in voltammetry.

In reversed-phase chromatography, the pH of the mobile phase was limited (pH < 9.0). A higher pH value in mobile phase is favourable for the regeneration of the CME surface but unsuccessful for the separation of amino acids. A 0.05 mol l^{-1} phosphate buffer (pH 8.7) was chosen as the mobile phase for the separation of serine and tyrosine (Fig. 5).

Calibration, detection limit and reproducibility

In the flow system, 1.0×10^{-5} mol l^{-1} $NiSO_4$ was added to mobile phase to make up for the stripping of Ni(II) from the surface of the modified electrode. With the chosen flow conditions, a series of amino acids were studied. For glycine, the linear response concentration range was between 5.0×10^{-6} and 0.1 mol l^{-1}. The detection limit was 1.0×10^{-5} mol l^{-1} (signal-to-noise ratio = 2). The reproducibility of the method was calculated by making nine replicate injections of 1.0×10^{-5} mol l^{-1} glycine; the relative standard deviation was 5.0% (Fig. 6). Finally, the repeatability of the CME response in the flow system appeared satisfactory for quantitative application. Long-term observation of the CME responses indicated a decrease in the analytical current of only 5% from day to day in a continuous-flow stream, even when the flow-rate was showed and the potentiostat was disconnected between working sections. These results indicate, analytically useful catalytic stability. The lifetime of this electrode is at least 1 week.

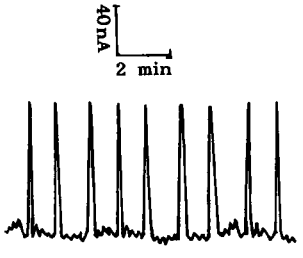

Fig. 6. Analytical signals at the CME for nine replicate injections of 1.0×10^{-5} mol l^{-1} glycine (20-μl injection). Other conditions as in Fig. 4.

The use of the Eastman-AQ–Ni(II) CME for oxidation of amines and amino acids is superior to that of metallic electrode substrates. For example, detection was performed at a constant potential with no need for specialized pulse sequences to enhance the electrode stability. Further, the linear concentration range extended over at least five orders of magnitude. The detection limit of glycine was 1.0×10^{-6} mol l^{-1}, which is better than that with a nickel electrode. In addition, this CME is suitable for buffered samples at lower pH with simple constant-potential chromatography and flow-injection analysis.

This project was supported by the National Natural Science Foundation of China.

REFERENCES

1 P.W. Alexander, P.R. Haddad, G.K.C. Low and C. Maitra, J. Chromatogr., 209 (1981) 29.
2 P.W. Alexander, C. Maitra, Anal. Chem., 53 (1981) 1590.
3 P.R. Haddad, P.W. Alexander and M. Troianowicz, J. Chromatogr., 315 (1984) 261.
4 A. Sauter and W. Frick, J. Chromatogr., 297 (1984) 215.
5 J.A. Polta and D.C. Johnson, J. Liq. Chromatogr., 6 (1983) 1727.
6 M.V. White, J. Chromatogr., 262 (1983) 420.

7 J.L. Meek, J. Chromatogr., 266 (1983) 401.
8 T.J. Mahachi, R.M. Carlson and D.P. Poe, J. Liq. Chromatogr., 298 (1984) 297.
9 L.C. Harsing, H. Nagashima, E.S. Vizi and D. Duncalf, J. Chromatogr., 383 (1986) 19.
10 W.A. Jacobs, Curr. Sep., 7 (1986) 39.
11 L.G. Harsing, H. Nagashima, E.S. Vizi and D. Duncalf, J. Chromatogr., 383 (1986) 19.
12 B.S. Hui and C.O. Huber, Anal. Chim. Acta, 134 (1982) 211.
13 J.B. Krafil and C.O. Huber, Anal. Chim. Acta, 139 (1982) 347.
14 M. Fleischmann, K. Korinek and D. Pletcher, J. Chem. Soc., Perkin Trans. 2 (1972) 1396.
15 T. Morrison, C.O. Huber, Anal. Chim. Acta, 120 (1980) 75.
16 C.J. Yuan and C.O. Huber, Anal. Chem., 57 (1985) 180.
17 E. Wang and A. Liu, J. Electroanal. Chem., 319 (1991) 217.
18 L.M. Santos and R.P. Baldwin, Anal. Chim. Acta, 206 (1988) 85.
19 A.M. Tolbert and R.P. Baldwin, Electroanalysis, 1 (1989) 389.
20 S.V. Prabhu and R.P. Baldwin, Anal. Chem., 61 (1989) 852.
21 S.V. Prabhu and R.P. Baldwin, Anal. Chem., 61 (1989) 2258.
22 P. Luo, S.V. Prabhu, R.P. Baldwin, Anal. Chem., 62 (1990) 752.
23 J. Wang, Z. Taha, Anal. Chem., 32 (1990) 1413.
24 H. Ji and E. Wang, Chinese Journal of Chromatography, 6 (1988) 1394.

Analytica Chimica Acta, 280 (1993) 231–238
Elsevier Science Publishers B.V., Amsterdam

Simple and rapid flow-injection spectrophotometric determination of carbaryl after liquid–liquid extraction

Karim D. Khalaf, A. Morales-Rubio and M. de la Guardia

Department of Analytical Chemistry, University of Valencia, 50 Dr. Moliner St., 46100 Burjassot, Valencia (Spain)

(Received 4th January 1993; revised manuscript received 16th February 1993)

Abstract

A simple procedure was developed for the spectrophotometric determination of carbaryl and its hydrolysis product 1-naphthol in water. These compounds are extracted into xylene and back-extracted, as the 1-naphtholate, with 0.2 M NaOH. A 600-μl volume of the alkaline extract is injected into a flow analysis manifold which provides the reaction between naphtholate and 50 μg ml^{-1} *p*-aminophenol solution in the presence of 0.004 M KIO_4 and spectrophotometric measurement is carried out at 596 nm. The method provides a limit of detection of 26.5 ng ml^{-1} carbaryl and a sample frequency of 110 injections per hour. Recoveries in different types of matrices vary from 95 to 102%.

Keywords: Flow injection; UV–Visible spectrophotometry; Carbaryl; Pesticides; Waters

Carbaryl (1-naphthyl methylcarbamate) is a carbamate pesticide widely used on farms as a contact insecticide because of its effectiveness against numerous insect pests of fruits, vegetables, cotton and many other crops.

The acute oral dose of carbaryl (LD_{50}) for male rats has been established as 850 mg kg^{-1} [1] or 560 mg kg^{-1} [2]. The biological potential activities of carbaryl and its major hydrolysis metabolite 1-naphthol have been studied, and it has been found that toxic effects are due to the inhibition of cholinesterase and the teratogenic character of these products [3–7]. Carbaryl causes nausea, vomiting, diarrhoea, bronchoconstriction, blurred vision, excessive salivation, muscle twitching, cyanosis, convulsion, coma and respiratory failure in humans. However, carbaryl has a short lifetime and a low toxicity for plants and mammals compared with other insecticides [8] and, for these reasons, carbaryl is currently marketed in wettable powder, bait, dust, liquid and aerosol forms.

Several methods have been reported for the determination of carbaryl and 1-naphthol. Thin-layer chromatography (TLC) [9–11] and gas chromatography (GC) [12–14], have been used for direct analysis and also after a previous derivatization step. Liquid chromatography (LC) has been successfully used, with or without postcolumn reaction detection, for the determination of trace levels of carbaryl [15–22].

Spectrofluorimetry has been used with high sensitivity and good selectivity, especially in the presence of micellar media which can improve the determination of carbaryl and 1-naphthol [23–25].

Spectrophotometric methods are not available for the direct determination of carbaryl, but the pesticide is easily hydrolysed to 1-naphthol, which can be coupled with different reagents in order to achieve an appropriate selectivity and sensitivity

Correspondence to: M. de la Guardia, Department of Analytical Chemistry, University of Valencia, 50 Dr. Moliner St., 46100 Burjassot, Valencia (Spain).

of the spectrophotometric measurements. For this purpose the following reagents have been proposed: diazotized sulphanilic acid [26], 4-aminophenazone [27], 3-methyl-2-benzothiazolinone hydrazone hydrochloride [28], *p*-aminophenol [29], 1-amino-2-naphthol-4-sulphonic acid and *p*-nitrobenzenediazonium fluoroborate [30], yielding coloured species that absorb at 475, 475, 500, 600, 700 and 590 nm, respectively.

The above studies were based on batch procedures, which need a lot of time, reagents and labour. However, so far flow-injection analysis (FIA) does not seem to have been used for the spectrophotometric determination of carbaryl.

The advantages of the automated FIA procedures, in order to save time and consumables in spectrophotometric measurements and to improve their selectivity [31–34], could be of interest in improving the determination of carbaryl.

Attempts have been made to develop FIA–spectrophotometric procedures for the determination of carbamate pesticides with on-line reaction with *p*-aminophenol (PAP), and encouraging results were obtained for the determination of propoxur [35].

This paper describes a FIA–spectrophotometric method for the determination of carbaryl and 1-naphthol in natural waters. The method is based on the alkaline hydrolysis of carbaryl, at room temperature, to yield 1-naphthol, which is coupled with PAP in an appropriate medium to produce a blue species that can be measured spectrophotometrically at 596 nm.

The developed method can be used for the analysis of real water samples after a previous liquid–liquid extraction with xylene and back-extraction with 0.2 M NaOH, which has the additional advantage of providing the complete hydrolysis of carbaryl.

EXPERIMENTAL

Reagents

Carbaryl (purity 99.5%) was obtained from Union Carbide. A stock solution of 15 μg ml^{-1} of carbaryl was prepared by dissolving 0.015 g of the pesticide in distilled water. This solution was kept under laboratory conditions, being highly stable to light, heat and hydrolysis under normal conditions.

p-Aminophenol (PAP) was purchased from Fluka (Buchs, Switzerland). A working standard solution of 50 μg ml^{-1} was freshly prepared by dissolving 0.025 g of PAP in 500 ml of boiled and cooled distilled water. This solution is stable for more than 8 h.

1-Naphthol and 2-Naphthol were obtained from Aldrich Chemie (Steinheim, Germany). Stock standard solutions were prepared by dissolving 0.01 g of each compound in 100 ml of distilled water, then 50 ml of each solution was diluted to 100 ml with distilled water in order to obtain a concentration of 50 μg ml^{-1}. An ultrasonic water-bath was used in all preparations to ensure the dissolution of the mentioned compounds in water.

Potassium metaperiodate and sodium hydroxide were purchased from Probus (Barcelona). A stock standard solution of potassium metaperiodate was prepared by dissolving 2.1 g in 500 ml of distilled water and then a 0.004 M KIO_4 solution was obtained by dilution with water. A 1 M stock standard solution of sodium hydroxide was prepared from the analytical-grade substance. Xylene solvent was purified by distillation of the technical-grade reagent. The fraction distilling between 138 and 142°C was collected and was used in the recommended liquid–liquid extraction procedure.

Apparatus

A Hewlett-Packard (HP) Model 8452 A diode-array spectrophotometer equipped with HP 89530 A MS-DOS UV–Visible software, with a response time of 0.1 s, was used for spectrophotometric determinations. A flow cell of 50 μl internal volume and 1 cm path length was used for absorbance measurements.

A Gilson P2 Minipuls peristaltic pump was used to transport the carrier solutions. A PTFE Type 50 injection valve (Rheodyne) was employed to provide appropriate injection volumes of the standard solutions and samples.

A four-channel flow manifold (Fig. 1) was used for the FIA–spectrophotometric determination of

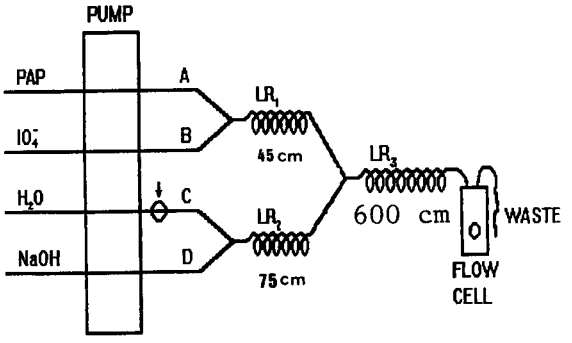

Fig. 1. FIA manifold used for the on-line oxidation of PAP, hydrolysis of carbaryl to 1-naphthol and reaction between the quinoneimine form of PAP and 1-naphthol.

carbaryl and 1-naphthol. Channel A was used to transport PAP solution, channel B to transport potassium metaperiodate solution, channel C for the introduction of samples and standards and channel D to transport sodium hydroxide solution. Channels A and B were connected by a Y-shaped merging zone in order to provide good mixing between PAP and periodate. Similar connection was made for channels C and D and to join all the channels before the measurement zone.

Flexible poly(vinyl chloride) tubes of 1.52 mm i.d. were used to provide a flow-rate of 4 ml min^{-1} in each channel.

A reaction coil of 45 cm (LR1) permits the quinoneimine form of PAP resulting from the oxidation of PAP by potassium metaperiodate to be obtained. An LR2 coil of length 75 cm ensures complete alkaline hydrolysis of carbaryl to 1-naphthol and at the same time provides an appropriate alkaline medium for the reaction between the quinoneimine and 1-naphthol. An LR3 reaction coil of length 600 cm was used to carry out the above-mentioned reaction in order to produce the indophenoldye, which was measured at 596 nm.

All the reaction coils used in the manifold were made of Teflon with an i.d. of 0.8 mm.

Preparation of environmental samples

Real irrigation, tap and well water samples were collected from different sources (minimum volume 500 ml) and spiked with several known amounts of carbaryl and 1-naphthol as stock solutions.

Extraction method

A 20-ml volume of the spiked sample was transfered into a 100-ml separating funnel and the insecticide was extracted with 10 ml of xylene by shaking for 10 min, then the two phases were allowed to separate. The aqueous phase was discarded, 5 ml of the xylene extract were transferred into another 100-ml separating funnel, 10 ml of 0.2 M sodium hydroxide were added and the mixture was shaken for 10 min and allowed to separate. The lower aqueous alkaline phase was taken for direct analysis.

RESULTS AND DISCUSSION

Hydrolysis of carbaryl

Figure 2a shows the UV spectrum of 2.5 μg ml^{-1} carbaryl in distilled water, indicating two

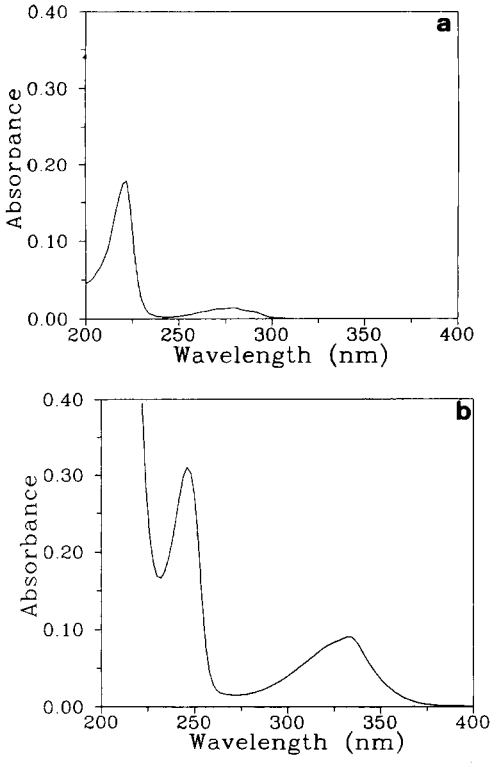

Fig. 2. UV absorption spectra of (a) 2.5 μg ml^{-1} carbaryl in distilled water and (b) the same concentration of carbaryl hydrolysed to 1-naphthol in 0.02 M NaOH.

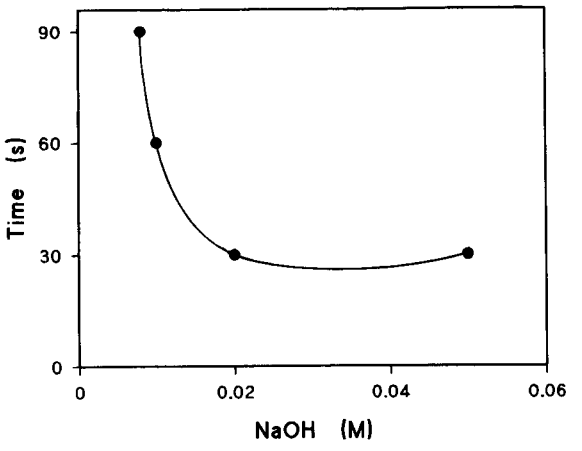

Fig. 3. Effect of sodium hydroxide concentration on the time required for the total hydrolysis of a 5 μg ml^{-1} solution of carbaryl.

absorption bands with maxima at 222 and 280 nm. Although it was mentioned that carbaryl is stable to light, heat and hydrolysis under normal conditions [1], 1-naphthol is obtained by the alkaline hydrolysis of the pesticide. Therefore, the effect of sodium hydroxide concentrations (from 0.008 to 0.05 M) on carbaryl hydrolysis was studied. The results show that carbaryl has a great tendency to hydrolyse to 1-naphthol even in highly diluted concentrations of sodium hydroxide, as indicated in Fig. 3, which shows that quantitative hydrolysis of carbaryl can be obtained in only 30 s using sodium hydroxide solutions with concentrations $\geqslant$ 0.02 M. The UV absorption spectrum of 1-naphthol obtained from the carbaryl hydrolysis shows also two absorption bands at 246 and 332 nm, as can be seen in Fig. 2b.

Reaction between 1-naphthol and PAP

It has been mentioned [36] that when PAP (**I**) is oxidized by molecular oxygen or other oxidizing agents in an alkaline medium, it yields a highly reactive benzoquinoneimine (**II**), which easily reacts at the free *para* position of phenols by electrophillic attack to produce **III**. Compound **III** undergoes rapid oxidation to yield a blue indophenol (**IV**), as is indicated in the following reaction scheme suggested by Sastry et al. [29]:

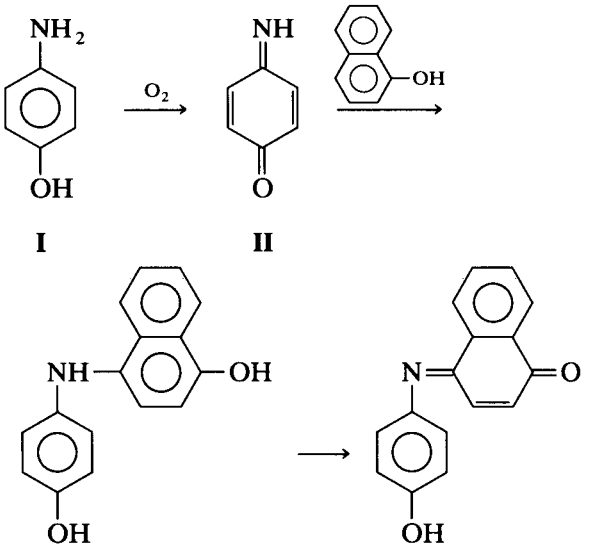

I **II** **III** **IV**

The blue colour of **IV**, which presents an absorption maximum at 596 nm, was developed in the presence of molecular oxygen and also in the presence of 0.004 M KIO_4, using both as oxidizing agents. Figure 4 shows that in the presence of molecular oxygen, the colour develops within the first 9 min and remains constant for more than 6 min, whereas in the presence of potassium metaperiodate the colour develops very rapidly during 1 min and remains stable for 9 min.

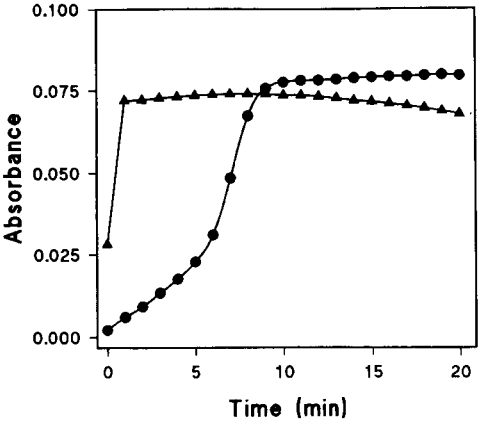

Fig. 4. Variation of the absorbance at 596 nm with time of reaction between 5 μg ml^{-1} carbaryl and 50 μg ml^{-1} PAP in 0.2 M NaOH and in the presence of (●) molecular oxygen and (▲) 0.004 M KIO_4.

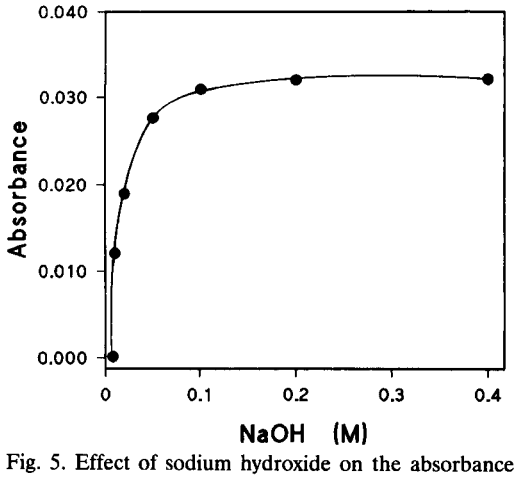

Fig. 5. Effect of sodium hydroxide on the absorbance at 596 nm, using fixed concentrations of 5 μg ml^{-1} carbaryl, 0.004 M KIO_4 and 100 μg ml^{-1} PAP.

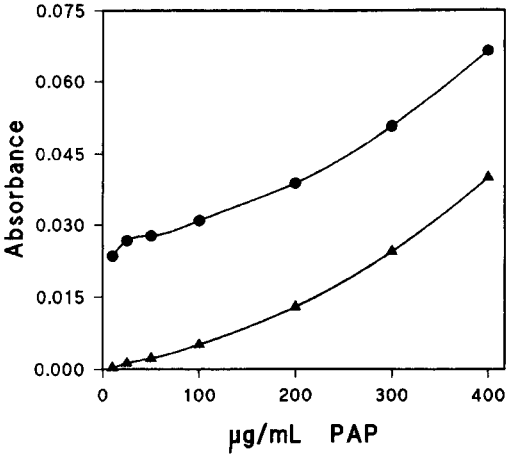

Fig. 6. Effect of PAP concentration on (●) the absorbance at 596 nm and (▲) the baseline for fixed concentration of 5 μg ml^{-1} carbaryl, 0.2 M NaOH and 0.004 M KIO_4.

The above reaction was applied to the flow-injection spectrophotometric determination of carbaryl and 1-naphthol.

Effect of NaOH concentration

Figure 5 shows the effect of sodium hydroxide concentration (from 0.008 to 0.4 M) on the absorbance at 596 nm at a fixed concentration of 0.004 M potassium metaperiodate and 100 μg ml^{-1} PAP. The absorbance increases with increasing concentration of NaOH up to 0.2 M, then remains constant.

Effect of PAP

The effect of PAP concentration (from 10 to 400 μg ml^{-1}) at fixed concentrations of 0.004 M KIO_4 and 0.02 M NaOH is shown in Fig. 6. With increasing PAP concentration high absorbance values can be obtained, but at the same time the baseline increases owing to the degradation of the excess of PAP added. Therefore, a concentration of 50 μg ml^{-1} PAP was used, which provides a low residual baseline absorption and good possibilities of measuring low concentrations of carbaryl.

Effect of FIA parameters

The effect of the flow-rate of the carrier streams (from 2 to 4 ml min^{-1}), length of reactions coils LR_1 (from 0 to 100 cm), LR_2 (from 0 to 200 cm) and LR_3 (From 100 to 1000 cm) and sample volume injected (from 100 to 800 μl) were studied (results not shown). Table 1 summarizes the best conditions of the flow-injection manifold for carrying out the reaction under study.

Figures of merit of the developed procedure

Under the optimum experimental conditions, a typical calibration graph was obtained for concentrations from 1.2 to 6 μg ml^{-1} carbaryl, showing the following regression equation:

$$A = 0.000 + 0.0216C$$

TABLE 1

Recommended conditions for the FIA–spectrophotometric determination of carbaryl with PAP

FIA condition	Value
Flow-rate (in each channel)	4 ml min^{-1}
Injection volume	600 μl
LR_1 length	45 cm
LR_2 length	75 cm
LR_3 length	600 cm
Reagent	**Concentration**
NaOH	0.2 M
KIO_4	0.004 M
PAP	50 μg ml^{-1}

where A = absorbance and $C = \mu g\ ml^{-1}$ 1-naphthol, with a regression coefficient of 0.9999 ($n = 6$). The 3σ [37] limit of detection (LOD) is 26.5 ng ml^{-1} carbaryl, which corresponds to 14.6 ng ml^{-1} 1-naphthol. The standard deviation of four replicate measurements of a solution containing 4.8 $\mu g\ ml^{-1}$ carbaryl was 0.14%.

In a similar manner, another calibration graph obtained for the direct determination of 1-naphthol (from 2 to 8 $\mu g\ ml^{-1}$) was carried out which provided the following regression equation:

$$A = 0.003 + 0.0216C$$

showing a regression coefficient of 0.9999 ($n = 6$) and a 3σ limit of detection of 11.8 ng ml^{-1}. The standard deviation of four replicate measurements of 4 $\mu g\ ml^{-1}$ 1-naphthol was 0.3%. Therefore, the proposed method permits the rapid and accurate spectrophotometric determination of the sum of both carbaryl and 1-naphthol in water samples, especially on using the proposed FIA methodology, which enables more than 110 measurements per hour to be carried out with very good reproducibility.

Figure 7 shows the FIA recordings obtained for a series of standard solutions of carbaryl.

Analysis of synthetic mixtures of 1- and 2-naphthol

A series of synthetic mixtures of 1- and 2-naphthol were prepared in distilled water and measured against a calibration graph for 1-naphthol. Table 2 shows that 2-naphthol does not interfere and high recoveries of 1-naphthol were obtained, because 2-naphthol does not react with PAP. Hence the method can be applied to selective determination of naphthols with a free *para* position.

TABLE 2

FIA–spectrophotometric analysis of synthethic mixtures of 1- and 2-naphthol in distilled water

1-Naphthol added ($\mu g\ ml^{-1}$)	2-Naphthol added ($\mu g\ ml^{-1}$)	1-naphthol found ($\mu g\ ml^{-1}$) [a]
2	4	2.05 ± 0.01
4	2	4.01 ± 0.01
3	3	3.02 ± 0.01
2	8	2.06 ± 0.01

[a] mean ± S.D. ($n = 3$).

Liquid–liquid extraction of carbaryl

The direct determination of carbaryl and 1-naphthol in natural water samples does not provide accurate results owing to the large number of interferences caused by the numerous matrix components. Therefore carbaryl and 1-naphthol were determined after a previous liquid–liquid extraction into xylene. Subsequently, back-extraction in 0.2 M NaOH was carried out, which prevents interference from other organic compounds which may be extracted into the organic

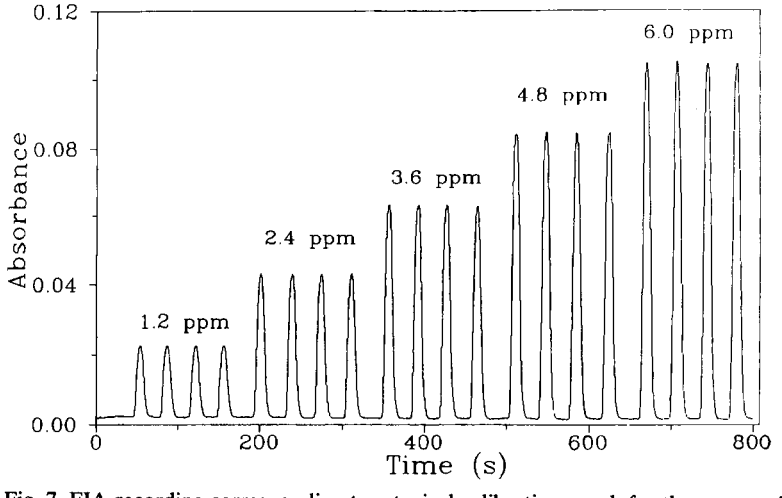

Fig. 7. FIA recording corresponding to a typical calibration graph for the spectrophotometric determination of carbaryl with PAP. Concentrations on peaks in $\mu g\ ml^{-1}$.

phase. In this case the FIA manifold can be simplified because carbaryl is already hydrolysed to 1-naphthol by the back-extraction process with NaOH and so a three-channel manifold can be used.

The extraction method provides a very good extraction yield because both carbaryl and 1-naphthol are highly soluble in xylene and slightly soluble in water. On the other hand, carbaryl is easily hydrolysed in the alkaline medium and this permits the back-extraction of both carbaryl and 1-naphthol from xylene into the alkaline aqueous phase as naphtholate.

The extraction method seems to be very rapid compared with other reported methods and does not require costly high-purity solvents. Also, it avoids other clean-up steps.

Analysis of spiked water samples

To confirm the applicability of the proposed method and the extraction method for the determination of carbaryl and 1-naphthol, three types of natural water obtained from different sources (irrigation, tap and well water) were fortified with different concentrations of carbaryl or with mixtures of carbaryl and 1-naphthol. The spiked samples were extracted and analysed by the recommended method. The results presented in Table 3 demonstrate the performance of extraction and measurement of low concentrations of carbaryl added to real water samples, providing recoveries of 98–101% for tap-water, 97.4% for well water and 98% for irrigation water.

TABLE 3

Recovery of carbaryl added to real water samples

Sample	Carbaryl added (μg ml^{-1})	Carbaryl found (μg ml^{-1})	Recovery (%)	R.S.D. [a] (%)
Tap water	0.5	0.505	101	1.2
	1	0.98	98	3.1
Well water	1	0.974	97	–
	2	1.947	97	0.4
Irrigation	2	1.964	98	0.3
water	3	2.950	98	0.1

[a] Relative standard deviation ($n = 3$).

TABLE 4

Recovery of carbaryl and 1-naphthol added to irrigation water

Carbaryl added (μg ml^{-1})	1-Naphthol added (μg ml^{-1})	Total amount of 1-naphthol added (μg ml^{-1})	1-Naphthol found (μg ml^{-1}) [a]	Recovery (%)
1.398	1.00	2.00	1.901 ± 0.004	95
2.795	2.00	4.00	3.83 ± 0.02	96
1.398	5.00	6.00	6.14 ± 0.05	102
5.589	4.00	8.00	7.78 ± 0.01	97

[a] Mean ± S.D. ($n = 3$).

Another series of spiked samples were prepared from irrigation water by adding different amounts of carbaryl and 1-naphthol. The spiked samples were extracted and measured by the proposed method against a calibration graph obtained from carbaryl standard. Table 4 recoveries of 95–102% of the total 1-naphthol.

The calibration equation obtained for carbaryl standards was

$$A = 0.000_1 + 0.0223C$$

where $C = \mu$g ml^{-1} 1-naphthol ($r = 0.9999$; $n = 6$), which is very similar to that obtained with the extracted carbaryl and 1-naphthol from the irrigation water, which shows the following regression line, $A = -0.000_1 + 0.0221C$ ($r = 0.9989$; $n = 6$). Therefore, it can be seen that both the hydrolysis of carbaryl to 1-naphthol and the extraction procedure are quantitative.

Conclusions

The FIA–spectrophotometric method developed for the determination of the total concentration of carbaryl and its hydrolysis product 1-naphthol in natural waters is simple and provides considerable saving in terms of labour and time. The only disadvantage is the impossibility of determining carbaryl and 1-naphthol separately in the same sample owing to the tendency of carbaryl to hydrolyse to 1-naphthol in the alkaline medium which is essential for carrying out the reaction between PAP and 1-naphthol.

The developed procedure, compared with the batch method [29], offers the advantages of the

automated procedures and provides a better recovery (between 95 and 102% compared with 83.89–98.6% for the batch method). The precision of the procedure (average relative standard deviation 1.02%) is also better than that reported for the batch procedure (1.58%). Further, the limit of detection (26.5 ng ml^{-1}) is better than that reported (ca. 800 ng ml^{-1}). Also, the extraction with xylene and back-extraction with NaOH avoids the tedious double extraction with $CHCl_3$ and evaporation of the solvent as recommended by Sastry et al. [29] for water analysis. The rapid hydrolysis of carbaryl, at room temperature, permits carbaryl to be determined selectively in the presence of propoxur [35], because the latter pesticide requires more than 6 min for total hydrolysis in 0.02 M NaOH compared with the high hydrolysis yield obtained for carbaryl in 1 min.

Karim D. Khalaf thanks the Spanish Institute of International Cooperation for financial support to carry out PhD studies in Spain.

REFERENCES

1 H. Martin and C.R. Worthing, Pesticide Manual, British Crop Protection Council, Nottingham, 5th edn., 1976.
2 M.C. Quintero, M. Silva and D. Perez-Bendito, Talanta, 35 (1988) 943.
3 R. Elespura, W. Lijinsky and J.K. Seltow, Nature, 247 (1974) 386.
4 M. Uchiyama, Bull, Environ. Contam. Toxicol., 14 (1974) 589.
5 J. Seifert and J.E. Casida, Biochem. Pharmacol., 27 (1978) 2611.
6 R.J. Bushway, J. Chromatogr., 211 (981) 135.
7 R.E. Gosselin, S.R. Powell, H.C. Hodge, R.P. Smith and M.V. Gleaon, Clinical Toxicology of Commercial Products, Williams and Wilkins, Baltimore, 4th edn., 1976, Sect. III, p. 79.
8 H.A. Stansbury and R. Miskus, in G. Zweig (Ed.), Analytical Methods for Pesticides, Plant Regulators and Food Aditives, Vol. 2, Academic, New York, 1976, p. 438.
9 M. Chiba and H.V. Morely, J. Assoc. Off. Agric. Chem., 47 (1964) 667.
10 G.F. Ernst, S.J. Roder, G.H. Tjan and J.T.A. Jansen, J. Assoc. Off. Anal. Chem., 58 (1975) 1015.
11 C.E. Mendoza, D.L. Grant, B. Braceland and K.A. McCully, Analyst, 9 (1969) 805.
12 O. Wueest and W. Meier, Z. Lebensm.-Unters.-Forsch., 177 (1983) 25.
13 M.D. Osselton and R.D. Snelling, J. Chromatogr., 368 (1986) 265.
14 S. Sakaue, Agric. Biol. Chem., 51 (1987) 1239.
15 M.C. Pietrogrande, G. Blo and C. Bighi, J. Chromatogr., 349 (1985) 63.
16 T.D. Spittle, R.A. Marafioti, G.W. Helfman and R.A. Morse, J. Chromatogr., 352 (1986) 439.
17 R.T. Krause, J. Assoc. Off. Anal. Chem., 63 (1980) 1114.
18 R.T. Krause and E.M. Agust, J. Assoc. Off. Anal. Chem., 66 (1983) 234.
19 M. Deberardinis and W.A. Wargin, J. Chromatogr., 246 (1982) 89.
20 B.D. McGarvey, J. Chromatogr., 481 (1989) 445.
21 J.G. Brayan, P.R. Haddad, G.T. Sharp and S. Dilli, J. Chromatogr., 447 (1988) 249.
22 R.T. Krause, J. Chromatogr., 442 (1988) 333.
23 F. Garcia-Sanchez and C. Cruces-Blanco, Talanta, 37 (1990) 573.
24 J. Sancenón, J.L. Carrión and M. de la Guardia, Fresenius' J. Anal. Chem., 336 (1990) 389.
25 J. Sancenón, J.L. Carrión and M. de la Guardia, Talanta, 36 (1989) 1165.
26 M.C. Quintero, M. Silva and D. Perez-Bendito, Talanta, 36 (1989) 717.
27 K.M. Appaiah, R. Ramakrishna, R.R. Sabbarao and O. Kapur, J. Assoc. Off. Anal. Chem., 65 (1982) 32.
28 C.S.P. Sastry and D. Vijaya, Talanta, 34 (1987) 372.
29 C.S.P. Sastry, D. Vijaya and D.S. Mangala, Analyst, 112 (1987) 75.
30 R. Miskus, H.T. Gordon and D.A. George, J. Agric. Food Chem., 7 (1959) 613.
31 M. Valcarcel and M.D. Luque de Castro, Flow Injection Analysis. Principles and Applications, Horwood, Chichester, 1987.
32 J. Ruzicka and E.H. Hansen (Eds.), Flow Injection Analysis, Wiley, New York, 2nd edn., 1988.
33 G.D. Christian and J. Ruzicka, Anal. Chim. Acta, 261 (1992) 11.
34 I. Lukkari and W. Lindberg, Anal. Chim. Acta, 211 (1988) 1.
35 K.-D. Khalaf, J. Sancenón and M. de la Guardia, Anal. Chim. Acta, 266 (1992) 119.
36 K.C. Brown, J.F. Corbett and R. Labinson, J. Chem. Soc., Perkin Trans. 2, (1978) 1292.
37 IUPAC, Anal. Chem., 48 (1976) 2294.

Analytica Chimica Acta, 280 (1993) 239–244
Elsevier Science Publishers B.V., Amsterdam

Electrospray mass spectrometry of zinc dithiophosphate derivatives and its application to the analysis of engine oil antiwear additives

Terence J. Cardwell, Ray Colton, Nick Lambropoulos and John C. Traeger

Department of Chemistry, La Trobe University, Bundoora, Victoria 3083 (Australia)

Philip J. Marriott

Department of Applied Chemistry, Royal Melbourne Institute of Technology, Melbourne (Australia)

(Received 2nd December 1992; revised manuscript received 15th February 1993)

Abstract

Electrospray mass spectrometry (ES-MS) has been applied to a variety of zinc *O,O'*-dialkyldithiophosphate (DTP) derivatives. The neutral $Zn(DTP)_2$ compounds were converted to the $[Zn(DTP)_3]^-$ anions by reaction with excess DTP^- and these principal anions are readily observed by ES-MS. Exchange reactions between two different zinc tris(DTP) anions leads to the simultaneous observation of zinc anions containing all possible combinations of ligands even though the species in solution are exchanging rapidly on the NMR timescale. Similar mass spectra are observed upon mixing $Zn(DTP)_2$ with a different DTP^- anion. Reaction of $Zn(DTP)_2$ with dimethylsulfoxide (DMSO) in methanol solution gives $[Zn(DTP)(DMSO)_{1,2}]^+$ and free DTP^- ions which are observed in the positive ion and negative ion ES mass spectra respectively. This latter reaction provides a convenient method for the characterisation and qualitative analysis of engine oil inhibitor and antiwear additives, which contain zinc dithiophosphates with alkyl and aryl substituents.

Keywords: Mass spectrometry; Antiwear additives; Engine oils; Zinc dithiophosphate

Electrospray mass spectrometry (ES-MS) provides a new method of transferring pre-existing ions from solution to the gas phase. The transfer is very soft and causes minimal fragmentation. ES-MS is now a well established technique in the structural analysis of large biomolecules such as proteins [1–3]. However, although the biochemical applications demonstrate that ES-MS links solution and gas phase studies, the technique has not yet been widely applied in a systematic manner to inorganic and organometallic systems.

Correspondence to: R. Colton, Department of Chemistry, La Trobe University, Bundoora, Victoria 3083 (Australia).

We have recently been investigating the use of ES-MS on a range of charged inorganic and organometallic compounds [4–8]. A feature of these studies is that the principal ions are always observed, often as the only significant peak in the mass spectrum, emphasising the soft nature of the process generating the gas phase ions. In the case of very labile species, such as $[Cu(PPh_3)_3]^+$ [8], daughter ions, formed by collisional activation within the electrospray ion source, are also observed. ES mass spectrometry reveals all the components of a system such as $[Cu(PPh_3)_x(PR_3)_{3-x}]^+$ (PR_3 = monodentate phosphine) in which the ligands are exchanging in solution at a rate which is fast on the NMR timescale [8].

The tetrahedral zinc dithiophosphates, $Zn[S_2P(OR)_2]_2$, $[Zn(DTP)_2]$, are widely used as additives to engine oils as inhibitors and antiwear agents. They readily react with excess dithiophosphate anion (DTP^-) to give the tris(dithiophosphate) anions $[Zn(DTP)_3]^-$ [9] and similar species are known with phosphinate (S_2PR_2) ligands [10]. In the solid state the zinc atom in these anions is essentially tetrahedrally coordinated by one bidentate and two monodentate ligands.

In this paper we describe the use of ES-MS in the study of zinc dithiophosphates and then apply the technique to the analysis of some engine oil additives. The neutral $Zn(DTP)_2$ compounds cannot be observed by ES-MS, but reactions with excess dithiophosphate ion or dimethylsulfoxide (DMSO) give ionic products which can be investigated by the technique.

EXPERIMENTAL

The zinc dialkyldithiophosphates were prepared by slight variations of standard methods [11–13] in which phosphorus pentasulfide was reacted with the appropriate alcohol. After evolution of H_2S had ceased dry ammonia was bubbled through the solution and the ammonium salt of the dithiophosphate was precipitated with ether. Excess zinc acetate was reacted with the ammonium salt in the appropriate alcohol and after gentle heating the solution was evaporated almost to dryness. The residue was dissolved in dichloromethane and the solution filtered and washed with the alcohol. After evaporation to dryness the solid was recrystallised from dichloromethane.

Electrospray mass spectra were recorded by using a VG Bio-Q triple quadrupole mass spectrometer (VG Bio-Tech, Altrincham) [14] with a water–methanol–acetic acid mobile phase. The zinc dithiophosphates or engine oil additives were dissolved in methanol (2 mM) and the appropriate reagent (DTP^- or DMSO) was added. The solution was then diluted 1:10 with methanol. The diluted solution was injected directly into the spectrometer via a Rheodyne injector using a Phoenix 20 micro LC syringe pump to deliver the solution to the vaporisation nozzle of the electrospray ion source at a flow-rate of 3 μl min^{-1}. Voltages at the first skimming electrode (B1) were varied between 80 V and the minimum possible consistent with retaining a stable ion jet. This varies from time to time but is usually in the range 25–30 V. Increasing the B1 voltage enhances the formation of daughter ions by collisions with solvent molecules within the ion source.

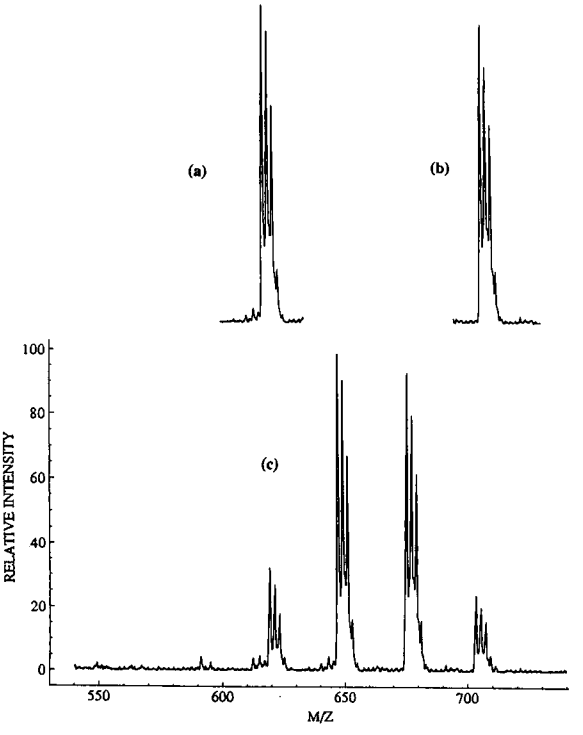

Fig. 1. Negative ion ES mass spectra of (a) $[Zn(Et_2DTP)_3]^-$, (b) $[Zn(Pr_2DTP)_3]^-$, (c) a mixture of $[Zn(Et_2DTP)_3]^-$ and $[Zn(Pr_2DTP)_3]^-$.

RESULTS AND DISCUSSION

Throughout this paper ions in the electrospray mass spectra will be identified by the m/z value for the most intense peak in the isotope mass distribution. In all cases the experimental and calculated isotopic mass distributions agreed well.

Zinc dithiophosphates

Figure 1a shows the negative ion ES mass spectrum of an approximately 0.2 mM methanol

TABLE 1

Electrospray mass spectra of zinc dithiophosphate anions

Compound	Principal anions (m/z)
$Zn(Et_2DTP)_2 + [Et_2DTP]^-$	$[Zn(Et_2DTP)_3]^-$ (619)
	$[Zn(Et_2DTP)_2(OAc)]^-$ (493), (476), (460)
$Zn(Pr_2DTP)_2 + [Pr_2DTP]^-$	$[Zn(Pr_2DTP)_3]^-$ (703)
	$[Zn(Pr_2DTP)_2(OAc)]^-$ (549), (532), (460)
$[Zn(Et_2DTP)_3]^- + [Zn(Pr_2DTP)_3]^-$	$[Zn(Pr_2DTP)_3]^-$ (703),
	$[Zn(Pr_2DTP)_2(Et_2DTP)]^-$ (675)
	$[Zn(Pr_2DTP)(Et_2DTP)_2]^-$ (647)
	$[Zn(Et_2DTP)_3]^-$ (619)
$Zn(Et_2DTP)_2 + [Bu_2DTP]^-$	$[Zn(Bu_2DTP)_3]^-$ (787),
	$[Zn(Bu_2DTP)_2(Et_2DTP)]^-$ (731)
	$[Zn(Bu_2DTP)(Et_2DTP)_2]^-$ (675)
	$[Zn(Et_2DTP)_3]^-$ (619)
$Zn(Pr_2DTP)_2 + [Me_2DTP]^-$	$[Zn(Pr_2DTP)_3]^-$ (703),
	$[Zn(Pr_2DTP)_2(Me_2DTP)]^-$ (647)
	$[Zn(Pr_2DTP)(Me_2DTP)_2]^-$ (591)
	$[Zn(Me_2DTP)_3]^-$ (535)

solution of $Zn(Et_2DTP)_2$ with excess $[Et_2DTP]^-$. The peak is due to the principal ion $[Zn(Et_2DTP)_3]^-$ (m/z 619). At lower m/z values there is a much weaker peak due to $[Zn(Et_2DTP)_2(OAc)]^-$ (m/z 493), the acetate being derived from the mobile phase in the spectrometer, and two other weak peaks at m/z 476 and 460 due to unidentified single charge anions containing zinc. No evidence was found for the species $[Zn(Et_2DTP)_4]^{2-}$. Figure 1b shows a similar ES mass spectrum for a solution containing $Zn(i\text{-}Pr_2DTP)_2$ and excess $[i\text{-}Pr_2DTP]^-$. Once again the mass spectrum is dominated by the peak due to the principal ion $[Zn(Pr_2DTP)_3]^-$, but as before there are weak peaks due to $[Zn(Pr_2DTP)_2(OAc)]^-$ (m/z 549) and the corresponding unidentified cations at m/z 532 and 516. Figure 1c shows the ES mass spectrum of the solution resulting from mixing the two tris(dithiophosphate) zinc anions. The four peaks correspond to zinc anions with all the possible combinations of dithiophosphate ligand, that is the original two species together with $[Zn(Et_2DTP)(Pr_2DTP)_2]^-$ (m/z 675) and $[Zn(Et_2DTP)_2(Pr_2DTP)]^-$ (m/z 647) in the statistical proportions. This mass spectrum shows that the zinc tris(dithiophosphate) anions completely exchange ligands on the timescale of some minutes, but in fact the ^{31}P NMR spectrum shows that they exchange rapidly on the NMR timescale

TABLE 2

Electrospray mass spectra of ions derived from zinc dithiophosphates by reaction with DMSO

Mixture	Principal cations (m/z)	Principal anions (m/z)
$Zn(Et_2DTP)_2$ + DMSO	$[Zn(Et_2DTP)(DMSO)_2]^+$ (405)	$[Et_2DTP]^-$ (185)
	$[Zn(Et_2DTP)(DMSO)]^+$ (327)	
	$[Zn(OAc)(DMSO)_2]^+$ (279)	
	$[Zn(OAc)(DMSO)]^+$ (201)	
$Zn(Pr_2DTP)_2$ + DMSO	$[Zn(Pr_2DTP)(DMSO)_2]^+$ (433)	$[Pr_2DTP]^-$ (213)
	$[Zn(Pr_2DTP)(DMSO)]^+$ (355)	
	$[Zn(OAc)(DMSO)_2]^+$ (279)	
	$[Zn(OAc)(DMSO)]^+$ (201)	

since only an average signal is seen for each dithiophosphate ligand in the mixed solution at room temperature. Thus, these zinc anions provide only the second example illustrating that ES mass spectrometry can be used to study the individual species in a rapidly exchanging inorganic system. The ES technique is successful because the ligand exchange ceases immediately the ions enter the gas phase.

Similar ES mass spectra were obtained for other combinations of dithiophosphate ligands by adding $[Bu_2DTP]^-$ to $Zn(Et_2DTP)_2$ and by adding $[Me_2DTP]^-$ to $Zn(Pr_2DTP)_2$. In all cases the distribution between the mixed ligand anions appears to be statistical. All data for these species are given in Table 1.

When $Zn(DTP)_2$ are reacted with DMSO in methanol at room temperature, peaks are observed in both the positive and negative ion modes. All data are given in Table 2. According to the ion source energy used, either or both of $[Zn(DTP)(DMSO)_2]^+$ and $[Zn(DTP)(DMSO)]^+$ are observed in the positive ion mass spectrum. Energies are varied by altering the voltage on the first skimming electrode (B1). At low ion source energies (B1 = 30 V) only $[Zn(DTP)(DMSO)_2]^+$ is observed, while at higher energies (B1 = 80 V) only $[Zn(DTP)(DMSO)]^+$ is seen. At intermediate energies both ions are observed. At higher voltages collisional activation with solvent molecules in the vicinity of the evaporation nozzle in the ion source (where the pressure is atmospheric) leads to increased formation of $[Zn(DTP)(DMSO)]^+$ showing that the bis(DMSO) cation is labile. Also at the lower ion source energies a weak peak is observed due to $[Zn(OAc)(DMSO)_2]^+$ and at higher energies $[Zn(OAc)(DMSO]^+$ appears. In the negative ion ES mass spectrum the free DTP^- ion is observed. The overall reaction is therefore

$$Zn(DTP)_2 + 2DMSO \rightleftharpoons [Zn(DTP)(DMSO)_2]^+ + DTP^-$$

and this provides a convenient method of analysis for materials containing zinc dithiophosphates and similar compounds.

TABLE 3

Electrospray mass spectra derived from reaction of engine oil additives with DMSO

Sample	Principal ions (m/z)	
Sample 1 + DMSO	Cations:	$[Zn(Hx_2DTP)(DMSO)_2]^+$ (517), $[Zn(Hx_2DTP)(DMSO)_2]^+$ (439)
	Anion:	$[Hx_2DTP]^-$ (297)
Sample 2 + DMSO	Cations:	$[Zn(Hx_2DTP)(DMSO)_2]^+$ (517), $[Zn(PrHxDTP)(DMSO)_2]^+$ (475), $[Zn(Hx_2DTP)(DMSO)]^+$ (439), $[Zn(Pr_2DTP)(DMSO)_2]^+$ (433), $[Zn(PrHxDTP)(DMSO)]^+$ (397), $[Zn(Pr_2DTP)(DMSO)]^+$ (355)
	Anions:	$[Hx_2DTP]^-$ (297), $[PrHxDTP]^-$ (255), $[Pr_2DTP]^-$ (213)

Analysis of engine oil additives

Three commercial engine oil additives were examined for their zinc dithiophosphate constituents by ES-MS using the DMSO method. When sample 1 was dissolved in methanol and DMSO added, the negative ion ES mass spectrum showed only one significant peak at m/z 297, corresponding to $[S_2P(OC_6H_{13})_2]^-$, $[Hx_2DTP]^-$. The positive ion ES mass spectrum exhibited peaks at m/z 517 and 439 which correspond to $[Zn(Hx_2DTP)(DMSO)_2]^+$ and $[Zn(Hx_2DTP)(DMSO)]^+$ respectively. ES-MS cannot distinguish between isomers of C_6H_{13} but the mass spectrum clearly indicates that a single alcohol was used to manufacture the dithiophosphate (compare with next samples). All data are given in Table 3.

After dissolution in methanol and addition of DMSO, the negative ion ES mass spectrum of sample 2 showed three peaks due to liberated DTP^- anions at m/z values of 213, 255 and 297. The lowest and highest values correspond to $[Pr_2DTP]^-$ and $[Hx_2DTP]^-$ respectively (Pr = C_3H_7 and Hx = C_6H_{13}) whilst the peak at m/z 255 corresponds to $[PrHxDTP]^-$. Thus this mixture of zinc dithiophosphates appears to have been manufactured from a mixture of propyl and hexyl alcohols in the approximate proportions of 40:60. The positive ion ES mass spectrum of the same solution shows peaks for both $[Zn(DTP)(DMSO)_2]^+$ and $[Zn(DTP)(DMSO)]^+$ for

each DTP^- anion, a total of six peaks altogether. All data are given in Table 3.

Upon reaction of sample 3 with DMSO in methanol both the positive and negative ion ES mass spectra reveal a complex mixture of dithiophosphates based upon aryl alcohols. Figure 2a shows the negative ion ES mass spectrum and the strongest peak at m/z 617 corresponds to $[S_2P\{OC_6H_4(C_{12}H_{25})_2\}_2]^-$. The peaks between m/z 477 and 659 are separated by 14 mass units, corresponding to a CH_2 group, and arise because a mixture of alcohols each differing by CH_2 in the side chain was used in the preparation of the dithiophosphates. In the data given in Table 4, the ions are listed by the sum of the two R groups in $[S_2P(OC_6H_4R)(OC_6H_4R')]^-$ because the ES mass spectrum cannot distinguish between different pairs of R groups giving the same mass. Thus the peak at m/z 617 is listed as $RR' = C_{24}H_{50}$,

TABLE 4

Electrospray mass spectra derived from reaction of engine oil additive (sample 3) with DMSO

$(R+R')$ in $[S_2P(OC_6H_4R)(OC_6H_4R')]^-$	Principal anion (m/z)	Principal cation (m/z)
$C_{14}H_{30}$	477	697
$C_{15}H_{32}$	491	711
$C_{16}H_{34}$	505	725
$C_{17}H_{36}$	519	739
$C_{18}H_{38}$	533	753
$C_{19}H_{40}$	547	767
$C_{20}H_{42}$	561	781
$C_{21}H_{44}$	575	795
$C_{22}H_{46}$	589	809
$C_{23}H_{48}$	603	823
$C_{24}H_{50}$	617	837
$C_{25}H_{52}$	631	851
$C_{26}H_{54}$	646	867
$C_{27}H_{56}$	659	879

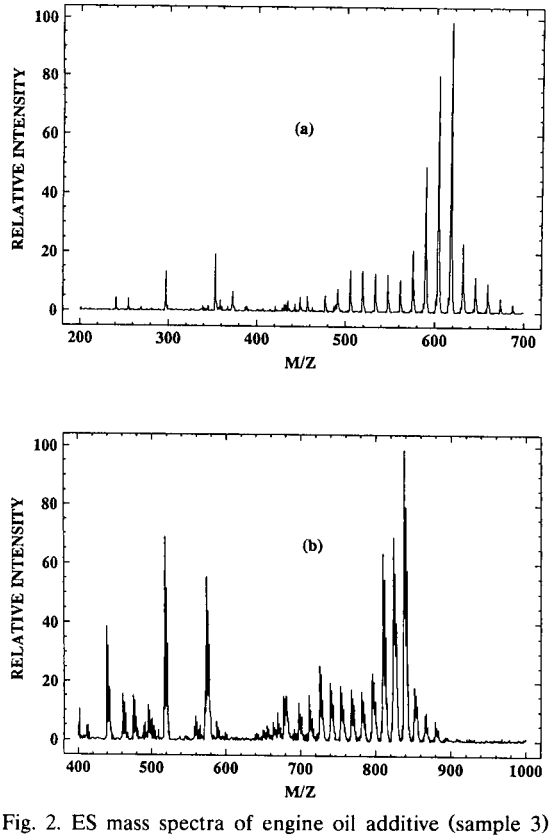

Fig. 2. ES mass spectra of engine oil additive (sample 3) in methanol after addition of DMSO. (a) negative ion ES mass spectrum, (b) positive ion ES mass spectrum.

which is predominantly due to $2(C_{12}H_{25})$ but there are contributions from $(C_{11}H_{23} + C_{13}H_{27})$, etc. The distribution shows that the major fraction of the alcohol was the one with the C_{12} side chain, but there was a significant amount of the C_{11} alcohol and small amounts of other alcohols with side chains between C_7 and C_{14}. Besides this family of peaks there are also two significant peaks at m/z 353 and 297 and a smaller one at m/z 241 which correspond to the aliphatic dithiophosphates $[S_2P(OC_8H_{17})_2]^-$, $[S_2P(OC_6H_{13})_2]^-$ and $[S_2P(OC_4H_9)_2]^-$ respectively. Figure 2b shows the positive ion ES mass spectrum for the ions $[Zn(DTP)(DMSO)_2]^+$ for the same solution. Upon expansion all of the peaks reveal the characteristic zinc isotope pattern. It is immediately obvious that for the aryl dithiophosphate derivatives the composition distribution is very similar to that observed for the anions, and in fact the two spectra are entirely equivalent as shown in Table 4. The shapes of the peaks in the region below m/z 800 are slightly distorted on the high mass side because of the presence of small amounts of $[Zn(DTP)(DMSO)]^+$ from the higher dithiophosphate derivatives. This assignment was confirmed by examining the spectra at

a higher ion source energy which accentuates these cations as described above.

The cations derived from the aliphatic dithiophosphates give very intense peaks compared with those observed in the negative ion spectrum. We believe this may be related to solubility effects since this particular sample dissolved only with difficulty and the final product appeared to be an emulsion. The simple aliphatic zinc dithiophosphates examined in the earlier part of this paper are all readily soluble, so it is the aryl derivatives which are less soluble and this might lead to decreased sensitivity in the ES mass spectrometer.

At this stage of development of ES-MS applied to inorganic systems, the technique is not a quantitative measure of concentrations. It has already been noted [5,8] that for spectra showing several ions which differ in charge or are labile, then the relative sizes of their peaks varies with the ion source voltage. Indeed, that is also seen in this paper for the $[Zn(DTP)(DMSO)_2]^+$ and $[Zn(DTP)(DMSO)]^+$ cations, and in order to make the technique quantitative spiking of the samples under standard conditions would be necessary. However, there is every reason to suppose that for a series of ions which are similar in mass, charge and structure then the peak heights should be a good measure of the relative proportions of those species in the solution. The fact that similar relative abundance profiles are observed for the aryl dithiophosphate derivatives in both the negative ion spectra (the DTP^- ions themselves, Fig. 2a) and in the positive ion spectra (Zn ions containing the DTP ligands, Fig. 2b) lends considerable support to this proposition, so it is likely that with spiking quantitative studies could be made. It is possible that the markedly different behaviour of the aliphatic dithiophosphates is due to different stabilities in the gas phase, but we favour the explanation based upon solubility differences outlined above.

We thank La Trobe University for a SCAEF grant to assist in the purchase of the electrospray mass spectrometer. TJC, NL and PJM thank the Australian Research Council for financial support.

REFERENCES

1 J.B. Fenn, M. Mann, C.K. Meng, S.F. Wong and C.M. Whitehouse, Science, 246 (1989) 64.
2 R.D. Smith, J.A. Loo, C.G. Edmonds, C.J. Barinaga and H.R. Udseth, Anal. Chem., 62 (1990) 882.
3 R.D. Smith, J.A. Loo, R.R. Ogorzalek Loo, M. Busman and H.R. Udseth, Mass Spectrom. Rev., 10 (1991) 359.
4 R. Colton and J.C. Traeger, Inorg. Chim. Acta, 201 (1992) 153.
5 R. Colton, J.C. Traeger and J. Harvey, Org. Mass Spectrom., 27 (1992) 1030.
6 R. Colton, V. Tedesco and J.C. Traeger, Inorg. Chem. 31 (1992) 3865.
7 I. Ahmed, A.M. Bond, R. Colton, M. Jurcevic, J.C. Traeger and J.N. Walter, J. Organomet. Chem., 447 (1993) 59.
8 R. Colton, B.D. James, I.D. Potter and J.C. Traeger, Inorg. Chem., in press.
9 R.S.Z. Kowalski, N.A. Bailey, R. Mulvaney, H. Adams, D.A. O'Cleirigh and J.A. McCleverty, Trans. Met. Chem., 6 (1981) 64.
10 J.A. McCleverty, R.S.Z. Kowalski, N.A. Bailey, R. Mulvaney and D.A. O'Cleirigh, J. Chem. Soc., Dalton Trans., (1963) 627.
11 V.P. Wystrach, E.O. Hook and G.L.M. Christopher, J. Org. Chem., 21 (1956) 707.
12 J.J. Dickert and C.N. Rowe, J. Org. Chem., 32 (1967) 647.
13 R.G. Cavell, E.D. Day, W. Byers and P.M. Watkins, Inorg. Chem., 11 (1972) 1759.

Analytica Chimica Acta, 280 (1993) 245–251
Elsevier Science Publishers B.V., Amsterdam

Electron impact mass spectral fragmentation patterns of 1-[(2′-carboxyl)pyrrolidinyl]-1-deoxy-D-fructose

Varoujan Yaylayan and Alexis Huyghues-Despointes

Department of Food Science and Agricultural Chemistry, McGill University, Macdonald Campus, 21,111 Lakeshore Road, Ste. Anne de Bellevue, Quebec H9X 1C0 (Canada)

Martine C. Bissonnette and J.R. Jocelyn Paré

Environment Canada, River Road Environmental Technology Centre, Ottawa, Ontario K1A 0H3 (Canada)

(Received 15th December 1992; revised manuscript received 8th February 1993)

Abstract

High resolution, linked-field scan and neutral loss experiments have indicated that 1-[(2′-carboxyl)pyrrolidinyl]-1-deoxy-D-fructose (proline Amadori product) followed two main pathways of fragmentation under electron impact conditions; one initiated by the ring oxygen and the other by the amino acid nitrogen, producing two well stabilized fragment ions; oxonium and imminium ions. In addition, *ortho*-elimination reactions initiated by O- or N-centred radical sites can produce the most intense peaks and diagnostically important ions for the identification of Amadori products.

Keywords: Mass spectrometry; Amadori; 1-[(2′-Carboxyl)pyrrolidinyl]-1-deoxy-D-fructose

The established importance of the decomposition products of 1-(amino acid)-1-deoxy-D-fructoses or Amadori rearrangement products (ARPs) (Scheme 1) in food and biological systems, led us to investigate their fragmentations under high resolution electron impact conditions [1,2]. ARPs are the key intermediates in the non-enzymatic interaction of reducing sugars with amino acid. The process is called non-enzymatic browning or the Maillard reaction [3]. With time, ARPs are decomposed to form various heterocyclic compounds, with important flavour characteristics, and intermediates that can cross-link proteins in food as well as in vivo, thus leading to the toughening of food products and in the case of biological systems, the stiffening of tissue (joint stiffness, atherosclerosis, etc.) symptoms associated with aging. The electron impact fragmentation patterns of ARPs could be a useful tool to predict their thermal degradation products. Such correlation's have been carried out with tryptophan Amadori product [4,5]. In addition it can be used to identify the presence of trace amounts of Amadori products in biological fluids using tandem mass spectrometry (MS–MS) or selected ion monitoring (SIM) techniques.

Previous studies have indicated that the sugar and amino acid moieties trigger the electron impact fragmentations of Amadori products and that in general, the mass spectra of Amadori compounds consisting of two non-interactive moieties (such as Amadori compounds with amino

Correspondence to: V. Yaylayan, Department of Food Science and Agricultural Chemistry, McGill University, Macdonald Campus, 21,111 Lakeshore Road, Ste. Anne de Bellevue, Quebec H9X 1C0 (Canada).

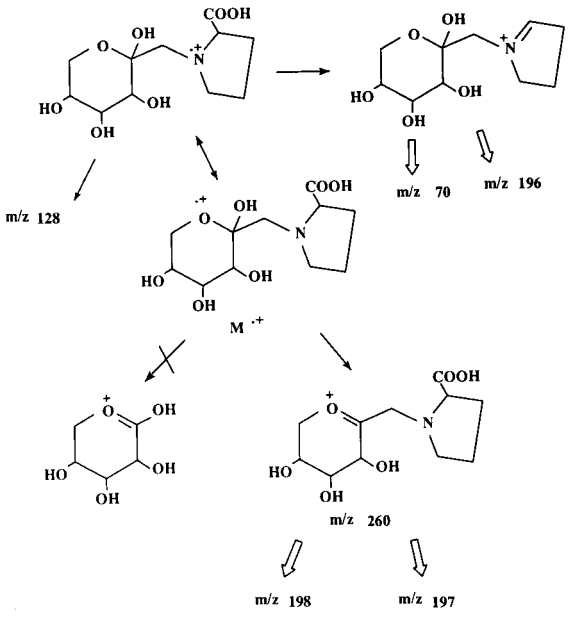

Scheme 1. Formation of oxonium and imminium ions by α-cleavage reactions.

acids containing alkyl side chains) show significant fragmentations characteristic of the two moieties, in addition to specific fragmentations characteristic of the compound. This observation is generally true for compounds in which the two moieties are connected at positions that do not influence markedly the characteristic fragmentations of each group. For example, N-substituted amino acids generally exhibit the same fragmentation pattern as unsubstituted amino acids [6] and C-1 substitution of fructose moiety is not expected to effect the overall mass spectral pattern of the molecule since the main bond fissions during electron impact fragmentation of fructose are governed by the substituents at C-2 and not by the substituents at C-1 [7]. However, for Amadori products containing interactive moieties (such as Amadori compounds of tryptophan or lysine) the predominant feature of their mass spectra are due to the intramolecular cyclization reactions producing β-carboline derivatives in the case of tryptophan ARP [4] and pyrrolidine and piperidine derivatives in the case of lysine [8].

MATERIALS AND METHODS

High resolution experiments

The high resolution electron impact mass spectra were determined on a high resolution double focusing mass spectrometer (MS-50, AEI, Manchester). The ionizing electron energy was 70 eV at a resolving power of 15000 and a source temperature and pressure of 180°C and 2×10^{-7}

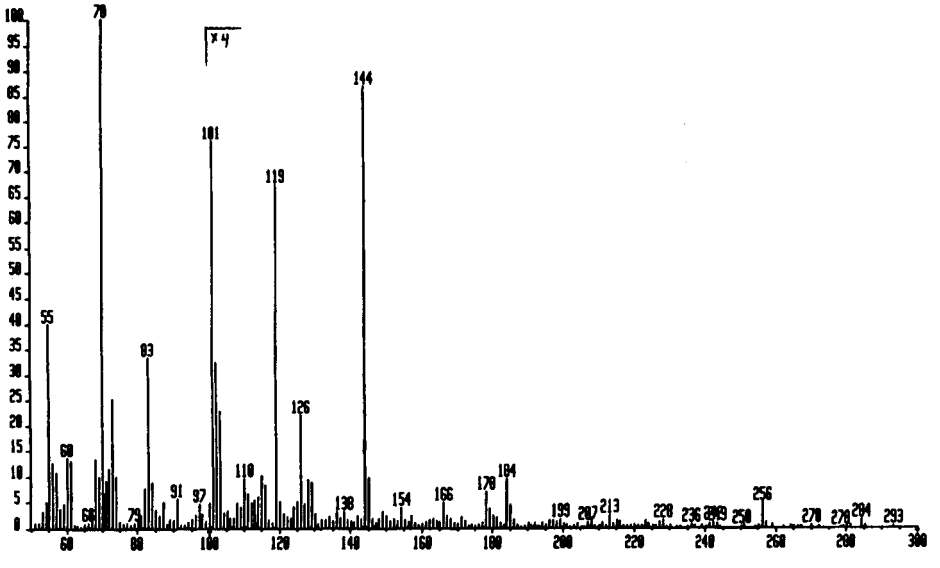

Fig. 1. EI mass spectrum of proline Amadori rearrangement product.

Torr (1 Torr = 133.3 Pa), respectively. The sample was introduced via a direct inlet probe heated to 180°C.

Synthesis of 1-[(2'-carboxyl)pyrrolidinyl]-1-deoxy-D-fructose (Proline Amadori product)

The synthesis was carried out according to published procedure [9].

Linked-scan and neutral loss experiments

Linked-scan experiments on the collision-induced decompositions were performed on a medium resolution mass spectrometer (7070-EHF, VG Analytical, Manchester) that was equipped with a data system (11–250, VG Analytical). The analyses were performed at 70 eV at a resolving power of 1000 and a source temperature and pressure of 180°C and 1×10^{-6} Torr, respectively. The sample was introduced via a direct inlet probe heated to 180°C.

RESULTS AND DISCUSSION

General fragmentation patterns of 1-[(2'-carboxyl)pyrrolidinyl]-1-deoxy-D-fructose

Amadori products can be considered as either N-substituted amino acids or as derivatives of D-fructose, consequently the characteristic fragmentations of amino acids and those of carbohydrates are expected to be found in their mass spectra. Extensive linked-field scan and neutral loss experiments have indicated that 1-[(2'-carboxyl)pyrrolidinyl]-1-deoxy-D-fructose (Proline Amadori product) followed two main pathways of fragmentation under electron impact conditions (see Fig. 1); one initiated by the ring oxygen and the other by the amino acid nitrogen, producing two well stabilized fragment ions; oxonium ions and imminium ions (see Scheme 1).

Funke et al. [10] studied TMS ether derivatives of several Amadori products formed from amines and similarly reported the formation of oxonium and imminium ions as the most prominent peaks in the mass spectra of Amadori compounds. These two parent ions can subsequently undergo secondary fragmentations and thermal dehydration of the sugar ring or thermal decarboxylation of the amino acid moiety. The oxonium ions can be formed by the α-cleavage reactions of the molecular ion centred at the ring oxygen. The α-cleavage of the anomeric hydroxyl group leads to the formation of two key ions m/z 198 and m/z 197. No evidence was found for α-cleavages of C_2–C_1, C_2–C_3 or C_6–O bonds.

Scheme 2 illustrates the formation of m/z 198 and m/z 197 fragment ions from the ion at m/z 259. B/E linked-field scan experiments (see Tables 1 and 2) have indicated that the oxonium ion m/z 260 is the daughter ion of m/z 277 (the molecular ion), that the ions at m/z 241 and 242 are the daughter ions of m/z 259 and that ion m/z 197 is the daughter ion of m/z 241 formed by the neutral loss of 44 a.m.u. (CO_2). This indicates that decarboxylation occurs after two dehydration steps. Similarly the ion at m/z 198 is postulated to be the result of the loss of a CO_2 molecule from ion at m/z 242 as shown in Scheme 2.

On the other hand the imminium ions can be formed by α-cleavage reactions of the molecular

TABLE 1

B/E linked-field scan data of fragment ions of proline Amadori compound with neutral loss confirmations

Precursor ion (m/z)	Corresponding product ions (neutral loss)
241	197 (44)
198	166 (32)
196	178 (18), 166 (30), 154 (42)
180	138 (42)
179	136 (43)
178	160 (18), 150 (28), 136 (42)
166	148 (18), 124 (42)
154	126 [a] (28)
153	126 [a] (27), 110 (43)
145	127 (18), 116 (29), 101 (44)
144	126 (18), 116 (28), 115 (29), 102 (42), 101 (43)
143	101 (42)
138	96 (42)
136	118 (18), 94 (42)
127	85 (42), 83 (44)
124	82 (42)
119	101 (18), 91 (28)
118	91 (27)
115	97 (18)
101	83 (18), 73 (28)

[a] 126.0919 ($C_7H_{12}N_1O_1$).

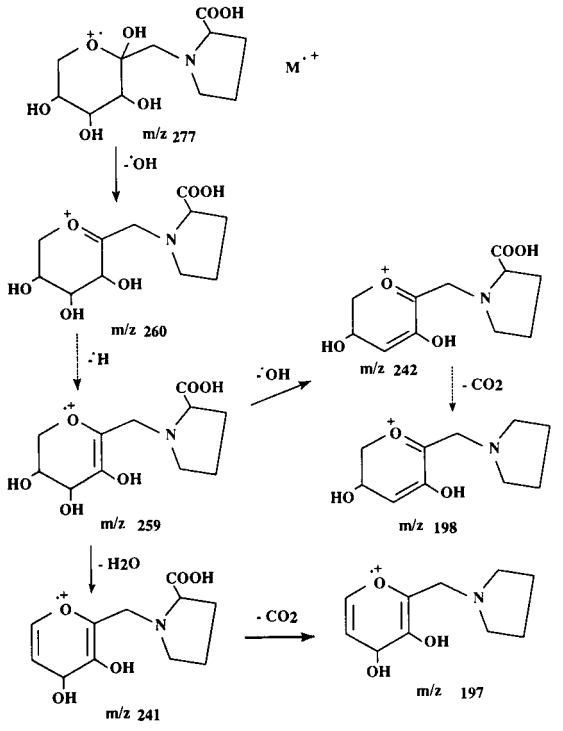

Scheme 2. Proposed mechanism of formation of ions at m/z 198 and m/z 197 from oxonium ion. Dotted arrows represent pathways with no confirmations, thin arrows represent pathways confirmed by B/E linked field scan and thick arrows represent pathways confirmed by B/E linked field scan and by neutral loss (also in Schemes 3–8).

TABLE 2

B/E linked-field scan data of fragment ions of proline Amadori compound

Precursor ion (m/z)	Corresponding product ions
277	260, 128
259	242, 241, 144, 145, 118, 115
198	128, 102
197	166, 127
180	153, 136, 102
166	138
160	142
154	136, 111, 97
153	97
148	105
144	127
143	126, 115
138	111
136	108
126	99, 97, 94, 85, 84, 83
124	96
118	101
97	82
91	73

Most of the fragmentation products of proline Amadori compound were assumed to originate from the pyranose form since, in equilibrated aqueous solutions this is the dominant structure which accounts for 80% of the tautomeric mix-

ion centred at the amino acid nitrogen. The α-cleavage of the bond bearing the carboxylic acid group can lead to the ion at m/z 196. The α-cleavage of the C_1–C_2 sugar bond can lead to m/z 128 which is the daughter of the molecular ion at m/z 277, as postulated in Scheme 3. According to the high resolution mass spectrum, this ion (m/z 128.0712) is four times more intense than the isomeric ion m/z 128.0465 ($C_6H_8O_3$) shown in Scheme 4. The electron donating ability of the nitrogen atom makes the N-centred α-cleavage reactions dominant in the fragmentation of Amadori products. The ion at m/z 128 was also identified in the mass spectrum of proline Amadori compound in the FAB positive ion mode [9]. This ion could have potential diagnostic value since it contains an intact amino acid moiety with a sugar fragment.

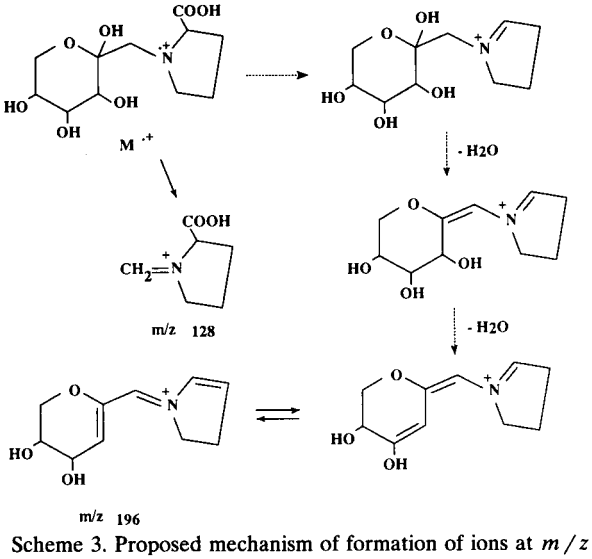

Scheme 3. Proposed mechanism of formation of ions at m/z 196 and m/z 128 from imminium ion.

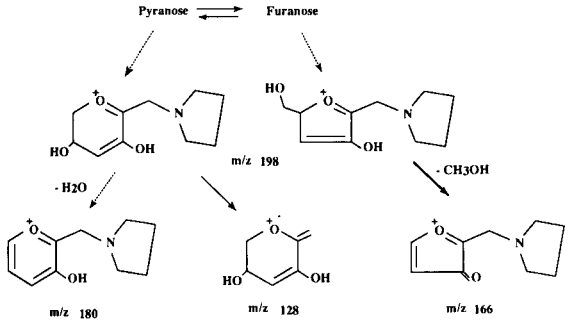

Scheme 4. Proposed fragmentations of ion at m/z 198.

ture. However, in gas phase ion chemistry, more furanose anomers are expected to be found since, generally, the furanose anomers are favoured kinetically, whereas pyranose anomers are favoured thermodynamically and thus are more abundant at equilibrium conditions [11]. Consequently it is reasonable to expect some furanose initiated fragmentations such as the ones shown in Schemes 4 and 5. These fragmentations can not be easily accounted for when originating from pyranose anomers.

Ortho-elimination reactions

Some of the important fragments, including the base peak at m/z 70, observed in the mass spectrum of proline Amadori product can be explained by what we termed *ortho*-elimination reactions. *Ortho*-elimination is a common feature in the mass spectra of Amadori products [12] and

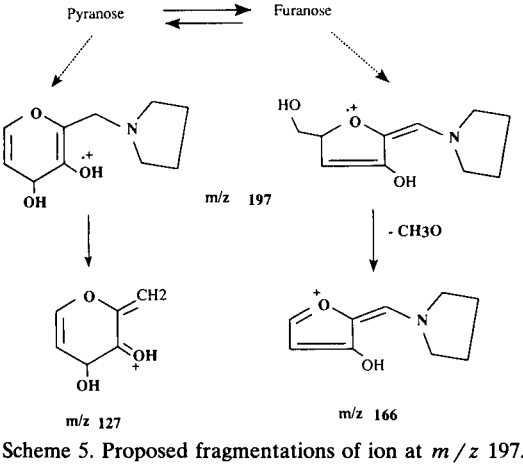

Scheme 5. Proposed fragmentations of ion at m/z 197.

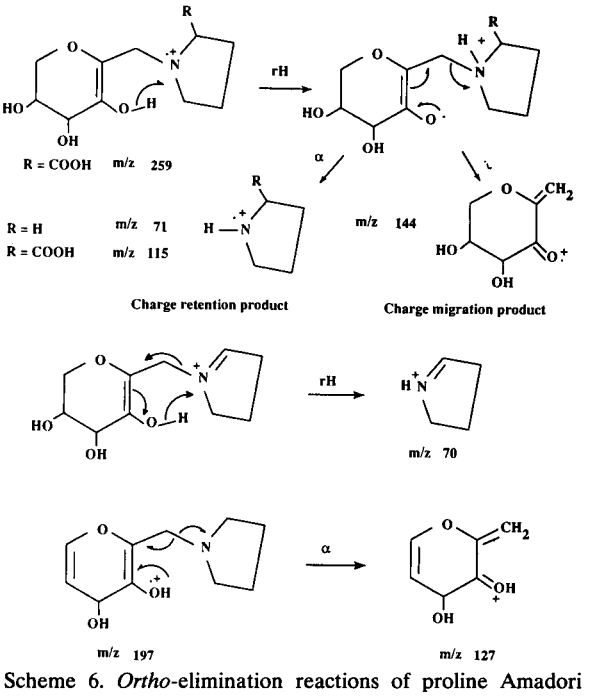

Scheme 6. *Ortho*-elimination reactions of proline Amadori product.

it leads to the fragmentation of Amadori products into sugar and amino acid moieties (Scheme 6). The process can be initiated from both N- and O-centred radical sites after the loss of anomeric hydroxyl group as water. Alternatively, the imminium ion can initiate a similar process that leads to the formation of the base peak at m/z 70. In most cases the reaction proceeds by charge retention.

The *ortho*-elimination reactions initiated at the nitrogen center radical site are triggered by intramolecular H transfer from the hydroxyl group to the nitrogen and this is followed by either an α-cleavage reaction to produce charge retention product or by charge-site initiated inductive cleavage (i) to produce the charge migration product such as sugar fragment m/z 144. The charge retention products are either intact amino acids or decarboxylated products such as the ions at m/z 71 or m/z 115. High resolution mass spectral data showed that the ion at m/z 115 is almost twice as intense as the isomeric m/z 115 shown in Scheme 4. The charge retention products could be used to identify unknown Amadori

products using MS–MS or SIM techniques. Linked-field scan experiments have indicated that both m/z 115 and m/z 144 are the daughter ions of m/z 259.

A similar process initiated by the imminium ion produces the base peak at m/z 70. In this case the even-electron ion decomposes by a concerted mechanism with concomitant transfer of proton from the hydroxyl group to the amino acid nitrogen. This type of ion decompositions in which the charge site retains its location and the electrons remain paired are usually energetically favourable and can provide valuable structural information. The imminium ions formed in diethylamine for example, undergo similar proton transfer to produce the second largest peak in the mass spectrum. The O-centred radical-site initiated *ortho*-eliminations can be considered as vinylogous α-cleavage reactions leading to ions m/z 127 or m/z 145 depending on the degree of dehydration of the sugar ring. B/E linked-scan studies have confirmed that ions at m/z 127 and m/z 145 are the daughter ions of m/z 197 and m/z 259 respectively. Scheme 5 shows the conversion of m/z 197 to m/z 127.

Fragmentations of m/z 198

Scheme 4 shows the fragmentations of ion m/z 198. Linked-field scan studies indicated that ions at m/z 166 and 128 are the daughter ions of m/z 198. The daughter ion m/z 166 can arise from the furanose form of m/z 198 this transformation was further confirmed by the detection of a neutral loss of 32 a.m.u. from m/z 198. The ion m/z 180 on the other hand is only postulated to be the daughter of m/z 198 formed by the loss of a water molecule.

TABLE 3

B/E linked-field scan data of ion m/z 126 generated from EI of proline Amadori product

Precursor ion	Corresponding product ions [a]
m/z 126	126, 99, 97, 94, 84, 85
Maltol [b]	126, 97, 94, 85

[a] Ions higher than 80 a.m.u. [b] Normal spectrum.

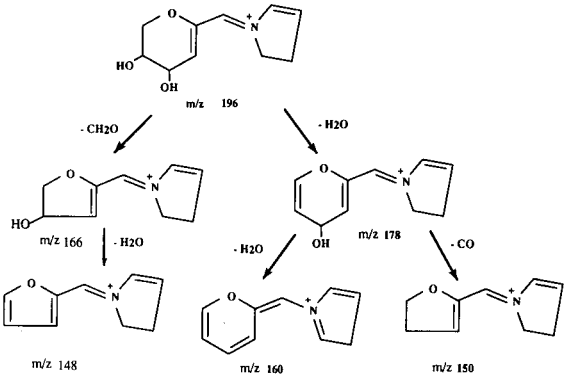

Scheme 7. Proposed fragmentations of ion at m/z 196.

Fragmentations of m/z 197

Fragment ion at m/z 197 undergoes O-centred radical-site initiated *ortho*-elimination as described in Scheme 5 to produce the daughter ion at m/z 127 as shown in Scheme 6. The ion m/z 127 in turn loses a neutral fragment CH_2CO as evidenced by the loss of 42 a.m.u. from m/z 127.

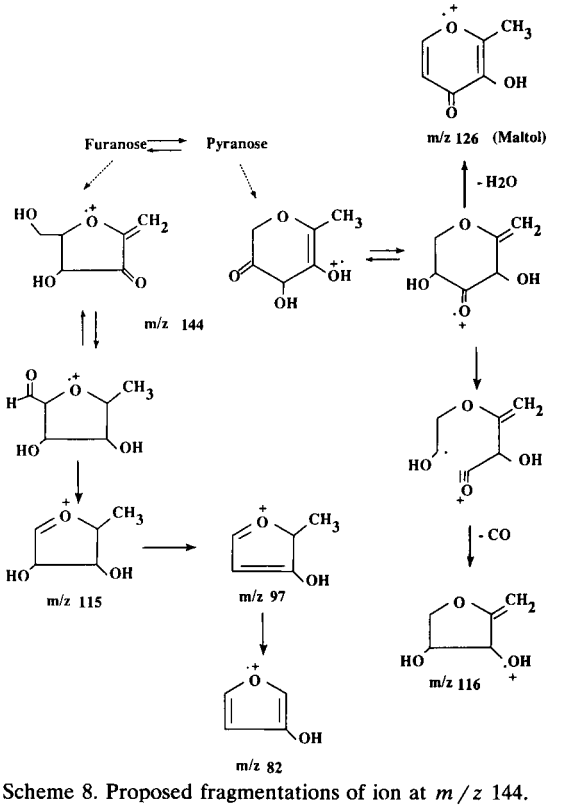

Scheme 8. Proposed fragmentations of ion at m/z 144.

The daughter ion m/z 166 could be formed from the furanose anomer of m/z 197 as confirmed by neutral loss of 31 a.m.u.

Fragmentations of m / z 196

The fragmentations of m/z 196 shown in Scheme 7 have been confirmed both by linked-field scan and neutral loss experiments. The ion can lose two molecules of water to produce the ions at m/z 178 and 160 respectively or it can produce the ion at m/z 166 by the loss of CH_2O which in turn loses a water molecule to give the ion at m/z 148.

Fragmentations of m / z 144

As shown in Scheme 8 the ion at m/z 144, which is the second highest peak, is the charge migration product of the *ortho*-elimination of m/z 259, this relationship was confirmed by B/E linked-field scan analysis. The ion m/z 144 loses a water molecule to produce m/z 126, the dehydration process was confirmed by linked-field studies and by neutral loss experiments. In addition m/z 126 represents commercially available 2-methyl-3-hydroxypyranone (maltol). The structure of m/z 126 was also confirmed by comparison of the ions in the normal mass spectrum of maltol to the daughter ions of m/z 126 as shown in Table 3. The other confirmed neutral loses such as CO and ·CHO are shown in Scheme 8.

One of the authors (VY) gratefully acknowledges funding for this research from the Natural Sciences and Engineering Research Council (NSERC) of Canada. We are grateful to Agriculture Canada's Food Research and Development Centre (St. Hyacinthe, Canada) and to the Department of Chemistry, University of Alberta (Edmonton, Canada) for the use of their mass spectrometry facilities.

REFERENCES

1 V. Yaylayan and P. Sporns, Food Chem., 26 (1987) 283.
2 V. Yaylayan and P. Sporns, Org. Mass Spectrom., 23 (1988) 849.
3 P.A. Finot, H.U. Aeschbacher, R.F. Hurrell and R. Liardon (Eds.). The Maillard Reaction in Food Processing, Human Nutrition and Physiology, Birkhäuser Verlag, Basel, 1990.
4 V. Yaylayan, J.R.J. Paré, R. Laing and P. Sporns, Org. Mass Spectrom., 25 (1990) 141.
5 V. Yaylayan and N. Forage, J. Agric. Food Chem., 39 (1991) 364.
6 K. Biemann, J. Seible and F. Gapp, J. Am. Chem. Soc., 83 (1961) 3795.
7 N.K. Kochetkov and O.S. Chizhov, Adv. Carbohydr. Chem., 21 (1966) 39.
8 V. Yaylayan, J.R.J. Paré, R. Laing and P. Sporns, in P.A. Finot, H.U. Aeschbacher, R.F. Hurrell and R. Liardon (Eds.), The Maillard Reaction in Food Processing, Human Nutrition and Physiology, Birkhäuser Verlag, Basel, 1990, pp. 115–120.
9 G. Vernin, L. Debrauwer, G.M.F. Vernin, R.-M. Zamkotsian, J. Metzger, J.L. Larice and C. Parkanyi, in G. Charalambous (Ed.), Off-flavors in Foods and Beverages, Elsevier, 1992, pp. 567–623.
10 W. Funke, D. Henneberg, C. von Sonntag and A. Klemer, Org. Mass Spectrom., 14 (1979) 220.
11 R.S. Shallenberger, C.Y. Lee, T.E. Acree, J. Barnard and M.G. Lindley, Carbohydr. Res., 58 (1977) 209.
12 V. Yaylayan, S. Mandeville and J.R.J. Paré, Spectroscopy Int. J., 9 (1991) 73.

Analytica Chimica Acta, 280 (1993) 253–261
Elsevier Science Publishers B.V., Amsterdam

Quantitative aqueous attenuated total reflectance Fourier transform infrared spectroscopy

Part II. Integrated molar absorptivities of alkyl carboxylates

Paul R. Pike, Pamela A. Sworan and Stephen E. Cabaniss
Department of Chemistry, Kent State University, Kent, OH 44242 (USA)

(Received 15th September 1992; revised manuscript received 9th February 1993)

Abstract

A quantitative attenuated total reflectance Fourier transform infrared (ATR-FT-IR) spectroscopic method is developed for the analysis of total carboxylate concentration, [COO^-], in aqueous solution. The short (12–13 μm) and highly reproducible pathlength of the ATR cell permits quantitative subtraction of the water peak at 1640 cm^{-1}. Carboxylate quantitation is based on the area of the asymmetric stretching peak, which is nearly independent of compound structure. The molar absorptivity of alkyl carboxylates in water is 438 ± 58 l mol^{-1} cm^{-1}, and the integrated molar absorptivity is $2.95 \pm 0.08 \times 10^4$ l mol^{-1} cm^{-2} ($n = 15$ compounds, 0.1 M $\leq$ [COO^-] $\leq$ 1.5 M). The [COO^-] in solutions of mixed carboxylates is measured with a root mean square error of 2.4% and a small (+1.5) positive bias. The accuracy of the method is limited by the assumption that integrated absorbance is constant for all COO^- groups.

Keywords: Infrared spectrometry; Alkyl carboxylates; Aqueous solutions; Quantitative analysis

Infrared spectroscopy (IR) is a popular tool for qualitative analysis of unknown compounds because of its speed, sensitivity and versatile sample handling. However, quantitative IR analysis typically requires standards, which complicates the analysis of unknown compounds and mixtures. In this paper, we measure the integrated molar absorptivity of carboxylate salts in water, and show that alkyl mixtures can be analysed for total carboxylate concentration, [COO^-], without knowing the structures of individual analytes.

The integrated molar absorptivity, B in the 'practical units' of l mol^{-1} cm^{-2} [1], is defined by

$$B = \int_{\nu_a}^{\nu_b} \epsilon_\nu \, d\nu \qquad (1)$$

Correspondence to: S.E. Cabaniss, Department of Chemistry, Kent State University, Kent, OH 44242 (USA).

where ν is the frequency in cm^{-1} and ν_a and ν_b are the frequencies at the bounds of the peak [1,2]. The decadic molar absorptivity at a single frequency, ϵ_ν, is given by

$$\epsilon_\nu = \frac{1}{bC} \log\left(\frac{I_0}{I}\right)_\nu \qquad (2)$$

where I_0 and I are the light intensities in the absence and presence of the sample at frequency ν, b is the pathlength in cm, and C is the concentration in mol l^{-1}. For convenience, we follow the practice of Wexler [1] and give all integrated molar absorptivity values in intensity units (IU) where 1 IU = 10^4 l mol^{-1} cm^{-2}.

The integrated molar absorptivity is often characteristic of a particular functional group. B is related to the change in dipole moment for a given vibration, and is unaffected by rotational broadening [3]. However, electronic, steric, and intermolecular (solvent) effects can affect inte-

grated molar absorptivity [4,5]. Consequently, although integrated molar absorptivity is more characteristic of a particular functional group than the peak molar absorptivity ϵ_{max} [5], not all vibrational bands have a truly characteristic B [4].

Steele and coworkers [6,7] have recently used integrated absorbances and factor analysis to determine $-CH_2-$ and $-CH_3$ abundances. Our approach emphasizes direct quantitation of total group concentrations in unknown mixtures, emphasizing aqueous systems of environmental and biological interest.

Carboxylate absorbance in water

IR spectra of carboxylates are distinguished by an asymmetric stretch band, ν_{as}, in the 1550–1610 cm^{-1} region and a symmetric stretch band, ν_s, in the 1350–1420 cm^{-1} region. Since the ν_{as} region typically has fewer interfering absorption bands, this peak is regarded as more diagnostic for carboxylates [8]. Studies of carboxylates in water are hampered by the strong water band near 1640 cm^{-1}, which often obscures the asymmetric band [9,10]. Successful subtraction of this peak requires a very short (< 20 μm) and highly reproducible pathlength, such as that provided by attenuated total reflectance (ATR) [10–12].

ATR is widely used for biochemical [13,14] and environmental [15,16] studies and for laboratory assays [17,18]. Radiation is reflected at the boundary between a medium of high refractive index (n_1) and a sample of lower refractive index (n_2), and a fraction of the light penetrates into the sample as an evanescent wave. A penetration depth, d_p, is defined as the depth required for the electric field intensity to decrease by a factor of e^{-1},

$$d_p = \frac{\lambda}{2\pi n_1 \sqrt{\sin^2\theta - n_{21}^2}} \quad (3)$$

where λ is the wavelength of the light, θ is the angle of reflection, and $n_{21} = n_2/n_1$ [11]. For a given cell and sample d_p is proportional to d_e, the equivalent depth of a single reflection [11,12]. d_e is defined as the thickness of a transmission cell which, when filled with the same sample, gives the same absorbance as a single ATR reflection [19,20]. The equivalent pathlength b_e for a multi-reflection cell can be obtained from the number of reflections N by $b_e = d_e \times N$. The equivalent pathlength is highly reproducible, although clearly dependent on light wavelength ν, cell construction (θ, n_1) and sample (n_2).

EXPERIMENTAL

Materials and methods

Reagent-grade chemicals from Aldrich and Sigma and deionized water were used for all solutions.

FT-IR spectra were collected using a Nicolet 740 FT-IR spectrometer and a Spectratech Horizontal ATR cell purged with N_2 or dry air. The ATR cell was fitted with a 45° ZnSe crystal with 12 reflections [21]. The spectrometer included a fluid-cooled Globar source, a KBr beamsplitter and a TGS (triglycine sulfate) detector. It was operated in single-beam mode with a mirror velocity setting of 30 (ca. 0.3 cm s^{-1}) and employed a Happ–Genzel apodization function. Spectra were acquired at 4 cm^{-1} resolution and 128 scans were averaged to reduce noise. Light throughput with an empty cell in place was at least 15% of the full (no accessory) signal, with an average of 20% throughput in the spectral region 1000–2000 cm^{-1}. Instrumental gain was typically set at 4 to compensate for decreased light throughput. Replicate scans of the empty ATR cell had < 0.001 absorbance units random noise.

Deionized water spectra were collected for background subtraction at least once per hour. The scaling factor F for background subtraction (difference = sample $- F \times$ background) was determined by eliminating the water absorbance peak near 2120 cm^{-1} [14,15]. Typical values of F were between 0.99 and 1.00, with some values as low as 0.98. Baselines of the resulting spectra were generally between -0.01 and 0.01 AU in the 1800–2000 cm^{-1} region.

Peak areas were obtained by integrating with respect to frequency (cm^{-1}). For isolated peaks, ν_a and ν_b were set at the ν for which the absorbance first reached zero. For imperfectly resolved peaks, the minimum absorbance between

the peaks was used as peak boundary. The peak width (FWHM, full width at half maximum) was measured for each ν_{as} band.

Peak and integrated molar absorptivities were determined from linear regression on peak heights or areas versus [COO^-]. After an initial instrumental purge to reduce the water vapor absorption below 0.001 AU, a series of 4–6 spectra were acquired in order of increasing concentration. A 5-min purge with dry N_2 or dry air preceded each spectral acquisition. Solution concentrations were typically between 0.1 and 0.5 M ([COO^-] from 0.1 to 1.5 M) to minimize relative errors in peak heights and areas.

RESULTS AND DISCUSSION

Carboxylate frequencies

Peak frequencies for carboxylate ν_{as} and ν_s are generally lower in aqueous solution than in solid or mull spectra [8]. Table 1 shows ν_{as} values lower in water than in solid spectra [22,23], and most of the ν_s peaks show a similar decrease.

The frequency of the asymmetric peak for acetate increases dramatically as Cl atoms are added from 1551 cm^{-1} (acetate) to 1668 cm^{-1} (trichloroacetate) (Table 1 and Fig. 1). However, peak splitting also increases (135 to 330 cm^{-1}), so that the center frequency of the two peaks, $\nu_{center} = (\nu_{as} + \nu_s)/2$, increases only slightly (1484 to 1502 cm^{-1}). ν_{center} is linearly related to the pK_a at ionic strength (I) = 0.1 M; the line is described by $pK_a = 327 - 0.2175\ \nu_{center}$, $r^2 = 0.9996$, $n = 4$. pK_a values were obtained from Smith and Martell [24]. This relationship is obscured in the solid state due to the anomalous behavior of trichloroacetate.

The hydroxy-acid spectra are complex, with ν_{as} frequencies increasing as –OH groups are added near the carboxylate (Table 1, Fig. 2). Glycolate and lactate, with one α-OH, have similar spectra and ν_{as} peak frequencies (1579 and 1574 cm^{-1}), while glyoxylic acid, which exists in solution as

TABLE 1

Carboxylate IR peak parameters

Compound	Aqueous peak frequencies (cm^{-1})		Molar absorptivities [a]	
	ν_{as}	ν_s	ϵ_{max}	B
Acetate	1550	1416	448 ± 3	3.01 ± 0.03
Chloroacetate	1589	1397	440 ± 4	2.97 ± 0.02
Dichloroacetate	1624	1378	482 ± 5	2.98 ± 0.05
Trichloroacetate	1668	1336	432 ± 4	2.97 ± 0.03
Glycolate	1579	1410	403 ± 2	2.87 ± 0.03
D-lactate	1574	1417	425 ± 4	2.86 ± 0.03
Glyoxylate	1595	1383	408 ± 5	3.04 ± 0.03
Gluconate	1587	1412	368 ± 2	2.78 ± 0.03
Oxalate	1569	1307	477 ± 1	2.89 ± 0.09
Malonate	1561	1356	481 ± 8	3.05 ± 0.04
Succinate	1552	1395	523 ± 7	3.02 ± 0.02
Glutarate	1547	1401	524 ± 7	2.86 ± 0.03
Formate	1580	1351	582 ± 11	3.17 ± 0.04
Cyanoacetate	1603	1366	467 ± 5	2.98 ± 0.04
Glutamate	1557	1401	296 ± 5	2.92 ± 0.09
Citrate	1568	1389	392 ± 5	3.00 ± 0.01
Average [b]			438	2.95
Relative standard deviation (%) [b]			13.2%	2.60%

[a] ± indicates standard deviation of the slope in Eqns. 5 and 6; the uncertainty due to calculated b_e is not included. [b] Formate not included.

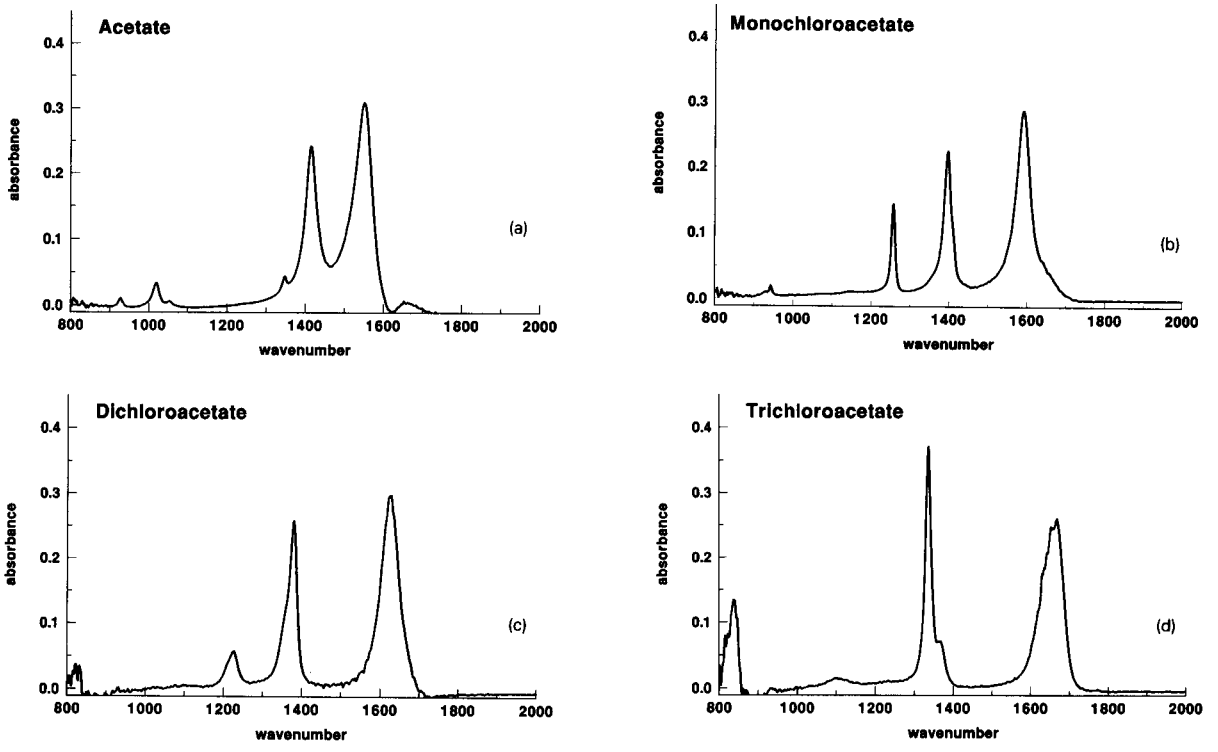

Fig. 1. Water-subtracted ATR-FT-IR spectra of 0.5 M solutions of (a) sodium acetate, (b) sodium chloroacetate, (c) sodium dichloroacetate, (d) sodium trichloroacetate.

the acetal with two α-OH, has a significantly higher ν_{as} peak (1595 cm^{-1}).

The dicarboxylate spectra are dominated by the COO^- bands, with increasing peak splitting as the number of CH_2 groups separating the COO^- groups decreases (Table 1, Fig. 3). ν_{center} is linearly related to the pK_a of the first proton released; $pK_{a1} = -123.9 + 0.0868\ \nu_{center}$, $r^2 = 0.996$. The closeness of the two groups influences pK_{a1} more than pK_{a2}. The interpretation of this relationship is not clear, especially since direct interaction between groups seems inevitable in the smallest dicarboxylates.

The formate spectrum is similar to those of other carboxylates (Fig. 4A), even though the carboxylate *C* is bonded to H instead of another C. Cyanoacetate has a high ν_{as} typical of electron-withdrawing substituents (Fig. 4B). Glutamate and citrate have broad carboxylate peaks due to the presence of non-identical acid groups (Fig. 4C and D). This effect is much more noticeable in glutamate, in which one COO^- is α to an amino group.

Quantitative aspects

Solvent subtraction is critical for quantitative aqueous FT-IR based on integrated molar absorptivity or ϵ_{max}. The absorbance of water near 1640 cm^{-1} was > 1.2 AU in this ATR cell, so even a 1% error in the factor *F* leads to > 0.012 AU error in peak height. With typical peak heights from 0.05 to 0.6 AU, 1% error in *F* corresponds to 2–24% error in peak height.

The interactive subtraction method attempted to eliminate the water band near 2120 cm^{-1} by obtaining a baseline slope of zero in the region 2000–2300 cm^{-1}, and gave good (1–3%) reproducibility in peak height. At high (> 0.3 M) $[COO^-]$, the water band could not be cleanly eliminated because the peak shifted to higher ν; a similar effect was observed by Bonn [15]. The resulting 'derivative-type' signal was considered

minimized when the positive and negative peaks were symmetrical. Use of an automated subtraction algorithm such as that recommended by Bonn [15] or Dousseau et al. [14] should produce more reproducible subtractions for the lower concentrations. However, since these algorithms assume no peak shift, their use is questionable for more concentrated solutions.

Numerical integration using a zero baseline introduced little uncertainty, since the criteria for selecting ν_a and ν_b were unambiguous. Numerical integration using a sloping, non-zero baseline was unsatisfactory on both theoretical and practical grounds. The baseline should be zero after water subtraction, and proportionality between concentration and area was not observed for peaks integrated with a non-zero baseline.

Long-term instrumental and cell alignment variability was estimated by measuring the water band near 1640 cm^{-1} over a one-month period. The relative standard deviation (R.S.D) for sixteen spectra was 0.6%. Combined short-term drift, subtraction and integration variability was estimated by measuring heights and areas of the ν_{as} on replicate aliquots on a single day; R.S.D. was 1–2%. The R.S.D. of carboxylate ν_{as} peak heights and areas ranged from 0.1 to 2.2% with an average of 1.2% for different solutions (> 0.2 M) analysed on different days. These results indicate that long-term drift and cell changes are less important sources of uncertainty than solvent subtraction.

The equivalent pathlength of the ATR cell was calibrated using absorbance of deionized water. The equivalent pathlength, b_e, at a given wavelength λ can be estimated within 2–3% using the relation

$$b_e = \lambda L \tag{4}$$

after calculating the calibration constant L from the height of the water absorption band near 2120 cm^{-1} [20]. The 45° ZnSe ATR cell used

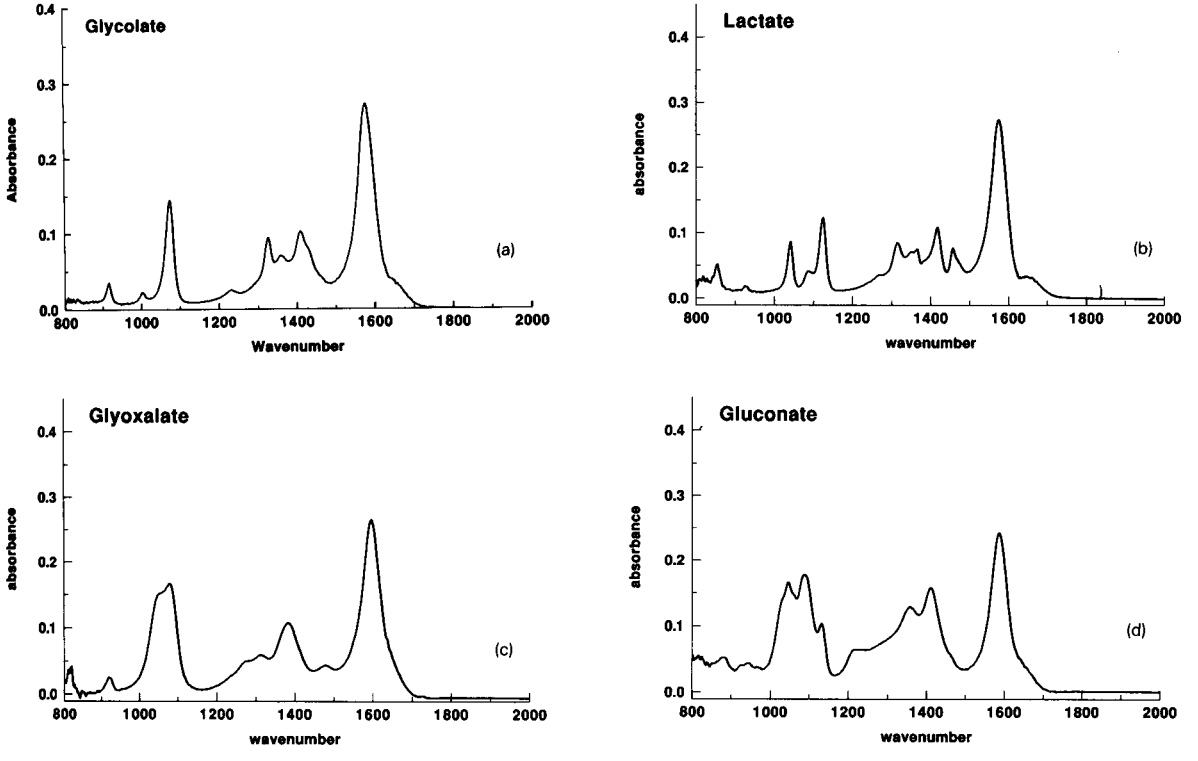

Fig. 2. Water-subtracted ATR-FT-IR spectra of 0.5 M solutions of (a) sodium glycolate, (b) sodium lactate (c) sodium glyoxalate, (d) potassium gluconate.

here has a calibrated $L = 2.03 \pm 0.05$, giving $b_e = 13.5 \pm 0.3$ μm at 1500 cm^{-1}.

Alkyl carboxylate B and ϵ_{max}

The molar absorptivity of the asymmetric peak for each carboxylate salt was determined by linear regression of peak maximum absorbance A versus $[COO^-]$, according to the equation

$$\frac{A}{b_e} = \epsilon[COO^-] \quad (5)$$

The regression r^2 was > 0.99 in each case; apparently Beer's law is obeyed in these solutions. The relative standard deviation in ϵ ranged from 0.3 to 1.9%, about one half the average experimental uncertainty for individual measurements (Table 1). Absolute bounds on ϵ are larger because of the uncertainty in b_e. However, this uncertainty affects all ϵ values nearly equally, and so can be disregarded when comparing ϵ for these compounds.

Molar absorptivities on a $[COO^-]$ basis vary from a low of 296 l mol^{-1} cm^{-1} for glutamate to a high of 582 l mol^{-1} cm^{-1} for formate, a range representing 60% of the average value 438 l mol^{-1} cm^{-1}. Discounting formate because it lacks a C–C bond for the carboxylate carbon, the relative standard deviation of 15 ϵ values is 13.2%, substantially higher than the uncertainty in the individual values. Chlorine containing compounds and dicarboxylates with identical COO^- groups had higher than average ϵ. Hydroxyacids and compounds with non-identical COO^- groups had lower than average ϵ.

Previous studies of ϵ in other matrices obtained substantially higher values. Flett [5] examined 10 alkyl carboxylate salts in KBr and found an average $\epsilon = 746 \pm 224$ (30%) l mol^{-1} cm^{-1}. Wexler [25] examined 36 alkyl carboxylates in methanol and found an average $\epsilon = 634 \pm 127$ (20%) l mol^{-1} cm^{-1}. The higher R.S.D. in KBr may be due to the difficulty of preparing homogeneous pellets [5].

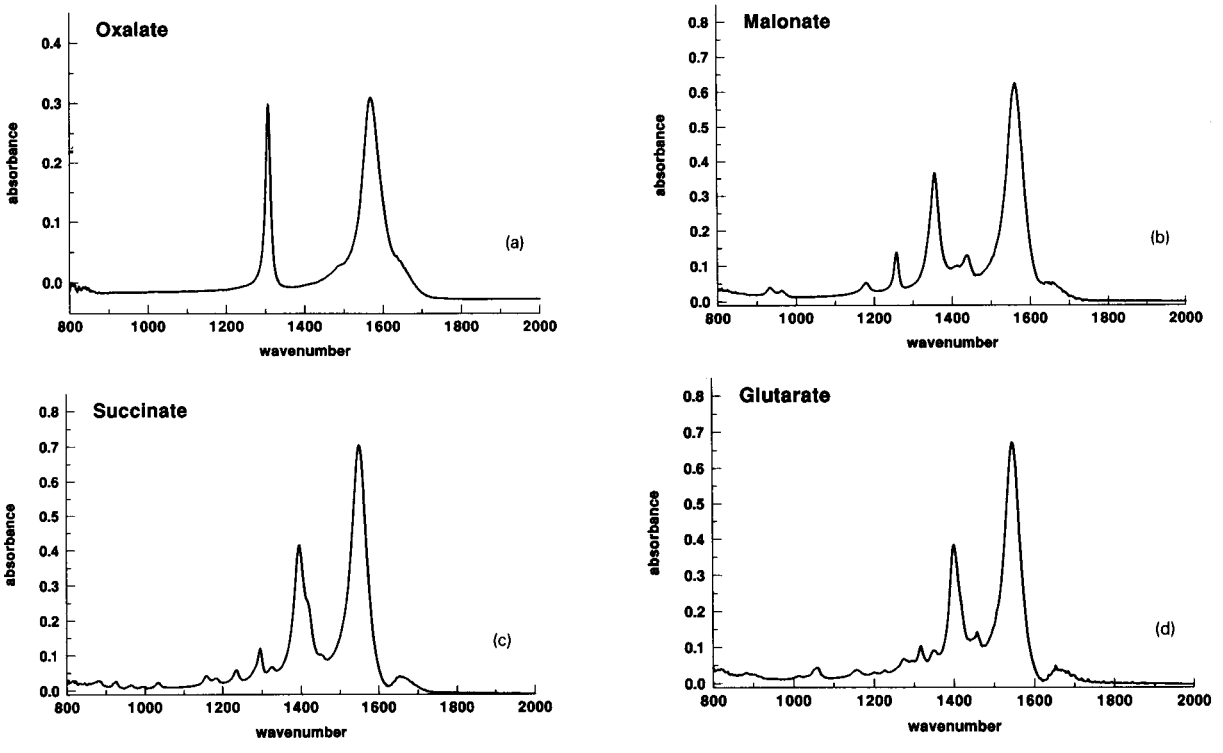

Fig. 3. Water-subtracted ATR-FT-IR spectra of (a) 0.25 M disodium oxalate, (b) 0.5 M disodium malonate, (c) 0.5 M disodium succinate and (d) 0.5 M disodium glutarate.

The integrated molar absorptivities of the asymmetric bands were determined by linear regression of peak area versus $[COO^-]$

$$\frac{\text{Area}}{b_e} = B[COO^-] \quad (6)$$

The Beer's law analogue for areas was obeyed, with $r^2 > 0.99$ for all compounds examined. The relative standard deviation in B was 1.3% (range 0.4 to 3.1%), lower than the average uncertainty in individual measurements.

Integrated molar absorptivities vary much less than the molar absorptivities among different compounds. The high integrated molar absorptivity of 3.05 for malonate and low of 2.78 for gluconate span a range 9% of the average of 2.95, compared to $> 50\%$ for ϵ. By comparison, the range of peak frequencies for ν_{as} is roughly 8% of the mean value. Discounting formate, the relative standard deviation in integrated molar absorptivity is 2.6%, nearly five-fold lower than the R.S.D. of ϵ.

This is a substantially (five-fold) lower R.S.D. of integrated molar absorptivity than previous determinations. Flett [5] measured an average integrated molar absorptivity of 3.6 ± 0.5 (13%) in KBr pellets ($n = 10$). Wexler [25] obtained an average integrated molar absorptivity of 2.9 ± 0.4 (13%) for methanol solutions ($n = 36$). The larger R.S.D. for integrated molar absorptivity and for ϵ in earlier studies relative to the present work might be due to experimental factors (single-point determinations rather than area versus molarity plots) or to matrix effects.

The variation in ϵ among solvents and among different compounds in the same solvent is much larger than the variation in B, confirming the anticipated effect of solvent and molecular structure on peak shape. Clearly, ν_{as} peaks are lower and broader in water than in KBr or methanol. The variation in shape among different compounds appears to be smaller in aqueous solution than in methanol, but this cannot be shown conclusively without a more rigorous comparison.

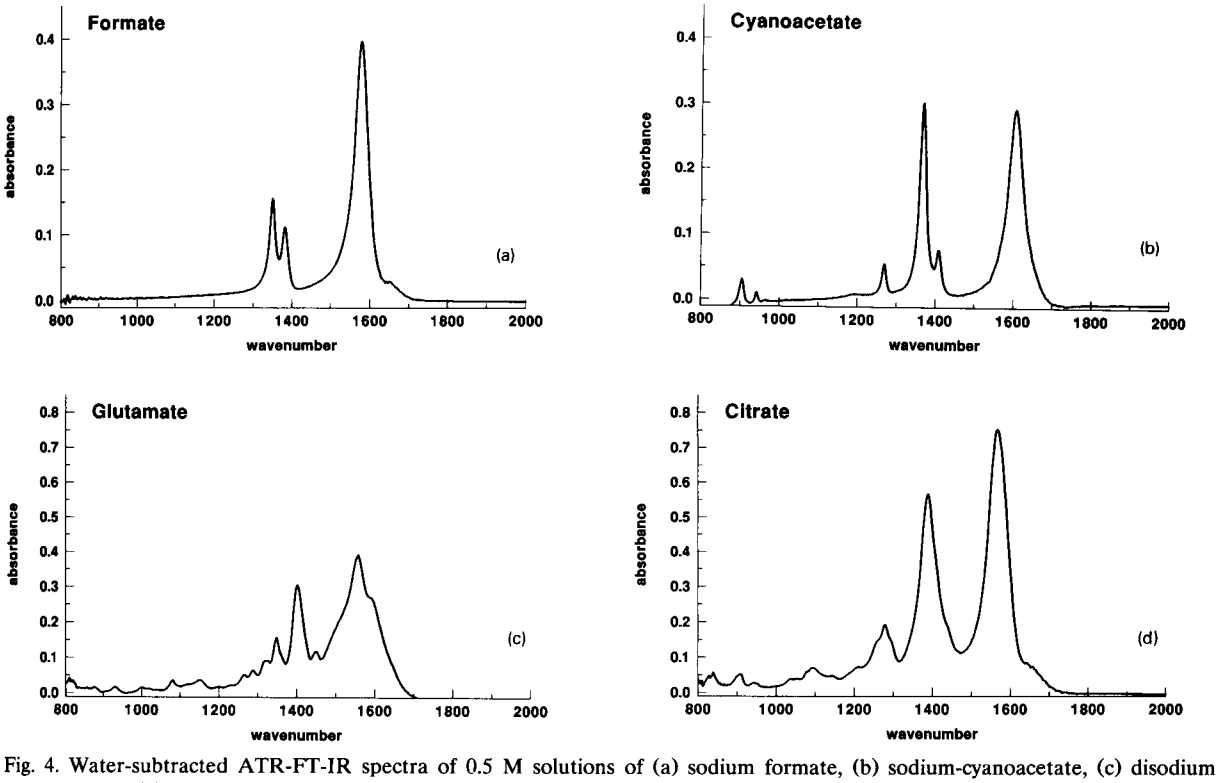

Fig. 4. Water-subtracted ATR-FT-IR spectra of 0.5 M solutions of (a) sodium formate, (b) sodium-cyanoacetate, (c) disodium glutamate and (d) trisodium citrate.

Some variations in peak shape obviously result from non-identical acid groups in the same molecule, i.e., the low, broad peaks of citrate and glutamate.

Analysis of mixtures

The goal of this project is to develop a quantitative method for functional group analysis in aqueous solution based on integrated peak absorbances. To test this, we analysed a set of mixed carboxylate solutions and compared $[COO^-]$ obtained from peak areas of ν_{as} with the known $[COO^-]$. The data was acquired and analysed by the same methods as the single-compound solutions. $[COO^-]$ was determined by

$$[COO^-] = \frac{\text{Area}}{\bar{B}b_e} \quad (7)$$

where $\bar{B}$ is an average value of B. The estimated uncertainty in calculated $[COO^-]$ is affected by the uncertainty in $\bar{B}$ and in peak area, but not by error in b_e. Given a 2.6% R.S.D. in $\bar{B}$ and a 1% error in peak area, the R.S.D. in $[COO^-]$ is estimated to be 2.8%; for a 2 or 3% error in area, 3.3 or 4% R.S.D. in $[COO^-]$, respectively.

Analysis of nine mixtures of acetate, glyoxylate, chloroacetate, glutarate, malonate, succinate, glycolate and lactate using this method gave calculated values of $[COO^-]$ within 4% of the true values (Table 2). The root mean square error (RMSE) in calculated $[COO^-]$ was 2.5%, but the error was not distributed evenly above and below the mean. The positive bias of the calculated $[COO^-]$, +1.5%, is at least partly due to the choice of $\bar{B} = 2.95$, the best overall value. If we set $\bar{B}$ to equal the actual average of the carboxylates in the mixtures, the bias is greatly reduced although the RMSE error drops only slightly. The uncertainties in the calculated $[COO^-]$ are within predicted limits. An improved value of $\bar{B}$ permits more accurate work, but may not always be available.

EVALUATION

The ATR-FT-IR method developed here provides rapid quantitation of $[COO^-]$ in aqueous solution. The precision, R.S.D. 2–3%, is limited principally by solvent subtraction and instrumental noise, and could be improved by working at lower concentrations with a more sensitive detector. In solutions with minimal interferences, the accuracy is limited by the degree to which $\bar{B}$ represents the average integrated molar absorptivity of the carboxylates; based on the average value of 2.95 ± 0.08, accuracy should be ± 2–3%. In solutions with interfering bands, the ability to remove interferences may limit accuracy.

TABLE 2

Analysis of mixtures

Mixture [a] (concentration in mM)	Peak (cm^{-1})	$[COO^-]$ (mM)		Error (%)
		Actual	Measured	
101 Glu + 102 Act + 99 Cla	1549	402	414	+3.1
205 Act + 99 Cla	1553	304	300	−0.5
102 Act + 99 Cla + 100 Glx	1557	301	312	+3.8
201 Glu + 200 Glx	1549	601	617	+2.7
101 Glu + 102 Act + 99 Cla	1551	502	496	−1.2
205 Act + 200 Glx	1558	405	415	+2.5
100 Suc + 102 Act + 101 Lac	1552	403	400	−0.8
100 Mal + 210 Gly + 101 Lac	1570	511	529	+3.5
102 Act + 105 Gly + 101 Lac	1570	308	308	0.0
RMSE (%)				2.5
Average (% bias)				+1.5

[a] Glu = Glutarate, Gly = Glycolate, Glx = Glyoxylate, Act = Acetate, Cla = Cloroacetate, Mal = Malonate, Suc = Succinate, Lac = Lactate.

The research was performed under the sponsorship of the U.S. Department of Energy Junior Faculty Award Program administered by Oak Ridge Institute for Science Education. The authors would like to thank Nancy Marley for making unpublished results available, and Sue Sutheimer for comments on the manuscript.

REFERENCES

1 A.S. Wexler, Appl. Spectrosc. Rev., 1 (1967) 29.
2 L. Dixlit, Appl. Spectrosc. Rev., 20 (1984) 159.
3 J. Overend, in M. Davies (Ed.), Infrared Spectroscopy and Molecular Structure, Elsevier, London, 1963, p. 345.
4 D. Hadzi, in M. Davies (Ed.), Infrared Spectroscopy and Molecular Structure, Elsevier, London, 1963, p. 226.
5 M.St.C. Flett, Spectrochim. Acta, 18 (1962) 1537.
6 D. Steele, Spectrochim. Acta, 44A (1988) 1255.
7 R.S. Emmence and D. Steele, Anal. Chem., 63 (1991) 2091.
8 L.J. Bellamy, The Infrared Spectra of Complex Molecules, Chapman and Hall, London, 1975.
9 R.C. Gore, R.B. Barnes and E. Petersen, Anal. Chem., 21 (1949) 382.
10 B. Katlafsky and R.E. Keller, Anal. Chem., 35 (1963) 1665.
11 N.J. Harrick, Internal Reflection Spectroscopy, Wiley New York, 1967.
12 N.A. Marley, J.S. Gaffney and M.M. Cunningham, Spectroscopy, 7 (1992) 44.
13 J.L. Kirsch and J.L. Koenig, Appl. Spectrosc., 43 (1989) 445.
14 F. Dousseau, M. Therrieu and M. Pezolet, Appl. Spectrosc., 43 (1989) 538.
15 B. Bonn, PhD Dissertation, Oregon Graduate Institute of Science and Technology, 1992.
16 S.E. Cabaniss, Anal. Chim. Acta, 255 (1991) 23.
17 R.T. Carl, Nicolet FT-IR Application Note AN-8819, Nicolet, Madison, WI, 1988.
18 J.H. Hopkinson, C. Moustou, N. Reynolds and J.E. Newbery, Analyst, 112 (1991) 501.
19 F.M. Mirabella, Jr., Appl. Spectrosc. Rev., 21 (1985) 45.
20 S.E. Cabaniss, unpublished results.
21 Spectra-Tech, Contact Sampler User's Manual, 1991, Stamford CT.
22 R.J. Keller, The Sigma Library of FT-IR Spectra, Vols. 1 and 2, Sigma, St. Louis, MO.
23 E. Spinner, J. Chem. Soc., 4217 (1964).
24 R.M. Smith and A.E. Martell, Critical Stability Constants, Plenum Press, New York, 1975, 1982 and 1989.
25 A.S. Wexler, Spectrochim. Acta, 23A (1967) 1319.

Analytica Chimica Acta, 280 (1993) 263–268
Elsevier Science Publishers B.V., Amsterdam

Surface-enhanced Raman spectrometry of amiloride on colloidal silver

N. Calvo, R. Montes and J.J. Laserna

Department of Analytical Chemistry, Faculty of Sciences, University of Málaga, E-29071 Málaga (Spain)

(Received 19th January 1993; revised manuscript received 23rd February 1993)

Abstract

Surface-enhanced Raman spectrometry (SERS) of the diuretic drug amiloride is discussed. The SERS-active substrate used is colloidal silver, which is prepared at room temperature by simple tetrahydroborate reduction of an aqueous solution of silver nitrate. SERS detection of amiloride in human urine is illustrated. The reproducibility of quantitative SERS data is supported by the simultaneous measurement of the scattering signal and transmitted light. Relative standard deviations at the 5% level are compatible with many practical analytical situations.

Keywords: Raman spectrometry; Amiloride; Pharmaceuticals; Urine

The detectability of trace concentrations of drugs by surface-enhanced Raman scattering (SERS) on silver colloids has been demonstrated [1–4]. The colloidal dispersion works as a derivatizing agent for the drug, i.e., it results in improved detectability of the analyte. In this instance, the resulting effect is an increase in the Raman scattering cross-section by factors as large as six orders of magnitude. Further advantages of silver hydrosols for this application include ease of formation and manipulation [5], a definite dependence of the enhancement factor on the morphology of silver particles [6] and simple substrate characterization by absorptiometric techniques [6]. Unfortunately, enhancement at metal surfaces is not as general a phenomenon as regular Raman scattering. In addition, the analyte-induced aggregation of the colloidal dispersion eventually causes instability of the system.

In a previous paper, a method for the simultaneous measurement of the SERS signal and transmittance changes occurring in colloid substrates was reported [7]. This method provides some information on the aggregation state of the colloid whilst the SERS signal is being recorded. The relationship between colloid aggregation and SERS intensity is thus readily established, allowing SERS spectra to be recorded under the most favourable conditions. In this work, the application of this method for improving the precision of quantitative SERS measurements is illustrated. The improvement of the signal reproducibility allowed the determination of amiloride [3,5-diamino-*N*-(aminoiminomethyl)-6-chloropyrazinecarboxamide] in a real urine sample. This compound is used clinically to treat hypertension and it is banned in official sport practices [8]. The compound is adsorbed from the gastrointestinal tract by 15–26% and it is excreted rapidly in urine in the native form [9].

Correspondence to: J.J. Laserna, Department of Analytical Chemistry, Faculty of Sciences, University of Málaga, E-29071 Málaga (Spain).

EXPERIMENTAL

Instrumentation

The excitation source consisted of an argon ion laser (Coherent Innova 70) tuned at 488 nm,

releasing about 30 mW at the sample. The sample was placed in a standard 1-cm square cell with four optical faces. Collection of the scattered light was at 90° to the excitation axis. Raman scattering was dispersed with a 0.22-m double-grating spectrometer (Spex Industries Model 1680B) and detected with a thermoelectrically cooled photomultiplier tube (Hamamatsu Model R928) and a photon-counting system (Stanford Research System Model SR400). Data acquisition, storage, processing and plotting were controlled by an IBM AT-compatible microcomputer using Stanford Research SR465 software. Spectral data were generated in binary code and converted to ASCII for processing in standard graphics software. The intensity of the laser beam transmitted by the sample was detected with a silicon photodiode. This approach provides real-time monitoring of the sample absorbance whilst the SERS spectrum is being recorded. The photodiode photocurrent was converted into voltage and amplified using a laboratory-made current follower. To avoid thermal drift in the photodiode response, the transmitted laser beam was chopped (24 Hz) prior to light detection. A standard chart recorder was used to acquire the transmitted signal.

Chemicals and procedure

Analytical-reagent grade chemicals and distilled, deionized water were used throughout. Amiloride (Sigma) was used as received. It was dissolved in water containing about 2% methanol to aid in drug dissolution. Silver colloids were prepared at room temperature by adding 1 ml of 1×10^{-3} M aqueous silver nitrate to 3 ml of 2×10^{-3} M aqueous sodium tetrahydroborate. The tetrahydroborate solution was aged for 4 h at room temperature before the experiment. The sample volume was 0.05 ml. Urine samples were filtered through 0.45-μm filter membranes. Intensity measurements were made at a Raman shift of 1375 cm^{-1} 10 min after adding the sample to the colloid. The laser beam entered the sample horizontally and the scattered light was collected at right-angles. The intensity of the transmitted light was monitored simultaneously vs. the baseline corresponding to the stopped beam.

RESULTS AND DISCUSSION

The intensity of vibrational modes in SER spectra has been shown to change with the evolution of the colloid during adsorbate-induced ag-

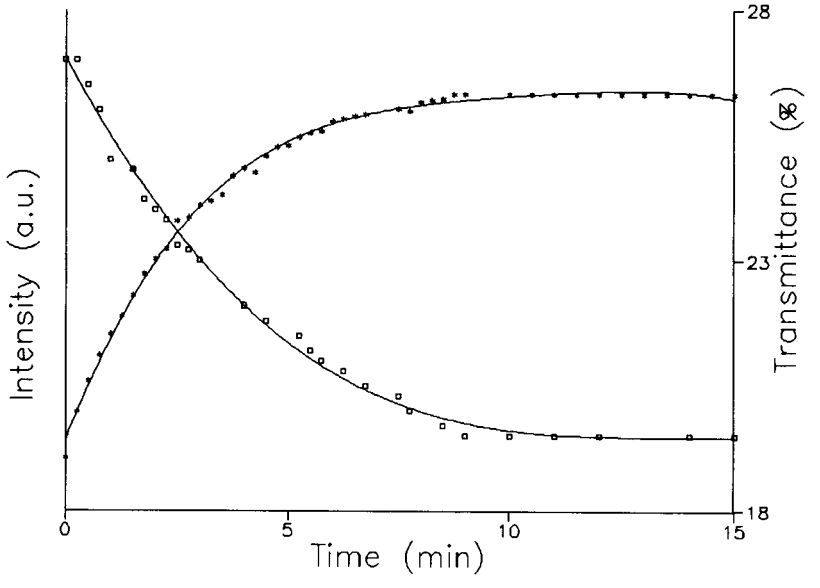

Fig. 1. SERS intensity (□) (Raman shift 1382 cm^{-1}) and transmittance (*) vs. time of a silver colloid with 5 μg ml^{-1} amiloride.

gregation [7]. Specific bands appear and disappear depending on the aggregation state of the colloid which is being recorded and may cause severe distortions in SERS intensities and, therefore, in quantitative measurements. The situation has been partially resolved by simultaneous mea-

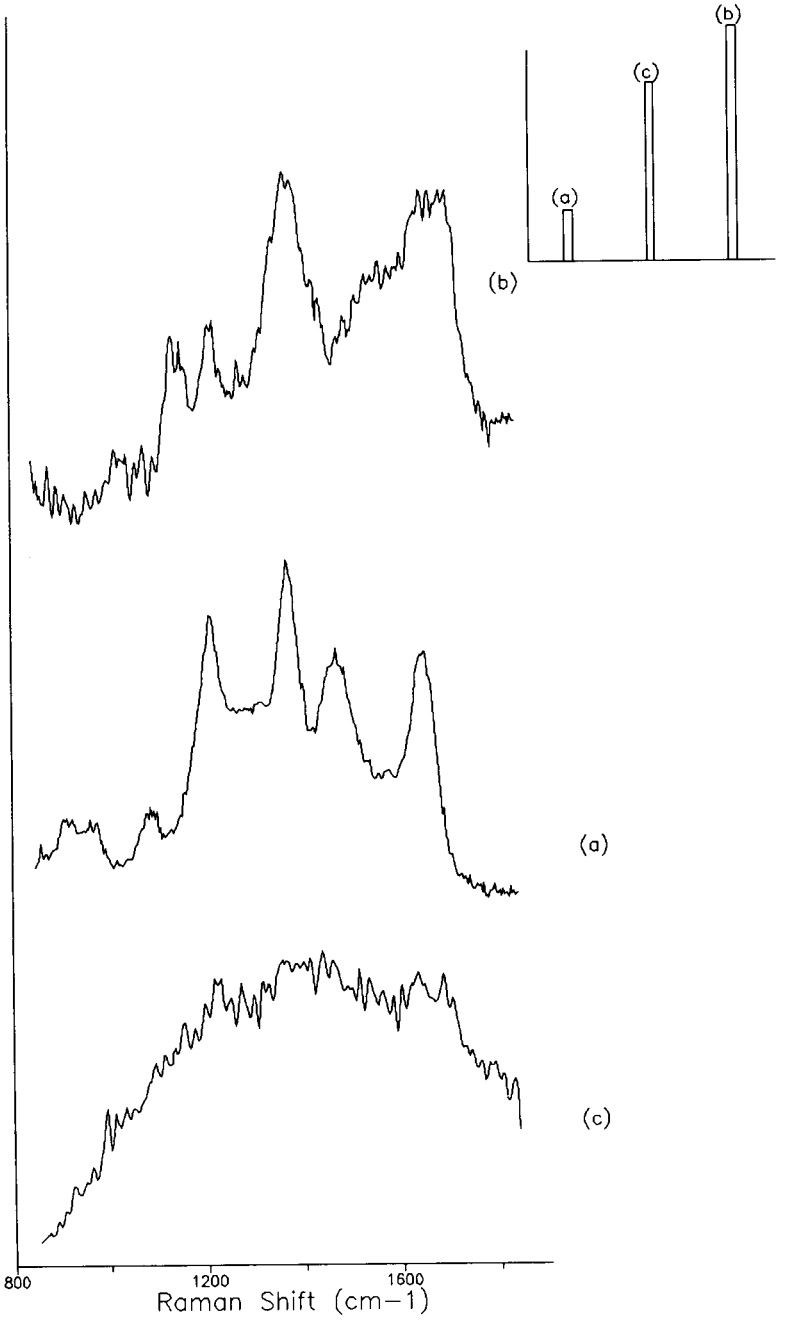

Fig. 2. (a) SERS spectrum of amiloride on colloidal silver. Amiloride concentration 5 μg ml^{-1}. (b) SERS spectrum of a urine sample containing 5 μg ml^{-1} amiloride. (c) SERS spectrum of urine blank, 5 min after addition to colloid.

surement of the scattering signal and transmitted light. Aggregation in colloidal systems proceeds concurrently with changes in the colour of the metal dispersions. These changes result from extinction bands associated with excitation of surface plasmons [10,11], and depend on the particle size [6] of the colloidal system. Thus the intensity of light transmitted by a colloid provides a real-time measurement of the aggregation state of the system.

Figure 1 shows the variation with time of scattering signal and transmitted light of a silver colloid aggregated with amiloride. The SERS signal increases with time as a result of aggregation, with a concomitant decrease in transmittance due to absorption by the colloid of the 488-nm exciting beam. Both signals reach stable readings simultaneously after about 10 min, indicating that a steady state has been achieved. It should be noted that the time needed for stable signals depends on the adsorbate concentration. Thus, in order to optimize the signal precision for quantitative purposes, the final value of the SERS intensities should be dictated by a stable reading of transmitted light. As shown below, this approach provides a further advantage in that the precision of transmittance measurements is better than that in SERS.

The SER spectrum of amiloride on colloidal silver recorded after constant transmittance is shown in Fig. 2a. The spectrum shows strong bands at Raman shifts of 1212, 1375, 1469 and 1648 cm^{-1}. Fig. 2b and c show the SER spectra of human urine spiked with amiloride and that of a urine blank, respectively. Urine samples show a strong signal background (Fig. 2c). As a broad band peaking at about 523.7 nm (1396 cm^{-1}), rather then a decaying background, is observed, the signal could be due to luminescence from urine components. The baseline of the spectra in Fig. 2 has been shifted for comparative purposes. The inset represents the intensities at 1375 cm^{-1} to scale. The amiloride bands at 1212 and 1375 cm^{-1} are easily recognized in the spectrum of spiked urine (Fig. 2b). No bands in this region appear in the spectrum of the urine blank. The broadening of the peak at 1375 cm^{-1} in urine is probably the result of the simultaneous existence of two or more surface environments for adsorbed amiloride in urine. Co-adsorption of endogenous urine components could also account for this observation, for the appearance of a peak at 1125 cm^{-1} and for a small intensity mode at 1020 cm^{-1}, which has previously been associated with urea [1].

Urine analysis

To evaluate possible matrix effects on the SERS response of amiloride, the analytical figures of merit of the SERS method were evaluated using water and urine as solvents for the drug. The results are summarized in Table 1. All quantitative data were taken after stable transmittance readings. As discussed earlier, urine causes a strong signal background, resulting in a higher intercept in the calibration graph. The analytical sensitivity of the method was calculated as the ratio of the calibration slope to the standard deviation. As the slope of the calibration graph is about four times larger in urine, the analytical sensitivity is also higher in this instance. The limit of detection (LOD) was calcu-

TABLE 1

Analytical figures of merit of the SERS method for amiloride

Matrix	Correlation coefficient	Intercept (arbitrary units)	Slope (μg^{-1} ml)	S_c [a] (arbitrary units)	LOD ($\mu g\ ml^{-1}$)	R.S.D. [b] (%)		
						T	S	C
Pure solvent	0.996	324	12.8	2.2	0.1	1.2	4.0	5.8
Urine	0.990	10800	46.2	6.2	6.9	1.7	5.5	7.5

[a] Analytical sensitivity, expressed as the ratio of the slope to the standard deviation. [b] Relative standard deviation of transmittance (T), SERS intensities at 1375 cm^{-1} (S) and amiloride concentration (C). The number of replicates was 10 at 100 $\mu g\ ml^{-1}$ amiloride.

lated as the concentration giving rise to a signal equal to the blank plus three times the standard deviation. The LOD for urine samples is poorer than that obtained with the pure solvent. This is due to the higher signal background of the blank and to the poorer precision of this method. The precision of transmittance measurements is much better than that of SERS intensities. This situation was expected as the signal levels involved in transmittance measurements are much higher. Nevertheless, the concentration relative standard deviations (R.S.D.s) provided by SERS are satisfactory.

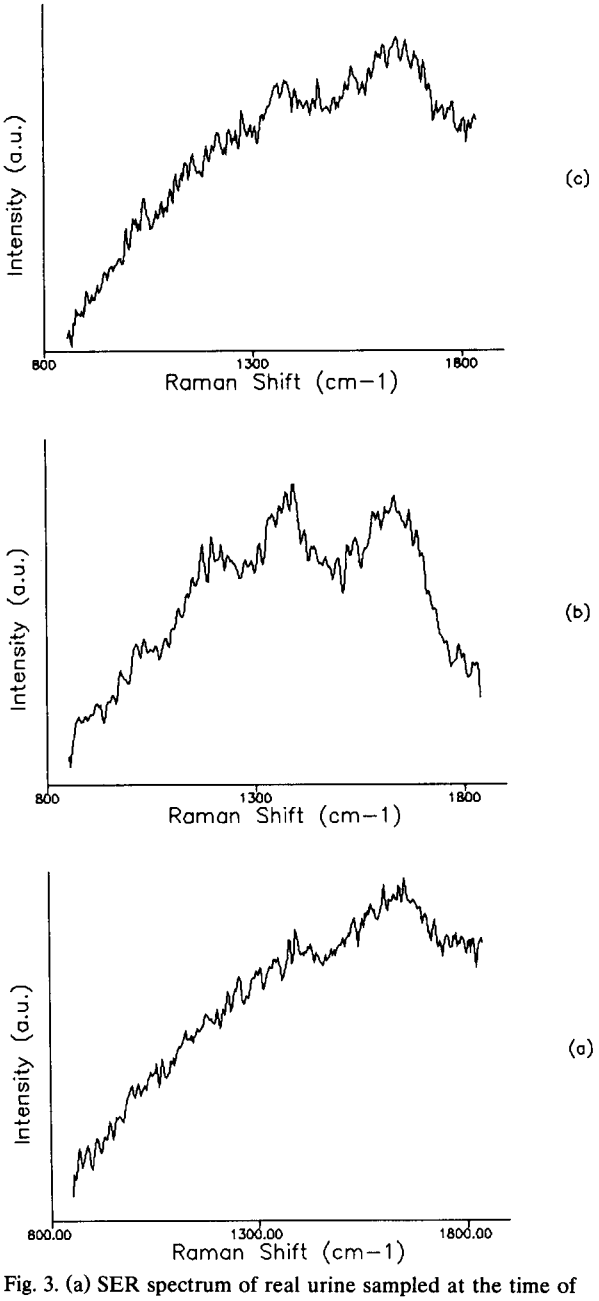

Fig. 3. (a) SER spectrum of real urine sampled at the time of a single oral dose of amiloride (2.5 mg). (b) SER spectrum of a urine sample taken 6 h after the dose. (c) SER spectrum of a urine sample taken 12 h after the dose.

Amiloride is rapidly excreted in urine in the native form, the concentration peaking 6–9.5 h after an oral dosis [9]. Three human urine samples were analysed following an oral dose of 2.5 mg. The SER spectra are shown in Fig. 3. As shown, amiloride can be recognized by the band at about 1375 cm^{-1}, which is more evident in the sample taken 6 h following the dose (Fig. 3b). The amiloride content of this sample obtained by the method of standard additions is about 6 μg ml^{-1}. Although these data have not been compared with those from another analytical technique, they indicate the potential of SERS for the detection of amiloride in urine.

Conclusions

Colloid SERS will not supplant other well established analytical techniques for the detection of drugs in urine samples in the near future. Urine is a complex mixture containing abundant suspended material and a variety of electrolytes. Thus, the SERS requirements for optimum colloid aggregation are difficult to achieve on a routine basis. Nevertheless, the results reported here demonstrate that the detection of amiloride in human urine by SERS on colloidal silver is feasible. The use of simultaneous transmittance and scattering measurements as demonstrated here is of help in improving signal reproducibility. The precision of 6–7% (R.S.D.) obtained with this approach is far better than the 15–20% level reported earlier for colloid SERS and tends to parallel that of state-of-the-art spectrochemical techniques.

This research was supported by the Dirección General de Investigación Científica y Técnica (Ministerio de Educación y Ciencia, Madrid, Pro-

ject PB87-0715) and the Dirección General de Universidades e Investigación (Consejería de Educación y Ciencia, Junta de Andalucía, Seville), Spain.

REFERENCES

1 A. Rupérez, R. Montes and J.J. Laserna, Vibr. Spectrosc., 2 (1991) 145.
2 W.S. Sutherland, J.J. Laserna, M.J. Angebranndt and J.D. Winefordner, Anal. Chem., 62 (1990) 689.
3 R. Montes and J.J. Laserna, Analyst, 115 (1990) 1601.
4 E.L. Torres and J.D. Winefordner, Anal. Chem., 59 (1987) 1626.
5 J.J. Laserna, E.L. Torres and J.D. Winedfordner, Anal. Chim. Acta, 200 (1987) 469.
6 J.A. Creighton, in R.K. Chang and T.E. Furtak (Eds.), Surface Enhanced Raman Scattering, Plenum, New York, 1982, p. 35.
7 R. Montes, C. Contreras, A. Rupérez and J.J. Laserna, Anal. Chem., 64 (1992) 2715.
8 C. Rodríguez, Dopaje, Interamericana, Madrid, 1992.
9 E.F. James (Ed.), Martindale. The Extra Pharmacopoeia, Reynolds, London, 29th edn., 1989.
10 M. Kerker, D.S. Wong, H. Chew, O. Siiman and L.A. Bumm, in R.K. Chang and T.E. Furtak (Eds.), Surface Enhanced Raman Scattering, Plenum, New York, 1982, p. 109.
11 P.C. Lee and D. Meisel, J. Phys. Chem., 86 (1982) 3391.

Analytica Chimica Acta, 280 (1993) 269–277
Elsevier Science Publishers B.V., Amsterdam

Simultaneous determination of traces of iron, cobalt, nickel, copper, mercury and lead in water by energy-dispersive x-ray fluorescence spectrometry after preconcentration as their piperazino-1,4-bis(dithiocarbamate) complexes

Oi-Wah Lau and Sing-Yiu Ho

Department of Chemistry, The Chinese University of Hong Kong, Shatin, NT (Hong Kong)

(Received 3rd December 1992; revised manuscript received 16th February 1993)

Abstract

A bidentate chelating agent has been proposed to preconcentrate seven metal ions dissolved in an aqueous sample for their simultaneous determination using energy-dispersive x-ray fluorescence spectrometry. The metal ions are precipitated as their polymeric piperazino-1,4-bis(dithiocarbamate) chelates, which are then collected by vacuum filtration on a Millipore membrane filter for direct examination by x-ray fluorescence analysis. Iron, cobalt, nickel, copper and zinc are determined by means of their K_α x-rays and mercury and lead by means of their L_α x-rays. A detection limit in the $\mu g\ l^{-1}$ range can be achieved for all metals tested in 250-ml water samples with a counting time of 600 s. Effective precipitation of all metals occurs at pH 6–7. The recoveries of eight analyses of the metals in a multielement standard using the proposed method ranged from 97 to 105% and the precision ranged from 2.3 to 3.1%. High concentrations of calcium and magnesium do not interfere with the method. The method is simple, sensitive and accurate, and has been used for the simultaneous determination of the seven metals under study in environmental samples and synthetic mixtures.

Keywords: X-ray fluorescence spectrometry; Chelation; Preconcentration; Trace metals; Waters

Energy-dispersive x-ray fluorescence spectrometry has become an important technique for the determination of trace elements in water [1] because of its capacity to perform simultaneous multielement analysis and its ability to display information on all elements at the same time [2]. The energy-dispersive spectrometers are less expensive than wavelength-dispersive spectrometers, although their resolution is much poorer than that of the latter. In determining trace metals in environmental water sample using energy-dispersive x-ray fluorescence spectrometry, a preliminary concentration step is usually necessary before the determination can be carried out.

Successful sample preparation procedures for x-ray fluorescence analysis are mostly based on the formation of insoluble compounds of trace metals with organic reagents, which are then collected as thin film deposits. Some reagents proposed for the purpose are 1-(2-pyridylazo)-2-naphthol [3], polyvinylpyrrolidone and thionalide [4]. Precipitation schemes using the dithiocarbamates with different organic substituents for preconcentrating the dissolved heavy metals have

Correspondence to: O.-W. Lau, Department of Chemistry, The Chinese University of Hong Kong, Shatin, NT (Hong Kong).

been described. Dithiocarbamates which have been used included diethyldithiocarbamate [5], pyrrolidinedithiocarbamate [6,7] and dibenzyldithiocarbamate [8–10]. However, these procedures required either a carrier element that has to be added to the sample to get an adequate amount of precipitate for trapping the trace metals or a long stirring and aging time, while dibenzyldithiocarbamate forms rather weak zinc complexes [8]. The use of a metal carrier would increase the absorption coefficient of the precipitate and result in lower x-ray intensities of the trace elements. In addition, the element used as a carrier cannot be determined in the sample.

The purpose of the present work was to assess a less common dithiocarbamate, disodium piperazino-1,4-bis(dithiocarbamate) [11] for the preconcentration of dissolved heavy metals in waters. The advantages of using the reagent are: (1) it forms with many metals polymeric chelates having low solubilities in water and organic solvents well suited for x-ray fluorescence spectrometry; (2) no carrier element is needed; and (3) it is easily prepared. The conditions for the preconcentration step have been optimised and the characteristics of the overall analysis procedure have been studied. The proposed method has been applied to determine the seven metals under study at the $\mu g\ l^{-1}$ levels in potable and polluted water samples.

EXPERIMENTAL

Apparatus

All x-ray measurements were carried out with a Tracor x-ray Spectrace 5000 energy-dispersive x-ray fluorescence spectrometer. The direct x-ray beam was provided by a low-power Rh target x-ray tube operated at 40 kV and 0.35 mA in an air environment for all x-ray measurements. The x-ray power supply allows a maximum operating voltage and current of 50 kV and 0.35 mA, respectively. An automated sample changer for ten samples and five sets of primary filters including aluminium, cellulose and thick and thin Rh filters between the x-ray tube and sample were provided. The characteristic x-rays were measured by a liquid nitrogen cooled lithium drifted silicon detector. A 0.05-mm Rh filter was used to reduce the scattering continuum. The typical counting time was 600 s livetime with system dead time losses averaging about 30%. The elements iron, cobalt, nickel, copper and zinc were determined by means of their K_α x-rays and mercury and lead by means of their L_α x-rays. The spectra were processed on a microcomputer using a peak fitting program, XML.

The filter equipment consisted of a Pyrex filter holder supplied by Millipore (Bedford, MA) and fitted with a reservoir, a circular fritted glass support and a metal clamp. The filter material used was HA type 47 mm diameter Millipore membrane filter of 0.45 μm pore size. The filtered sample supported on the membrane filter was protected with a 3.6 μm thick Mylar film and mounted on the plastic sample holder.

Reagents

All chemicals used were of analytical-reagent grade.

Distilled water which was further purified with a Milli-Q water purification system (Millipore) was used for preparing reagents and standard solution.

Disodium piperazino-1,4-bis(dithiocarbamate) was prepared as reported previously [11]: 11 g of piperazine hexahydrate in 30 ml of ethanol were added to 8.5 g of sodium hydroxide in 8 ml of pure water and 20 ml of ethanol at 10°C, and 15 g of carbon disulphide were added to the mixture at 10°C. The residue was recrystallized twice from a water–ethanol mixture (1:3, v/v). A 1% (w/v) aqueous solution of the reagent was used as the precipitating reagent. The solution was stored in a polyethylene bottle and kept in a refrigerator.

Stock solutions (1000 mg l^{-1}) were prepared as follows. Stock solutions of five metals, namely, iron, nickel, copper, zinc, and lead were prepared by dissolving 1.0000 g of the respective pure metal in a minimum amount of concentrated nitric acid and diluting to exactly 1 l with dilute nitric acid (ca. 0.1 M). Mercury(II) chloride (1.3603 g) was dissolved in 1 l of dilute nitric acid (ca. 0.1 M). Cobalt(II) sulphate heptahydrate (4.8180 g) was dissolved in 1 l of dilute nitric acid (ca. 0.1 M).

Intermediate standard solutions were prepared by appropriate dilution with purified distilled water. The multielement standards for calibration were prepared from these standards.

Ammonium acetate buffer solutions were prepared as follows. (a) Buffer of pH 6.5 was prepared by dissolving 154.2 g of ammonium acetate in 900 ml of pure water and adjusting to a pH of 6.5 with glacial acetic acid. The solution was diluted to 1 l. (b) Buffer of pH 3.7 was prepared by dissolving 120 ml of acetic acid and 27 g of ammonium acetate in 1 l of water. (c) Buffer of pH 9.5 was prepared by dissolving 200 g of ammonium acetate and 70 ml of concentrated ammonia in 1 l of water. (d) Other buffer solutions with pH 3.0–10.0 were prepared by adjusting buffers of pH 3.7 and 9.5 with either ammonia or acetic acid to obtain the desired pH value.

All buffer solutions were purified by removing the heavy metals with the precipitating agent followed by filtration.

Procedure

All glassware, beakers, pipettes and plastic bottles were cleaned by soaking them for one day in 10% nitric acid and rinsing with Milli-Q-grade water.

Precipitation of metal ions. To 250 ml of sample in a 400-ml beaker, 10 ml of 2 M ammonium acetate buffer solution of pH 6.5 were added, followed by the addition of 2 ml of 1.0% disodium piperazino-1,4-bis(dithiocarbamate) solution. The solution was stirred for 5 min. The precipitate formed was filtered off under suction on a 47-mm diameter, 0.45 μm pore size membrane filter and collected as a solid film, which was placed in a Petri dish and allowed to dry in air or in an oven at 50°C for 1 h. The filter was mounted with a 3.6-μm Mylar film in a plastic sample holder and subjected to x-ray fluorescence analysis.

Sample analyses. (a) Citrus leaves. About 0.5 g of citrus leaves was placed in a crucible and ashed in a furnace at 500°C for 2 h. The residue was wet with 5 drops of water and 2 ml of (1 + 1) nitric acid and evaporated on a hot plate. The residue was further ashed for 1 h at 500°C, and was then dissolved in 5 ml of (1 + 1) hydrochloric acid and diluted to 50 ml with purified distilled water. (b) Aluminium and Nimonic alloys. About 0.1 g of the sample was dissolved in the minimum amount of concentrated hydrochloric acid and diluted to 100 ml with purified distilled water. (c) Water samples were filtered through a 0.45 μm pore size membrane filter before the analysis.

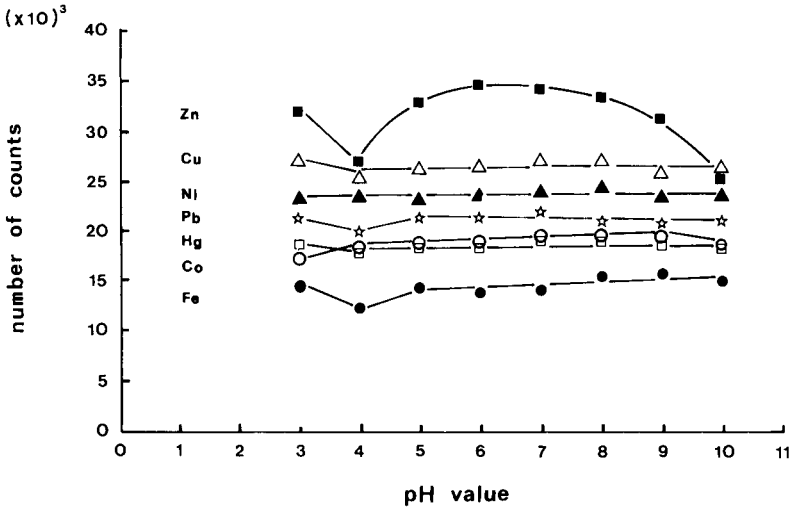

Fig. 1. Variation of count intensity of 25 μg of each metal with pH.

RESULTS AND DISCUSSION

Optimum conditions for the preconcentration step

The effect of the pH of the solution on complex formation was studied over the pH range of 3–10. Aliquots (5 ml) of the multielement standard solution containing 25 μg of each metal under study were used in the investigation. The pH profiles for each element under study are shown in Fig. 1, where it can be seen that the count number remained almost constant for each element except zinc in the pH range 5–9 indicating that the effect of pH on the complex formation of each element except zinc is slight in this range. For zinc, the effect of pH is slight in the pH range 6–7. Thus, the pH for complex formation for all elements was chosen to be 6.5.

The effect of the stirring time on the collection efficiency of the metals was studied. Several 5.0-ml aliquots of the multielement standard solution containing 2.5 μg of each metal were used, and 2.0 ml of 1% ligand solution were added to each solution, which were stirred for 1, 2, 5, 10 and 30 min, respectively. It was found that increasing the stirring time had little effect on the amount of metal complexes collected. The final procedure adopted a stirring time of 5 min, which is sufficient for complete collection of all elements under study and yet not unduly long for sample preparation.

The metal ions in aqueous solutions would eventually be collected as a solid film on the membrane filter prior to x-ray fluorescence analysis. The effect of the volume of samples containing the same absolute amount of metals on the collection efficiency of metals was investigated. Multielement standard solutions were made up to contain 25 μg of each metal under study but with volumes varying from 50 ml to 500 ml. They were then subjected to the same analytical procedure. Results obtained from measurements of the samples are summarized in Table 1, where it can be seen that the intensity counts for all metals remained relatively constant when the volume of sample solution increased, indicating that the volume of solution had little effect on the recovery of the metal ions under study. A sample volume of 250 ml was chosen to give adequate detection limits to the elements determined and the advantages of easy handling and short filtration time.

The water used for preparing reagents and standard solutions was distilled then purified with a Milli-Q water purification system. All buffer solutions were further purified by removing the heavy metals by pretreatment with the proposed reagent. The x-ray spectrum of the reagent blank did not exhibit any signals above the detection limits of the metals under study, and thus no correction was deemed necessary.

Calibration, recovery tests, precision and detection limits

The method of multielement calibration was used to simulate the composition of samples and to detect any interelemental effect. An x-ray

TABLE 1

A study of the effect of sample volume [a]

Volume (ml)	Counts/600 s						
	Fe	Co	Ni	Cu	Zn	Hg	Pb
50	15725	20443	25148	28431	34799	20146	22933
100	14899	19846	24346	27968	33000	19207	21726
150	15104	19770	24402	27926	34396	18991	22235
200	14692	19356	24464	28070	33694	18820	21606
250	14093	19528	23989	27206	33088	18351	21059
300	14820	19197	24219	27725	33484	18789	21867
500	14719	18690	23976	27466	32522	18312	21012
Mean intensity	14865	19547	24363	27827	33569	18945	21777
R.S.D.(%)	3.3	2.8	1.6	1.5	2.4	3.3	3.1

[a] Each solution contained 25 μg of each metal.

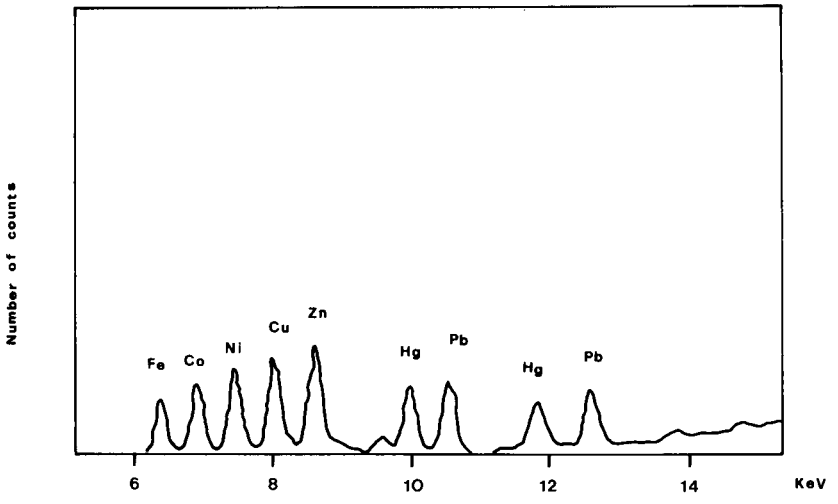

Fig. 2. X-ray spectrum of a standard mixture containing 25 μg of each metal under study. Tube voltage, 40 kV. Live time 600 s.

TABLE 2

Calibration parameters of the elements under study

Element	Slope [a]	Intercept [b]	Correlation coefficient [c]	Detection limits [d] (μg)
Fe	0.2333	−0.0003	0.9998	0.140 (0.560)
Co	0.3185	0.1333	0.9999	0.100 (0.400)
Ni	0.3925	0.1509	0.9999	0.083 (0.332)
Cu	0.4383	0.4682	0.9998	0.071 (0.284)
Zn	0.5120	0.7660	0.9999	0.075 (0.300)
Hg	0.3035	0.3374	0.9997	0.119 (0.476)
Pb	0.3475	0.5119	0.9998	0.105 (0.420)

[a] In count s^{-1} l μg^{-1} using 250 ml of solution. [b] In count s^{-1}. [c] 7 calibration results. [d] Concentration in 250 ml of solution (in μg l^{-1}) is given in parentheses.

TABLE 3

Recovery tests

	Element						
	Fe	Co	Ni	Cu	Zn	Hg	Pb
First multielement standard mixture							
Amount taken (μg/l)	100	80	60	40	20	40	60
Amount found [a] (μg/l)	101	81	60	40	21	42	60
R.S.D. (%)	2.1	3.0	4.1	5.0	3.9	2.8	4.1
Recovery (%)	101	101	100	100	105	105	100
Second multielement standard mixture							
Amount taken (μg/l)	20	40	60	80	100	20	40
Amount found [b] (μg/l)	20.3	40	60	82	103	19.4	40.8
R.S.D. (%)	2.6	3.1	2.3	2.3	2.6	3.0	2.4
Recovery (%)	101	100	100	102	103	97	102

[a] Average of three determinations. [b] Average of eight determinations.

spectrum showing the characteristic peaks of all elements under study is shown in Fig. 2. Linear relationships were obtained for the seven metals under study. Regression lines were found by the least-squares method and the corresponding calibration parameters are shown in Table 2.

Recovery tests were performed using two synthetic samples containing the metal ions under study in different ratios. The results are given in Table 3 where it can be seen that the recoveries range from 97 to 105% with most in the range of 100–102%. Hence, the result may be considered quite good and also indicate that in the proposed method negligible interelemental effect was observed.

An estimate of the precision (%R.S.D.) for each element at the respective concentration shown in Table 3 was determined from eight different trials, as summarized in the table. The relative standard deviation (R.S.D.) varies from 2.3 to 3.1%, and may be considered good for determinations at the $\mu g\ l^{-1}$ levels.

The detection limits, calculated as the amount of each element giving a signal equal to three times the square root of that of the average background [5], are in the range of 0.07–0.14 μg, as shown in Table 2. These limits correspond to concentrations in the range 0.28–0.56 $\mu g\ l^{-1}$ when 250-ml water samples are used.

Interference studies

Synthetic sea water was prepared with a composition shown in Table 4 and spiked respectively with 5 and 25 μg of each metal under study, and the amount of each metal added was determined. The results are shown in Table 4. It can be seen that a large excess of alkali and alkaline earth ions in the sample matrix has a negligible effect on the determination.

TABLE 5

Determination of Fe, Cu, Zn and Pb in citrus leaves [a]

	Element			
	Fe	Cu	Zn	Pb
Certified value [g] ($\mu g\ g^{-1}$)	90 (10)	16.5 (1.0)	29.0 (2.0)	13.3 (2.4)
Value found [b] ($\mu g\ g^{-1}$)	99 (5.8)	17.5 (0.72)	30.1 (1.6)	13.3 (1.5)

[a] NBS standard reference material 1572. [b] Values in parentheses are standard deviations ($n = 6$).

Analysis of standard reference materials and water samples

The accuracy of the proposed method was checked by determining the contents of heavy metals under study simultaneously in three standard reference materials, namely, citrus leaves (NBS Standard Reference Material 1572), aluminium (BCS Certified Reference Material 1813) and Nimonic alloys (BCS Certified Reference Material 310/1). The results are shown in Tables 5–7, respectively. It can be seen that there is an excellent agreement between the certified values and the experimentally determined values, demonstrating the accuracy of the proposed method.

The applicability of the proposed method to the determination of heavy metals in potable and waste waters was examined by analysing 250-ml aliquots of a tap water sample, a sea water sample collected from Tolo Harbour close to the

TABLE 4

Interference study on synthetic sea water sample [a]

Mixture	Element found (μg)						
	Fe	Co	Ni	Cu	Zn	Hg	Pb
1 [b]	5.2	5.07	5.1	5.2	5.2	5.2	5.05
Relative error (%)	4.0	1.4	2.0	4.0	4.0	4.0	1.0
2 [c]	24.0	25.6	25.8	26.0	26.0	25.7	26.0
Relative error (%)	−4.0	2.4	3.2	4.0	4.0	2.8	4.0

[a] Composition (concentration in g l^{-1}): NaCl, 25.40; $MgCl_2 \cdot 6H_2O$, 10.85; $CaCl_2 \cdot 2H_2O$, 1.46; KCl, 0.72; H_3BO_3, 0.026; and $Sr(NO_3)_2$, 0.27. [b] Mixture containing 5 μg of each element. [c] Mixture containing 25 μg of each element.

TABLE 6

Determination of Fe, Ni, Cu and Zn in an aluminium alloy [a]

	Element			
	Fe	Ni	Cu	Zn
Certified value (%)	0.72	2.00	2.48	2.52
Content found [b] (%)	0.75 (0.037)	2.01 (0.04)	2.45 (0.04)	2.61 (0.04)

[a] BCS certified reference material 1813. [b] Values in parentheses are standard deviations ($n = 6$).

TABLE 7

Determination of Co and Ni in a Nimonic alloy [a]

	Element	
	Co	Ni
Certified value (%)	17.0	58.6
Content found [b] (%)	16.4 (0.4)	59.3 (1.7)

[a] BCS Certified reference material 310/1. [b] Values in parentheses are standard deviations ($n = 6$).

TABLE 8

Determination of metals in tap water sample [a]

	Element						
	Fe	Co	Ni	Cu	Zn	Hg	Pb
Amount found: ($\mu g\ l^{-1}$)							
Trial [b] 1	11.30	N.D.	0.24	N.D.	24.60	N.D.	N.D.
2	11.69	N.D.	0.26	N.D.	24.12	N.D.	N.D.
Average [c]	11.5 (0.28)		0.25 (0.01)		24.4 (0.34)		
Spiked result [d] ($\mu g\ l^{-1}$)							
Trial 1	76.12	60.50	60.42	59.85	84.68	59.79	60.28
2	74.74	60.14	62.28	62.30	84.81	62.26	62.90
Average [c]	75.4 (0.98)	60.3 (0.25)	61 (1.32)	61 (1.73)	84.7 (0.09)	61 (1.75)	62 (1.85)
Recovery (%)	106	100	101	102	101	102	103

[a] Sample volume, 250 ml. [b] N.D. = not detected. [c] Values in parentheses are standard deviations ($n = 2$). [d] Spike, 60 $\mu g\ l^{-1}$.

TABLE 9

Determination of metals in sea water sample [a]

	Element						
	Fe	Co	Ni	Cu	Zn	Hg	Pb
Amount found ($\mu g\ l^{-1}$)							
Trial [b] 1	1.50	N.D.	4.38	0.84	10.01	N.D.	N.D.
2	1.21	N.D.	3.94	0.81	10.70	N.D.	N.D.
Average [c]	1.4 (0.21)		4.2 (0.31)	0.83 (0.02)	10.4 (0.49)		
Spiked result [d] ($\mu g\ l^{-1}$)							
Trial [b] 1	22.19	19.17	23.82	20.53	31.27	20.88	18.91
2	21.89	19.47	25.43	21.48	30.35	19.82	19.36
Average [c]	22.0 (0.21)	19.3 (0.21)	25 (1.14)	21.0 (0.67)	30.8 (0.65)	20.4 (0.75)	19.1 (0.32)
Recovery (%)	103	96.6	104	101	102	102	95.5

[a] Sample volume, 250 ml. [b] N.D. = not detected. [c] Values in parentheses are standard deviations ($n = 2$). [d] Spike, 20 $\mu g\ l^{-1}$.

TABLE 10

Determination of metals in water sample [a] collected from Fo Tan nullah

	Element						
	Fe	Co	Ni	Cu	Zn	Hg	Pb
Amount found ($\mu g\ l^{-1}$)							
Trial [b] 1	583.9	0.46	11.07	14.62	180.9	N.D.	16.60
2	575.4	0.54	11.14	14.94	177.7	N.D.	16.12
3	581.3	1.10	10.27	14.00	176.3	N.D.	15.91
Average [c]	580	0.7	10.8	14.5	178		16.2
	(4.36)	(0.35)	(0.48)	(0.48)	(2.36)		(0.35)
Spiked result [d] ($\mu g\ l^{-1}$)							
Trial 1	636.9	57.13	65.69	71.44	227.1	57.06	73.19
2	632.2	57.06	67.17	71.39	231.9	58.02	74.43
3	653.4	59.15	69.80	74.10	240.2	58.71	76.55
Average [c]	640	58	68	72	233	57.9	75
	(11.1)	(1.19)	(2.08)	(1.55)	(6.58)	(0.83)	(1.70)
Recovery (%)	100	95.5	95.3	95.8	91.7	96.5	98.0

[a] Sample volume, 250 ml. [b] N.D. = not detected. [c] Values in parentheses are standard deviations ($n = 3$). [d] Spike, 60 $\mu g\ l^{-1}$.

University and a waste water sample collected at Fo Tan, an industrial area near the university, and two treated waste water samples. Analysis was repeated after spiking each water sample with known amounts of the metal ions under study. The results are collected in Tables 8–12. It can be seen that concentrations of these metals at the $\mu g\ l^{-1}$ levels can be determined with good precision and recoveries using the proposed method. It is worthy to note that appreciable amounts of copper, lead, nickel and zinc were found in the water sample collected from a nullah (Table 10), which were thought to be due to illegal discharge of effluents from the metal plating industry nearby. Similarly, the heavy metals found in the treated waste water samples might

TABLE 11

Determination of metals in treated effluent sample [a] from Shatin sewage treatment works

	Element						
	Fe	Co	Ni	Cu	Zn	Hg	Pb
Amount found ($\mu g\ l^{-1}$)							
Trial [b] 1	5.28	N.D.	62.79	0.261	18.68	N.D.	N.D.
2	4.45	N.D.	59.90	0.57	15.78	N.D.	N.D.
3	5.62	N.D.	60.22	0.66	17.72	N.D.	N.D.
Average [c]	5.1		61	0.5	17		
	(0.60)		(1.58)	(0.21)	(1.48)		
Spiked [d] *result* ($\mu g\ l^{-1}$)							
Trial 1	25.24	18.77	78.45	19.46	36.37	18.05	18.36
2	25.85	19.38	79.58	20.70	35.82	18.02	19.20
3	24.65	18.19	78.90	19.52	35.12	18.39	18.44
Average [c]	25.2	18.8	79.0	19.9	35.8	18.2	18.7
	(0.60)	(0.59)	(0.57)	(0.70)	(0.62)	(0.21)	(0.46)
Recovery (%)	101	94	90	97	94	91	94

[a] Sample volume, 100 ml. [b] N.D. = not detected. [c] Values in parentheses are standard deviations ($n = 3$). [d] Spike, 20 $\mu g\ l^{-1}$.

TABLE 12

Determination of metals in treated effluent sample [a] from Tai Po sewage treatment works

	Element						
	Fe	Co	Ni	Cu	Zn	Hg	Pb
Amount found ($\mu g\ l^{-1}$)							
Trial [b] 1	9.18	N.D.	18.03	33.63	53.07	N.D.	3.68
2	8.39	N.D.	17.96	32.19	50.97	N.D.	3.38
3	9.43	N.D.	19.33	33.44	55.10	N.D.	3.40
Average [c]	9.0		18.4	33.1	53		3.5
	(0.54)		(0.77)	(0.78)	(2.07)		(0.17)
Spiked result [d] ($\mu g\ l^{-1}$)							
Trial 1	26.74	18.73	36.85	53.48	71.31	19.54	23.26
2	25.18	19.19	37.90	53.27	72.92	19.35	22.49
3	28.18	18.50	38.18	54.94	76.66	19.39	23.93
Average [c]	27	18.8	37.6	53.9	74	19.4	23.2
	(1.50)	(0.35)	(0.70)	(0.91)	(2.74)	(0.10)	(0.72)
Recovery (%)	90	94	96	104	105	97	99

[a] Sample volume, 250 ml. [b] N.D. = not detected. [c] Values in parentheses are standard deviations ($n = 3$). [d] Spike, 20 $\mu g\ l^{-1}$.

also come from the metal plating industry. The recoveries for some of the metals in the waste water samples shown in Tables 10–12 were relatively low compared to earlier results possibly due to the complexity of the matrix studied in which different elemental species may be present.

Conclusions

A simple, sensitive, efficient and accurate method has been developed for the simultaneous determination of iron, cobalt, nickel, copper, zinc, mercury and lead using energy-dispersive x-ray fluorescence spectrometry. Negligible interelemental effects were detected and detection limits down to the $\mu g\ l^{-1}$ level were obtained. The metals in solution are collected by forming insoluble polymeric chelates with piperazino-1,4-bis(dithiocarbamate), which have low solubilities in water and organic solvents so that no carrier ion is needed. A commparatively wide pH range for the formation of the complex makes time-consuming pH adjustment unnecessary. The procedure gives the specimen in the form of a thin homogeneous film supported on a membrane filter, which may be examined again if necessary. The method has the advantages of allowing convenient multielement determination in contrast to the single element determination in atomic absorption spectrometry. In comparison with neutron activation analysis x-ray fluorescence spectrometry is less expensive and not limited by the proximity of a suitable reactor. The proposed method is suited for the simultaneous determination of traces of many heavy metals under study in both polluted and unpolluted water samples.

REFERENCES

1 K. Hirayama, and D.E. Leyden, Anal. Chim. Acta, 188 (1986) 1.
2 R. Jenkins, X-ray Fluorescence Spectrometry, Wiley, New York, 1988, p. 93.
3 P. Pueschel, Talanta, 16 (1969) 351.
4 R. Panayappan, D.L. Venezky, J.V. Gilfrich and L.S. Birks, Anal. Chem., 50 (1978) 1125.
5 H. Watanabe, S. Berman and D.S. Russell, Talanta, 19 (1972) 1363.
6 A.J. Pik, A.J. Cameron, J.M. Eckert, E.R. Sholkovitz and K.L. Williams, Anal. Chim. Acta, 110 (1979) 61.
7 T. Tisue, C. Seils and R.T. Keel, Anal. Chem., 57 (1985) 82.
8 H.R. Linder, H.D. Seltner and b. Schreiber, Anal. Chem., 50 (1978) 896.
9 G.S. Caravajal, K.I. Mahan and D.E. Leyden, Anal. Chim. Acta, 135 (1982) 205.
10 D.E. Leyden, K. Goldbach and A.T. Ellis, Anal. Chim. Acta, 171 (1985) 369.
11 S.P. Gupta and D.M.L. Garg, J. Indian Chem. Soc., 42 (1965) 412; CA, 63 (1965) 11562a.

Analytica Chimica Acta, 280 (1993) 279–287
Elsevier Science Publishers B.V., Amsterdam

Kinetic determinations of reactants utilizing uncatalyzed reactions

Horacio A. Mottola

Department of Chemistry, Oklahoma State University, Stillwater, OK 74078–0447 (USA)

(Received 15th December 1992; revised manuscript received 16th March 1993)

Abstract

Kinetic-based determinations of reactants utilizing uncatalyzed chemical reactions do not match the popularity of catalytic methods for the determination of catalysts (particularly transition metal ions) or reactants (e.g., in enzymatic reactions) and this reflects on the scarcity of reviews on the topic. In some cases, however, advances in instrumentation and data manipulation provide competitive alternatives to nonkinetic-based methods for single as well as multispecies determinations. Such advances are reviewed here and applications illustrated.

Keywords: Kinetic methods; Review; Uncatalyzed reactions

Recorded kinetic analytical applications of systems in which a catalytic cycle or a rate-modifying effect is not in operation are considerably fewer than those in which catalysis, in particular, is exploited for practical purposes. In some instances, however, thanks to advances in instrumentation (e.g., stopped-flow mixing) and in data manipulation (e.g., predictive equilibrium-value methods) uncatalyzed reactions provide competitive alternatives to the solution of analytical problems.

In contrast to catalytic or catalysis-related methods, uncatalyzed ones are not primarily used to determine low concentrations. The bulk of analytical applications of uncatalyzed reactions can be classified as:

(1) Determination of single species (this includes several applications of luminescence);

(2) Simultaneous determination of two or more species (commonly known as *differential methods*)

Correspondence to: H.A. Mottola, Department of Chemistry, Oklahoma State University, Stillwater, OK 74078–0447 (USA).

Some determinations are based on measurement or calculation of the rate of change of signal (proportional to concentration) and should properly be designated as *rate methods*. All rate methods are kinetic in nature; there are, however, kinetic-based methods in which a rate of change of signal is not used for determination and the designation of rate method is unwarranted.

From a practical viewpoint, methods based on uncatalyzed reactions for reactants determination have proved more useful in the determination of organic species, although in a few instances that of inorganic species by these methods have also been proposed.

The considerations presented here focus on methods based on the rate of change of chemical composition with time. Equally important however, are rates of change of physical properties of the system because physical time-dependent processes have a clear impact on contemporary analytical chemistry (Chap. 1 in [1]). Although most of the points addressed in this review apply equally to kinetic determinations based on catalyzed reactions, the scope has been limited here

to uncatalyzed ones in order to single out progress in this particular area.

DETERMINATION OF SINGLE SPECIES

Rate considerations

Uncatalyzed reactions used in chemical analysis can mechanistically be classified as following pseudo-zero-order, first-order, or pseudo-first-order kinetics (Chap. 6 in [1]). Table 1 summarizes the mathematical relationships operative in the most relevant determinations of a single species in uncatalyzed processes and for the most common case, a bimolecular reaction of the type:

$$A + R \underset{k_b}{\overset{k_f}{\rightleftharpoons}} P$$

where A = species of analytical interest (analyte), R = added reagent, P = products, k_f = forward rate coefficient, and k_b = backward rate coefficient.

If different chemical species in a mixture have significant different rates of reaction with a common reagent, it may be possible to treat each species separately. Conditions under which one of the components can be determined in a mixture undergoing reaction without a significant error are not difficult to find in such cases [1,2]. The criteria for neglecting a slower-reacting or a faster-reacting component are the ratio of the corresponding rate coefficients, the time selected for measurement, and the tolerable error. If the ratio of rate coefficients is 463 : 1, it is possible to find a reaction time at which 99% of the faster component has reacted but only about 1% of the slower one. The situation is in essence a special case of differential methods [1].

Instrumentation

Conventional instrumental requirements for kinetic methods (Chap. 9 in [1], Chap. 7 in [3]) apply to determinations of reactants making use of uncatalyzed reactions. Two instrumental approaches are receiving attention in this kind of determinations. Stopped-flow mixing permits study of systems with relatively fast reactions, while continuous addition of reagent at a constant rate provides an alternative to stopped flow [4].

Data manipulation and errors

Error analysis in kinetic-based determinations has been dealt in general in Chap. 10 in [1]. The

TABLE 1

Mathematical relationships of application in the determination of a single species in uncatalyzed processes [1]

Mathematical relationship	Comments
$d[P]_t/dt = k_f[A]_0[R]_0 = \text{constant}$	This relationship provides the basis for initial rate measurements under pseudo-zero-order conditions. If $[R]_0$ is constant, the initial rate plotted agains $[A]_0$ should be a straight line (working curve for the determination of $[A]_0$). k_f = forward rate coefficient
$d[P]_t/dt = k_f[A]_0 \exp(-k_f t)$	This relationship applies if $[R]_0$ is absent (first-order conditions) and a "derivative approach" to measurement is used
$[A]_t = [A]_0 \exp(-k_f t)$	This relationship applies if $[R]_0$ is absent and integral approaches are chosen for measurement (e.g., fixed-time or variable-time approaches)
$d[P]_t/dt = k_f[R]_0[A]_t = k_f'[A]_t$	This equation permits pseudo-first order reactions to be mathematically treated as true first-order reactions. In this case $[R]_0$ is sufficiently large that it can be considered constant
$d[P]_t/dt = k_f([A]_0 - [P])[R]_0$	This applies when reaction conditions are such that the reaction is second order

choice of methods of manipulation of collected data is intimately linked to the measurement approach and error associated with the approach. Three basic approaches deserve consideration: (a) single-rate measurement, (b) two-rate measurement, and (c) multi-rate measurement. Such measurements are basically the common ones in kinetic-based determinations:

(1) Initial rate estimation, which can be by either a differential, quasi-differential, or integral method. Differential measurement involves direct evaluation of d[signal]/dt. Quasi-differential measurements result from either a fixed-time approach (measurement of Δ[signal] during a finite but short Δt) or variable-time approach (measurement of Δt needed to attain a finite but small Δ[R]). Integral methods, as their name implies, are based on the integration of the corresponding rate expressions over a finite, constant, and normally small time interval $t_2 - t_1$ (t_1 may be equal to zero). If these measurements are performed when no more than about 2% reactant conversion has been allowed to occur, the measurement qualifies as *initial rate*.

(2) Intermediate-rate measurements involve evaluation of d[signal]/dt or, for methods with linear response, Δ[signal]/Δt at any given time during the reaction. This approach is normally used in association with multipoint rate evaluations.

Pardue [5] has subdivided methods for single-component determination as methods without error compensation and with error compensation. Table 2 is based on this grouping. Single-rate and two-rate measurement approaches exemplify direct computation, while multi-rate measurements, although also amenable to direct computation, are better served by curve-fitting procedures. Recent work has shown an increased use of curve-fitting methods over the traditional approach by direct computation. The availability of low-cost computational tools is in part responsible for this, but the recognition of better utilization of experimental information and the usefulness of predictive (extrapolative) approaches also enter in the picture. Direct computational approaches used fixed mathematical expressions to extract the concentration of the sought-for species. Curve-fitting methods, on the other hand, compute values of parameters (e.g., signal) representing the *best fit* of a mathematical model describing the signal vs. time data. Least-square methods are commonly used but the utility of other curve-fitting approaches such as the Kalman filter [6] has also been demonstrated. Curve-fitting has been applied to both linear models [7] and nonlinear ones [8]. Predictive approaches are based on curve-fitting and permit deriving from a large but incomplete number of data points in the signal vs. time profile, the *best estimate* of the signal change expected if the system were allowed to reach equilibrium. Predictive methods are particularly useful in kinetic determinations based on uncatalyzed reactions, since catalysts are not amenable to determination by this approach. They can be used, however, to determine the reactant of a catalyzed reaction (e.g., the substrate in an enzyme-catalyzed one).

TABLE 2

Classification of single-component determinations based on measurement and data processing approaches [5]

Methods without error compensation	
Direct computational methods:	integral methods (e.g., fixed- and variable-time)
	Rate methods (e.g., initial rate and intermediate-rate measurements)
Curve-fitting methods:	integral methods (linear responses, nonlinear responses, rate methods)
Methods with error compensation	
Direct computational methods:	integral methods (rate constant, four-point, three-point, partial sums, two-point fixed time, and rate methods)
	Curve-fitting methods (integral and rate methods)

Error compensation is targeted at minimizing the effect that experimental variables have on rate coefficients. This recognizes that those effects affect rate coefficients to a greater extent than they affect the equilibrium concentration ratio (equilibrium constant). Error compensation by direct computation may involve a single rate measurement [9], two rate measurements [10], or multi-point curve-fitting methods (particularly for predictive purposes) [8,11].

Applications of single-component determinations using uncatalyzed reactions

As already stated, single-component determinations based on uncatalyzed reactions have been used chiefly for determination of organic species. A few methods, however, have been proposed for inorganic species. Tables 6.1 and 6.2 in [1] and pp. 142 to 147 in [3] are sources recommended to the interested reader. Updates of these listings can be found in the biennial *Analytical Chemistry*

TABLE 3

Selected determinations of inorganic and organic species by means of rates of uncatalyzed reactions

Species determined	Comments	Ref.
Determination of inorganic species		
Aluminum	Fluorescence measurement. Metal chelate formation with 2-hydroxy-1-naphthaldehyde *p*-methoxybenzoyl-hydrazone. Initial rate determination of aluminum in serum	15
Europium	Sensitive determination by microsecond time-resolved fluorometry. Fluorescence results from complexation with 4,7-bis(chlorosulfophenyl)-1,10-phenanthroline-2,9-dicarboxylic acid	16
Niobium	Photometric monitoring of color formation with 4-(2-pyridylazo)resorcinol. Fixed-time method. Interference from tantalum(V) eliminated by masking with tartrate	17
Nitrite	Photometric monitoring of the Griess reaction (red azo dye formation from sulfanilic acid and 1-naphthylamine). Stopped-flow mixing. Variable-time procedure. Determination in the 10^{-6} M range	18
Vanadium	Photometric monitoring of color formation with 1,8-diamino-4,5-dihydroxyanthraquinone-2,7-disulfonic acid. Method of tangents. Determination of nonvolatile V(V) in crude oil samples	19
Determination of organic species		
Methemoglobin	Reaction with cyanide. Absorbance monitoring (630 nm) and curve fitting. Determination of hemoglobin in whole blood after reaction with hexacyanoferrate(III). Stopped-flow or centrifugal mixing used	20
Methyl parathion	Determination of the insecticide in commercial formulations and aqueous samples of environmental origin. Rate method based on the alkaline hydrolysis of the analyte	21
Aminoaryl sulfonamides	Initial rate data treatment. Monitoring absorbance of azo dye produced by reaction with 1-naphthol (acetate buffer, pH 4.15) and continuous addition of nitrite as developing reagent	22
Tartaric acid	Determination in pharmaceutical preparations and in impure citric acid. Reaction with periodate monitored with a periodate ion-selective electrode. Initial rate measurement	23
Theophylline	Formation of a 1:1 complex between the oxidation product of theophylline and Ce(IV), the oxidant. Stopped-flow mixing. Determination in commercial pharmaceutical samples	24
Thiamine	Continuous addition of reagent. The oxidation of the analyte by hexacyanoferrate (III) produces a fluorescent product. Initial rate treatment of rate information	25
Uric acid	Determination in serum and urine. Stopped-flow mixing and fluorometric monitoring	26
Zineb	Zinc-containing dithiocarbamate-type pesticide and fungicide. Decomposition of zineb and complexation of the liberated zinc with zincon. Continuous addition of reagent and photometric monitoring. Determination in vine and olive leaves	27

Fundamental Reviews published by the American Chemical Society via its journal *Analytical Chemistry* [12,13]. Table 3 illustrates, with selected examples, typical applications for inorganic as well as organic species.

SIMULTANEOUS DETERMINATION OF TWO OR MORE SPECIES (DIFFERENTIAL METHODS)

Since conditions for determining more than one species simultaneously are difficult to design, differential rate determinations are less frequently described in the literature than some other kinetic methods, particularly those exploiting catalysis. The use of the word *differential* has no mathematical connotation and only implies the possibility to differentiate chemical species by simultaneous determination without prior separation. The terminology of *simultaneous kinetic-based determinations* has been proposed as a better alternative [14]. The designation of *differential kinetic methods* is widely accepted and, consequently, will be used here. This is in recognition that other terminologies (e.g., chromatography and flow-injection analysis) are equally open to criticism but widely used.

Differential methods fall into two broad categories depending on the approach used: (1) methods based on graphical treatment of data, and (2) methods based on mathematical computations.

These approaches have some common features, and sometimes the classification must be based on the predominant ones. Differential rate determinations are not designed, in most cases, to measure low concentrations and most applications are for the determination of organic species.

Rate considerations

Mark and Rechnitz [2] have proposed a classification of differential reaction rate methods based on reaction order. Figure 1 illustrates such a classification. A few differential reaction rate methods are based on the measurement of initial rates; since in these cases the kinetics becomes pseudo-zero-order, they are not included in Fig. 1. A critical evaluation of the different methods is available [28].

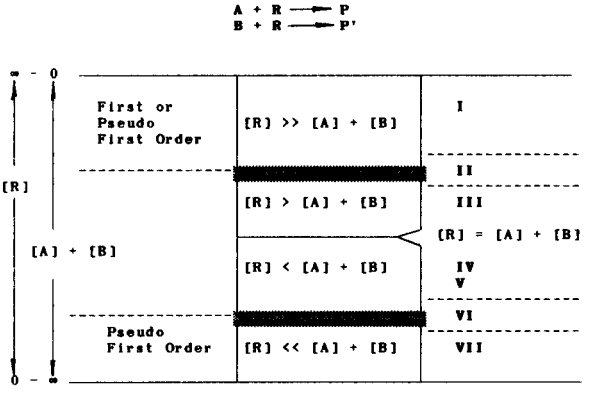

Fig. 1. Classification of differential reaction rate methods based on reaction order (adapted from p. 79 in [2]).

Whenever possible, the conditions for the bimolecular reactions of a binary (or by extension any number of target analytes) mixture of components A and B with a common reagent R are adjusted so that pseudo-first-order kinetics is followed. A 50-fold or greater excess of reagent or reactant (regions I and VII in Fig. 1) provides such a condition. Experimental conditions in the bulk of published applications fall in Region I of Fig. 1. Mathematical equations on which the methods of Region I are based are summarized in Table 4.

Instrumentation

Many differential rate determinations need only conventional means of mixing, but stopped-

TABLE 4

Mathematical relationships that apply in differential methods based on first-order or pseudo-first-order kinetics ([R] ≫ [A] + [B])

Method	Mathematical relationship
Logarithmic extrapolation	$\ln([P]_{inf} - [P]_t) = \ln([A]_t + [B]_t) = -k_B t + \ln[B]_0$
Single-point	$[A]_t + [B]_t / [A]_0 + [B]_0 = [\exp(-k_A t) - \exp(-k_B t)] \{[A]_0 / ([A]_0 + [B]_0)\} + \exp(-k_B t)$
Tangent	$\ln[B]_0 = \ln[B]_t + k_B t = \ln([P]_{inf} - [P]_t) + k_B t$
Proportional equations	$[P]_{t1} = \phi_{A1}[A]_0 + \phi_{B1}[B]_0$, and $[P]_{t2} = \phi_{A2}[A]_0 + \phi_{B2}[B]_0$

flow and most recently continuous-flow sample/reagent(s) processing (e.g., flow-injection analysis) have made a lasting impact in this area of kinetic methods. For systematic presentation of methods of mixing the reader is referred to Chap. 9 in [1]. The continuous addition of reagent in differential rate determinations, also of recent application, has been evaluated [29].

Detection approaches are like those used in the determination of a single component, which in turn are also similar to those used in catalyzed reactions. Computers have made calculations more accessible to the practitioner, particularly in handling graphical displays and facilitating calculations when the method of proportional equations or curve-fitting procedures are used.

Data manipulation and errors

Logarithmic extrapolation treats the data graphically by plotting either $\ln([A]_t + [B]_t)$ or $\ln([P]_{inf} - [P]_t)$ versus time. The resulting straight line has a slope of $-kB$ and an intercept (at $t = 0$) of $\ln[B]_0$. The value of $[A]_0$ may be obtained by subtracting $[B]_0$ from the total initial concentration of A and B in the mixture. This total concentration can be determined by independent methods or can be calculated from $[P]_{inf}$, provided the reaction mechanism does not change during the final stages of the reaction. The single-point method makes use of calibration graphs prepared by measuring the extent of reaction of pure A and pure B at a given selected time t. By labelling as mole fraction (e.g., of species A) the x-axis, the two points are entered in the corresponding y-axis drawn at mole fractions 0 and 1 for component A. A straight line is then drawn between the two points. A convenient alternative is to calculate the intercepts from a knowledge of the corresponding rate coefficients. For each case there is an optimum time for measurement that can be estimated from:

$$t_{opt} = \ln(k_A/k_B)/(k_A - k_B)$$

The tangent method, also known as the reaction rate method, utilizes the equation listed in Table 4. A knowledge of the rate coefficient for the slower-reacting component, k_B, permits calculation of $[B]_0$ from the equation. The concentration of the faster-reacting component A must be determined from an independently measured value of $[A]_0 + [B]_0$ or from $[P]_{inf}$. This method, however, is not a popular one and only a few applications are recorded in the literature.

TABLE 5

Classification of differential reaction rate methods based on approaches to data treatment [5]

Direct-computation methods	
Integral methods:	(a) sequential single-component
	(b) simultaneous method (one-point or two-point fixed-time methods)
Rate methods	
Curve-fitting methods	
Integral methods:	(a) logarithmic extrapolation
	(b) nonlinear curve-fitting

The method of proportional equations, based on the principle of constant fractional life, is frequently employed by simultaneous solution of the equations presented for this approach in Table 4. It requires determination of the proportionality constants from the appropriate reactions involving the pure analytes. The sum of the initial concentrations of the reactants does not need to be known; consequently the method can be applied to any number of chemical species reacting with a single reagent and to a mixture of species forming various reaction products with a common reagent.

Pardue [5] classifies differential rate methods, according to the way data are treated, as direct-computation and curve-fitting methods. Table 5 summarizes the grouping of these methods according to this criteria for classification.

Chapter 7 in [2] discusses general error analysis for the graphical extrapolation method, the method of proportional equations, and first-order and pseudo-first-order methods when concentrations of analytes are much less than the concentration of reagents. All these methods, when $[R] \gg [A]_0 + [B]_0$, are mathematically based on the general equation that follows:

$$[P]_{inf} - [P]_t = [A]_0 \cdot \exp(-k_A t) + [B]_0 \cdot \exp(-k_B t) \quad (1)$$

In the method of proportional equations we recognize that $[P]_{inf}$ is a constant for each case under consideration and $[P]_t$ is indirectly measured under two different conditions of the system (e.g., at two different times). Hence, it is valid to conclude that in actuality all approaches are special cases of the method of proportional equations. For example, in cases where contributions from one of the components can be disregarded, logarithmic extrapolation and the method of tangents apply and, by simply dividing Eqn. 1 by a constant ($[P]_{inf}$) results in the single point method.

Therefore, we are dealing with the indirect determination of two chemical species without their separation and in such a case, the relative error for each species can be derived from the simultaneous equations for the method of proportional equations:

$$Q_1 = K_{A,1}[A]_0 + K_{B,1}[B]_0$$

$$Q_2 = K_{A,2}[A]_0 + K_{B,2}[B]_0$$

in which Q_i is the result of a measurement under conditions i, and $K_{X,i}$ are the respective rate proportionality coefficients for each component X at a given condition i. If dQ is the absolute error in the measurement of Q_i values, and this error is the same under all conditions i, the following can be derived:

$$d[A]_0/[A]_0 = dQ[K_{B,1} + K_{B,2}]/[Q_2K_{B,1} - Q_1K_{B,2}] \quad (2)$$

and

$$d[B]_0/[B]_0 = dQ[K_{A,1} + K_{A,2})]/[Q_2K_{A,1} - Q_1K_{A,2}] \quad (3)$$

Equations 2 and 3 define the relative concentration error for each component. These equations indicate that such errors depend on: (a) the uncertainty in the measurement of Q, (b) the absolute value of the quantities Q_i, and (c) the ratio of the values of the rate proportionality coefficients. Since, in general, the errors will be controlled by:

$$\xi = dQ[1 + (K_{A,1}/K_{A,2})]/[Q_2 - Q_1(K_{A,2})/(K_{A,1})] \quad (4)$$

TABLE 6

General recommendations for differential rate methods (adapted from [31])

Collection of multiple data rates should give approximately the same number of data points per three half-lives of each component
Weighting factors are not recommended unless the product of the rate coefficient for the fastest-reacting component multiplied by the uncertainty of the mixing time exceeds 0.10
Calibration runs should be performed with pure components and under exactly the same conditions as in determination runs
Linear least-squares regression is possible for up to five components with on-line operation using microcomputers
The technique of centering the data and the use of a correlation matrix are recommended
Tests in which the residuals are displayed against the data points should be performed to detect incorrect or missing rate coefficients
The ratio of the concentrations of analytes should not greatly exceed the ratio of their rate coefficients
Nonlinear least squares can be used for a small number of components if the rate coefficients of the pure components under reaction conditions are not known accurately
Synergistic effects should be totally absent, and the kinetics of the system should be well defined

equations such as 4 also point to the fact that in two component determination it is difficult to select optimum conditions since the overall error of the determination is mainly dependent on the composition of the mixture under analysis. Doerffel [30] has studied the problem of precision in indirect multicomponent determinations and critically concludes that experimental work should stress the need of exact measurement and of knowing with great reliability the value of the individual coefficients.

Ridder and Margerum [31] have emphasized the importance of using the entire signal–time response. Present-day availability of computers makes easy the task of collecting data at i different conditions such that $i \gg n$ (n = number of unknowns in the mixture). General recommendations given by these authors are summarized in Table 6. Synergism is not frequently observed; although, as indicated in Table 6, it should be avoided, means to treat data under synergistic

TABLE 7

Typical determinations using differential rate approaches

Species determined	Comments	Ref.
Inorganic species		
Zn(II), Mg(II), Cu(II), Ni(II)	Rate difference by ligand substitution of the complexes with 3-hydroxy-4-(2-hydroxy-5-methylphenylazo)naphthalene-1-sulfonic acid (camalgite) and EDTA. Stopped-flow mixing and photometric monitoring. Logarithmic extrapolation. No interference from calcium. Analysis of binary and ternary mixtures	32
Cu(II)/Co(III), Co(III)/Ni(II)	Binary mixtures. Complexation with 3-(1*H*-1,2,4-triazolyl-3-azo)toluene-2,6-diamine. Single-point method. Application to the analysis of steel hydrofining catalysts	33
Co(II)/Fe(III)	Determination based on differential rate of ligand displacement by 4-(2-pyridylazo) resorcinol on the complexes with EGTA	34
Co(II)/Ni(II)	Continuous-flow/stopped-flow system with determination based on the large rate differential in the ligand substitution reaction of the metal ion complexes with 2-(5-bromopyridylazo)-5-(*N*-propyl-*N*-sulfopropylamino)aniline and nitrilotriacetic acid	35
Ga(III)/Al(III)	Room temperature phosphorimetry after complexation with 7-iodo-8-hydroxyquinoline-5-sulfonic acid and sulfite as oxygen scavenger. Kalman filtering of the data permits the deconvolution of the phosphorescence spectra and the simultaneous determination	36
Organic species		
Histidine/ histamine	Fluorometric monitoring based on the increase in the fluorescence intensity of the 1,1,3-tricyano-2-amino-1-propene/hydrogen peroxide/Cu(II) system. Synergistic effects are taken into consideration	37
Amino acids	Application of linear Kalman filtering to the reaction of amino acids with 2,4,6-trinitrobenzenesulfonic acid	38
Zineb/maneb	Zineb = zinc ethylenebis (dithiocarbamate); maneb = manganese ethylenebis(dithiocarbamate). Determination based on continuous addition of zincon and differences in the rate of Zn(II) and Mn(II) displacement by the added reagent	39
Epinephrine/ norepinephrine	Determination in urine. Stopped-flow mixing and fluorometric monitoring of reaction with trihydroxyindole. The method is an extension of the method of proportional equations using a kinetic measurement (initial rate) and an equilibrium parameter (intensity of steady-state signal)	40
Alkylamines	Determination of normal and isoalkylamines in their mixtures. Reaction with carbon disulfide [in presence of Cu(II)] to form dialkyldithiocarbamates. Stopped-flow mixing. Calculations are based on mathematical expressions making use of rate coefficients	41

influence for some cases have been discussed ([3], pp. 169–172).

Applications of differential reaction rate methods

The reader interested in surveying typical applications of differential reaction rate methods is referred to Table 7.1 in [1] and pp. 172–187 in [3]. As already mentioned for single-component determinations, *Analytical Chemistry Fundamental Reviews* updates the listing of applications every two years [12,13]. Table 7 is offered here to illustrate typical applications.

REFERENCES

1 H.A. Mottola, Kinetic Aspects of Analytical Chemistry, Wiley, New York, 1988.
2 H.B. Mark, Jr. and G.A. Rechnitz, Kinetics in Analytical Chemistry, Wiley, New York, 1968, pp. 72–75.
3 D. Perez-Bendito and M. Silva, Kinetic Methods in Analytical Chemistry, Ellis Horwood, Chichester, 1988, Chap. 7.

4 M. Marquez, M. Silva and D. Perez-Bendito, Analyst (London), 113 (1988) 1733.
5 H.L. Pardue, Anal. Chim. Acta, 216 (1989) 69.
6 S.D. Brown, Anal. Chim. Acta, 181 (1986) 1; S. Rutan, J. Chemom., 1 (1987) 7.
7 H.L. Pardue, Clin. Chem. (Winston-Salem, NC), 23 (1977) 2189.
8 J.W. Skoug and H.L. Pardue, Anal. Chem., 58 (1986) 2306; B.A. Dilena, M.J. Peake, H.L. Pardue and J.W. Skoug, Clin. Chem. (Winston-Salem, NC), 32 (1986) 486.
9 F.J. Holler, R.K. Calhoum and S.F. McClanahan, Anal. Chem., 54 (1982) 755.
10 P.D. Wentzell and S.R. Crouch, Anal. Chem., 58 (1986) 2851.
11 R.C. Harris and E. Hultman, Anal. Biochem., 83 (1977) 767.
12 H.A. Mottola, D. Perez-Bendito and H.B. Mark, Jr., Anal. Chem., 60 (1988) 181R; H.A. Mottola, D. Perez-Bendito and H.B. Mark, Jr., Anal. Chem., 62 (1990) 441R.
13 H.A. Mottola and D. Perez-Bendito, Anal. Chem., 63 (1992) 407R.
14 H.L. Pardue, personal communication.
15 P.C. Ioannou and E.A. Piperaki, Clin. Chem. (Winston-Salem, NC), 32 (1986) 1481.
16 T.K. Christopoulos and E.P. Diamandis, Analyst (London), 116 (1991) 627.
17 A.M. Albretch-Gary, G. Nemra, T. Nguyen and Ch.-M. Wolff, Analusis, 13 (1985) 394.
18 M.I. Karayannis, E.A. Piperaki and M.M. Maniadaki, Anal. Lett., 19 (1986) 13.
19 E. Alvarez-Manzaneda and M.T. Gamiz-Garofano, Anal. Lett., 21 (1988) 233.
20 H.R. Cummings and H.L. Pardue, Clin. Chem. (Winston-Salem, NC), 33 (1987) 493.
21 C. Cruces Blanco and F. Garcia Sanchez, Int. J. Environ. Anal. Chem., 38 (1990) 513.
22 M. Marquez, M. Silva and D. Perez-Bendito, Anal. Chim. Acta, 237 (1990) 353.
23 V.H. Hartofylax, C.E. Efstathiou and T.P. Hadjiioannou, Microchem. J., 33 (1986) 9.
24 M.C. Gutierrez, A. Gomez-Hens and D. Perez-Bendito, Analyst (London), 113 (1988) 559.
25 M. Marquez, M. Silva and D. Perez-Bendito, Anal. Lett., 22 (1989) 2485.
26 D. Perez-Bendito, A. Gomez-Hens, M.C. Gutierrez and S. Anton, Clin. Chem. (Winston-Salem, NC), 35 (1989) 230.
27 M.C. Quintero, M. Silva and D. Perez-Bendito, Talanta, 38 (1991) 359.
28 H.A. Mottola, CRC Crit. Rev. Anal. Chem., 4 (1975) 229.
29 M. Marquez, M. Silva and D. Perez-Bendito, Anal. Chim. Acta, 239 (1990) 221.
30 K. Doerffel, Statistik in der Analytischen Chemie, VEB Deutscher Verlag fuer Grundstoffindustrie, Leipzig, 1966.
31 G.M. Ridder and D.W. Margerum, Simultaneous Kinetic Analysis, in E. Wanninnen (Ed.), Analytical Chemistry: Essays in Memory of Anders Ringbom, Pergamon, New York, 1977, pp. 515–528; G.M. Ridder and D.W. Margerum, Anal. Chem., 49 (1977) 2090.
32 E. Mentasti, V. Dlask and J.S. Coe, Analyst (London), 110 (1985) 1451.
33 J.J. Arias, A.I. Jimenez and F. Jimenez, Mikrochim. Acta, I (1989) 303.
34 M. Romero-Saldana, A. Rios, M.D. Luque de Castro, and M. Valcarcel, Talanta, 38 (1991) 291.
35 T. Yamane and C. Ishimizu, Mikrochim. Acta, I (1991) 121.
36 Y-M. Liu, M.R. Fernandez de la Campa, M.E. Diaz Garcia and A. Sanz-Medel, Mikrochim. Acta, I (1991) 53.
37 M.C. Gutierrez, A. Gomez-Hens and M. Valcarcel, Anal. Chim. Acta, 185 (1986) 83.
38 P.D. Wentzell, M.I. Karayannis and S.R. Crouch, Anal. Chim. Acta, 224 (1989) 263.
39 M. del C. Quintero, M. Silva and D. Perez-Bendito, Analyst (London), 115 (1990) 1261.
40 M.P. Llavero, S. Rubio, A. Gomez-Hens and D. Perez-Bendito, Anal. Chim. Acta, 229 (1990) 27.
41 S. Tagashira, Y. Sasaki, K. Hayashi and G. Fukuhara, Anal. Chim. Acta, 244 (1991) 239.

Analytica Chimica Acta, 280 (1993) 289–298
Elsevier Science Publishers B.V., Amsterdam

Fiber diameter measurement of bulk man-made vitreous fiber

A.R. Koenig [1], R.D. Hamilton [2], T.E. Laskowski [3], J.R. Olson [4], J.F. Gordon [5], V.R. Christensen [6] and C.D. Byers [7]

[1] *Center For Applied Engineering, 10301 9th. N., St. Petersburg, FL 33716 (USA);* [2] *Health, Safety and Environmental Department, Schuller International Inc., P.O. Box 5108, Denver CO 80217–5108 (USA);* [3] *Owens Corning Fiberglas, Technical Center, 2790 Columbus Road, Route 16, Granville, OH 43023–1200 (USA);* [4] *The Carborundum Company, P.O. Box 808, 2351 Whirlpool Street, Niagara Falls, NY 14302–0808 (USA);* [5] *Certain Teed, 1400 Union Meeting Rd., Blue Bell, PA 19422 (USA);* [6] *Rockwool International A / S, DK-2640 Hedehusene (Denmark);* [7] *USG Corporation, P.O. Box 6721, Chicago, IL 60606–4678 (USA)*

(Received 2nd November 1992; revised manuscript received 18th February 1993)

Abstract

This procedure describes a method for determining the distribution of fiber diameters of man-made vitreous fibers (MMVF) in bulk products by optical microscopy. Although some very thin fibers may be present in a typical bulk MMVF sample, repeated studies have shown that optical techniques provide a satisfactory method for the determination of the fiber diameter distribution for any product with an anticipated mean fiber diameter of 1 μm or larger. This procedure is applicable for the determination of the diameter distribution of bulk samples only and is not intended for use with aerosol samples where the number of particles is an important consideration.

Keywords: Fibres; Microscopy; Vitreous fibres

The diameter of individual fibers in a typical man-made vitreous fiber (MMVF) product varies widely due to the random nature of the processes that manufacture the fibers. Even in products with an average fiber diameter of 5 μm or larger, there are invariably some fibers that are thinner than 1 μm and some that may be thicker than 20 μm. In addition, certain manufacturing processes produce a large number of roughly spherical particles (shot), mostly larger than 60 μm. Given this range of diameters, it is appropriate to discuss the fiber diameter of MMVFs found in bulk products in terms of statistical measures of the distribution of fiber diameters.

Correspondence to: A.R. Koenig, Center For Applied Engineering, 10301 9th. N., St. Petersburg, FL 33716 (USA).

There is no known method for directly measuring the diameter of MMVFs without first separating the fibers. In all known cases, extraction of the fiber sample from the product mass breaks all or a significant portion of the fibers into shorter lengths, causing a loss of information about how many fibers originally had a given diameter. In fact, most practical methods of preparation simply break the fibers in order to obtain a representative sample with lengths suitable for microscopic measurement. Since MMVFs are known to break only perpendicular to the longitudinal direction, this reduction in length does not change the diameter of the individual fibers. However, it is likely that fibers of different diameters may break into different lengths. The lengths obtained vary considerably within a sample and typically will range from 5 μm up to several hundred micrometers.

Under these circumstances, it is not meaningful to report the number of fibers within a certain range of diameters, because the number of fibers actually determined depends upon how the sample was prepared and bears no relationship to the number in the original product. The most logical method for overcoming this sample preparation bias is to base the analysis on a length-weighted basis (as described further on). Two techniques are recommended for obtaining this length-weighted result. These include a direct method and a probabilistic weighted method. The direct method involves the measurement of both the length and the diameter of the fibers allowing the data to be compiled in any desired way. The method requires that the lengths of the sample fibers be reduced to around 20 to 30 times the diameter so that complete fiber segments are contained within the viewing area. For the probabilistic length-weighted method, only fibers that pass through a thin line drawn through the viewing area are measured for diameter. This method does not require that the actual lengths of the fibers be measured. The laws of probability dictate that longer fibers are more likely to cross the line, and thus be counted, than shorter fibers [1,2]. The method does not require that the fibers be of any particular length and thus sample preparation may be simpler. Reduced sample preparation time, coupled with the fact that the determination of the actual fibers lengths are not required, make this method substantially faster. However, under certain circumstances, the length information may be desired. The best method for any given analysis will depend upon the purpose of the measurement and the capabilities of the individual laboratory.

SAMPLE PREPARATION

Sample selection

Sample selection and sample preparation techniques are critical factors involved in obtaining an unbiased test result. Before selecting a sampling technique, one should consider what population is being estimated (i.e. a small sample, a bag or pallet of material, or a production lot). Standard methods of obtaining a statistically representative sample of the population should be used [3].

Sample processing

Many MMVF products contain an organic phase that must be removed prior to slide preparation. Organic phase removal is most easily accomplished by heating the sample in a muffle furnace or equivalent at a temperature which is just high enough to decompose the organic without causing dimensional changes to the fiber. The best temperature for processing glass and refractory ceramic fibers has been found to be 425°C. The sample should be heated until all organic material is removed. Rock/slag wool samples may be heated to temperatures as high as 550° to 600°C to enhance sample processing during additional preparation stages.

Slide preparation

Three acceptable methods have been found to process the sample into a suitable form for microscope slide preparation although other procedures that produce equivalent results may be used. It is up to the user to determine if an alternate method employed gives equivalent results. A particular method may be found to be more advantageous for a specific fiber type. Each of the three specified methods involves (1) separating the fibers, (2) depositing a very small amount (pin head size) of the fibers onto a slide, and (3) adding a refractive index oil and cover slip. The proper index oil has an index that is at least 0.03 units higher or lower than the refractive index of the fiber. Typical MMVF products have refractive indices that range from 1.5 to 1.7. To avoid contamination of the index oil, never allow the oil dropper to come in contact with any surface other than a clean slide. Acceptable methods are.

Grinding method (use for fiber samples which contain low quantities of shot). In a well ventilated area, grind at least 2 cm^3 of the organic-free fiber sample with acetone in a mortar until a uniform mixture of fibers is obtained. The fiber slurry should be free of visible lumps or fibers greater than about 1 mm in length. Care should be taken to avoid grinding the sample too much which may

destroy coarser fibers. The proper technique will require some experimentation. After the acetone has evaporated, scrape the material into a loose pile. A very small sample is removed with a spatula and placed in the center of a clean slide on which 1 or 2 drops of index oil has been placed. Distribute the fiber–oil mixture over approximately 2 cm^2 of the center area of the slide, thoroughly mixing the fiber with the oil. Place a cover slip on top of the fiber–oil mixture and press firmly against the slide to remove any air bubbles.

Chopping method (use for fiber samples that contain low quantities of shot). Place a small tuft of the organic free fiber sample (approximately 1 cm in diameter) on a clean cutting surface. Holding two single edge razor blades firmly together so that there is an approximate 1 mm gap between them, press down with both blades firmly through the center of the fiber tuft and cut completely through to the cutting surface. Lift up the blades, separate them and drop the fiber from between the blades into a 20 ml scintillation vial. Add 2 ml of methanol to the vial, cap the vial and shake vigorously until the fiber is dispersed. Draw 2 or 3 drops of the slurry into a clean disposable dropper. Squeeze out all of the slurry as adjacent droplets near the center of the slide. The dropper used for sampling the slurry must have a hole that is at least 2 mm in diameter so that long fibers are not excluded. Sampling must be conducted with or immediately after agitation to prevent settling of larger fibers. Allow the methanol to evaporate either naturally or by placing the slide on a hot plate. Add 1 or 2 drops of index oil to the center of the slide and thoroughly mix the fiber and oil. Place a cover slip on top of the fiber/oil mixture and press firmly against the slide to remove any air bubbles.

Screening method (use for fiber samples that contain significant quantities of shot). To assure that the cover slip will sit tightly over the slide, it may be desirable to remove most of the shot during sample preparation. A commonly used method to accomplish this task is to place approximately 10 g of the organic free sample on the surface of the top screen in a sieve stack. The sieve stack is comprised of an 8 inch full height US 60 mesh (250 μm) sieve placed over a US 230 mesh (63 μm) sieve along with a pan and a lid. Each of the sieves should contain 4 rubber stoppers, 23–27 mm in diameter and 25 mm in height. Place the assembled sieve stack on a testing sieve shaker and shake till all fibers have passed through to the pan (approximately 10 min). Using a spatula, mix the material in the pan and remove a very small sample. Place this sample in the center of a clean slide together with a few drops of a suitable index oil and thoroughly mix the fiber and oil. Place a cover slip on top of the fiber–oil mixture and press firmly against the slide to remove any air bubbles.

Due to the possibility of preferential migration patterns of fibers in index oil, prepared slides should be analyzed soon after preparation. Permanent mounting is possible using standard preparation methods. However, it is generally preferable to save the remainder of the prepared sample in a labeled container for future reference.

FIBER DIAMETER MEASUREMENT

Microscope set-up

The heart of any fiber diameter measurement system is a good quality optical microscope. The specific operating procedures for each individual microscope varies between manufacturers. Therefore, manufacturer's literature should be consulted regarding specific details.

The use of transmitted light is essential for measuring fiber diameters. Dark field or phase contrast microscopy techniques are not recommended; these techniques yield images in which the fiber edges are very difficult to accurately locate and measure. Under transmitted light it is important to establish proper positioning of the various optical elements of the microscope (lamp condenser, substage condenser, objective, ocular and light source). The preferred set-up is Köhler illumination [4].

When selecting the optical elements, the important factor is not the magnification used but the resolution achieved. The maximum useful magnification (MUM) should not exceed 1000

times the numerical aperture (NA) of the objective used, otherwise empty magnification will occur. Image quality and resolution are not achieved by the magnification of the oculars or objectives used, but instead by the NA of the objective and substage condenser (which should match or be greater than the NA of the objective) used. The higher the NA, the greater the resolving power. However, by increasing the NA, the depth of field is decreased.

A guide for selecting a combination of optical elements that achieves the best image quality and resolution for a sample containing a broad range of fiber diameters is given below:

Objective Magnification	*Objective NA*	*Condenser NA*
40×	0.65, 0.70 or 0.85	0.9
63×	0.80 or 0.85	0.9
100×	1.30	0.9

Other researchers prefer other lens combinations that give similar results.

In order to measure samples which contain a significant number of fibers below 1 μm, a numeric aperture of at least 1.20 with immersion oil is necessary to satisfy resolution needs. Failure to obtain adequate image quality in terms of resolution will bias the results obtained.

A set of test slides [a] that have known diameter distributions should be used to verify the resolution limits of the microscope optics on a regular basis.

Fiber measurement and calibration

Many techniques are available for the measurement of fiber length and diameter using both direct and projected images. Direct measurement of the image with a graticule in an ocular or a filar eyepiece is entirely satisfactory in terms of accuracy and precision but the process is labor intensive and fatiguing to the analyst. Thus, the measurement of a projected image, either manually employing a ruler or automatically by use of a computer-assisted technique, is generally preferred. With any technique employed, calibration must be established and maintained using adequate reference standards. A standard stage micrometer calibrated in tens of micrometers is satisfactory for calibration of most optical systems.

When using image projection systems the resolution must be carefully checked to ensure that the image has not suffered a loss of resolution. The projected image should always be checked and compared with the direct image.

Focus. The dimensions of any fiber can only be measured when the fiber is in focus so that the edges are clearly in view. The cylindrical nature of MMVFs generate false Becke lines along the fiber edges. Depending upon the focus, the center of the fiber may appear much darker or lighter than the background and the apparent edge of the fiber will move as the focus is changed. Proper focus is achieved when the center of the fiber is the same shade as its background and the edges of the fiber are defined by a pair of sharp thin black and white lines.

Fiber selection. The use of a valid set of rules for selecting fibers to be measured is critical for obtaining a correctly length-weighted average diameter. Simply measuring all fibers that are present in a field of view yields a value which is neither length nor number weighted but is a blend of both factors. Since the proportion of the two factors in the blend is unknown, and may vary based on sample preparation techniques and the relationship between average fiber length and diameter, this counting rule is unsuitable for this determination.

Either of two methods are recommended for achieving a correctly length-weighted measurement. The length-weighted method requires that both the diameter and the length of each selected fiber be measured. The direct method is the more difficult of the two methods because two dimensions of each fiber must be measured and the fiber selection rules are more complex. However, this method provides information about the length distribution which may be desired for certain applications. The probabilistic length-weighted method requires only that the diameter be measured, selecting fibers for measurement in a

[a] A set of suitable slides to check microscope resolution can be obtained from Schuller International, Mountain Technical Center, Littleton, CO (USA).

length-weighted manner. The probabilistic method is simpler and faster and yields a statistically equivalent result.

These two methods are adapted from the counting rules for airborne fiber samples as specified by WHO [5] and NIOSH [6]. The WHO and NIOSH counting rules provide limits on the diameter, length, and aspect ratio in the definition of a fiber. These definitions are relevant for counting airborne fibers but are not appropriate for the present purpose. When measuring the diameter of fibers that have been artificially shortened, it is necessary to measure virtually every fiber segment regardless of its diameter, length, or aspect ratio. In practice, all particles that have parallel sides are measured. Jagged shards, irregularly shaped, or spherical particles should not be measured.

It is also necessary to deviate from the WHO and NIOSH rules in one other detail. Many products contain a small proportion of fibers that are fused together along their entire length. In the case where two fibers are merely touching, not fused, they should be measured separately according to the WHO and NIOSH rules. However, if the two fibers are actually fused, then they act for all purposes as a single fiber, and they should be measured as one. In practice, two fibers are considered to be fused into one if they are parallel, touching along their entire length, and if the ends are broken nearly coincident. It is unlikely that two unfused fibers would meet these criteria by chance. With either method, a large portion of the sample area should be traversed, and the fields selected for counting should be chosen randomly based on the techniques outlined in the WHO and NIOSH references. Once a field is selected, the two recommended methods differ in how the fibers in the field are measured.

Direct length-weighted method. In this method, the diameter and length of a fiber is measured if at least one end of the fiber is inside the reticle. If neither end of the fiber is within the reticle, it is ignored. The length and diameter of any fiber with both ends inside the reticle is entered into the data set twice, as if it had been encountered twice. For fibers with only one end visible in the reticle, its diameter and its entire length are measured, even if the microscope stage must be moved to locate the end outside of the field. The measured length and diameter of such a fiber is entered only once in the data set.

The length of a curved fiber is estimated as that length that would be measured if the fiber were completely straightened. For fibers with diameters that vary along their length, the average diameter is estimated. For other unusual fiber arrangements, the WHO and NIOSH rules should be used to measure them.

It may not be immediately obvious that the dimensions of fibers that have both ends inside the reticle should be entered into the data set twice. The rationale for this procedure is to reduce each fiber to a single reference point and to measure it only if that reference point is inside the reticle. Which point on a fiber to use as a reference point is arbitrary, but it could be the right end, for instance. Thus, a fiber passing through the reticle with no end inside, definitely does not have its right end inside and should be ignored. A fiber with both ends inside has its right end inside and is measured. But a fiber with only one end inside the reticle would be measured only half the time, on average, whenever the right end is the one inside. Rather than entering the length and the diameter of such a fiber into the data set with one-half its length, it is simpler and faster to enter it once, and to enter twice those fibers for which both ends are visible.

When using the direct length-weighted method, it is convenient if most of the fibers are considerably shorter than the size of the reticle, so that their length may be more easily measured. The method is also more practical when the reticle is much smaller than the entire field of view, so that long fibers may be tracked easily. If the fibers are very long compared to their diameters, this method may be impractical and the probabilistic length-weighted method should be used.

Probabilistic length-weighted method. In this method, the ocular is provided with a reticle containing a straight line such as one axis of a cross-hair. The diameter of each fiber is measured only if it crosses or touches this line. All other fibers visible in the field are ignored. The

diameter of each selected fiber is measured at any convenient representative point along its length. For unusual arrangements of fibers, the WHO and NIOSH rules are applied. Average values and other statistics are calculated from the data in the normal way. Such statistics are properly length-weighted in spite of the fact that no lengths are measured because the fibers are selected in proportion to their length. The method is easy to implement, and may be the only practical method of measurement in cases where the fibers are very long, such as those on slides that were prepared using the chopping method of preparation.

Fiber number. For each sample a minimum of 100 fibers should be measured. If the diameter distribution is relatively narrow the 100 measurements will give an accurate representation of both the mean and the distribution of the diameters about the mean. If the distribution is broad, a greater number of fibers should be measured (see Precision and accuracy – *diameter distribution statistics*).

CALCULATION

A set of length-weighted fiber diameter data for a bulk MMVF product sample may be conveniently summarized by the length-weighted arithmetic mean diameter, the length-weighted standard deviation and the length-weighted median diameter. The mean and median are two different measures of the central tendency of the diameter distribution, whereas the standard deviation is a measure of the spread or width of the distribution.

When the probabilistic length-weighted method is used, these quantities may be calculated from the set of measured diameters in the normal manner. If the direct length-weighted method is used, the average diameter D for a number of fibers each having a diameter D_i and length L_i can be calculated as

$$D = \frac{\sum_i D_i L_i}{\sum_i L_i} \quad (1)$$

where the sums run from $i = 1$ to n, the number of fibers measured. In the same way, the length-weighted arithmetic standard deviation σ, is given by

$$\sigma = \sqrt{\frac{\sum_i (D_i - D)^2 L_i}{\sum_i L_i}} \quad (2)$$

More information about the diameter distribution of a bulk MMVF fiber sample can be obtained by plotting the cumulative length-weighted fiber diameter. This chart is obtained by plotting, for each diameter, the percent of the total measured fiber length that was found to be less than this diameter. The length-weighted median may be read from this chart and is defined as the diameter at the 50% point. The cumulative diameter chart has an advantage over a diameter histogram presentation in that the cumulative diameter plot is a reasonably smooth curve from which one may reliably determine such quantities as the median or the fraction of the product within any given diameter range.

An alternative is to plot the cumulative length-weighted diameter on standard probability distribution graph paper to obtain information concerning the shape of the distribution curve. If the diameter axis chosen is linear, and if the fiber diameter distribution of the sample is normally distributed, the resultant curve is a straight line. If the diameter axis chosen is logarithmic, and the fibers in the sample have a log normal diameter distribution, the resultant curve is also straight line.

PRECISION AND ACCURACY

An incorrect estimate of the fiber diameter distribution of a test specimen is likely to occur from two sources; (a) improper sample preparation, microscope configuration and calibration, and/or fiber measurement techniques, (b) operator technique or bias.

Fiber measurement

Calibration. It is suggested that available stage micrometers be used for calibration. Any potential error involved in the use of a calibration standard is likely to be insignificant. There is also some error that may be introduced by measuring thick fibers having a circular cross section after calibration with a two dimensional standard. This error is also likely to be small in comparison to the random error associated with the measuring process.

Bias. Systematic errors associated with operator bias are generally related to evaluation of the optical image. The diffraction effects associated with cylindrical, refracting fibers make focusing of the image and the location of the fiber edge a subjective process. As a result operators measure an apparent diameter rather than a true diameter. Systematic differences of 0.1–0.3 μm between operators are common. Relative operator bias can be determined by a comparison of data from each individual operator. When only a single operator is used within a laboratory, operator bias becomes laboratory bias.

Random error. The random error as expressed by the standard deviation (s) associated with the measuring process at about 1000 × has been found, by repeated tests, to be in the range of 0.1–0.2 μm for fibers in the diameter range of 1–10 μm (Table 1). The optical measurement of fiber diameters that are less than about 0.4 μm ($D < 2s$) is, based on the available data, subject to significant error. This limit corresponds closely to the theoretical limit of resolution of a typical optical microscope.

If the direct length-weighted method of diameter measurement is used, then errors associated with the measurement of fiber lengths must also be recognized. The magnitude of these errors have been found to be relatively insignificant for two reasons. First, length measurements are not influenced as strongly as diameter measurements by the problems associated with image focus and edge location. Length measurements are, however, strongly influenced by fiber morphology and the problems associated with determining the true length of irregularly shaped fibers. Experiments have shown that the errors associated with length measurement increase with increasing fiber length and have standard deviations in the range of 0.2 to 0.4 μm (Table 1). The fractional error associated with the length determination is equal to or less than that associated with the diameter determination when employing the direct length-weighted method. Secondly, as can be noted by referring to Eqns. 1 and 2, diameter measurements are both multiplied and divided by the fiber length, thus the random and systematic errors approximately cancel.

Diameter distribution statistics

Typical MMVF fiberization processes produce a range of diameters that are distributed about a central value. Experience has shown that the distribution is generally not normally distributed. The standard deviation of the population mea-

TABLE 1

Precision of single fiber measurements [a]

Analyst	S.D. (μm)					
	1 μm Diam.	3 μm Diam.	10 μm Diam.	5 μm Length	10 μm Length	50 μm Length
A	0.13	0.13	0.21	0.17	0.11	0.50
B	0.14	0.13	0.10	0.21	0.33	0.41
C	0.12	0.15	0.14	0.24	0.26	0.41
D	0.17	0.15	0.17	0.31	0.34	0.33
E	0.14	0.11	0.10	0.26	0.32	0.32
Average	0.14	0.13	0.14	0.24	0.27	0.39

[a] Based on 50 measurements of a single fiber by each analyst.

sured gives a general indication of the variation or dispersal of the diameters. In this case, the standard deviation is not a measure of the precision with which the diameters are determined but is rather a characteristic of the fiberization process.

The precision with which the mean diameter of the population is determined depends on the dispersion of the fiber population sampled and the number of fibers measured. No matter how the fiber diameters are distributed, the mean diameters obtained from multiple determinations are approximately normally distributed about the true mean. The standard deviation of the mean diameter σ_m, can be calculated from the standard deviation of the population, σ, and the number of fibers measured, N, according to the relation:

$$\sigma_m = \frac{\sigma}{\sqrt{N}} \quad (3)$$

MMVF fiber samples have standard deviations ranging from 0.5 to over 5 μm and it is not unusual for the standard deviation to be roughly equal to the mean diameter. Table 2 illustrates the problems associated with accurate mean diameter determinations when the standard deviation is large. In many cases a standard deviation of 0.3–0.5 μm is all that can be reasonably expected. It is also clear from the table that increasing the number of fibers measured from 100 to 300 or even 1000 yields only a modest increase in precision.

TABLE 2

Number of measurements required to obtain a desired confidence interval [a]

σ	Desired σ_m (μm)			
	1.0	0.5	0.3	0.1
5.0	68	272	756	6806
4.5	55	221	613	5513
4.0	44	174	484	4356
3.5	33	133	371	3335
3.0	25	98	272	2450
2.5	17	68	189	1702
2.0	11	44	121	1089
1.5	6	25	68	613
1.0	3	11	30	272
0.5	1	3	8	68

[a] For a population with a dispersion of σ, N measurements are required to determine the mean diameter to within $\pm\sigma_m$ at the 90% (1.65σ) confidence level.

TABLE 3

Measurement of fiber diameter of two MMVF samples in different laboratories

	Slag wool			
	Measured Mean (μm)	Diameter S.D. (μm)	Total fibers measured	Estimated S.D. of the mean (μm)
A	5.32	3.78	300	0.22
B	5.56	3.50	200	0.24
C	4.66	3.79	300	0.22
D	4.35	3.05	200	0.22
E	4.29	3.33	200	0.24
Average	4.84 μm			
S.D.	0.58 μm			
	Rotary glass wool			
	Measured Mean (μm)	Diameter S.D. (μm)	Total fibers measured	Estimated S.D. of the mean (μm)
A	4.38	1.81	900	0.06
B	4.36	1.93	800	0.08
C	4.42	1.99	700	0.08
D	4.91	1.81	1000	0.04
Average	4.52 μm			
S.D.	0.26 μm			

An estimate of the precision of the mean fiber diameter obtained from measuring any given number of individual fibers can be obtained by reference to Table 2. In practice, the actual precision of the mean diameter is considerably larger than this estimate. Operator and laboratory bias, sample inhomogeneity, and artifacts of sample preparation usually contribute to increasing the variation in the observed mean fiber diameter. As an illustration, Table 3 exhibits the results of the measurement of two different MMVF wool insulations in several different laboratories. For each laboratory measuring the sample, the observed mean and standard deviation is shown along with the number of fibers measured to determine this mean and standard deviation. The last column of Table 3 shows the estimated standard deviation of the mean, calculated from Eqn. 3. Since similar measurements were done in different labora-

tories, one may calculate the average and the standard deviation of these measured means, which is shown for each of the two samples. It is clear from Table 3 that the actual variation of the mean fiber diameter, as measured by the "SD of the means," is two to three times any of the "estimated SD's of the mean" calculated from Eqn. 3. Such an increase in the actual variation compared to that estimated from Eqn. 3 is typical of fiber diameter measurements of MMVF wool samples.

The recommended method for determining how many fibers must be measured to accurately estimate the mean fiber diameter is to measure 100 or more fibers initially. The mean and the standard deviation of this sample along with the estimated standard deviation of the mean, employing Eqn. 3, are then calculated. If the standard deviation of the mean is small enough, keeping in mind that the actual S.D. is usually several times larger, then the measurement is complete. If not, then 100 more fibers may be measured and the calculation repeated until the precision of the mean is as small as desired. In practice, however, it is seldom feasible to obtain the mean more precisely than 0.3–0.5 μm.

It is recommended that three or more slides be prepared and evaluated for each sample. As few as 25 or as many as 100 or more fibers on each slide should be measured to determine the mean fiber diameter. When several slides are measured, it is instructive to compute the mean and standard deviation separately for each slide and compare the variation in the means with the estimated values just as was done for the different laboratories in Table 3. A better estimate of the true variation in the mean is given by the variation between slides.

Although the preceding discussion has focused on estimating the mean fiber diameter and its precision, another statistic often desired is the length-weighted fraction of the fiber that is less than 1 μm in diameter or some other limit. Whereas the total number of fibers measured plays a central role in establishing the precision of the mean, it is the total number of fibers measured that are less than 1 μm in diameter that is critical to establishing the precision of the fraction less than 1 μm. If N fibers are measured by the probabilistic length-weighted method and n of them are less than 1 μm in diameter, then an estimate of the fraction of length that is less than 1 μm in diameter is

$$f = \frac{n}{N} \tag{4}$$

It is reasonable to assume that the number of fibers counted is Poisson distributed, so that the standard deviation of n is equal to the square root of its mean. It follows then that an estimate of the standard deviation of f is

$$\sigma_f = \frac{\sqrt{n}}{N} \tag{5}$$

While Eqns. 4 and 5 (as well as Eqn. 3) are strictly true only for the Probabilistic length-weighted method, they are a useable approximation for the direct length-weighted method.

When the fraction of fibers less than or equal to 1 μm in diameter (for example) must be determined, it is recommended that 100 or more fibers be measured initially. Then f and σ_f may be computed and a decision made as to whether the precision obtained is sufficient. It should be recognized from the outset, however, that the fraction of fibers under 1 μm in diameter will necessarily be inaccurately estimated from the counting of any reasonable number of fibers in a typical MMVF wool insulation sample with a mean diameter in the range of 3–5 μm. This is true not only because only a small number of fibers under 1 μm can be found, but also because many submicrometer fibers are finer than the resolving power of the microscope system.

The authors greatfully acknowledge the technical assistance provided by Dick Cunningham, Harry Causway, John Copham, T.M. Singh, Brian Ence, Chuck Axten, and Carey Towe. We also thank Walter Eastes and Jim Bird for providing assistance with the statistical analysis of the data and other valuable contributions too numerous to detail.

REFERENCES

1 T. Schneider, Ann. Occup. Hyg., 21 (1978) 341.
2 T. Schneider and E. Holst, J. Aerosol Sci., 14 (1983) 139.
3 ASTM, D1060-85, Annual Book of ASTM Standards, Part 07.01, Method D1060-85 1991.
4 O. Goldberg, Microscope, 28 (1980) 15.
5 WHO/EURO Technical Committee for Monitoring and Evaluating Airborne Man-Made Mineral Fibers, WHO, Copenhagen, 1985.
6 National Institute for Occupational Safety and Health, NIOSH Manual of Analytical Methods, Method 7400, Revision 3, 5/15/89, U.S. Government Printing Office, Washington, DC, 1989.

Analytica Chimica Acta, 280 (1993) 299–307
Elsevier Science Publishers B.V., Amsterdam

Mechanistic interpretation of photochemical thallimetric oxidations catalysed by chloride and bromide ions

S.R. Sagi, K. Appa Rao and M.S. Prasada Rao

Inorganic Chemistry Laboratories, Andhra University, Visakhapatnam 530 003 (India)

(Received 30th October 1992; revised manuscript received 4th February 1993)

Abstract

The thallimetric oxidation of carboxylic acids appears to proceed through free radical and intermediate activated complex mechanisms. The thermal and photochemical uncatalysed oxidation reactions appear to proceed through the formation of an intermediate metal–substrate complex that eventually decomposes to give the products. However, photochemical oxidation in the presence of chloride and bromide ions appears to proceed through a two-electron step via a halo bridge mechanism. In the presence of bromide at 2–3 times the concentration of thallium(III), the photochemical reduction mainly proceeds through a free radical mechanism involving a one-electron step via the formation of thallium(II) species. The nature and concentration of halide ions appear to be critical in deciding the path of the reaction.

Keywords: Carboxylic acids; Oxidation; Photochemical oxidation; Thallimetric oxidation

Thallium usually exhibits oxidation states of I and III. The redox chemistry of thallium mainly depends on the oxidizing power of thallium(III) and the special stability associated with thallium(I). Thallium(II) is unstable and is often suggested as an intermediate in redox reactions of thallium(I) and thallium(III). The reduction of thallium(III) by iron(II), the oxidation of thallium(I) by $^{\cdot}OH$ radicals in aqueous solution and the catalysis of thallium(I)–thallium(III) electron exchange by iron(II) provide persuasive evidence for the existence and participation of thallium(II) in these reactions [1].

The electron exchange reaction between thallium(III) and thallium(I) in perchloric and sulphuric acid media in the presence and absence of chloride or bromide ions has been thoroughly investigated. Sykes [2] presented convincing evidence for a single-stage two-electron exchange.

Gupta and co-workers [3–7] studied in detail the reactivity of chloro complexes of thallium(III) with various reducing agents in aqueous solutions. They concluded that the dependence of the reduction of thallium(III) on chloride may be divided into two classes.

(a) One class includes the oxidation reactions of hydrazine [3], formic acid [8] and arseneous acid [4], which are decelerated by chloride ions. All these reactions are reported to proceed through the formation of an intermediate complex between thallium(III) and substrate in the absence of chloride ions. When chloride ions are present they block the coordination sites on thallium(III) and thus inhibit the formation of an intermediate complex and decrease the rate of thallium(III) reduction.

Correspondence to: M.S. Prasada Rao, Inorganic Chemistry Laboratories, Andhra University, Visakhapatnam 530 003, India.

(b) The other class includes the oxidation of iron(II) [9], antimony(III) [5], hypophosphite [8] and phosphite [7] and the thallium(III)–thallium(I) exchange reaction [10], where chloride ion accelerates the rate of the reaction. The catalysis by chloride ions is explained by invoking a bridge-activated mechanism with chlorine as the bridge atom.

In addition to the above thermal reactions, some photochemical studies on thallium salts have also been reported [11–19]. Most of these reactions are reported to proceed through the formation of free radicals and thallium(II) as intermediates.

Sagi's group [20–29] has investigated the photochemical and thermal oxidations of various organic and inorganic substrates with thallium(III) and proposed convenient methods for the analysis of these substrates and also thallium(III). These reactions were also studied in the presence and absence of halides as catalysts. Utilizing the conditions for selective oxidation of these substrates, methods were suggested for the analysis of mixtures [23,30–32]. In photochemical thallimetric oxidations under optimum conditions the chloride ions are found to catalyse only some of the reactions whereas bromide ions catalyse almost all the reactions reported. In this paper a mechanistic interpretation of the photochemical thallimetric oxidations of some carboxylic acids, for which analytical procedures have been described previously, is presented.

EXPERIMENTAL

Reagents

Thallium(III) solutions in perchloric and sulphuric acid were prepared and standardized as reported previously [33,34]. All other reagents were of analytical-reagent grade.

Apparatus

The photochemical reactions described were done with a Philips high-pressure mercury vapour lamp (200/250 V, 125 W) as the light source, placed 15 cm above the test solutions, which were contained in colourless, uncovered glass vessels.

The thermal studies were carried out by refluxing the reaction mixture in a 250-ml round-bottomed flask fitted with a water-cooled condenser.

A Shimadzu UV-260 recording spectrophotometer with silica cells of 1 cm path length was used for absorbance measurements.

Free radical test with acrylonitrile

Laboratory-grade acrylonitrile was washed with 1% sodium hydroxide and water, dried over anhydrous calcium chloride and distilled. The fraction distilling between 77 and 79°C was collected and used immediately. A 5-ml volume of 0.5 M perchloric acid (or 0.25 M sulphuric acid) and 1 ml of 0.01 M thallium(III) were placed in the lower limb of a Thumberg tube. In the upper limb 0.2 ml of acrylonitrile, different amounts of halide and organic substrates were placed. The tube was closed and air inside was removed by using a

TABLE 1

Summary of results of thermal thallimetric oxidations

Substrate	Tl(III):Tl(III)* ratio [a]	Reflux time (min)	Probable route
Oxalic acid (OA)	2:1	2	OA → CO_2
Malonic acid (MA)	4:1	120	MA → TTA → MO → OA → CO_2
Formic acid (FA)	6:1	120	FA → CO_2
Mesoxalic acid (MO)	6:1	10	MO → OA → CO_2
Glyoxylic acid (GOA)	6:1	240	GOA → FA/OA → CO_2
Tartronic acid (TTA) (Hydroxymalonic acid)	5:1	120	TTA → MO → OA → CO_2

[a] Tl(III)* indicates the amount of thallium(III) required theoretically for complete oxidation. Tl(III) indicates the amount of thallium(III) actually present in the reaction mixture at the start of the experiment.

vacuum pump. Then both solutions were mixed by shaking and the tube with the reaction mixture was exposed to radiation from the mercury vapour lamp.

RESULTS AND DISCUSSION

The important observations made during the investigation of the thallimetric oxidation of different organic substrates, namely oxalic acid, malonic acid, formic acid, formaldehyde, glyoxylic acid, mesoxalic acid, glycolic acid and tartronic acid (hydroxymalonic acid), are summarized in Tables 1 and 2.

The following observations were also made during these studies: chloride ions inhibit the thermal reactions at all the concentrations studied; bromide ion interferes in the thermal thallimetric oxidations by itself being oxidized to bromine; the quantitative oxidation of malonic and tartronic acid to carbon dioxide does not

TABLE 2

Summary of results of photochemical thallimetric oxidations [a]

Substrate	Tl(III):Tl(III)* ratio [b]	Irradiation time (min)	Catalytic/retardation effect of						Probable route
			Chloride		Bromide		Mn(II)		
			Tl(III):Cl^- ratio	Effect [c]	Tl(III):Br^- ratio	Effect [c]	Tl(III):Mn(II) ratio	Effect [c]	
Oxalic acid (OA)	2:1	120	1:2	10	2:1	5	1:3	Nil	OA → CO_2
			1:10	20	10:1	11			
			10:1	20	1:1	6			
			≥ 1:3	R	1:2	15			
					1:3	80			
					≥ 1:4	R			
Formic acid (FA)	6:1	300	[d]	R	4:1	10	1:3	R	FA → CO_2
					10:1	30			
					≥ 1:3	R			
Formaldehyde (F)	16:1	600	[d]	R	2:1	240	1:3	R	F → FA FA → CO_2
					1:2	480			
					≥ 1:3	R			
Glyoxylic acid (GA)	16:1	360	[d]	R	2:1	20	1:3	R	GA → OA/FA OA/FA → CO_2
					10:1	55			
					1:1	30			
					1:2	150			
					≥ 1:3	R			
Mesoxalic acid (MOA)	8:1	120	[d]	R	2:1	1	1:3	Nil	MOA → OA ↘ ↙ CO_2
					64:1	4			
					1:1	2			
					1:2	30			
					1:3	80			
					≥ 1:4	R			
Glycolic acid (GL)	3:1	720	[d]	R	2:1	240	1:3	R	GL → F F → FA FA → CO_2
					20:1	360			
					1:1	360			
					1:2	720			
					≥ 1:3	R			

[a] Polymer formation is observed in the test with acrylonitrile when the reactions are carried out in the presence of bromide, under light. A decrease in the rate of the reaction with increase in hydrogen ion concentration is observed for all the reactions except with formaldehyde and glycolic acid. [b] Tl(III)* indicates the amount of thallium(III) theoretically required for complete oxidation. Tl(III) indicates the amount of thallium(III) actually present in the reaction mixture at the start of the experiment. [c] Time taken for the quantitative oxidation to take place in 1.0 M perchloric acid is given in minutes. R indicates retardation of the reaction compared with that in the absence of Cl^-, Br^- or Mn^{2+}. [d] Any ratio > 1:0.

take place in less than 3.0 M perchloric acid medium; for the oxidation of the other acids studied, the time taken for quantitative oxidation decreases with increase in perchloric acid concentration; when solutions containing formaldehyde and thallium(III) are boiled, polymeric resin formation on the walls of the reaction vessel is observed and once the resin has been formed it resists further oxidation, resulting in only partial oxidation of formaldehyde; and in the oxidation of glycolic acid, formaldehyde is formed as the intermediate, and hence its oxidation to carbon dioxide and water is not quantitative.

In perchloric acid medium the reactions between thallium(III) and these reducing substances proceed at a negligible rate in the dark at room temperature. However, these reactions are catalysed either photochemically or thermally, or both.

Bis- and monooxalato complexes of thallium(III) have been reported [35,36] to be present in 0.2 and 1.0–0.3 M perchloric acid solutions, respectively. Aggarwal and Srivastava [37] observed that whenever a bisoxalatothallate(III) complex was isolated from 0.1 M acid medium some of the thallium(III) was always reduced to thallium(I). The mechanism of oxidation of oxalic acid by thallium(III) in 3 M perchloric acid medium was explained by Mønsted et al. [36] by assuming the existence of $Tl(C_2O_4)^+$ as the reactive species. Spectral evidence was also provided for the formation of a complex between thallium(III) and oxalic acid in 3.0 M perchloric acid medium. Farver [38] studied the effect of oxalic acid on the rate of the thallium(I)–thallium(III) exchange reaction and explained the decrease in the exchange quantitatively by considering the formation of $Tl(C_2O_4)^+$ species, which did not participate in the exchange reaction. Halvorson and Halpern [39] studied the kinetics of the reaction between thallium(III) and formic acid in perchloric acid medium. To explain the results they proposed a thallium(III)–formic acid complex as the reaction intermediate, which is in rapid equilibrium with the reactants. They also presented spectral evidence for the formation of a complex between thallium(III) and formic acid in 3.0 M perchloric acid medium. Ignaczak and Andrijewski [40] obtained kinetic evidence for the formation of complexes of thallium(III) with glyoxylic and glycolic acids.

Basing on the above reports, it can be concluded that these uncatalysed reactions proceed through the formation of a complex between thallium(III) and the reactant that is in rapid equilibrium with the reactants. This intermediate complex obviously decomposes both photochemically and thermally to give the products.

Role of chloride ion

Chloride ions retard all the thermal and photochemical reactions reported except for the photochemical oxidation of oxalic acid. Obviously in these reactions the chloride ions block the coordination sites on thallium(III), thereby decreasing the possibility of complex formation between thallium(III) and the substrate, resulting in negative catalysis by chloride ions.

With oxalic acid also chloride ions retard the thermal reaction, but at low concentrations the chloride ion catalyse the photochemical reaction. The catalytic activity of chloride ion in this instance is through a chlorine bridge mechanism.

In solutions containing chloride ion at concentrations equal to or less than that of thallium(III) all the chloride is present in the form of $TlCl^{2+}$ and when the thallium(III) to chloride ratio is 1:2 it is in the form of $TlCl_2^+$ [40]. $TlCl_3$ is the principal species only in the narrow range of thallium(III) to chloride ratio of 1:2.5 to 1:3. Further, disproportionation of a considerable proportion of $TlCl_3$ into $TlCl_2^+$ and $TlCl_4^-$ has been reported [41]. When the thallium(III) to chloride ratio is between 1:4.5 and 1:10, the stability constants show that most of the thallium(III) exists in the form of $TlCl_4^-$. Therefore, in solutions containing thallium(III) and chloride under the conditions where the chloride catalysis is observed, the principal thallium(III) chloride species present are $TlCl^{2+}$ and $TlCl_2^+$.

At a concentration ratio where a minimum in the rate of exchange between thallium(III) and thallium(I) in the presence of chloride ions [42] is observed, the catalysis of the photochemical reaction between thallium(III) and oxalic acid is observed to be maximum. This indicates the pres-

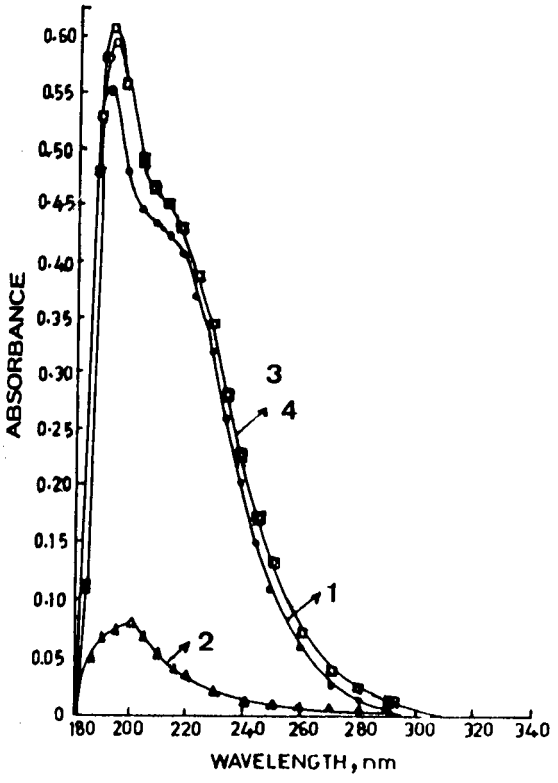

Fig. 1. Absorption spectra of (1) Tl(III)+Cl^-; (2) oxalic acid; (3) Tl(III)+Cl^-+oxalic acid (computed); (4) Tl(III)+Cl^-+oxalic acid (recorded).

ence of two competing reactions, electron exchange between thallium(I) and thallium(III) and electron transfer from oxalate to thallium(III):

$$Tl(III) + 2\,e^- \longrightarrow Tl(I)$$

$$Tl(III) + C_2O_4^{2-} \longrightarrow 2CO_2 + Tl(I)$$

The electron exchange between thallium(I) and thallium(III) in the presence of chloride ion is explained through the formation of chlorine bridges. The catalytic activity is observed to be a maximum at high chloride on concentrations [42].

However, the rate of electron exchange between thallium(I) and thallium(III) is found to be a minimum when the thallium(III) to chloride ratio is 1:2. Under these conditions the lower chlorothallium(III) species is likely to be present in the solution. No spectral evidence could be obtained for the formation of a complex between chlorothallium(III) species and oxalate (Fig. 1). It may be assumed that the chloride ion will be slightly depleted of electron density when it is attached to a tripositive metal ion and the oxalate ion attacks the halide ion attached to the highly positive metal centre, resulting in a chlorine bridge between the metal and substrate. After the bridge formation, photochemically aided transfer of electron density from the substrate to the metal is facilitated, thus resulting in reduction of thallium(III) to thallium(I). A similar mechanism was proposed by Gupta and Gupta [6,7] to explain chloride catalysis in the reduction of thallium(III) by hypophosphite and phosphite. Here the active form of the substrate is believed to attack the electron-depleted chloride ion attached to the tripositive metal ion, thereby facilitating the electron transfer.

In the majority of the cases, such a type of electron transfer and subsequent reduction of thallium(III) are not observed in solutions containing high chloride ion concentrations. This appears to be due to two reasons: the thallium(I) and thallium(III) exchange rate is facilitated in high chloride medium, and in higher chlorothallium(III) species the electrophilic nature decreases, thereby making the attack by the nucleophilic substrate less favourable. Hence the reaction rate decreases.

A similar type of chlorine bridge can be assumed with other substrates also, but the absence of catalytic activity in these instances may be due to the inability of the chlorine bridge to facilitate such an electron transfer as it does with oxalate ion. However, bromide, being a better bridging ligand with a greater ease of electron transfer, is able to catalyse the reaction with the other substrates also.

Role of bromide ion

In spite of the difference in the nature of the reducing substances studied, the photochemical oxidations catalysed by bromide have many similarities. Considerable catalysis is observed in the oxidation of organic substrates with thallium(III) where thallium(III) to bromide ratio is in the range 10:1 to 1:1. A considerable decrease in catalytic activity is observed in reaction mixtures containing thallium(III) and bromide in ratios

between 1:2 and 1:3 [20–23,25–27]. When the ratio of thallium(III) to bromide is 1:4 and above, a drastic decrease in the rate of oxidation of the organic substrate is observed, apparently because the thallium(III) ion forms various bromo complexes that differ greatly in their reactivities and the overall reaction is determined by the properties of the individual species and by their concentrations in the system. From the observations recorded in these studies, it appears that the thallimetric photochemical oxidations proceed via two different mechanisms.

Basing on the stability constants data of bromothallium(III) species [43], Rao [28] calculated the percentage populations of various bromothallium(III) species at different bromide ion concentrations. From these data it is clear that under the present conditions where catalytic activity is observed the main bromothallium(III) species existing in the reaction mixture are $TlBr^{2+}$ and $TlBr_2^+$.

Hence the bridge mechanism proposed for chloride ion can be invoked to explain the reaction between thallium(III) and the organic substrates in the presence of bromide ions also. Here also the thallium(I)–thallium(III) exchange reaction in the presence of bromide is observed to be the slowest under the conditions when the photochemical reactions are the fastest. Hence the bromide ion attached to thallium(III) in the lower bromothallium(III) species is assumed to be attacked by the nucleophilic substrate, thus forming a bridged complex, and subsequent transfer of electron density will be facilitated in the presence of light. The higher bromothallium(III) species are ineffective in bringing about the reactions.

However, in the presence of bromide ion these reaction mixtures, under radiation from mercury vapour lamp, are able to initiate polymerization in acrylonitrile, indicating the formation of free radicals, whereas such free radical formation is absent in the case of chloride ion. Schafer [17] observed that on UV irradiation $TlBr_2^+$ and $TlBr_3$ species reversibly decompose to give thallium(II) and bromine radical, whereas $TlBr^{2+}$ remains as a stable species. Reversible equilibria similar to decomposition may be assumed to occur under radiation from the mercury vapour lamp. The bromide radicals formed in this manner are obviously responsible for the initiation of the polymerization reaction. Hence the highly reactive thallium(II) species and the bromide radicals appear to be responsible for bringing about the oxidations of the studied substrates by thallium(III).

It was thought that the proof for the existence of such reactive species could also be obtained from a study of the role of manganese(II) in the present reactions, as thallium(II) is known to oxidize manganese(II) to manganese(III). Hence the following investigation was undertaken.

Role of manganese(II)

Manganese(II) ions are found to retard the rate of oxidation of formic acid [23] by thallium(III). In addition to manganese(II), other ions such as iron(III) and chromium(III) also retard the photochemical thallimetric oxidation of formic acid. Obviously these interferences are due to the reaction with either of the chain carriers, namely thallium(II) species or the bromine free radical. As these ions interfere in the bromimetric titration of thallium(I), which was used for monitoring the progress of the reactions, further detailed studies could not be carried out in the presence of these ions. However, manganese(II) does not interfere in the bromimetric determination of thallium(I), hence, the effect of manganese(II) on these reactions was investigated further.

Falcinella et al. [44] reported that in the presence of an excess of manganese(II), thallium(II), in addition to undergoing decay by disproportionation, also oxidizes manganese(II) to manganese(III). Hence solutions containing thallium(III) and bromide in different ratios in the presence of excess of manganese(II) were exposed to radiation from the mercury vapour lamp. Spectral evidence showed the presence of manganese(III) during the reactions, thereby indicating the formation of thallium(II) as the intermediate species:

$$2Tl(II) \longrightarrow Tl(III) + Tl(I)$$

$$Tl(II) + Mn(II) \longrightarrow Tl(I) + Mn(III)$$

Obviously the concentration of manganese(III) will be proportional to the concentration of thal-

lium(II). Experiments were therefore done to establish the extent of thallium(II) formed by observing the extent of manganese(III) formation in the reaction mixtures containing thallium(III) and bromide in different ratios. These reactions were carried out in the presence of excess of manganese(II) and in the absence of the reducing substance. The reaction mixtures were exposed to radiation from the mercury vapour lamp and after 120 min the solutions had turned pink; further exposure did not increase the intensity of the colour. For the solutions containing the same thallium(III) to bromide ratio, the intensity of the pink colour was greater in sulphuric acid than in perchloric acid medium, and also the intensity increased with increase in sulphuric acid concentration.

When these coloured solutions were kept in the dark, they gradually became colourless. The development of pink colour is obviously due to a purely photochemical phenomenon, as no pink colour developed in the reaction mixtures when kept in dark, even after 1 month. With the same solution the process of development of pink colour in the light and its disappearance in dark were observed repeatedly during a span of 4 months. The absorption spectrum of the reaction mixture after irradiation for 120 min was recorded with reference to a similar reaction mixture left unexposed. The spectrum obtained was identical with that of manganese(III) in 4.0 M sulphuric acid medium reported by Purdy and Hume [45] and is shown in Fig. 2.

Hence it is clear that in the presence of bromide, thallium(III) photochemically oxidizes manganese(II) to manganese(III) and in the dark the reduction of manganese(III) takes place. No pink colour developed in solutions containing thallium(III) and manganese(II) in the absence of bromide. The absorbance of the reaction mixture recorded at 500 nm after irradiation for 120 min is plotted against the bromide to thallium ratio in Fig. 3.

It is clear that when the thallium(III) to bromide ratio is ca. 1:2 to 1:3, maximum formation of manganese(III) occurs. Based on previous reports and the results of the present experiments it can be concluded that the $TlBr_2^+$ and $TlBr_3$ species when exposed to radiation from the mercury vapour lamp readily decompose to form thallium(II) and bromine radicals. This observation is in accordance with the report of Schafer [17]. Hence the observations in this experiment support the mechanism proposed earlier.

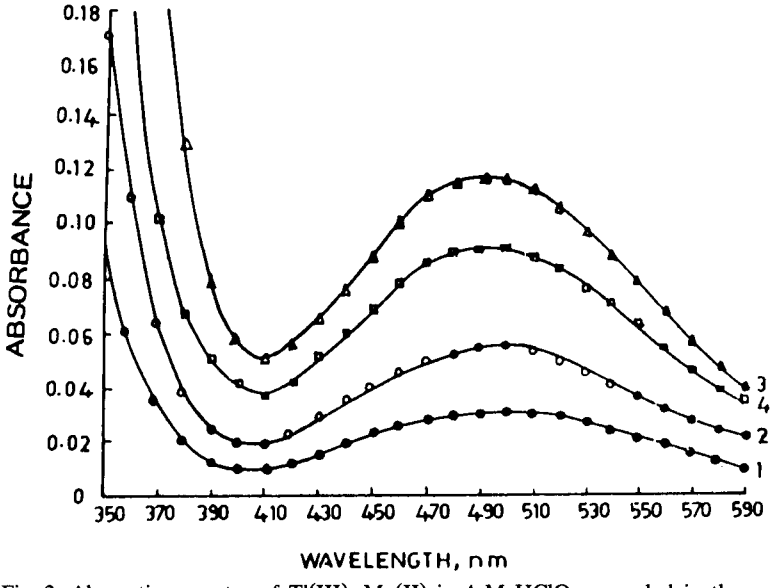

Fig. 2. Absorption spectra of Tl(III), Mn(II) in 4 M $HClO_4$ recorded in the presence of different concentrations of Br^- ion. Exposure time = 120 min. $[Tl^{3+}]:[Br^-]$ ratio: (1) 2:1; (2) 1:1; (3) 1:2; (4) 1:3. $[Tl^{3+}] = 0.008$ M; $[Mn^{2+}] = 0.08$ M.

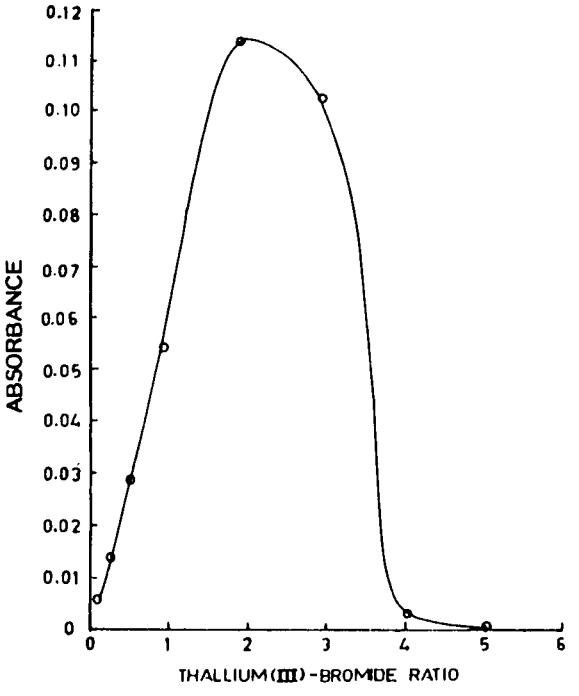

Fig. 3. Optical densities of the reaction mixtures recorded at different Tl(III) and Br^- ratios. Exposure time = 120 min. $[Tl^{3+}] = 0.008$ M; $[Mn^{2+}] = 0.08$ M; $[HClO_4] = 4.0$ M.

As already stated, manganese(II) when present even at low concentrations is able to retard the bromide-catalysed photochemical oxidation of formic acid. Probably manganese(II) is complexed with the substrate, thereby decreasing the availability of the substrate for the photochemical reaction to take place, and also the manganese(II) formic acid complex is oxidized to manganese(III) formate, which is resistant to further redox decomposition [46].

The effect of manganese(II) on the photochemical oxidation of formaldehyde, glyoxylic acid and glycolic acid may be explained similarly.

With oxalic acid, the retarding influence of manganese(II) is not observed as the intermediate manganese(III) formed readily oxidizes oxalic acid [46,47].

From the results in Table 2, it can be seen that in the uncatalysed reaction only a large excess of manganese can influence the rate or course of the reaction. This is obviously due to the preferential coordination of manganese(II) with oxyanions [48]. Hence in the presence of a large excess of manganese(II) a considerable amount of organic substance may be coordinated with it. The redox potential data [44] show that thallium(III) cannot oxidize manganese(II) to manganese(III). However, in the presence of some ligands the manganese(II) complex may be oxidized to the manganese(III) complex by thallium(III) [46]. As manganese(III) cannot oxidize formic acid readily, inhibition in the oxidation of formic acid is observed.

With glyoxylic acid, the manganese(III)–glyoxylic acid complex undergoes redox decomposition in such a way that formic acid is formed as the intermediate. Hence further oxidation becomes slow, thereby accumulating formic acid as the intermediate in sufficient amounts and it could be identified by a spot test. However, with oxalic and mesoxalic acid the manganese(III)–substrate complex readily undergoes redox decomposition to give corresponding products.

Finally, the rapid photochemical oxidation of oxalic and mesoxalic acid can be attributed to the type of bond that is broken during the oxidation. With these two substrates relatively easy homolytic fission of C–C bonds takes place. However, with the other substrates difficult heterolytic fission of C–H bonds has to take place, which eventually slows the reaction.

Hence it can be concluded that the bromide catalysis in these photochemical reactions takes place through a bridge mechanism as proposed for chloride when the thallium(III) to bromide ratio is $\leq 1:1$. At higher bromide ion concentrations the free radical mechanism also appears to be operative and dominating over the bridge mechanism. This assumption is based on the fact that the electrophilic nature of thallium(III) is less in higher bromo species.

REFERENCES

1 H.A. Schowarg, D. Comstock, J.K. Yandell and R.W. Dodson, J. Phys. Chem., 78 (1984) 488.
2 A.G. Sykes, J. Chem. Soc., (1961) 5549.
3 B.M. Thakuria and Y.K. Gupta, J. Chem. Soc., Dalton Trans., (1975) 2541.

4 P.D. Sharma and Y.K. Gupta, J. Chem. Soc. A, (1973) 52.
5 P.D. Sharma and Y.K. Gupta, J. Chem. Soc., Dalton Trans., (1973) 789.
6 K.S. Gupta and Y.K. Gupta, Inorg. Chem., 13 (1974) 851.
7 K.S. Gupta and Y.K. Gupta, Inorg. Chem., 14 (1975) 2000.
8 H.N. Halvorson and J. Halpern, J. Am. Chem. Soc., 78 (1956) 5562.
9 F.R. Duke and B. Bornong, J. Phys. Chem., 60 (1956) 1015.
10 G.M. Waind, Discuss. Faraday Soc., 29 (1960) 136.
11 N.A. Maier, G.P. Korityshova and Yu.A. Lodekop, Zh. Obshch. Khim., 38 (1968) 2384.
12 J.K. Kochi and T.N. Bethea, J. Org. Chem., 33 (1968) 75.
13 C.E. Burchill and W.H. Wolodrarsky, Can. J. Chem., 48 (1970) 2955.
14 Z. Böti, I. Horvath, Z. Szil and I.J. Csanyl, J. Chem. Soc., Dalton Trans., (1978) 1012.
15 D.R. Shranks and J.K. Yandell, J. Phys. Chem., 73 (1969) 840.
16 H. Schafer, Z. Anorg. Allg. Chem., 64 (1960) 305.
17 H. Schafer, Naturwissenschaften, 48 (1961) 302.
18 M. Lefort and Y. Tarragoa, J. Chem. Phys., 57 (1960) 38.
19 G. Laurence and V. Balzani, Inorg. Chem., 13 (1974) 2976.
20 S.R. Sagi, G.S.P. Raju, K. Appa Rao and M.S. Prasada Rao, Talanta, 29 (1982) 413.
21 S.R. Sagi, K. Appa Rao and M.S. Prasada Rao, Talanta, 30 (1983) 282.
22 S.R. Sagi, K. Appa Rao and M.S. Prasada Rao, Can. J. Chem., 61 (1983) 2795.
23 S.R. Sagi, K. Appa Rao and M.S. Prasada Rao, Analyst, 109 (1984) 53.
24 S.R. Sagi, K. Appa Rao and M.S. Prasada Rao, Talanta, 31 (1984) 209.
25 A. Ramamohana Rao, M.S. Prasada Rao, K.V. Ramana and S.R. Sagi, Talanta, 36 (1989) 686.
26 M.S. Prasada Rao, A. Ramamohana Rao, K.V. Ramana and S.R. Sagi, Talanta, 37 (1990) 753.
27 M.S. Prasada Rao, A. Ramamohana Rao, K.V. Ramana and S.R. Sagi, Talanta, 38 (1991) 337.
28 A. Ramamohana Rao, PhD Thesis, Andhra University, Visakhapatnam, 1991.
29 K. Appa Rao, PhD Thesis, Andhra University, Visakhapatnam, India, 1991.
30 S.R. Sagi, K. Appa Rao and M.S. Prasada Rao, Indian J. Chem., 22A (1983) 95.
31 M.S. Prasada Rao and A. Ramamohana Rao, Anal. Chim. Acta, 242 (1991) 229.
32 M.S. Prasada Rao and A. Ramamohana Rao, Anal. Chim. Acta, 257 (1992) 159.
33 S.R. Sagi and K.V. Ramana, Talanta, 16 (1969) 1217.
34 S.R. Sagi and M.S. Prasada Rao, Talanta, 26 (1979) 52.
35 S.R. Sagi and K.V. Ramana, Z. Anal. Chem., 245 (1969) 320.
36 L.B. Mønsted, O. Mønsted and G. Nord, Trans. Faraday Soc., 66 (1970) 936.
37 R.C. Aggarwal and A.K. Srivastava, Indian J. Chem., 3 (1965) 494.
38 O. Farver, Acta Chem. Scand., 26 (1972) 534.
39 H.N. Halvorson and J. Halpern, J. Am. Chem. Soc., 78 (1956) 5562.
40 M. Ignaczak and G. Andrijewski, Pol. J. Chem., 55 (1981) 277.
41 T.G. Spiro, Inorg. Chem., 4 (1965) 731.
42 C.H. Brubaker, Jr., K.O. Groves, J.P. Micke and C.P. Knop, J. Am. Chem. Soc., 79 (1957) 4641.
43 L.G. Carpernter, H.M. Ford-Smith, R.P. Bell and R.W. Dodson, Discuss. Faraday Soc., 29 (1960) 92.
44 B. Falcinella, D. Felgate and G.S. Laurence, J. Chem. Soc., Dalton Trans., (1975) 1.
45 W.C. Purdy and D.N. Hume, Anal. Chem., 27 (1955) 256.
46 V.S. Srinivasan and N. Venkatasubramanian, Indian J. Chem., 11 (1973) 702.
47 M. Ishivoshi, T. Shigematsu and S. Shivata, Jpn. Anal., 8 (1959) 380.
48 K.K. Sengupta and J. Sarkar, Tetrahedron, 31 (1975) 123.

ANALYTICA CHIMICA ACTA, VOL. 280 (1993)

AUTHOR INDEX

PUBLICATION SCHEDULE FOR 1993

	S'92	O'92	N'92	D'92	J	F	M	A	M	J	J	A
Analytica Chimica Acta	267/1 267/2	268/1 268/2	269/1 269/2	270/1 270/2	271/1 271/2	272/1 272/2 273/1–2	274/1 274/2	275/1–2 276/1 276/2	277/1 277/2	278/1 278/2	279/1 279/2	280/1 280/2
Vibrational Spectroscopy		4/1			4/2		4/3	5/1		5/2		5/3

INFORMATION FOR AUTHORS

Detailed "Instructions to Authors" for *Analytica Chimica Acta* was published in Volume 256, No. 2, pp. 373–376. Free reprints of the "Instructions to Authors" of *Analytica Chimica Acta* and *Vibrational Spectroscopy* are available from the Editors or from: Elsevier Science Publishers B.V., P.O. Box 330, 1000 AH Amsterdam, The Netherlands. Telefax: (+31-20) 5862845.

Manuscripts. The language of the journal is English. English linguistic improvement is provided as part of the normal editorial processing. Authors should submit three copies of the manuscript in clear double-spaced typing on one side of the paper only. *Vibrational Spectroscopy* also accepts papers in English only.

Abstract. All papers and reviews begin with an Abstract (50–250 words) which should comprise a factual account of the contents of the paper, with emphasis on new information.

Figures. Figures should be prepared in black waterproof drawing ink on drawing or tracing paper of the same size as that on which the manuscript is typed. One original (or sharp glossy print) and two photostat (or other) copies are required. Attention should be given to line thickness, lettering (which should be kept to a minimum) and spacing on axes of graphs, to ensure suitability for reduction in size on printing. Axes of a graph should be clearly labelled, along the axes, outside the graph itself. All figures should be numbered with Arabic numerals, and require descriptive legends which should be typed on a separate sheet of paper. Simple straight-line graphs are not acceptable, because they can readily be described in the text by means of an equation or a sentence. Claims of linearity should be supported by regression data that include slope, intercept, standard deviations of the slope and intercept, standard error and the number of data points; correlation coefficients are optional.

Photographs should be glossy prints and be as rich in contrast as possible; colour photographs cannot be accepted. Line diagrams are generally preferred to photographs of equipment.

Computer outputs for reproduction as figures must be good quality on blank paper, and should preferably be submitted as glossy prints.

Nomenclature, abbreviations and symbols. In general, the recommendations of the International Union of Pure and Applied Chemistry (IUPAC) should be followed, and attention should be given to the recommendations of the Analytical Chemistry Division in the journal *Pure and Applied Chemistry* (see also *IUPAC Compendium of Analytical Nomenclature, Definitive Rules*, 1987).

References. The references should be collected at the end of the paper, numbered in the order of their appearance in the text (*not* alphabetically) and typed on a separate sheet.

Reprints. Fifty reprints will be supplied free of charge. Additional reprints (minimum 100) can be ordered. An order form containing price quotations will be sent to the authors together with the proofs of their article.

Papers dealing with vibrational spectroscopy should be sent to: Dr J.G. Grasselli, 150 Greentree Road, Chagrin Falls, OH 44022, U.S.A. Telefax: (+1-216) 2473360 (Americas, Canada, Australia and New Zealand) or Dr J.H. van der Maas, Department of Analytical Molecule Spectrometry, Faculty of Chemistry, University of Utrecht, P.O. Box 80083, 3508 TB Utrecht, The Netherlands. Telefax: (+31-30) 518219 (all other countries).

0003-2670/93/$06.00

This issue is printed on acid-free paper.

PRINTED IN THE NETHERLANDS

TrAC - Trends in Analytical Chemistry: Reference Edition

Volume 11: 1992

TrAC Compendium Series Volume 11

The Reference Edition of Trends in Analytical Chemistry (TrAC) is a compilation of the archival material reprinted from the regular issues of the journal. TrAC provides a topical digest of current developments and new ideas in the analytical sciences. It does so in the form of broadly-based, easy-to-read scientific reviews, backed up by news and other features of interest to the international analytical chemistry community. For subscribers to the library edition of TrAC, the reference editions form an integral part of the annual subscription, but for others these indispensable sources of information can be purchased individually. They provide informative and stimulating reading for all those who use analytical methods.

This latest volume contains all the archival material published in 1992. It covers a wide range of analytical techniques and applications of interest to academic and research workers in chemistry, biochemistry, clinical chemistry, pharmaceutical chemistry and toxicology.

A selection of the Contents.

Capillary Electrophoresis in Chemical/Pharmaceutical Quality Control *(A. Pluym, W. Van Ael, M. De Smet)*. Image Analysis in Chemistry. I. Properties of Images, Greylevel Operations, the Multivariate Image. II. Multivariate Image Analysis *(P. Geladi et al.)*. Silica Based, Solid Phase Reagents for Derivatizations in Chromatography *(F.-X. Zhou, J.M. Thorne, I.S. Krull)*. Mapping Post-Translational Modifications of Viral Proteins by Mass Spectrometry *(J.J. Gormann)*. Fluorescence Detection in Capillary Electrophoresis *(L.N. Amankwa, M. Albin, W.G. Kuhr)*. Biomolecular Tracing through Accelerator Mass Spectrometry *(J.S. Vogel, K.W. Turteltaub)*. Solid-Phase Reactors in Flow Injection Analysis *(M.D. Luque de Castro)*. Capillary Electrophoresis: A Powerful Tool for Biomedical Analysis and Research? *(D. Perrett, J. Ross)*. Bioanalytical Sample Preparation using Microdialysis and Ultrafiltration Capillaries *(M.C. Linhares, P.T. Kissinger)*. Models of Time-Series Analysis - a Helpful Tool for Evaluation of Noisy Data in Distribution Analysis *(K. Doerffel)*. Bio-Analytical Applications of Fourier Transform Infrared Spectroscopy *(M. Jackson, H.H. Mantsch)*. X-ray Absorption Spectroscopy in Chemistry. I. Extended X-ray Absorption Fine Structure. II. X-ray Absorption near Edge Structure *(P. Behrens)*. Mechanism of the Peroxyoxalate Chemiluminescence Reaction *(P.J.M. Kwakman, G.J. de Jong, U.A.Th. Brinkman)*. Plasma Spectrometric Detection for Supercritical Fluid Chromatography *(J.M. Carey, J.A. Caruso)*. Electrochemistry of Biopolymers *(J.A. Cox, A. Pryzjazny)*. High-Field NMR Spectroscopy as an Analytical Tool for Quantitative Determinations: Pitfalls, Limitations and Possible Solutions *(Cs. Szántay, Jr.)*. Abrasive Stripping Voltammetry - an Electrochemical Solid State Spectroscopy of Wide Applicability *(F. Scholz, B. Lange)*. Polymer Coatings as Stationary Phases in High-Performance Liquid Chromatography *(M. Hanson, K.K. Unger)*. Lasers in Mass Spectrometry *(J. Gorbally)*. Author Index. Subject Index.

1993 viii + 402 pages
Price: US $ 354.25 / Dfl. 620.00
ISBN 0-444-89926-X

ELSEVIER
SCIENCE PUBLISHERS

ORDER INFORMATION

For USA and Canada
ELSEVIER SCIENCE PUBLISHERS
Judy Weislogel
P.O. Box 945
Madison Square Station,
New York, NY 10160-0757
Tel: (212) 989 5800
Fax: (212) 633 3880

In all other countries
ELSEVIER SCIENCE PUBLISHERS
P.O. Box 211
1000 AE Amsterdam
The Netherlands
Tel: (+31-20) 5803 753
Fax: (+31-20) 5803 705

US$ prices are valid only for the USA & Canada and are subject to exchange rate fluctuations; in all other countries the Dutch guilder price (Dfl.) is definitive. Customers in the European Community should add the appropriate VAT rate applicable in their country to the price(s). Books are sent postfree if prepaid.

0003-2670(19930816)280:2;1-9